

THE ALTERATION HISTORY OF A SERIES OF
SHEAR ZONES, MIRAGE ISLANDS,
YELLOWKNIFE BAY, N.W.T.

CENTRE FOR NEWFOUNDLAND STUDIES

**TOTAL OF 10 PAGES ONLY
MAY BE XEROXED**

(Without Author's Permission)

CAROLYN DIANE RELF



National Library
of Canada

Bibliothèque nationale
du Canada

Canadian Theses Service

Service des thèses canadiennes

Ottawa, Canada
K1A 0N4

NOTICE

The quality of this microform is heavily dependent upon the quality of the original thesis submitted for microfilming. Every effort has been made to ensure the highest quality of reproduction possible.

If pages are missing, contact the university which granted the degree.

Some pages may have indistinct print especially if the original pages were typed with a poor typewriter ribbon or if the university sent us an inferior photocopy.

Previously copyrighted materials (journal articles, published tests, etc.) are not filmed.

Reproduction in full or in part of this microform is governed by the Canadian Copyright Act, R.S.C. 1970, c. C-30.

AVIS

La qualité de cette microforme dépend grandement de la qualité de la thèse soumise au microfilmage. Nous avons tout fait pour assurer une qualité supérieure de reproduction.

S'il manque des pages, veuillez communiquer avec l'université qui a conféré le grade.

La qualité d'impression de certaines pages peut laisser à désirer, surtout si les pages originales ont été dactylographiées à l'aide d'un ruban usé ou si l'université nous a fait parvenir une photocopie de qualité inférieure.

Les documents qui font déjà l'objet d'un droit d'auteur (articles de revue, tests publiés, etc.) ne sont pas microfilmés.

La reproduction, même partielle, de cette microforme est soumise à la Loi canadienne sur le droit d'auteur, SRC 1970, c. C-30.

THE ALTERATION HISTORY
OF A SERIES OF SHEAR ZONES, MIRAGE ISLANDS,
YELLOWKNIFE BAY, N.W.T.

BY

© Carolyn Diane Relf, B.Sc.

A thesis submitted to the School of Graduate
Studies in partial fulfillment of the
requirements for the degree of
Master of Science.

Department of Earth Sciences
Memorial University of Newfoundland

January, 1988

St. John's

Newfoundland

Permission has been granted to the National Library of Canada to microfilm this thesis and to lend or sell copies of the film.

The author (copyright owner) has reserved other publication rights, and neither the thesis nor extensive extracts from it may be printed or otherwise reproduced without his/her written permission.

L'autorisation a été accordée à la Bibliothèque nationale du Canada de microfilmer cette thèse et de prêter ou de vendre des exemplaires du film.

L'auteur (titulaire du droit d'auteur) se réserve les autres droits de publication; ni la thèse ni de longs extraits de celle-ci ne doivent être imprimés ou autrement reproduits sans son autorisation écrite.

ISBN 0-315-45079-7

ABSTRACT

The Mirage Islands are part of a north-facing Archean supracrustal sequence which is dominated by felsic to intermediate volcanoclastic rocks interlayered with mafic flows, and cut by gabbroic dykes and sills. The western-most islands are intruded by granitoid veins, inferred to have been derived from an unexposed pluton centred south of the West Mirage Islands.

Two metamorphic events have been recognized in the area. The first involved amphibolite facies metamorphism (M1), interpreted to have been caused by the intrusion of the inferred pluton. Temperatures approached 600°C and pressures were between approximately 2 and 5 kbar. The second metamorphic event (M2) entailed regional greenschist facies metamorphism, with temperatures near 450 to 500°C and pressures of about 2 to 4 kbar. M2 may have overlapped in time with M1, but it has overprinted (and therefore outlasted) M1 assemblages on the Mirage Islands.

A series of steeply dipping east-west striking shear zones cut the rocks on the Mirage Islands, and are well exposed in metabasic rocks. Equilibration temperatures in the shear zones were calculated from the fractionation of

^{18}O between quartz and chlorite. They have a bimodal distribution which corresponds to the temperatures determined for M1 and M2, and thus it is interpreted that the shear zones formed during M1 and that some of them have subsequently re-equilibrated during M2.

The source of the hydrothermal fluids cannot be established unequivocally from isotope data, but it is suggested that the fluids which were present in the shear zones during M1 were of igneous origin, and that metamorphic and meteoric fluids moved through the shear zones as the temperature decreased.

Quartz veins in the shear zones are host to fluid inclusions with a range of compositions and homogenization temperatures. High salinities determined by fluid inclusion analyses support the interpretation that the hydrothermal fluid was in part meteoric. No primary inclusions were identified, however a few inclusions had sufficiently high homogenization temperatures that an estimate of their maximum trapping pressure could be made using formation temperatures calculated from isotope data. These pressure estimates are all less than 0.75 kbar.

Alteration in the shear zones has resulted in the formation of new mineral assemblages and changes in the

bulk chemistry of the sheared rocks. The oxidation states of iron in sheared samples suggest that the hydrothermal fluids were ascending, reducing fluids. In general, the changes in bulk composition of the sheared rocks may be predicted from alteration reactions between sheared and unsheared mineral assemblages. Estimates of minimum fluid:rock volume ratios are on the order of 10:1, but may be as high as 100:1 or more locally. It is possible semiquantitatively to monitor the alteration progress in the shear zones, and it was found that the enrichment or depletion of some elements varies systematically with the extent of alteration.

The shear zones are interpreted to have formed during the intrusion of the pluton south of the Mirage Islands. Alteration, which began in the presence of igneous fluids, continued variably into the regional greenschist facies event which followed plutonism. The calculated variations in equilibrium temperature, isotopic composition, bulk chemistry and fluid:rock ratio are attributed to a variable time of closure of each shear zone.

ACKNOWLEDGEMENTS

The author wishes to acknowledge the assistance and support of several people during the course of this project.

Dr. T. Rivers is thanked for his supervision, constructive comments and financial support. This study has benefited greatly from his ideas and enthusiasm.

Dr.s D. Wilton and A. Nutman each critically reviewed several chapters, and their comments have helped to improve the text.

Financial and logistical support for field work were provided by the Department of Indian and Northern Affairs in Yellowknife. C. Nicholson is thanked for his capable field assistance, and his help in the last minute preparations of the manuscript.

G. Goldak kindly allowed me access to confidential assessment work, and has shared ideas with me.

Chemical analyses were carried out by G. Veinnott and G. Andrews, and polished thin sections were produced by the lapidary laboratory at Memorial University. Oxygen

isotope analyses were done by Dr. F. Longstaffe at the University of Alberta.

Laboratory expenses were covered by an NSERC grant to T. Rivers. Financial support for the author was provided by a Memorial University Graduate Scholarship (1985-1987).

Finally, I have benefited from stimulating discussions with many individuals, including F. Mengel, A. Nutman, F. Longstaffe, and H. Helmstaedt of Queen's University.

TABLE OF CONTENTS

	page
ABSTRACT	ii
ACKNOWLEDGEMENTS	v
 CHAPTER 1: REGIONAL AND LOCAL GEOLOGY OF THE MIRAGE ISLANDS	
Introduction	1
Objectives of Study	2
Location and Access	2
Regional Geology	3
The Yellowknife Greenstone Belt	7
Stratigraphy	8
Structure and Metamorphism	14
Mirage Islands	20
Mirage Island Map Units	21
Unit 1	23
Unit 2	24
Unit 3	33
Unit 4	33
Unit 5	33
Unit 6	37
Unit 7	37
Unit 8	37
Structure in the Mirage Islands	38
Shear Zones	40
 CHAPTER 2: METAMORPHISM	
Introduction	51
Petrography	52
Mineral chemistry: Plagioclase	61
Amphibole	70
Pressure, Temperature Determinations	73
Geothermometry	73
Geobarometry	81
Summary	90
 CHAPTER 3: STABLE ISOTOPES	
Introduction	92
Sample Selection	93
Analytical Techniques	94
Thermometry	94
Results and Calculations from Quartz - Chlorite Pairs	94
Results from Carbonate-bearing Shear Zones	112
Whole Rock Oxygen Isotopes	115
Conclusions	122

CHAPTER 4: FLUID INCLUSION ANALYSES	
Introduction	125
Analytical Techniques	127
Results	129
Composition of Inclusions	138
Thermobarometry	151
Discussion	158
CHAPTER 5: SHEAR ZONE GEOCHEMISTRY AND REACTIONS	
Introduction	165
Analytical Techniques	165
Calculations and Results	166
Bulk Chemistry	166
Mineral Reactions	180
Composition of Hydrothermal Fluids	198
Oxidation State	199
Summary	208
CHAPTER 6: REACTION PROGRESS	
Introduction	213
Methodology	214
Alteration Index	216
Reaction Progress	226
Conclusions	241
CHAPTER 7: DISCUSSION AND CONCLUSIONS	
Summary	246
Shear Zone Model	250
REFERENCES	263
APPENDIX A	278
APPENDIX B	301
APPENDIX C	304
APPENDIX D	306
APPENDIX E	308
APPENDIX F	315
APPENDIX G	331
APPENDIX H	334
GEOLOGY MAP OF THE WEST MIRAGE ISLANDS	BACK POCKET
SAMPLE LOCATION MAP	BACK POCKET

LIST OF FIGURES

	page
Figure 1.1 Simplified geological map of the Slave Structural Province	6
Figure 1.2 Geological map of the Yellowknife Bay area, modified after Helmstaedt and Padgham, 1986	10
Figure 1.3 Schematic diagram showing sequence of quartz vein formation within major shear zones at Yellowknife from Kerrich and Allison (1978) and Allison and Kerrich (1981)	19
Figure 1.4 Stratigraphy of the West Mirage Islands	21
Figure 1.5 Soft sediment features in tuffaceous sediments	27
Figure 1.6 Fragmental volcanoclastic unit	29
Figure 1.7 Heterogeneous, poly lithic volcanic breccia	32
Figure 1.8 Plagioclase porphyritic dyke intruding an intermediate volcanoclastic rock and cut by a later gabbro	32
Figure 1.9 Gabbro dyke bearing zoned plagioclase megacrysts	36
Figure 1.10 Anastomosing shear zone 1 m in width hosted in gabbro	43
Figure 1.11 5, m wide shear zone in mafic flow	45
Figure 1.12 Rose diagram showing the range of shear zone orientations in the West Mirage Islands	47
Figure 1.13 Map showing distribution of shear zones on the West Mirage Islands	49

Figure 2.1	Fine grained mafic tuff interlayered with intermediate tuff	57
Figure 2.2	Intermediate fragmental volcaniclastic rock	57
Figure 2.3	Metagabbro showing partial alteration of amphibole to chlorite and plagioclase to sericite and epidote	60
Figure 2.4	Histogram of plagioclase compositions determined by probe analyses	63
Figure 2.5	Schematic temperature vs. time graph showing relative timing of M1 and M2 ...	67
Figure 2.6	Compositions of amphiboles from gabbros from the West Mirage Islands	69
Figure 2.7	Histograms showing temperatures determined from plagioclase-hornblende thermometry .	80
Figure 2.8	Qualitative estimate of metamorphic pressure using compositions of amphiboles from Mirage Islands	85
Figure 2.9	Qualitative geothermobarometer of Plyusnina, 1982	89
Figure 3.1	Histogram of temperature determinations from oxygen isotope fractionation between chlorite and quartz	100
Figure 3.2	Graph of isotopic composition of quartz veins vs. shear zone temperature .	106
Figure 3.3	Whole rock oxygen isotope compositions of typical unaltered igneous rocks compared to Mirage Islands samples	118
Figure 4.1	Histograms of homogenization temperatures of fluid inclusions in quartz veins from shear zones	136
Figure 4.2	Homogenization temperature vs. melting temperature for CO ₂ -bearing inclusions ..	139
Figure 4.3	Histogram showing the range of eutectic temperatures found in inclusions.	146

Figure 4.4	Salinity vs. solution temperature for inclusions bearing daughter minerals ...	150
Figure 4.5	Schematic diagram of a shear zone in which localized movement produces a dilatent zone, causing a drop in pressure and concomitant silica precipitation ..	161
Figure 5.1	Sample isocon diagram for a shear zone ..	170
Figure 5.2	Graphs showing gains and losses of elements in shear zones hosted in metabasic rocks	172
Figure 5.3	Graphs showing gains and losses of elements in shear zones hosted in felsic to intermediate volcanics	174
Figure 5.4	Graphs showing gains and losses of elements in shear zones hosted in metabasic rocks predicted by balanced chemical reactions	193
Figure 5.5	Graphs showing gains and losses of elements in shear zones hosted in felsic to intermediate volcanics predicted by balanced chemical reactions	197
Figure 5.6	Schematic diagram showing local downward convection of hydrothermal fluids in a shear zone with a net upward flow	210
Figure 6.1	Graphs of AI vs. change in concentration of elements across shear zones	223
Figure 7.1	Contact metamorphic aureole around pluton intruding supracrustal rocks	252
Figure 7.2	Formation of shear zones by subhorizontal stresses imposed by pluton	255
Figure 7.3	Alteration of shear zones by fluids ...	258
Figure 7.4	Temperature vs. time plot showing variable timing of shear zone closures ..	261

LIST OF TABLES

	page
Table 1.1 Simplified stratigraphy of the Yellowknife Greenstone Belt	10
Table 2.1 Comparison of the mineral assemblage(s) in each rock type on the West Mirage Islands	54
Table 2.2 Comparison of the mean An content of plagioclase with the composition of amphibole and the amount of chlorite replacing amphibole	72
Table 2.3 Equilibrium temperatures from plagioclase-hornblende thermometry	78
Table 3.1 Temperatures from oxygen isotope thermometry	102
Table 3.2 Comparison of the whole rock oxygen isotope compositions of unsheared and sheared West Mirage Island samples	121
Table 4.1 Comparison of homogenization temperatures, eutectic temperatures, melting temperatures and salinities of fluid inclusions	131
Table 4.2 Critical point and triple point temperatures of various species known to occur in fluid inclusions	141
Table 4.3 Comparison of homogenization temperature of fluid inclusions to formation temperature (from independent thermometers)	154
Table 5.1 Changes in concentration of elements predicted by alteration reactions	191
Table 5.2 Comparison of oxidation state of Fe in unsheared and sheared samples	201

Table 5.3	Table showing fluid:rock ratios calculated from silica enrichment/depletion	206
Table 6.1	Comparison of ΔAI between shear zones ...	218
Table 6.2	Comparison of ΔAI with change in concentration of elements across shear zones	221
Table 6.3	Additive and exchange components for the minerals involved in the net transfer reactions used to characterize alteration of the Mirage Islands	229
Table 6.4	Estimates of reaction progress variables for shear zone reactions	243

CHAPTER 1: REGIONAL AND LOCAL GEOLOGY OF THE MIRAGE ISLANDS

Introduction

Gold mining in the Yellowknife area has dominated the mineral industry of the Northwest Territories since it began in the late 1930's. Major shear zones and their associated quartz veins are host to the most important gold deposits in the Yellowknife area, and several studies have been undertaken in order to better understand the conditions under which these gold-bearing chlorite-sericite-carbonate schists formed, including those of Boyle (1961), Kerrich *et al.*, (1977), Kerrich and Allison (1978), and Kerrich and Fyfe (1981).

One of the two main gold-bearing shear zones at Yellowknife strikes into Great Slave Lake, and recent exploration in the area (G. Goldak, personal communication, 1986) has involved lacustrine geophysical studies to delineate the shear zone under water and to locate the extension of the gold-bearing zone under the waters of Yellowknife Bay.

This study is centred on a series of shear zones on the Mirage Islands in Yellowknife Bay, where the southern-most exposures of the volcanic rocks of the

Yellowknife Greenstone Belt occur.

Objectives of Study

The timing of shear zone formation and the type and extent of chemical alteration in the major gold-bearing shear zones at Yellowknife have been studied by Boyle (1961); Kerrich et al. (1977); Kerrich and Allison (1981); and Kerrich (1981), among others. The results of these studies provide the background for the present study, in which whole rock geochemical analyses and microprobe analyses of minerals, together with oxygen isotope and fluid inclusion studies on samples from the Mirage Islands and the Octopus Islands are compared with the data from the Yellowknife area. The analytical results are combined with geological data to produce a model for the formation and alteration history of the Mirage Island shear zones.

Location and Access

The Mirage Islands lie about 25 km south of Yellowknife, at the mouth of Yellowknife Bay. They comprise two groups of islands named the West and East Mirage Islands. They are accessible by boat or float plane from Yellowknife.

Field work in the area was carried out during 10 days in late August of 1984, and from mid-June to the end of August 1985, under the auspices of the Geology C.O.S.E.P. program of the Department of Indian and Northern Affairs, Canada. Field work entailed detailed (1:2200) geological mapping of the islands and systematic sampling across the shear zones. Although the majority of the map area lies under water, the shoreline exposure is superb, giving a clear view of various contact and intrusive relationships and of the shear zones which form the subject matter of this study.

Regional Geology

The Slave Structural Province is located in the Northwest Territories (Figure 1.1), and covers an area of almost 190,000km² (McGlynn and Henderson, 1972). It is underlain by an Archean granitoid basement dated between 2.7 and 3.2 Ga (Easton, 1984), over which lies a late Archean supracrustal succession of metavolcanic and metasedimentary rocks, intruded by syn- and post-volcanic granitoids. The supracrustal sequence has been named the Yellowknife Supergroup by Henderson (1970), and covers about half of the Slave Province.

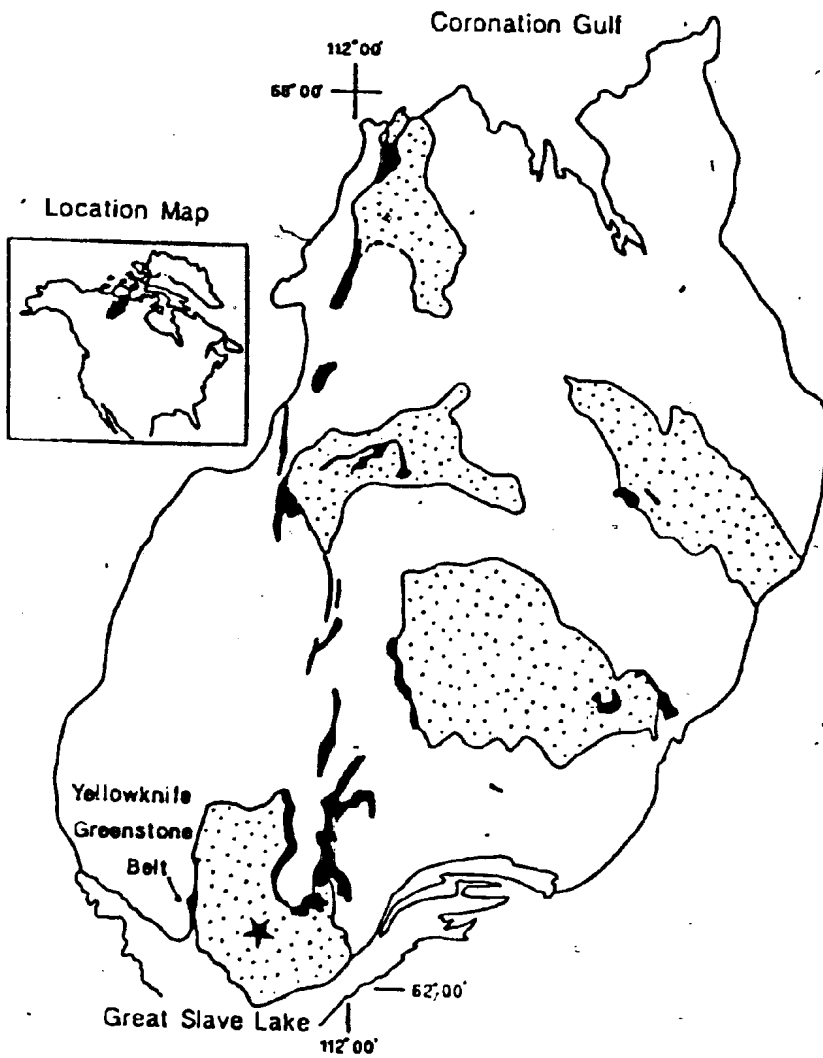
The evolution of the Slave Province is presently under

debate, and two models are currently being considered. One involves extensional tectonics with continental rifting, and the other calls upon compressive tectonics, involving accretion of suspect terranes. Both models are described briefly below.

Within the Slave Province five separate supracrustal terranes - defined by large areas of turbiditic metasediments flanked by volcanic rocks of tholeiitic to calc-alkaline affinity - have been delineated by Padgham (1985) (Figure 1.1). According to the first model, these terranes represent remnants of volcanosedimentary basins which are believed to have formed by east-west extension of the basement, producing graben structures that were infilled by clastic material derived from the adjacent uplifted blocks (Henderson, 1981). In this model, volcanism is considered to have occurred as a result of extension along the steep faults bounding the basins.





In the second model, extensive areas of supracrustal rocks are thought to be essentially allochthonous with respect to the structurally-underlying Slave basement (Hoffman, 1986). Volcanic belts are considered to be Archean equivalents of accreted fore-arc complexes, and the extensive turbiditic sediments associated with the

Figure 1.1 Simplified geological map of the Slave Structural Province, outlining the five supracrustal basins defined by Padgham (1985). Inset figure shows the location of the Slave Province in northwestern Canada.

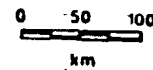


SLAVE STRUCTURAL PROVINCE

Legend

-  Slave Supracrustal Basins
-  Yellowknife Supracrustal Basin
-  Volcanic Belts
-  Granite; Granitic Gneiss

scale



greenstones are compared to modern distal pelagic sediments (Hoffman, 1986).

Proponents of both models acknowledge that widespread granitic plutonism largely postdated the deposition of the supracrustal units, and produced contact metamorphic aureoles in the surrounding country rocks. Most plutons have yielded radiometric dates between 2.5 and 2.6 Ga (Padgham, 1985). Complex folding and faulting accompanied the earlier stages of post-depositional plutonism, and resulted in the rotation of the supracrustal sequences into their present, sub-vertical orientations. The emplacement of the latest granitoid bodies did not produce significant structural overprinting of the country rocks (King *et al.*, 1988).

Detailed structural mapping is required to discriminate between these two opposing models.

The Yellowknife Greenstone Belt

The Yellowknife greenstone belt lies on the western margin of the southwestern-most supracrustal basin (Figure 1.1). It is exposed for over 40 km, extending northwards from the mouth of Yellowknife Bay in Great Slave Lake. The overall strike of the lithologies is NNE with tops

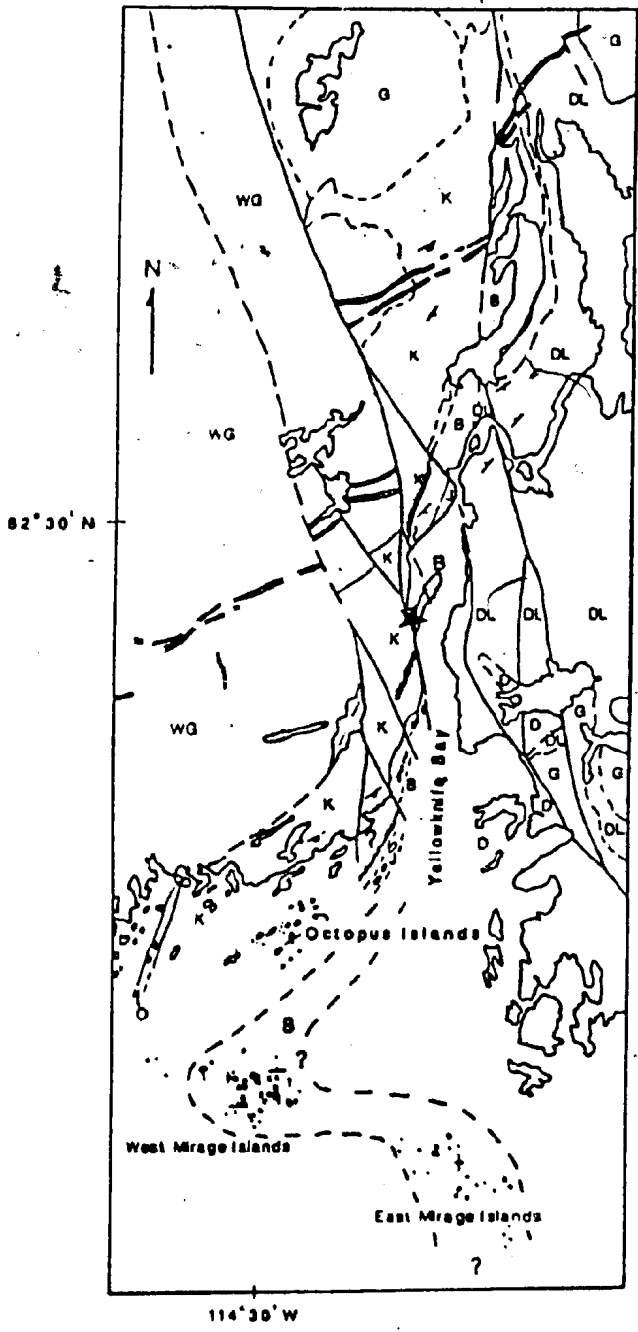
facing east, into the basin.

The stratigraphy has been defined by a number of workers, including Joliffe (1938, 1946), Henderson and Brown (1966), Henderson (1970, 1981), and most recently by Helmstaedt and Padgham (1986). The stratigraphy of Helmstaedt and Padgham (1986) is shown in Table 1.1 and Figure 1.2, and is discussed briefly below.

Stratigraphy

Helmstaedt and Padgham (1986) have subdivided the Yellowknife Supergroup at Yellowknife into three conformable groups, known as the Kam Group, composed mainly of tholeiitic basalts; the Banting Group, a calc-alkaline volcanic suite; and the Duncan Lake Group, made up of predominantly turbiditic metasediments (see Table 1.1). The Kam Group unconformably overlies the Octopus Formation, a poorly-exposed unit composed of metamorphosed volcanics and sediments which are interpreted to be part of an earlier volcanic cycle (Helmstaedt and Padgham, 1986). Banting Group metavolcanics and Duncan Lake metasediments interfinger and overlie the Kam Group (Padgham, 1985; Helmstaedt and Padgham, 1986).

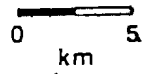
Figure 1.2 Geological map of Yellowknife Bay area, modified after Helmstaedt and Padgham (1986), showing the three main groups (the Kam, Banting and Duncan Lake Groups) of the Yellowknife Supergroup, the location of the Western Granodiorite (a phase of the Western Plutonic Complex), and the location of the major gold-bearing shear zones. The location of the Kam/Banting boundary in the area of the Octopus Islands (informally named) is presently under dispute. This map shows the interpreted boundary of Belletier (personal communication, 1986). That of Helmstaedt (personal communication, 1987) lies north of the Octopus Islands.



Geology of Yellowknife Bay Area

- Major Gold-bearing Shear Zones
- Bedding
- Pillows
- Late Faults
- Proterozoic Diabase Dykes
- Granitoids - undifferentiated
- Western Granodiorite
- Jackson Lake Formation
- Duncan Lake Group
- Duck Formation
- Banting Group
- Kam Group
- Octopus Formation
- City of Yellowknife

Archean



modified from Helmstaedt and Padgham, 1986

The basal Kam Formation is composed of sheeted gabbro dykes and pillow basalts. It is interpreted to represent an initial phase of rifting following extension of the basement (Helmstaedt and Padgham, 1986).

On the east side of Yellowknife Bay lies the Duck Formation, which is dominated by pillowed basaltic flows whose chemistry is transitional between tholeiitic and calc-alkaline trends (Cunningham (1984) in Helmstaedt and Padgham, 1986). The Duck formation may have originated from a different volcanic centre to the Kam and Banting volcanics, and has been included as part of the Duncan Lake Group by Helmstaedt and Padgham (1986).

The supracrustal rocks of the Yellowknife area are intruded by a number of granitic plutons, including a composite granodiorite batholith known as the Western Plutonic Complex which lies to the west of the greenstone belt. The Western Granodiorite (Figure 1.2) is one phase of the Western Plutonic Complex. The earliest phases of this complex may be synchronous with Banting Group volcanism (Easton, 1984).

Table 1.1 Simplified stratigraphy of the Yellowknife
Greenstone Belt, after Helmstaedt and Padgham, 1986.

Jackson Lake Formation
(conglomerate)

unconformity ~~~~~

Duncan Lake Group
(metaturbidites)

Banting Group
(calc-alkaline metavolcanics
and volcaniclastics)

initiation of
plutonism

Kam Group
(tholeiitic metavolcanics)

unconformity ~~~~~

Octopus Lake Formation
(metavolcanics and metasediments)

Unconformably overlying the Yellowknife stratigraphy is the Jackson Lake Formation, which is a conglomerate composed in part of granitoid clasts derived from the Western Plutonic Complex. The base of the Jackson Lake Formation cuts down through the Kam Formation, and its deposition is believed to have been confined to a narrow fault-bounded channel (Helmstaedt and Padgham, 1986).

Structure and Metamorphism

The supracrustal rocks at Yellowknife define a homocline striking NNE and generally dipping steeply to the east. The Duncan Lake Group metasediments are complexly folded and dip and young both east and west, although the overall direction of younging preserved in the more competent volcanic rocks is eastward, away from the Western Plutonic Complex. To date no evidence for large-scale thrusting has been found in the Yellowknife Greenstone Belt (Helmstaedt, personal communication, 1987).

Metamorphic grade in the Yellowknife Greenstone Belt is low to intermediate; mostly greenschist facies except adjacent to the Western Plutonic Complex, where amphibolite facies assemblages occur. Metamorphic index

minerals in mafic metavolcanics and intrusives include albite, actinolite, chlorite and locally hornblende, and in the metasediments include biotite, muscovite, and in places cordierite and andalusite,

A series of steep, anastomosing shear zones is developed in the Yellowknife greenstone belt (Figure 1.2). They strike both obliquely across and parallel to the bedding. These shear zones, which are spatially associated with the Western Plutonic Complex are considered by Helmstaedt and Padgham (1986) to have formed near the brittle/ductile transition zone between amphibolite and greenschist facies conditions. Helmstaedt and Padgham (1986), observed that the shear zones define steep conjugate pairs, and concluded that they formed following eastward rotation of the volcanic sequence. Furthermore, Drury (1977) suggested that the bedding-parallel shear zones probably formed during tilting of the volcanics, synchronous with granitoid intrusion.

The shear zones themselves vary in width from 10 to 150 m, and display greenschist facies assemblages as a result of retrograde metamorphism within them. The shear zones formed through simple shear, dominated by dip slip offset, with west side up movement (Henderson and Brown,

1966).

Three deformational episodes, each associated with a characteristic geochemical signature, have been identified in the shear zones by Kerrich and Allison (1978), and Allison and Kerrich (1981) (Figure 1.3). An early set of en-echelon sigmoidal quartz veins is interpreted to have developed coevally with the formation of the schistosity (Figure 1.3a). These are barren quartz veins that are believed to have formed by the migration of SiO_2 in solution from the surrounding schists (Allison and Kerrich, 1981). Fluid transport is considered to have occurred only on a local scale in this early phase.

The second deformational episode within the shear zones involved hydraulic fracturing parallel to schistosity (Figure 1.3b). Allison and Kerrich (1981) have shown that this could have been achieved under stress conditions identical to those interpreted for the first phase of deformation. Fracturing parallel to the schistosity produced dilatant zones in the shears into which large volumes of fluids flowed and reacted with the surrounding wallrock. Kerrich (1981) has suggested that these fluids were derived from the products of prograde metamorphism at depth. Igneous fluids circulating about the Western Plutonic Complex, which is believed to have

intruded coevally with shear zone formation (Drury, 1977; Helmstaedt and Padgham, 1986), may also have contributed to alteration in the shear zones.

Phase two quartz veins are gold-bearing, and are surrounded by alteration haloes distinguished by reduced Fe and extensive sericitization (Kerrich, 1981; Allison and Kerrich, 1981; Kerrich et al., 1977a). Typically, fluid:rock ratios of the order of 150:1 or more have been calculated for this phase of shear zone alteration (Kerrich et al., 1977a).

In the third deformational event, further displacement along the shear zones produced joints normal to the schistosity, which were infilled with gold-bearing quartz veins (Allison and Kerrich, 1981) (Figure 1.3c). Material in these veins is believed to have been remobilized from phase two quartz veins (Kerrich and Allison, 1978).

Near Yellowknife, the second and third generations of quartz veins in the Campbell and Giant Shear Zones are being mined, and to date they have produced over 330,000 kg of gold (Padgham, 1983).

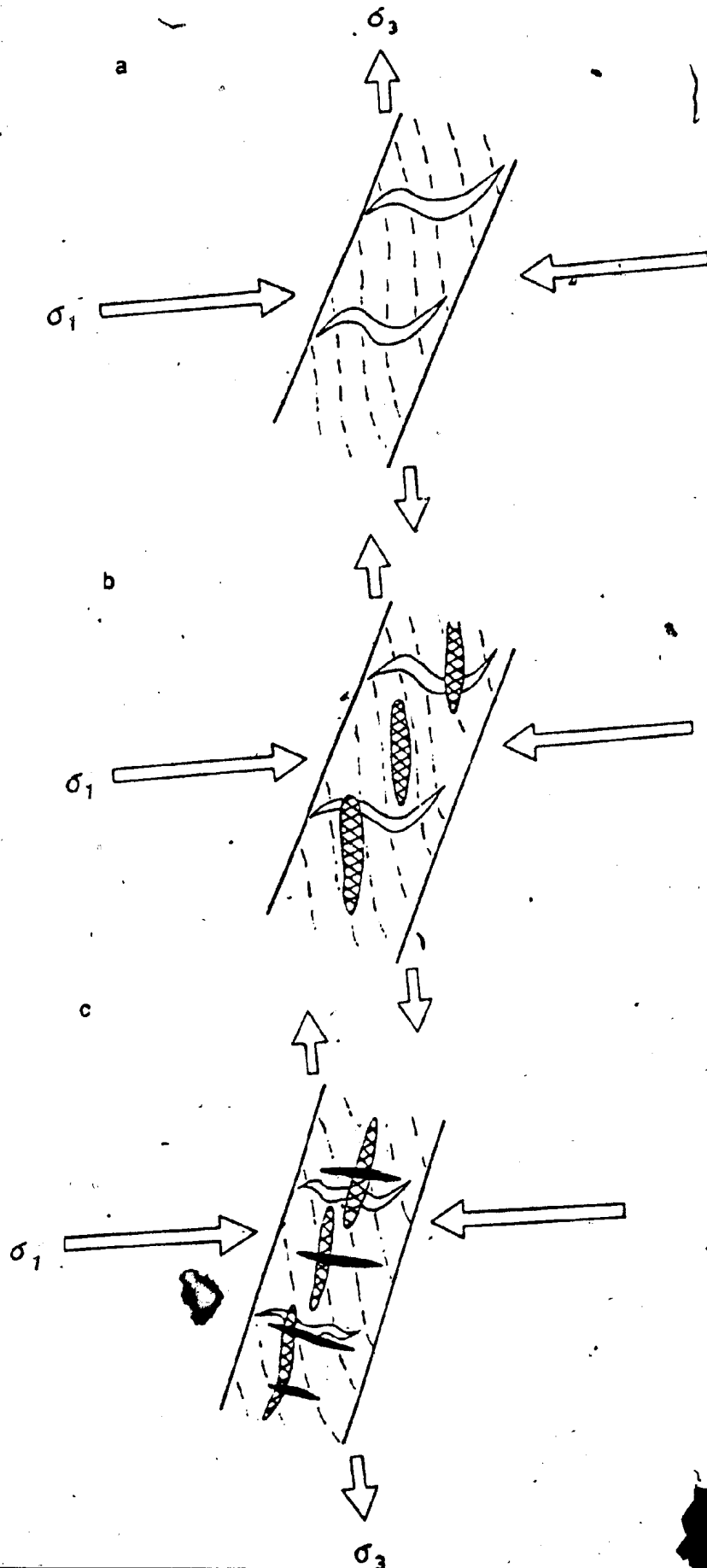
Late Proterozoic sinistral faulting has offset the

Figure 1.3 Schematic diagram showing sequence of quartz vein formation within major shear zones at Yellowknife, from Kerrich and Allison (1978), and Allison and Kerrich (1981).

a) initial en-echelon quartz vein formation, resulting from local migration of SiO_2 .

b) schistosity-parallel gold-bearing quartz veins, resulting from hydraulic fracturing.

c) gold-bearing quartz veins filling joints at high angles to schistosity, resulting from continued displacement along shear zone.



rocks and the gold-bearing shear zones in the Yellowknife area (Figure 1.2), so that the continuation of the Campbell Shear Zone lies somewhere under the waters of Yellowknife Bay. The Mirage Islands and informally named Octopus Islands (Figure 1.2) are the only outcrop in the region of the inferred extension of the shear zone, and so represent the simplest and cheapest means of sampling in the area. If minor shear zones on the islands show similar types of alteration to those of the large shear zones near Yellowknife, it may be inferred that both were formed during the same structural event and underwent the same physicochemical processes which produced the major concentrations of gold near Yellowknife.

Mirage Islands

The Mirage Islands comprise the southern-most exposures of the Yellowknife Greenstone Belt. The bedrocks consist of a suite of calc-alkaline rocks correlative with the Banting Group.

Lithologies on the West Mirage Islands strike east-west, and dips are steep. Beds generally young to the north, with a few local reversals. Strikes on the East Mirage Islands are variable, with a dominant trend nearly north-south. Because the East Mirage Islands are

smaller and more widely spaced than the West Mirage Islands, most units could not be interpolated between islands, or between the two groups of islands.






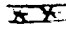
Mirage Island Map Units

The stratigraphy of the Mirage Islands is shown in Figure 1.4. Units are labelled numerically according to their relative positions and to cross-cutting relationships. There are some gaps in the stratigraphy due to lack of exposure between the islands. No attempt has been made to correlate with Banting Group stratigraphy because the closest exposure of Banting rocks lies 22 km to the north, and distinctive marker units do not occur.

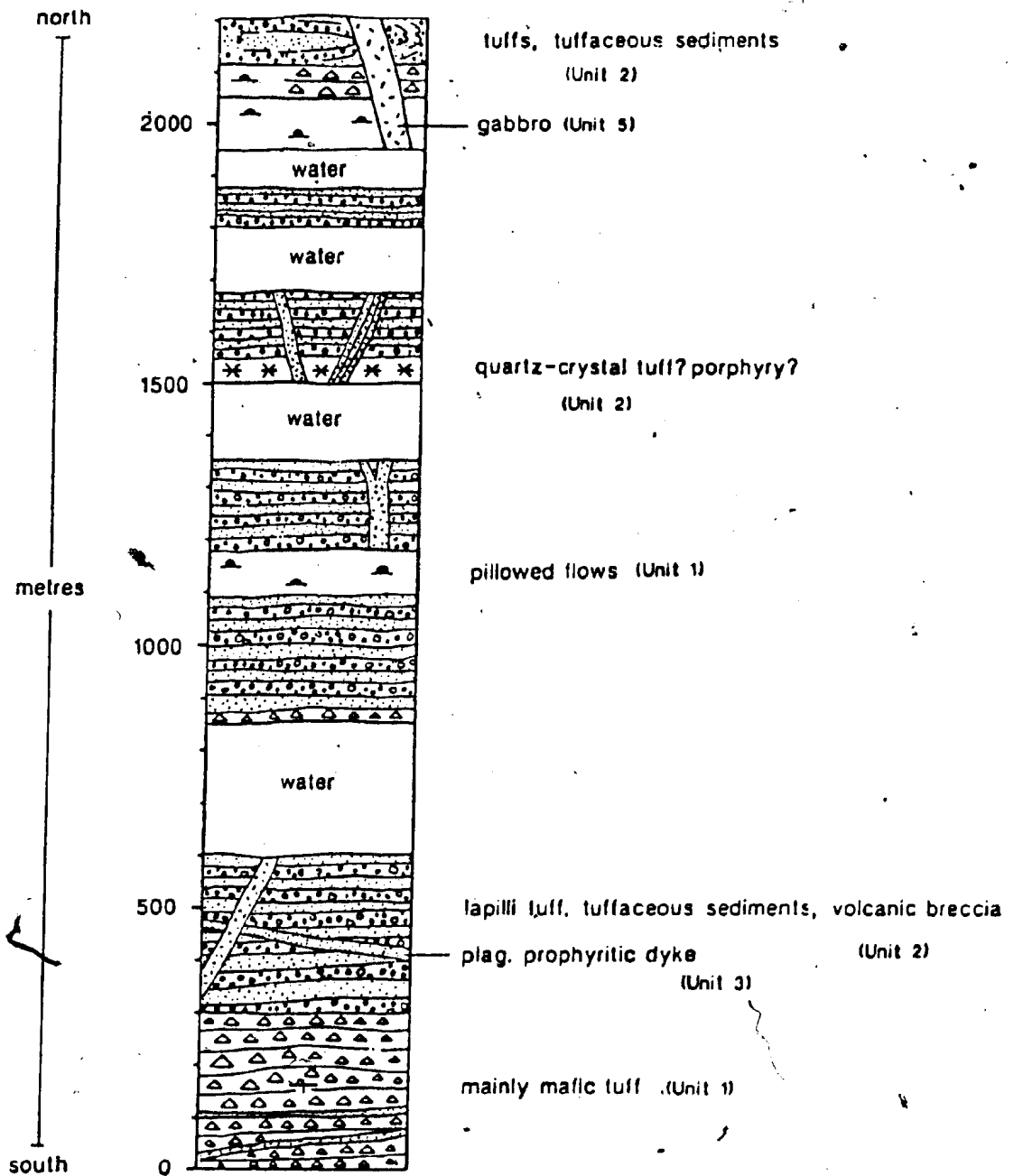
The rocks exposed on the West Mirage Islands have been informally named the Mirage Formation by the author (Relf, 1986a), and are considered to be part of the Banting Group. Two maps showing the geology of the islands and sample locations are presented in the back pocket of the thesis, and detailed geology maps are available as open file maps from the Department of Indian and Northern Affairs, Canada, in Yellowknife (Relf, 1986b).

Figure 1.4 Stratigraphy of the West Mirage Islands. The exposed base is dominated by mafic tuffs and volcanoclastic rocks, overlain by more than 1500 metres (possibly thickened by folding) of felsic to intermediate tuffs, tuffaceous sediments, and fragmental volcanoclastic rocks, interlayered with minor basalt flows, and intruded by gabbro dykes. This sequence is topped by thinly-bedded, isoclinally-folded tuffs and tuffaceous sediments.

Legend:

-  - dominantly mafic tuffs
-  - mixed felsic and intermediate volcanoclastic rocks, tuffs, tuffaceous sediments
-  - pillowed basalts (tops N)
-  - gabbro
-  - plagioclase porphyry
-  - quartz crystal tuff (porphyry?)

Stratigraphy of West Mirage Islands



Unit 1

Mafic volcanic rocks of basaltic to andesitic composition comprise Unit 1. The southern-most West Mirage Islands, at the base of the exposed section, are almost entirely composed of well-bedded mafic tuffs. In three localities, tops were found to face north. Beds dip steeply north and south, with bedding overturned in places.

In the top half of the stratigraphic section, pillowed and massive flows are intercalated with felsic to intermediate volcanoclastic rocks (Unit 2). Where the pillows are not too deformed, the flows can be seen to young towards the north. Recrystallized quartz amygdules are common in both the massive and the pillowed flows, and locally mafic amygdules of actinolite +/- chlorite +/-biotite are present.

A number of pillowed flows are overlain by pillow breccia. These breccias consist of broken fragments of pillow selvages supported in an aphanitic, mafic groundmass. Generally the pillow breccias are less than a metre or so in thickness.

Unit 2

Unit 2, which consists of intermediate to felsic volcanoclastic rocks, encompasses a wide variety of lithologies and can be subdivided into a number of sub-units. Well-bedded tuffs and tuffaceous sediments comprise a large part of Unit 2. The tuffs are composed of very fine grained material of intermediate to felsic composition, and locally such sedimentary features as normal graded bedding, flame structures, cross-stratification, and in one place, slump structures can be seen (Figure 1.5). Where such sedimentary features are displayed, the rocks are interpreted to be reworked aquagene tuffaceous sediments.

Tops are preserved in places in the tuffaceous sediments, and are found to face both north and south, indicating the presence of tight to isoclinal folds. Bedding is steep and locally overturned.

Fragmental volcanoclastic rocks make up a significant part of Unit 2 (see Figure 1.6). Their compositions vary from felsic to intermediate, and the fragments range in

Figure 1.5 Soft sediment features in tuffaceous sediments.

- a) Flame structures in tuffaceous sediments, West Mirage Islands. Pencil is approximately 15 cm long.
- b) Slump structures in tuffaceous sediments, West Mirage Islands. Lens cap is 5 cm in diameter.



Figure 1.6 Fragmental volcanoclastic unit.

a) Intermediate lapilli tuff, fragments showing flattening parallel to bedding. Pencil is approximately 15 cm long.

b) Intermediate volcanogenic unit containing block-size fragments. Pencil (approximately 15 cm long) is parallel to bedding.



size from lapilli to blocks up to 30 cm or more in diameter. Lapilli tuffs are most common.

In general, the fragments are more felsic than the surrounding matrix, and appear as buff-coloured clasts which weather higher than the groundmass.

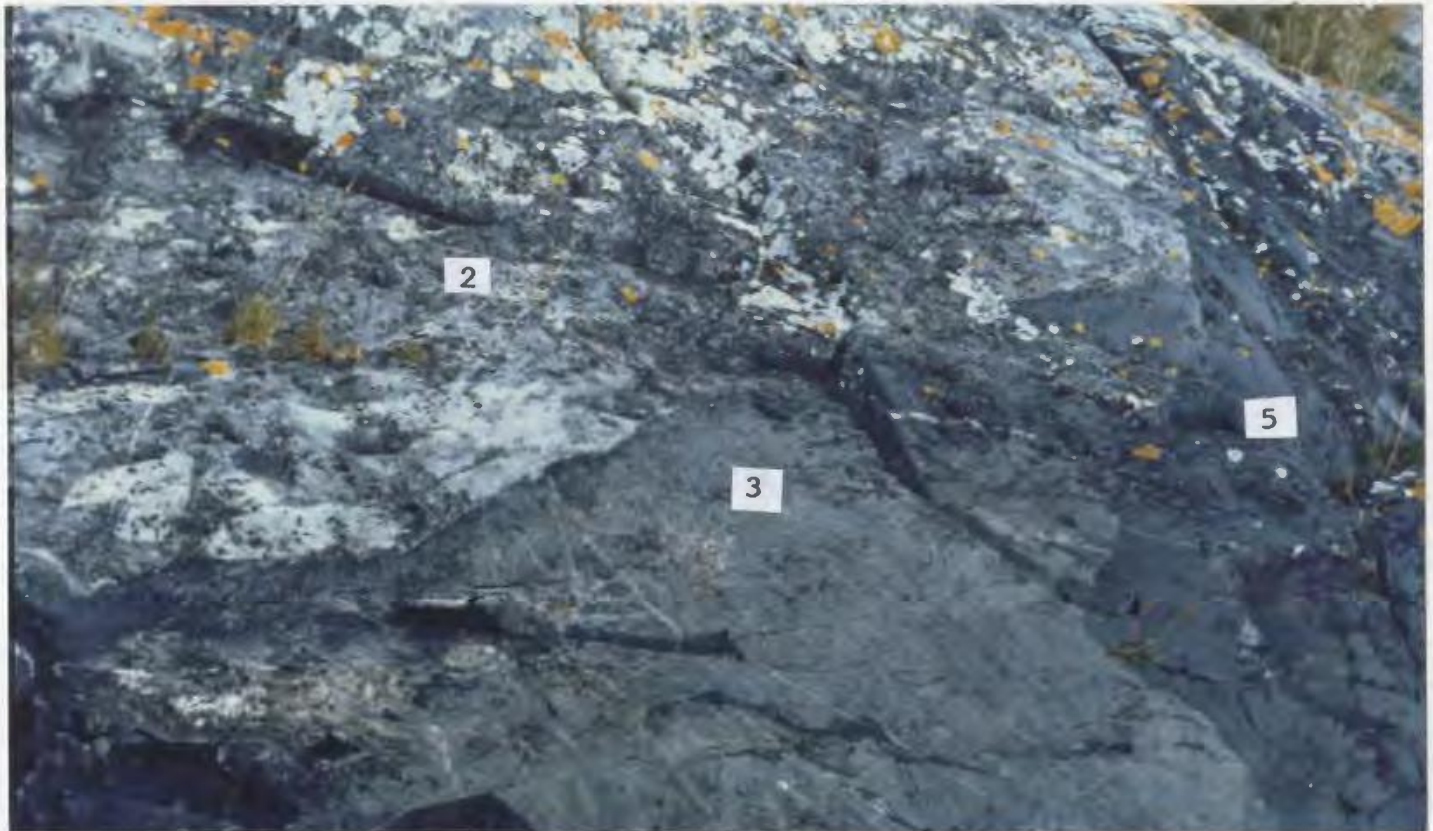
The appearance of the fragmental volcanoclastic rocks varies considerably. Some are well-bedded, matrix-supported units, with bedding thicknesses of 2 to 20 cm. Others contain irregularly-shaped lapilli (and locally blocks) in massive layers 1 to 5 m thick with weakly defined internal layering. These may be matrix- or clast-supported.

A unit containing angular to sub-rounded, poorly-sorted, heterogeneous volcanic clasts supported in an ash matrix is present in a few localities (Figure 1.7). This unit shows little or no internal sorting, typically is less than 2 metres thick, and rarely extends for more than 15 - 20 m. In the field it was called a volcanic breccia, although its origin is uncertain. It may either be the result of explosive volcanism, or it may be a laharcic breccia.

Other lithologies in Unit 2 include a quartz crystal

Figure 1.7 Heterogeneous, poly lithic volcanic breccia
(Unit 2). Diameter of lens cap is 5 cm.

Figure 1.8 Plagioclase porphyritic dyke (3) intruding an
intermediate volcanoclastic rock (2), and cut by a later
gabbro (5). Width of photo covers approximately 5 m.



tuff (flow?), and a few thin (5 - 10 cm) cherty horizons which may be either sedimentary cherts or silicified sediments or tuffs.

Unit 3

Unit 3 consists of a felsic, aphanitic, plagioclase-porphyry which both cross-cuts and in places is conformable with the bedding. Where conformable it is uncertain whether this unit is intrusive or extrusive.

This unit is cross cut by gabbro, but locally intrudes the volcanics (Figure 1.8), and so is interpreted to be late syn-volcanic in age.

Unit 4

Unit 4 is composed of a series of aphanitic felsic dykes less than 1 m in width which cut the volcanics at low angles. These dykes weather buff to pink, and are commonly flow-banded parallel to their margins.

Unit 5

Unit 5 consists of dykes and sills of gabbroic to dioritic composition. Gabbro is a field term commonly

applied in the Slave Province to mafic intrusive rocks that are spatially associated with volcanic packages (e.g. Bostock, 1980, Helmstaedt and Padgham, 1986, Helmstaedt et al., 1986). It is used here to describe unit 5, even where albite is the dominant plagioclase composition, and igneous plagioclase is not recognized.

At least four generations of gabbroic intrusions have been identified in the area, and cross-cutting relationships indicate that dykes striking between north and northeast are the youngest. Plagioclase-porphyrific gabbros are fairly common, and locally contain zoned plagioclase phenocrysts as large as 10X10 cm on the outcrop surface (Figure 1.9).

Near the bottom of the volcanic pile, gabbro is intruded in places by felsic dykes of Unit 4. Higher up in the section, Unit 4 is consistently cut by the gabbro. Assuming that all of the felsic dykes are coeval (in contrast to the gabbros which intrude one another, the felsic dykes show no crosscutting relationships with other felsic dykes), then the gabbro dykes near the base of the pile represent an early phase of mafic intrusion, and may be feeders to the mafic flows higher up.

Figure 1.9 Gabbro dyke bearing zoned plagioclase megacrysts in places up to 10 cm across. Diameter of lens cap is 5 cm.



Unit 6

Unit 6 is a foliated intrusive unit varying in composition from a tonalite to a gabbro. The end member compositions are distinguished by the greater modal abundance of quartz (>20%) and fewer mafic minerals (about 10 to 20% in the former), and a lower quartz content (<5%) and greater mafic content (>35%) in the latter. The western-most West Mirage Islands are intruded by unit 6. Contacts between the gabbro and tonalite are locally gradational and poorly-defined. Elsewhere, younger gabbros clearly intrude the tonalite-gabbro.

Unit 7

Unit 7 is a foliated leucocratic granite to granodiorite, and is exposed as roughly north-south striking veins up to one metre in width on the western-most West Mirage Islands. These veins crosscut the supracrustal rocks on the islands, but locally are intruded by the youngest northeast-striking gabbro dykes.

The extrapolated extension of the Western Plutonic Complex in Great Slave Lake lies about 5 km west of the West Mirage Islands. Where the complex is exposed

farther north, granitoid veins extend between 200 m and 1 km into the adjacent volcanic rocks (Henderson and Brown, 1966). This implies that: 1) the contact of the Western Plutonic Complex does not continue SSW, but swings eastward towards the West Mirage Islands; or 2) there is another plutonic body nearby which is located near the western-most West Mirage Islands.

Unit 8

Undeformed diabase dykes comprise Unit 8. In the Mirage Islands, these dykes are typically less than 1 metre in width, and strike between north and northwest. They weather a distinct rusty brown colour, typical of Proterozoic diabase dykes exposed elsewhere in the Slave Province.

Structures in the Mirage Islands

In the West Mirage Islands, the lithologies strike east-west, with tops facing north, implying the presence of a large fold in Yellowknife Bay (Figure 1.2). Lacustrine seismic studies (G. Goldak, personal communication, 1987) have outlined a sharp bend in the structural trend which accords with this inferred fold.

Neither axial planar cleavage nor minor asymmetric folds, spatially associated with the axial trace of the fold were found in the area, although on the western-most islands a strongly developed, east-west trending, steep foliation is present. This fabric implies a north-south directed subhorizontal stress field, and may have resulted from the intrusion of a plutonic body to the south of the islands. The presence of such a body could explain the sharp, pinched shape of the fold in the volcanic belt, and also the presence of abundant granitoid veins on the western most islands. Because these granitoid veins are locally cut by gabbro, it is believed that this inferred pluton is temporally related to the Western Plutonic Complex, which is late syn- to post- Banting Group in age (Easton, 1984).

Tight to isoclinal folds were observed in tuffaceous metasediments of Unit 2, with half wavelengths of about 1 metre. These folds are correlated with the F1 folds farther north in the volcanic belt. An associated S1 foliation in the volcanic rocks is weakly developed to absent.

Exposure in the East Mirage Islands is sparse, with an average strike of bedding approximately north-south (Figure 1.2). A weak foliation is present and is subparallel to bedding.

Shear Zones

The shear zones in the Mirage Islands are similar to those at Yellowknife in that they strike nearly parallel to bedding and dip steeply to vertically (Figures 1.10 and 1.11). The mean strike of the shear zones is 098° (Figures 1.12, 1.13). Locally shear zones cross-cut and offset one another, although apparently no one orientation of shear zone is consistently younger than the others. This suggests that they formed more or less synchronously.

Because most outcrop surfaces on the islands are near-horizontal and the shear zones dip subvertically, kinematic indicators for dip slip movement were rarely observed. Locally, moderately plunging mineral lineations (mainly of chlorite) are exposed on the schistosity planes within shear zone boundaries. Elsewhere, offsets of units across the shear zones were employed to determine the magnitude and direction of displacement in the horizontal plane, although the amount of dip slip offset could not generally be determined.

Most shear zones on the Mirage Islands are between 1 and 5 m wide and are characterized by retrograde

assemblages with respect to the surrounding rocks. They commonly contain anastomosing quartz veins which are subparallel to the schistosity, and less commonly contain carbonate veins which transect the schistosity at low to moderate angles. Locally less deformed augen are preserved within the shear zone boundaries, and are characterized by assemblages which are less hydrated than the surrounding schistose rocks.

Shear zones cutting gabbro are more abundant than shear zones in the volcanic rocks, perhaps indicating that the supracrustal rocks deformed in a ductile manner by folding, whereas the more competent gabbros deformed by faulting and shearing.

A shear zone cutting a felsic lapilli metatuff (Unit 2) on one island displays a protomylonitic texture. Offset in the plane of the outcrop is approximately 30 cm in a dextral sense. Elsewhere, shear zones cutting the felsic volcanic rocks are marked by steeply-dipping schistose zones, similar in appearance to shear zones in gabbro.

Near Yellowknife, the shear zones strike parallel to the contact of the Western Plutonic Complex, whose intrusion is believed to have initiated the deformation

Figure 1.10 Anastomosing shear zone 1 metre in width hosted in gabbro. Note the less deformed augen preserved in the shear zone. Scale is 9 cm long.



Figure 1.11 5 m wide shear zone in mafic flow, with
• discontinuous anastomosing quartz veins which are
subparallel to schistosity. Hammer handle is
approximately 1 m long.



Figure 1.12 Rose diagram showing the range of shear zone orientations in the West Mirage Islands. Dip of the shear zones is essentially vertical. n = 34.

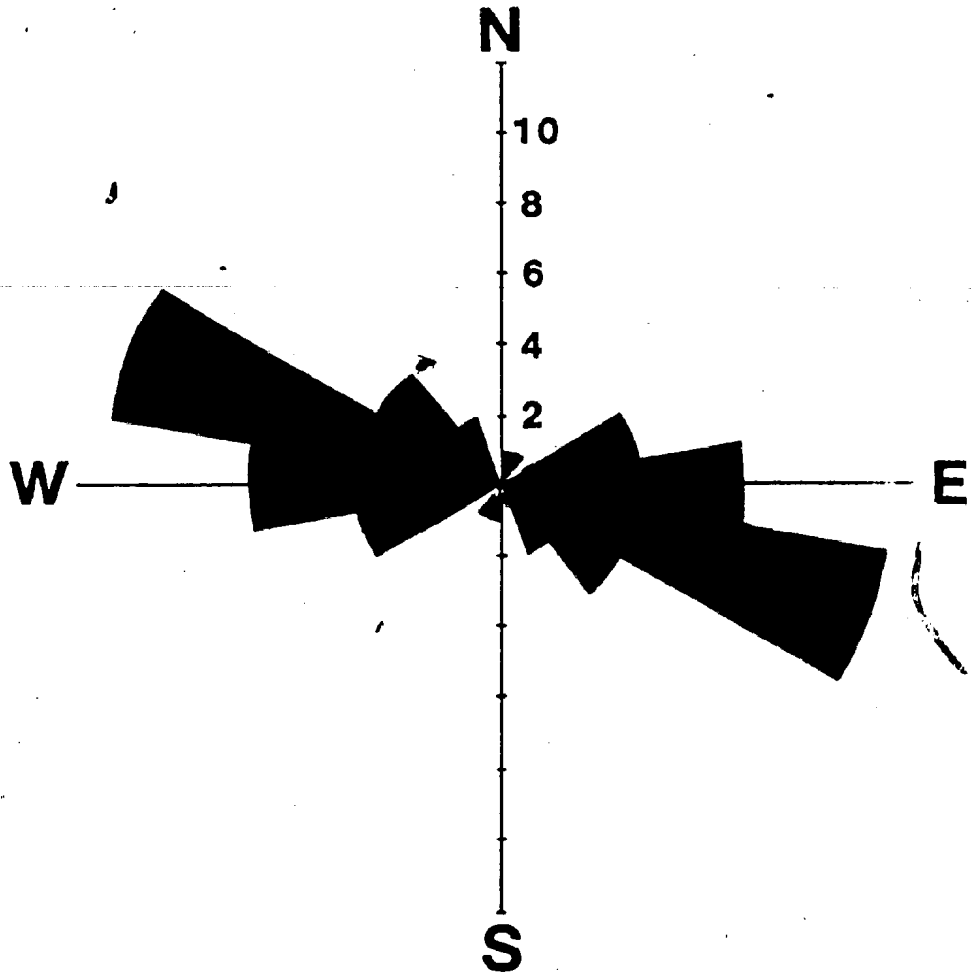
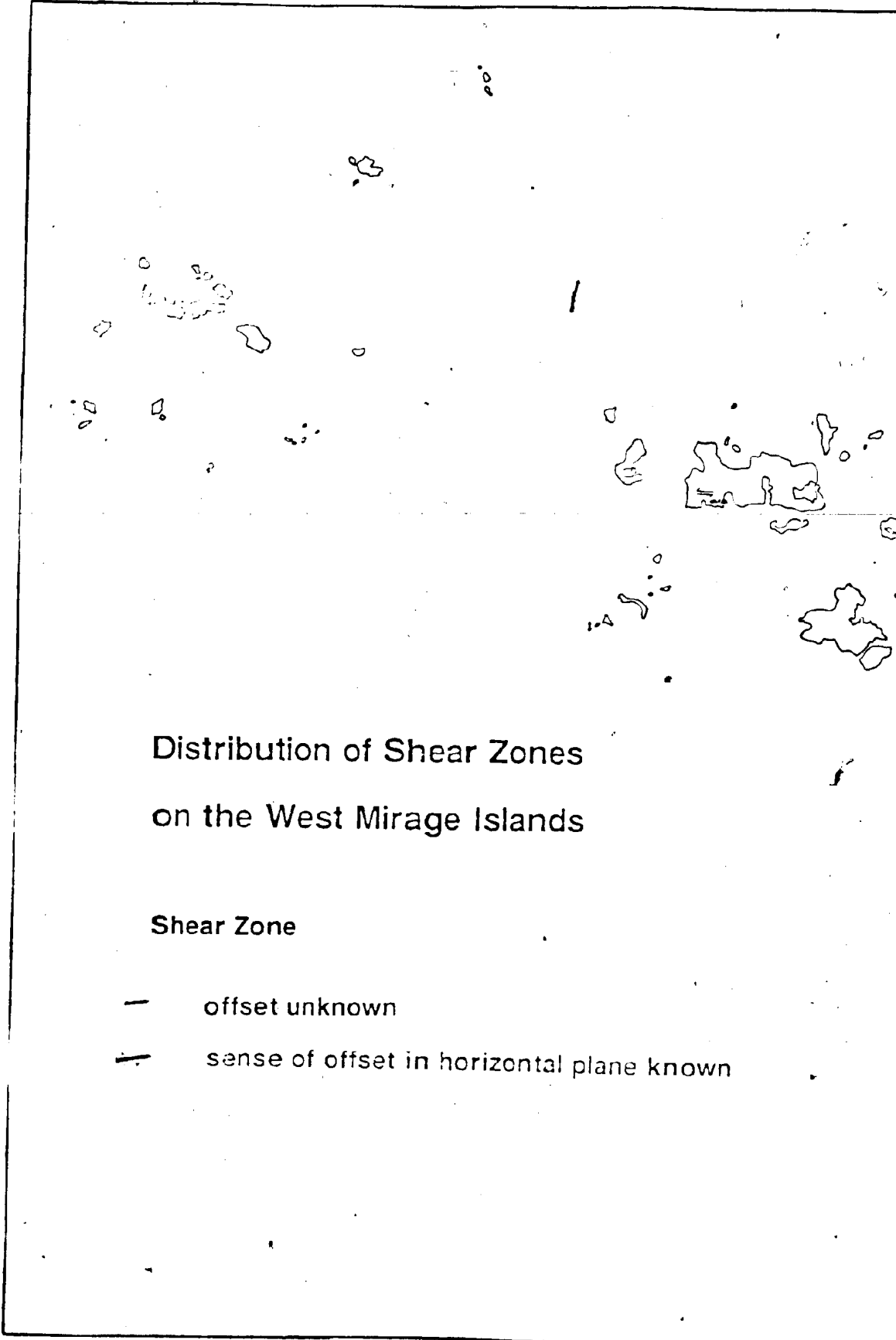


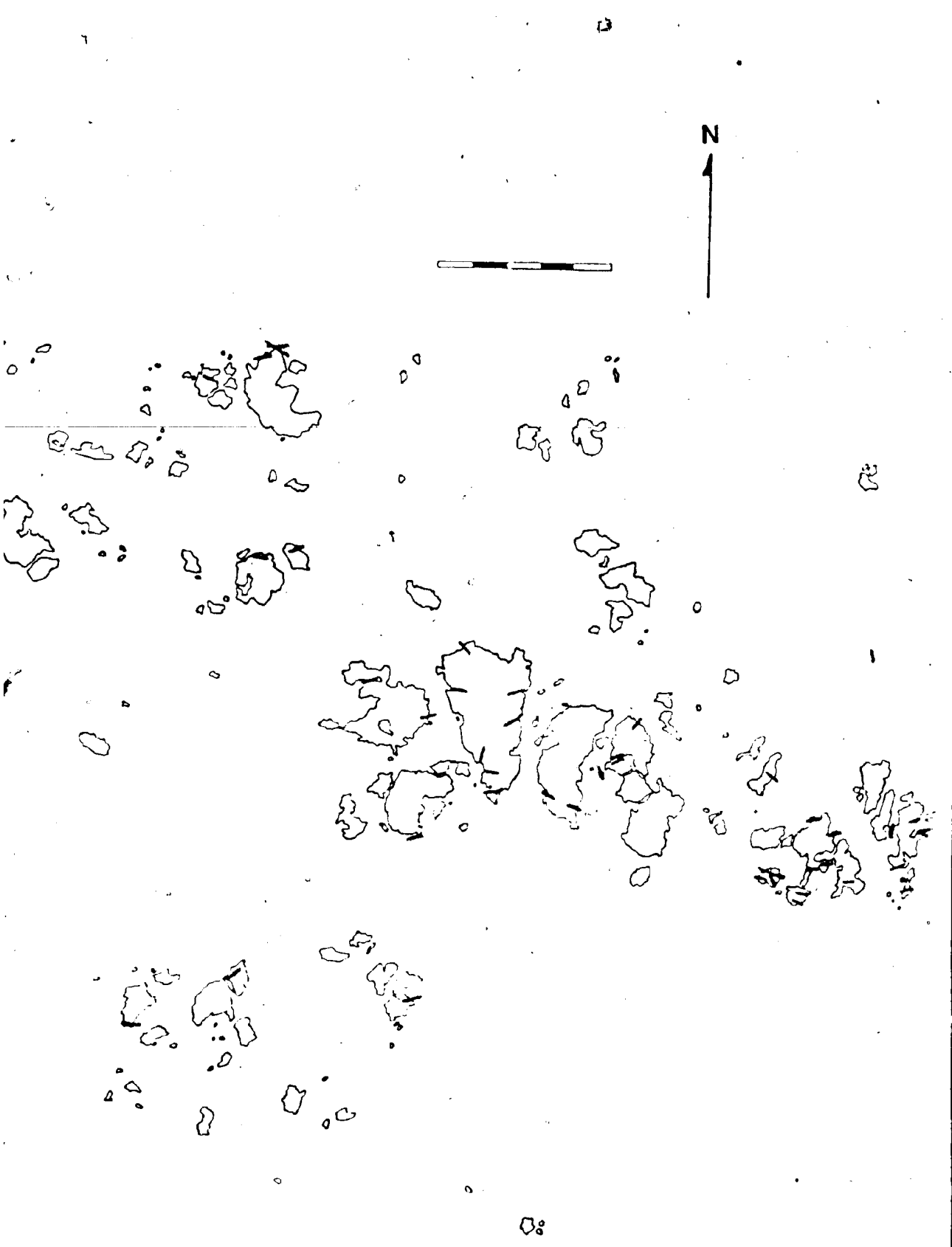
Figure 1.13 Map showing distribution of shear zones on the West Mirage Islands. Bar scale is 500 m.



Distribution of Shear Zones
on the West Mirage Islands

Shear Zone

- offset unknown
- sense of offset in horizontal plane known



that produced the shear zones (Helmstaedt and Padgham, 1986; Drury, 1977). In the West Mirage Islands, the shear zones have a mean strike near east-west, and a pluton is inferred to lie south of the islands. It is possible therefore, that a similar shearing mechanism was operative in the Mirage Islands.

CHAPTER 2: METAMORPHISM

Introduction

The Yellowknife Greenstone Belt has undergone regional greenschist facies metamorphism, accompanied by amphibolite facies contact metamorphism adjacent to large plutonic bodies (Henderson and Brown, 1966). Rocks on the Mirage Islands similarly record evidence of two metamorphic events; an amphibolite facies contact thermal event, and a regional greenschist facies event. Mineral textures indicate that the greenschist facies assemblages equilibrated after amphibolite facies assemblages on the Mirage Islands, although the onset of greenschist facies metamorphism may have been synchronous with, or even predated the amphibolite facies metamorphic event.

Samples from each of the seven Archean units were examined in thin section. Although primary structures such as bedding and igneous textures are preserved, the mineral assemblages, especially in the mafic rocks, are essentially metamorphic. Glassy fragments in the felsic volcaniclastic rocks are devitrified, and aphanitic-textured volcanic rocks contain fine grained metamorphic assemblages. In many cases, microprobe analysis of minerals in the fine grained rocks is

difficult, and thus the majority of analyses are from the coarser-grained gabbros.

Petrography

Mineral assemblages from the map units in the Mirage Islands are given in Table 2.1.

The mafic tuffs are composed of very fine grained plagioclase (partly replaced by epidote and calcite), mats of intergrown actinolitic hornblende and actinolite, chlorite, biotite, and minor disseminated pyrite (Figure 2.1). This assemblage indicates a metamorphic grade between upper greenschist and lower amphibolite facies conditions.

The mineral assemblage of the basalts is indicative of greenschist facies conditions. Earlier plagioclase is replaced by oligoclase + albite + epidote +/- white mica. Mafic minerals comprise about 50% of the rock, and are predominantly actinolite, chlorite and minor biotite. In the field, some brown-weathered orthopyroxene was found in one locality, and is interpreted to be igneous in origin. Minor calcite is present, and trace amounts (<1%) of pyrite are disseminated through the rocks.

Table 2.1 Comparison of the mineral assemblage(s) in each
rock type found on the Mirage Islands.

Unit #	Rock Type	Mineral Assemblage
1	meta-basalt	albite to oligoclase + actinolite (+/- actinolitic hornblende) + chlorite + epidote + quartz + calcite +/- sericite, biotite, pyrite, sphene
1	meta-mafic tuff	albite to oligoclase + actinolite to hornblende + chlorite + biotite + epidote +/- calcite, quartz, pyrite, sphene
2	felsic to intermediate meta-volcaniclastics	quartz + plagioclase + K-feldspar + biotite + muscovite +/- chlorite, actinolite, sphene
3	plagioclase porphyry	oligoclase phenocrysts, groundmass - quartz + feldspar* + biotite + chlorite +/- pyrite
4	felsic dykes	aphanitic to very fine grained quartz + feldspar* + minor muscovite, biotite
5	metagabbro	greenschist facies: albite + actinolite + chlorite + epidote + quartz + calcite +/- sericite, biotite, pyrite amphibolite facies: labradorite + hornblende to actinolitic hornblende + epidote + quartz +/- calcite, actinolite, chlorite, clinopyroxene, pyrite, sphene
6	tonalite to gabbro	albite to oligoclase + quartz + hornblende + actinolite + biotite +/- chlorite, sphene albite to oligoclase + hornblende + actinolite + quartz +/- chlorite, sphene, epidote
7	granite to granodiorite	albite to oligoclase + quartz + K-feldspar + biotite +/- chlorite, sphene

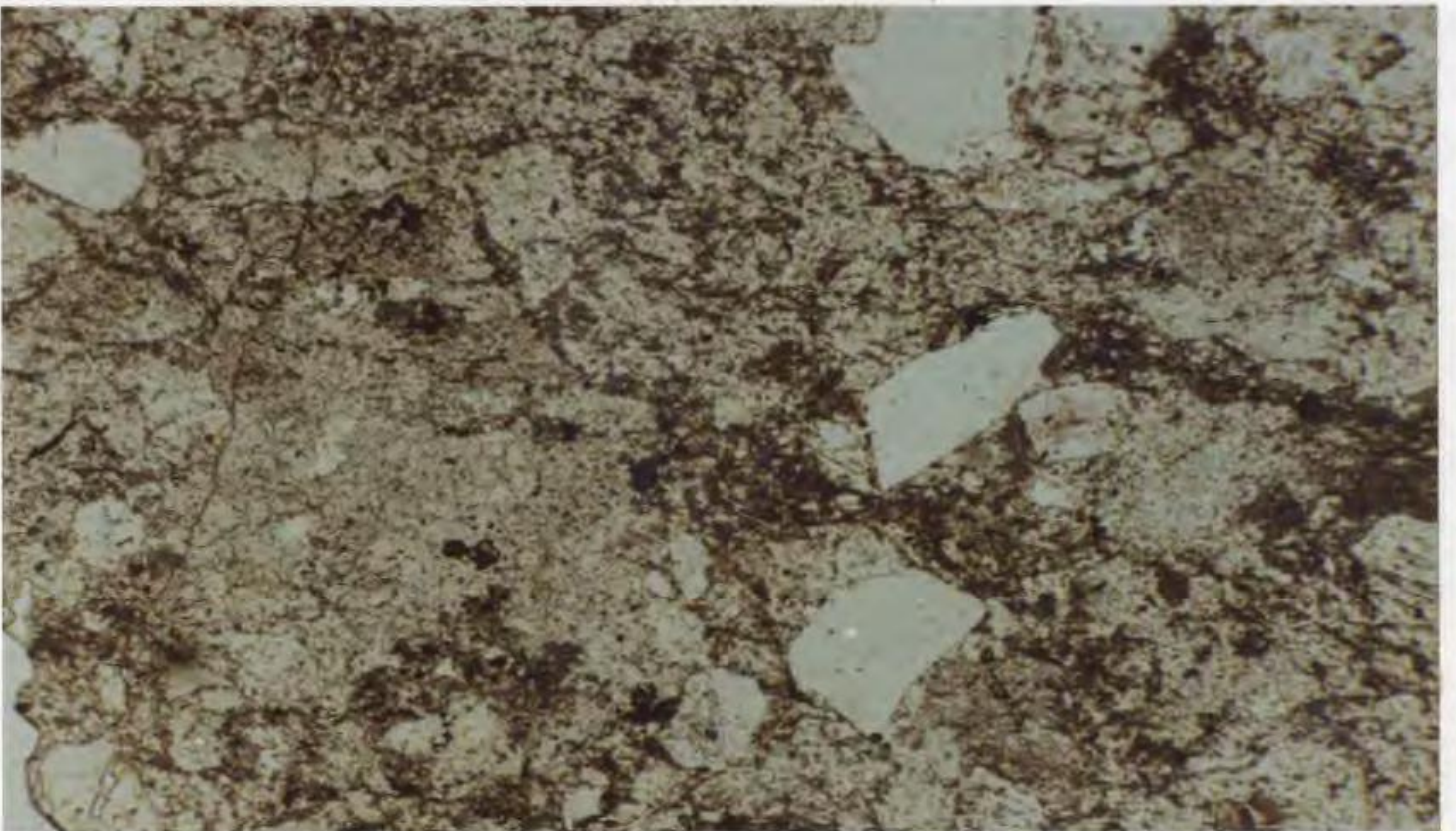
* groundmass too fine grained to distinguish plagioclase and K-feldspar optically.

The mineral assemblages of the felsic to intermediate volcanoclastic rocks are difficult to distinguish in most samples, due to their very fine grain size. However, a few of the samples are sufficiently coarse-grained that individual minerals can be recognized in thin section. Quartz, plagioclase and K-feldspar together comprise in general about 60 - 80% of these rocks, the rest being very fine grained biotite +/- chlorite +/- muscovite (Figure 2.2), which commonly define a compositional layering interpreted to be bedding. This assemblage is indicative of greenschist facies metamorphism. In mica-poor rocks, this layering may be defined by different grain sizes of the felsic minerals, and diagnostic assemblages of metamorphic facies are not present.

The felsic plagioclase porphyry unit (unit 3), contains randomly-oriented oligoclase phenocrysts 1 - 1.5 mm in length which are partly altered to sericite and epidote. The groundmass is composed of about 85% quartz and feldspar (the feldspar is too fine grained to distinguish plagioclase from K-feldspar in thin section), and 15% intergrown biotite + chlorite. The micas define a moderate foliation visible in thin section, and are concentrated in the pressure shadows of the phenocrysts. Fine grained pyrite is spatially associated with the

Figure 2.1 Fine grained mafic tuff (top) interlayered with intermediate tuff (bottom). Mineral assemblage is albite, chlorite, epidote, biotite, and minor actinolite, calcite and quartz. Plane polarized light. Bar scale is 1 mm long.

Figure 2.2 Intermediate fragmental volcanoclastic rock. Clasts are made up of quartz (80%) and recrystallized lithic fragments (20%). Matrix consists of very fine grained quartz + plagioclase + K-feldspar + muscovite + minor biotite + chlorite. Plane polarized light. Bar scale is 1 mm long.



biotite. The coexistence of chlorite and biotite implies a metamorphic grade between mid greenschist and lower amphibolite facies.

The gabbro dykes are hydrated to varying degrees, and mineral assemblages record metamorphic conditions ranging from greenschist to amphibolite facies. A typical greenschist facies assemblage in gabbro consists of albite, actinolite, chlorite, epidote, sericite, minor quartz, calcite, +/- trace amounts of biotite, sphene, and pyrite. Amphibolite facies gabbros contain labradorite, hornblende, sericite, minor actinolite, chlorite, calcite, epidote and quartz, +/- traces of sphene and pyrite. This is not an equilibrium assemblage, and an examination of the minerals reveals that chlorite, calcite and actinolite are replacing hornblende and epidote.

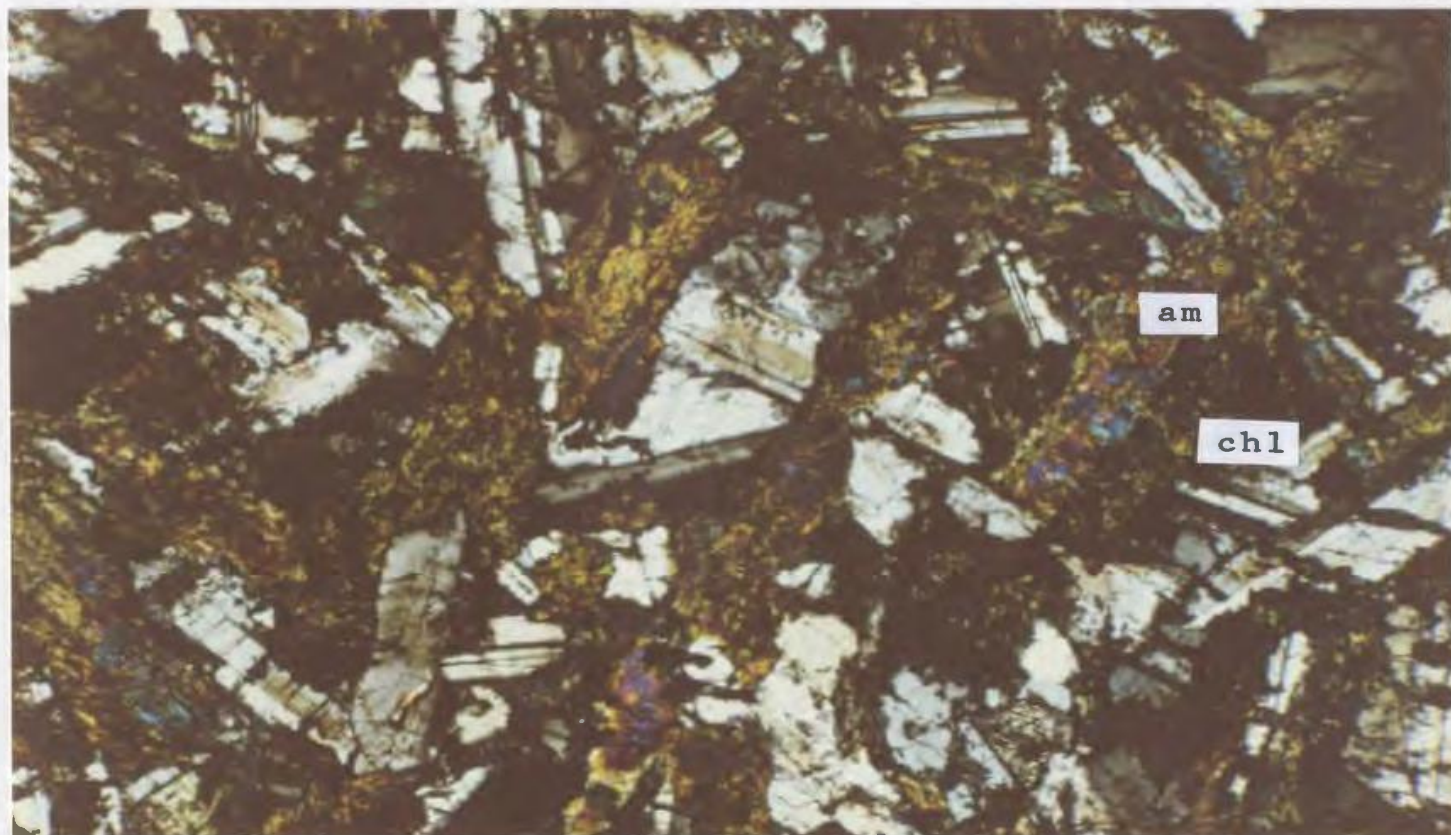
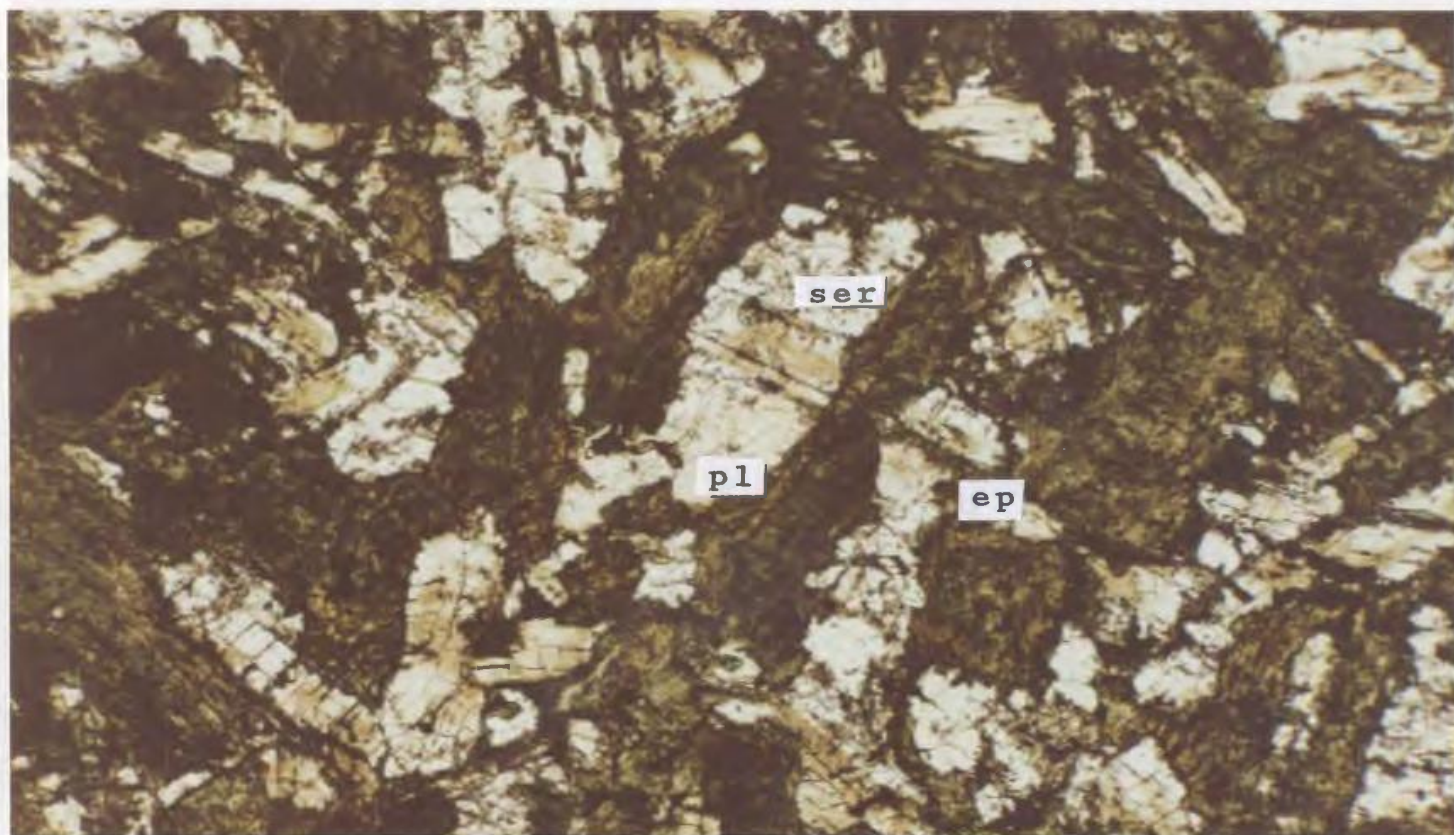
Most of the Mirage Island gabbros contain one of these two assemblages, although a mineralogical continuum exists between the two end members. Petrographic textures show that the greenschist facies minerals are replacing the amphibolite facies assemblage (Figure 2.3), implying an early medium to high grade metamorphic event, followed by a retrograde event in which complete equilibrium was not achieved in all samples. Perhaps the coarse grain size of

Figure 2.3 Metagabbro showing partial alteration of amphibole (am) to chlorite (chl) and plagioclase (pl) to sericite (ser) and epidote (ep).

a) Plain polarized light

b) Crossed polars

Bar scale is 1 mm long.



the gabbro relative to the basalt, and its lack of structural anisotropy (such as bedding or cleavage) along which hydrating fluids could penetrate has ensured the preservation of the amphibolite facies assemblage locally.

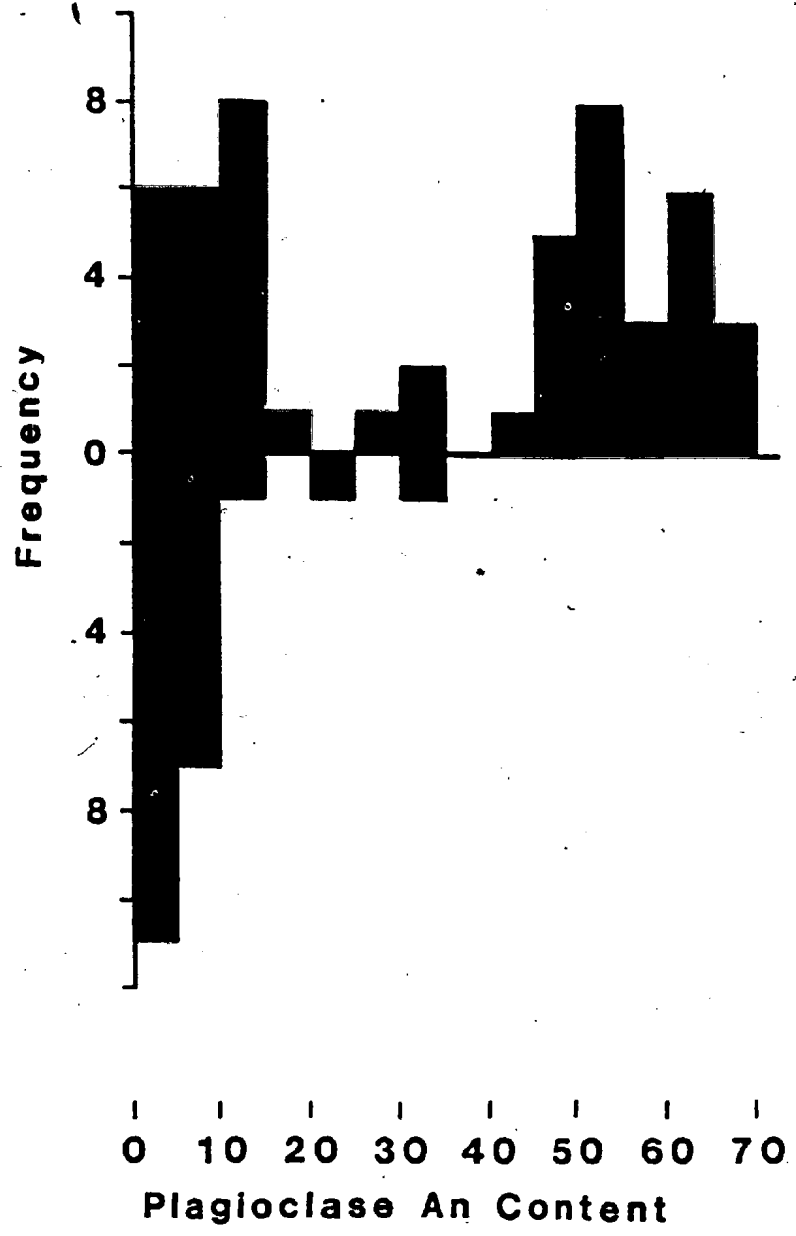
The tonalites are distinguished from the gabbros by the smaller proportion of mafic minerals (20-30%), and by the presence of more than 20% quartz. Plagioclase composition ranges from An₀ to An₁₀. Hornblende, actinolite and biotite, (the latter locally replaced in part by chlorite) make up the mafic component of the rock. The two amphiboles appear to be in equilibrium, indicating lower amphibolite facies metamorphic conditions.

Mineral Chemistry

Plagioclase

Although the quality of some of the microprobe data is suspect (see discussion in Appendix A), it is sufficient to show that the plagioclase has a bimodal distribution of anorthite content, with one mean near the albite-oligoclase boundary, and another in the labradorite range (Figure 2.4).

Figure 2.4 Histogram of plagioclase compositions determined by microprobe analyses from unsheared metabasic rocks (top half) and sheared metabasic rocks (bottom half) from the Mirage Islands. Unsheared plagioclase grains have a bimodal distribution of An content, and petrographic textures indicate that assemblages bearing the more calcic plagioclase are being replaced by assemblages bearing more sodic plagioclase. Plagioclases from sheared samples are sodium-rich.



The basic volcanic and volcanoclastic units are characterized by abundant micas (especially chlorite), a paucity of amphiboles, and plagioclase compositions near albite, although plagioclase phenocrysts not uncommonly preserve compositions of An₂₀₋₂₅. The plagioclase composition then, is compatible with the greenschist facies mafic minerals present.

The gabbros, which have been subjected to the same greenschist facies metamorphic event, have locally preserved more calcic plagioclase (as high as An₆₇ in one sample); less modal chlorite and concomitantly more amphibole; and in one thin section, some relict clinopyroxene. These features attest to the lower permeability of these rocks, and thus to less extensive reaction with hydrothermal fluids.

The more calcic plagioclase (andesine-labradorite) preserved in the unsheared gabbros is indicative of middle amphibolite facies metamorphic conditions, whereas albite is characteristic of greenschist facies. The bimodal distribution of plagioclase composition may be explained by two distinct metamorphic events, in which an amphibolite facies metamorphism was followed and overprinted by a greenschist facies event. It is possible that the most calcic plagioclase (defining a minor peak

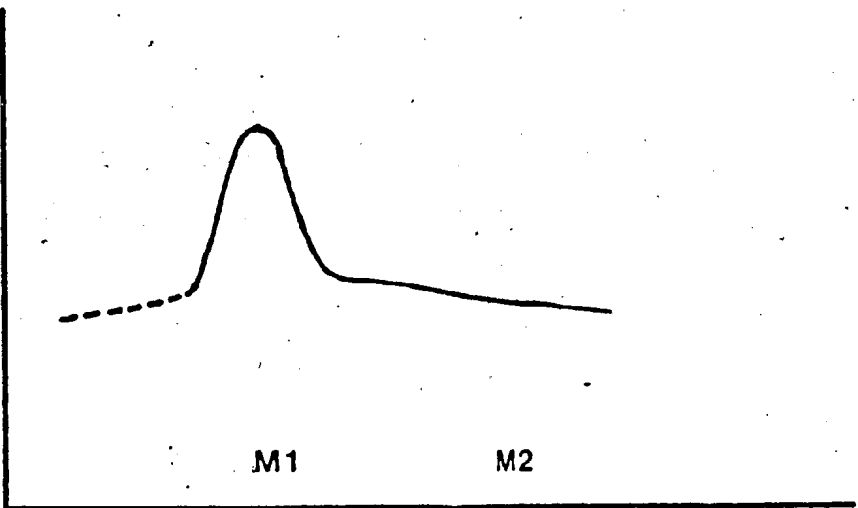
between An₆₀ and An₇₀) is relict igneous plagioclase.

Throughout the Yellowknife Greenstone Belt, regional greenschist facies metamorphism is recognized, and amphibolite facies aureoles are spatially associated with large plutons (Henderson and Brown, 1966). Although the lower grade regional metamorphism may have begun before or during peak contact metamorphism, no evidence was found from the Mirage Islands that the greenschist facies event bracketed the time span of the amphibolite facies event. Amphibolite facies assemblages, where they are preserved, are partly replaced by, and therefore predate greenschist facies assemblages. Thus, the amphibolite grade metamorphism is referred to as M₁, since it is the first recognizable metamorphic event in the area, and the greenschist facies event is referred to as M₂. It is important to recognize, however, that M₂ may have been initiated before M₁, and that the regional metamorphism of the area is called M₂ because it outlasted and overprinted contact metamorphic (M₁) assemblages (Figure 2.5).

The average plagioclase composition in sheared rocks is that of albite (near An₀₅; Figure 2.4), which is compatible with the greenschist facies mafic minerals preserved in the shear zones. It is inferred from this that the shear zone assemblages equilibrated during

Figure 2.5 Schematic temperature vs time graph showing the relative timing of M1 and M2, as recorded in the Mirage Islands. M1 represents amphibolite facies metamorphism, most likely caused by the intrusion of the inferred pluton, or the Western Plutonic Complex, or both. Peak M1 metamorphism was followed by regional greenschist facies metamorphism (M2), which overprinted amphibolite facies assemblages. M2 may have begun during or before M1, as indicated by the dashed line.

Temperature

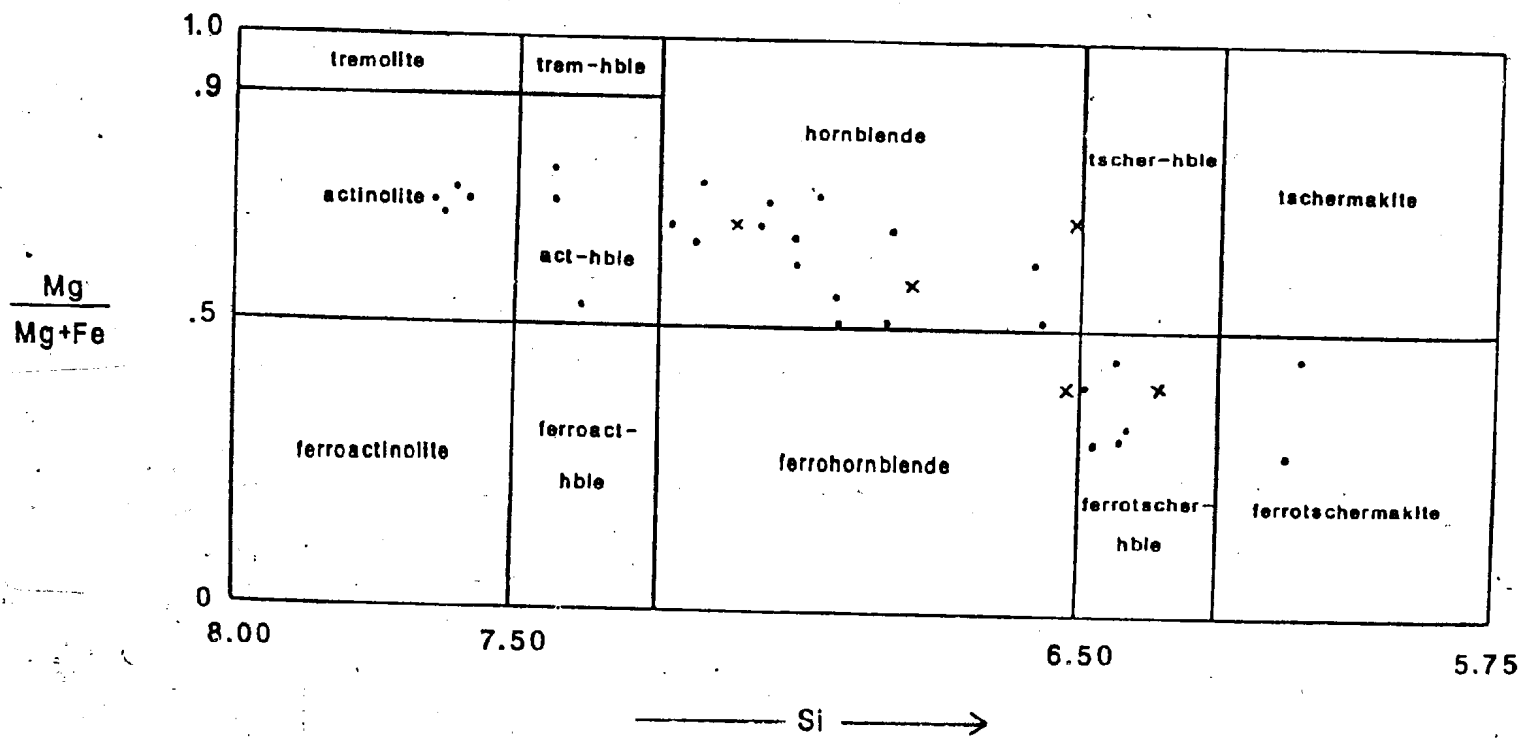


M1

M2

Time

Figure 2.6 Composition of amphiboles from unsheared gabbros (dots) and sheared gabbros (X's) from the Mirage Islands. Abbreviations: trem-hble - tremolitic hornblende, act-hble - actinolitic hornblende, tscher-hble - tschermakitic hornblende. Diagram from Leake, 1978.



$(\text{Na}+\text{K})_A < 0.5$ $\text{Ti} < 0.5$

greenschist facies (M2) metamorphism.

Amphibole

Microprobe analyses of amphiboles yielded compositions ranging from ferrotschermakite to actinolite (calculated after the method of Leake, 1978; Figure 2.6). The former coexists with andesine, but the latter occurs in association with both albite and labradorite, making it difficult to predict the Ca-content of plagioclase from amphibole composition, and vice versa. However, the extent to which the amphibole is altered to chlorite correlates well with the An content of the plagioclase. The most calcic plagioclases occur in association with the least hydrated amphiboles, and the most sodic plagioclases occur in more chloritic assemblages (see Table 2.2).

Amphibole is rarely preserved in the shear zones, having been hydrated to chlorite. However, local low strain augen within the shear zones contain hornblende or ferrotschermakitic hornblende. As in the unsheared rocks, the highest An contents of plagioclases occur in those parts of the shear zones that have undergone the least amount of deformation and hydration, and that contain the largest modal quantities of amphibole.




Table 2.2 Comparison of the mean anorthite (An) content of plagioclase with the composition of co-existing amphibole, and the amount of chlorite replacing the amphibole. Chlorite content and An composition show a good correlation, with the most sodic plagioclase occurring in the most chloritic assemblages.

Lithology (Sample no.)	An(plag) (ave)	Amphibole	% Chlorite replacement
CWM-141A	An61	act-hbl	5%
CWM-160A	An57	act, act-hbl	7%
CWM-35A	An54	act-hbl, hbl	11%
CWM-142A	An50	act, act-hbl	15%
CWM-82	An50	act, act-hbl	<5%
CWM-127	An35	fer-tsch	<2%
CWM-41A	An12	act	33%
CWM-34A	An12	act, act-hbl, hbl	21%
CWM-149A	An09	act-hbl, hbl	13%
CWM-83	An05	none	99%
CWM-163A	An04	act-hbl	22%

Data arranged in order of increasing albite content.

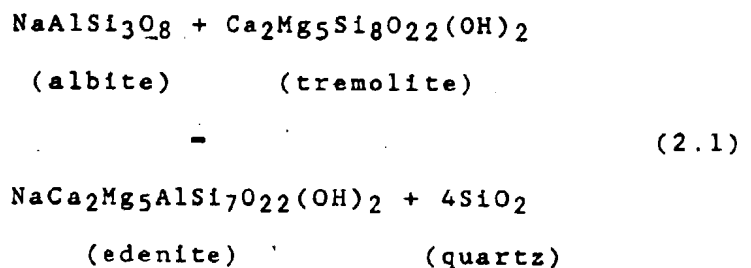
Pressure, Temperature Determinations

Geothermometry

In this section, calculations of equilibrium temperatures are made using mineral compositions determined by microprobe analysis. As discussed in Appendix A, some probe results were found to have fairly significant errors, thus only plagioclase analyses with weight % totals between 98 and 102% were used in the following calculations. Those inside this range but outside the range 99 - 101 % are indicated with an asterisk (*), and have larger temperature errors associated with them.

Spear (1980,1981) defined a geothermometer which is based on the distribution of Na between plagioclase and the A site in amphibole to determine the temperature of equilibration. At low temperatures, albite is stable, and coexists with an amphibole approaching the tremolite end-member, while at higher temperatures, the An content of plagioclase increases, and edenite is the stable amphibole.

Spear (1981) used the following mass transfer reaction to characterize this relationship:



He suggested that the equilibration temperature could then be calculated using:

$$\begin{aligned}
 T &= 3560.6 - .129 * P \\
 &3.452 - \ln K_{id}
 \end{aligned}$$

where $K_{id} = \frac{X_{\text{Na},A}}{X_{,A} * X_{ab}}$

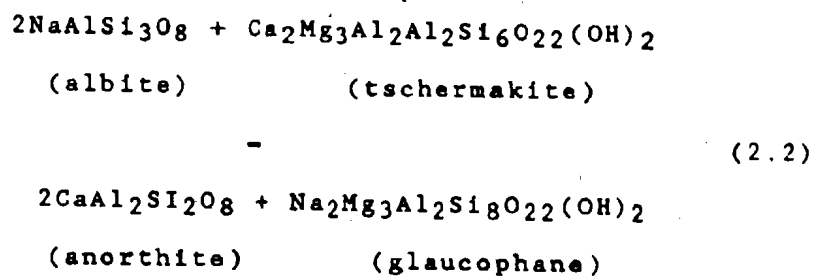
and $X_{\text{Na},A}$ - mole fraction of Na in A site of amphibole
(ideally 1 in edenite)

$X_{,A}$ - mole fraction of vacancy in A site of amphibole
(ideally 0 in tremolite)

X_{ab} - mole fraction of Na in plagioclase.

An activity coefficient of 1 is assumed here, for simplicity.

The exchange reaction:



was proposed by Spear (1980), for which he derived the following relationship:

$$T = 11826.9 - \frac{.0604 * P}{11.14 - \ln K_D}$$

$$\text{where } K_D = \frac{X_{\text{Ca,pl}} * X_{\text{Na,M4}}}{X_{\text{Na,pl}} * X_{\text{Ca,M4 am}}}$$

and $X_{\text{Ca,pl}}$ - mole fraction of An in plagioclase

$X_{\text{Na,pl}}$ - mole fraction of Ab in plagioclase

$X_{\text{Na,M4(am)}}$ - mole fraction of Na in M4 site of
amphibole

$X_{\text{Ca,M4(am)}}$ - mole fraction of Ca in M4 site of
amphibole.

For simplicity, ideal mixing between plagioclase end

members is assumed.

Both of these reactions have only a very small dependence on pressure, and calculations at various crustal pressures yield temperatures with a range of only a few degrees. Calculations using both of these equations yield similar temperatures (Table 2.3, Figure 2.7), and the estimated error associated with the determinations is approximately 50°C for plagioclase analyses with weight % totals between 99 and 101%, and 70°C for plagioclases with totals between 98 and 99% and 101 and 102%. It is clear from Table 2.3 and Figure 2.7 that there is a bimodal distribution of temperatures outside the shear zones, as expected from the bimodal plagioclase compositions. The mean temperature for M1 is 585°C, and for M2 is 460°C.

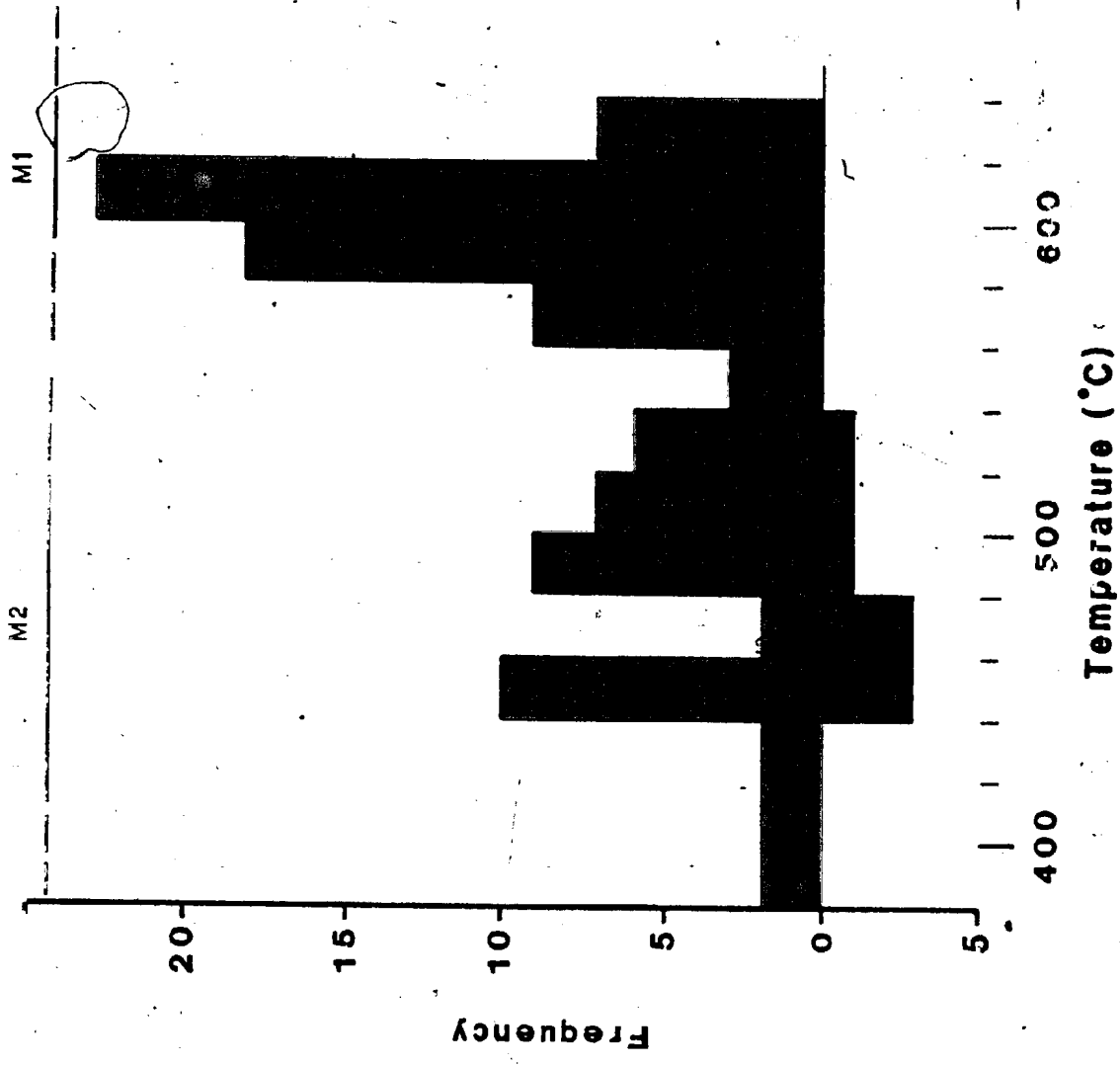
Amphiboles are not commonly preserved in the sheared gabbros, although they were found locally. Spear's (1980, 1981) thermometers yielded an average temperature near 490°C for sheared assemblages bearing amphibole. Since the mineral assemblages in most shear zones consist mainly of chlorite + albite + quartz (i.e. lacking amphibole), it is very likely that the shear zones formed at temperatures of less than 490°C.

Table 2.3 Equilibrium temperatures calculated from the plagioclase-hornblende geothermometers of Spear (1980, 1981) for samples from the Mirage Islands and the Octopus Islands. The mean temperature and the standard deviation of the mean are also presented for each sample. Temperatures calculated from plagioclase analyses with wt % totals between 98-99% and 101-102% are indicated by * ; the remaining temperatures were calculated from plagioclases with wt % totals of 99-101%.

Sample no.	Temperatures	Mean	σ
Mirage Islands			
CWM-34A	524 537 496 509 522 535 515* 516* 520* 489* 489* 493* 514* 514* 518*	513	13
CWM-35A	608 603 561 573 582 636 631 587 600 610 636 631 587 600 610	604	22
CWM-41A	437 455 446 429 458 451	446	10
CWM-82	588 601 602 598 601 597 595 601	598	4
CWM-126	443 448 445 450 481 483 488 449 454 481* 470* 487* 475* 523* 511*	470	18
CWM-127	589 617 585* 613* 550* 575*	588	22
CWM-141A	601* 601* 591* 602* 601* 591* 606* 605* 595*	599	5
CWM-142A	596 631	613	17
CWM-156	558 563	560	2
CWM-160	578 589 547 594 569 575 612 624 579 630 603 610 594 606 562 611 585 592	592	21
CWM-163A	387* 417* 398* 409*	403	11
Sheared sample			
CWM-142B	444 446* 444*	445	1
CWM-155B	521* 479* 480* 503* 463* 464*	485	21
Octopus Islands			
CO-22A	501 505 480 483 481 484 504 507	493	11
CO-23A	620 626 638* 644*	632	10

* Plagioclase analyses with wt % totals between 98 - 99% and 101 - 102% (indicated by *) have errors estimated to be +/- 70°C; totals between 99 - 101% have errors of +/- 50°C.

Figure 2.7 Histograms showing temperatures determined from plagioclase-hornblende thermometry (after Spear, 1980, 1981) for unsheared metabasites (upper half) and sheared metabasites (lower half). Estimated temperatures outside the shear zones have a bimodal distribution, and define two thermal events: M1, with a mean temperature of 585°C, and M2, with a mean temperature of 460°C. M1 is correlated with the amphibolite facies contact metamorphic event, and M2 with the regional greenschist facies event. Inside the shear zones, most temperatures correspond to the M2 thermal event, or are intermediate between M2 and M1.



Geobarometry

The pressure sensitive assemblage biotite + muscovite + chlorite + quartz (Powell and Evans, 1983) is present in several intermediate volcanoclastic rocks. However, the grain size of these rocks was found to be too small to obtain precise microprobe analyses from the micas, and therefore this barometer could not be used.

Mineral assemblages in the mafic rocks do not contain any known quantitative barometers. However, a qualitative estimate of metamorphic pressure has been made using pressure fields defined for various amphibole compositions, as determined by Laird and Albee (1981), and using a semiquantitative geothermobarometer calibrated by Plyusnina (1982).

In their study, Laird and Albee (1981) considered a series of mafic schists interlayered with metapelites. The "common assemblage" amphibole + chlorite + epidote + plagioclase + quartz + Ti-phase + carbonate + K-mica +/- Fe^{3+} oxide was ubiquitous throughout their study area, from greenschist to lower amphibolite grade. However, the composition of the amphibole at different grades was found to be variable, and the "...variations in mineral

chemistry can be related to differences in metamorphic grades..." (Laird and Albee, 1981 page 132).

As a result of their study, Laird and Albee (1981) were able to delineate low, medium and high pressure fields on four different binary plots on the basis of amphibole compositions.

In this study, calcic amphibole analyses were normalized to 13 cations excluding Ca, Na and K (after Robinson *et al.*, 1982). Various cation ratios were calculated, which were then plotted against each other, and these are superposed on the pressure fields of Figure 12 of Laird and Albee (1981). All four plots were designed so that an increase in temperature is qualitatively shown as a shift in the positive direction along the horizontal axis, and a qualitative increase in pressure corresponds to a shift in the positive direction along the vertical axis.

In Figure 2.8a, $Na/(Na+Ca)$ is plotted against $Al/(Al+Si)$. This is independent of the amphibole normalization scheme used. Amphiboles from the Mirage Islands have a fairly narrow range in pressure, corresponding mainly to the medium pressure field of Laird and Albee (1981), with a few points approaching the low pressure field. Amphiboles

which yielded M2 temperatures have a wider compositional range and approach the low pressure field more closely than the M1-equilibrated amphiboles (Figure 2.8a). Although it may be suggested from this that M2 pressures were lower than M1 pressures, given the qualitative nature of this barometer, it is probably more reasonable to simply infer that the pressure during both metamorphic events was low to medium.

The points show a wider horizontal distribution, inferring a broad temperature range, which is compatible with the large variation in temperature found using Spear's (1980, 1981) thermometers, although absolute values can not be attached to temperatures.

In the other three diagrams the variables plotted are dependent on the amphibole normalization scheme used. Figures 2.8b and 2.8d indicate medium to low pressures compatible with Figure 2.8a, whereas points are widely scattered in Figure 2.8c. If amphibole stoichiometry is normalized to 15 cations excluding Na and K, the points on Figure 2.8c all plot within the medium pressure field.

07

Figure 2.8 Qualitative estimates of metamorphic pressure using the composition of amphiboles from the Mirage Islands. Amphibole stoichiometry normalized to 13 cations excluding Ca, Na and K (after Robinson *et al.*, 1982). Figure 2.8a is independent of amphibole normalization.

2.8a $100\text{Na}/\text{Na}+\text{Ca}$ vs. $100\text{Al}/\text{Al}+\text{Si}$. Amphiboles plot in the areas delineated for low to medium pressure.

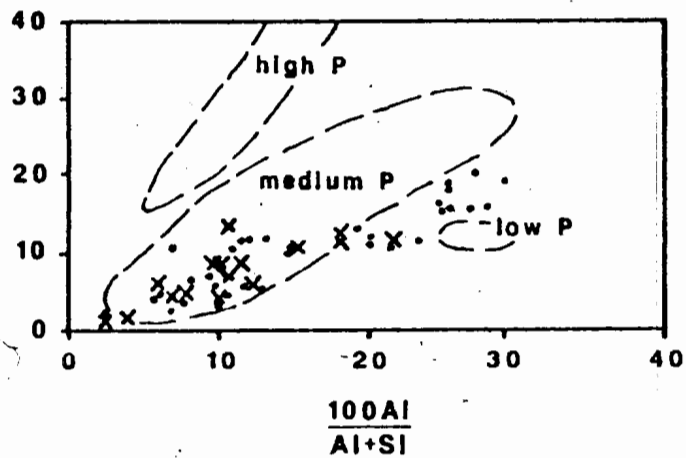
2.8b Na^{M4} vs. $\text{Al}^{\text{VI}} + \text{Fe}^{3+} + \text{Ti} + \text{Cr}$. Amphiboles plot in the areas delineated for low to medium pressure.

2.8c $\text{Al}^{\text{VI}} + \text{Fe}^{3+} + \text{Ti} + \text{Cr}$ vs. Al^{VI} . Amphiboles plot in the areas delineated for low, medium and high pressure.

2.8d Na^{M4} vs. $(\text{Na} + \text{K})^{\text{A}}$. Amphiboles plot in the areas delineated for low to medium pressure.

Pressure fields were defined by Laird and Albee, 1981.

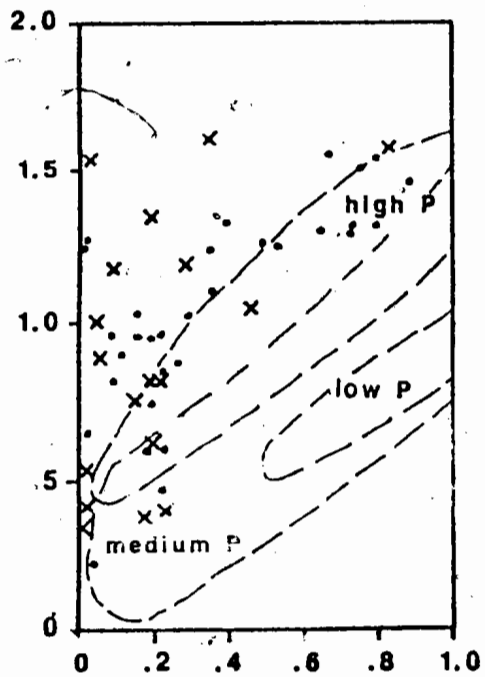
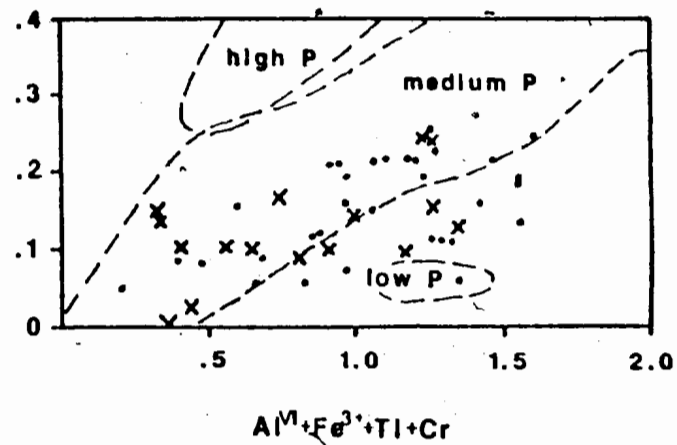
$\frac{100\text{Na}}{\text{Na}+\text{Ca}}$



a

Na^{M4}

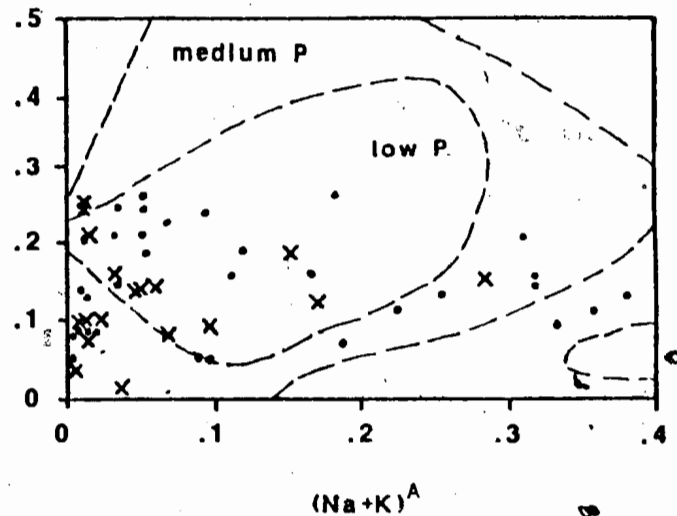
c



b

Na^{M4}

d

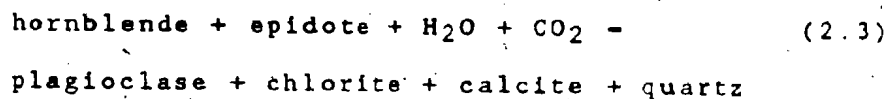


x = M1

• = M2

Because of the dependence on amphibole normalization inherent in Figure 2.8b to 2.8d, only the results of Figure 2.8a are considered reliable. The Mirage Island amphiboles have Na/Na+Ca and Al/Al+Si ratios which are the same as low to medium pressure amphiboles in mafic schists from Vermont (Laird and Albee, 1981), and suggest a fairly wide range of equilibration temperature.

A semi-quantitative geothermobarometer was developed by Plyusnina (1982) for the reaction



The thermometer/barometer was calibrated experimentally, and is based on the temperature and pressure-dependence of Al-content in plagioclase and Ca-amphibole, respectively.

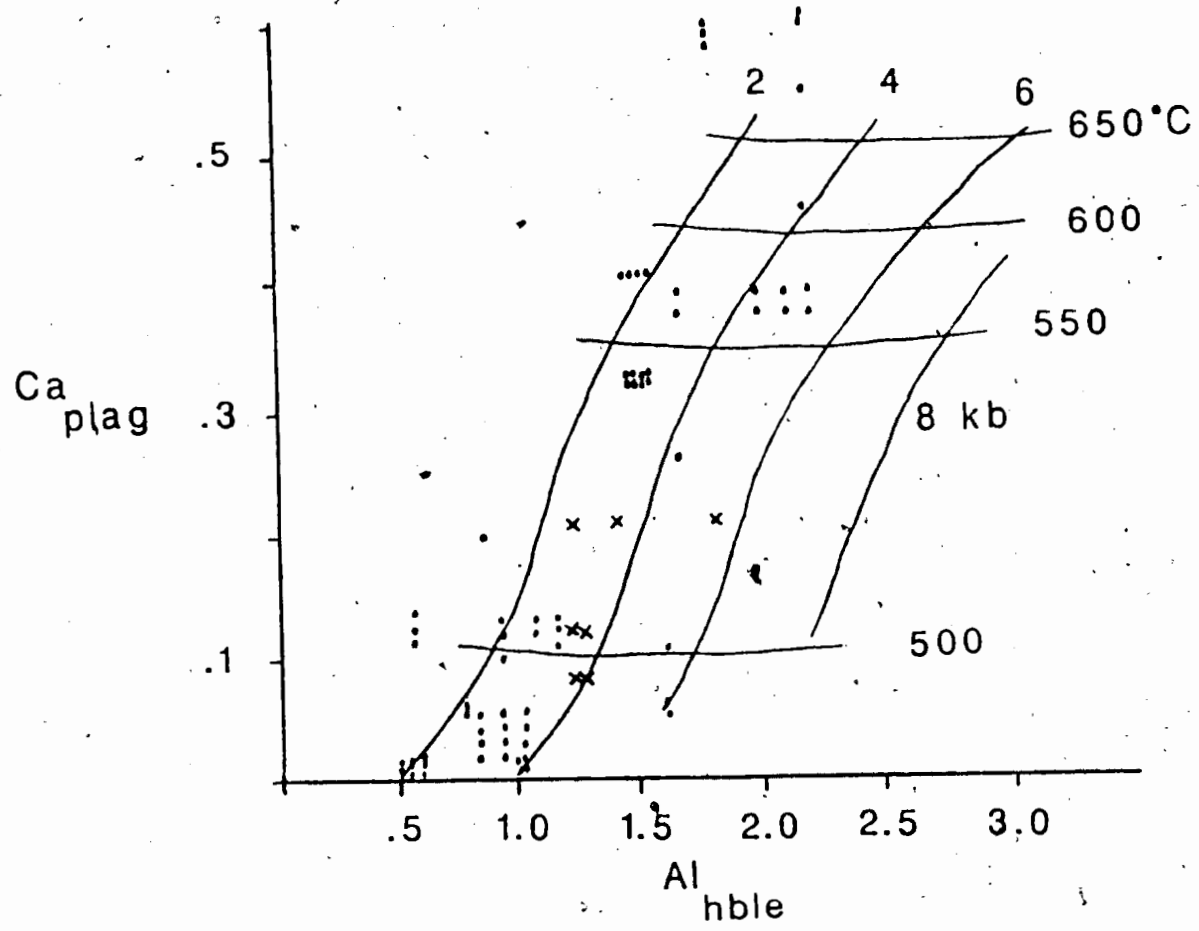
The assemblage amphibole + epidote + plagioclase + chlorite + calcite + quartz is common in the Mirage Islands, and the compositions of coexisting mineral pairs are plotted in Figure 2.9. Isotherms are defined by the Al content of plagioclase, and isobars are dependent on

the total Al content of amphibole.

Data on plagioclase and amphibole compositions are selected from unshered gabbro samples containing mineral assemblages which appeared to be at or near equilibrium. The samples show a concentration of estimates from about 450 to 500°C and 2 to 4 kbar, and another concentration at about 545 to >650°C and 2 to 5 kbar. These data are compatible with the M1 and M2 temperatures indicated by Spear's (1980, 1981) thermometers, suggesting a middle amphibolite facies metamorphic event and a greenschist grade event. As was found with the amphibole barometer used previously, it appears that M1 and M2 pressures overlapped, but that the mean M2 pressure may have been slightly lower than that of M1.

A limited number of data from sheared samples containing amphibole + epidote + plagioclase + calcite + quartz are also available, and they indicate similar equilibration temperatures and pressures to their unshered greenschist facies counterparts, with temperatures ranging from about 480 to 530°C, and pressures between 2 to 4 kbar (Figure 2.9).

Figure 2.9 Plot of Ca content of plagioclase vs total Al in amphibole. Isobars and isotherms are defined from experimental studies of Plyusnina (1982). Unsheared samples (dots) from the Mirage Islands have a bimodal distribution, with temperature and pressure ranges of 545 to >650°C and 2 to 5 kbar, and 450 to 500°C and 2 to 4 kbar. Sheared samples (X's) overlap with the lower temperature and pressure data described above.



after Plyusnina, 1982

Summary

In the Yellowknife Greenstone Belt, the intrusion of the Western Plutonic Complex produced a mid-amphibolite facies metamorphic aureole adjacent to the batholith (Henderson and Brown, 1966; Padgham, 1983). Elsewhere, the supracrustal rocks bear greenschist facies assemblages as a result of regional metamorphism. Although it is uncertain which thermal event was initiated first on the Mirage Islands, regional metamorphism outlasted the contact metamorphism, as indicated by retrograde mineral textures. Therefore, the amphibolite facies contact metamorphism has been called M1, and the regional greenschist facies metamorphism M2.

On the Mirage Islands, the thermal source for M1 is considered to be the inferred plutonic body located south of the West Mirage Islands, or the Western Plutonic Complex, or both. Temperatures during M1 approached 600°C, and pressures were medium to low (2-5 kbar).

During M2 metamorphism, amphiboles in the metabasic rocks were hydrated to chlorite, and labradorite was replaced by less calcic plagioclase. Temperatures generally were less than 500°C, and pressure was probably

lower than during M1 (2-4 kbar).

Metamorphic conditions calculated for a few sheared samples correspond to M2 conditions. These samples come from the least sheared and hydrated parts of the shear zones, and so probably record the highest equilibrium temperatures preserved in the shear zones.

CHAPTER 3: STABLE ISOTOPES

Introduction

Oxygen is present in many common minerals as well as in all known hydrothermal fluids. It has three stable isotopes, ^{16}O , ^{17}O and ^{18}O , whose abundances in any given phase are a function of the environment in which the phase formed (Faure, 1977). ^{16}O and ^{18}O respectively make up approximately 99.75% and 0.205% of the oxygen in the earth's crust, and the fractionation of these two isotopes between minerals is dependent on temperature (ibid.). Thus the measurement of the oxygen isotopic composition of a rock and its constituent minerals, when coupled with geological data, can be a useful tool in determining both the temperature at which the phases equilibrated and the environment in which equilibration occurred.

In this chapter, isotopic data on mineral separates from sheared samples and on whole rock powders from sheared and unsheared rocks are examined. The distribution of ^{18}O between chlorite and quartz from within 13 shear zones is used to estimate the equilibrium temperature and the $\delta^{18}\text{O}$ content of the associated hydrothermal fluid. Whole rock $\delta^{18}\text{O}$ values of unsheared rocks are compared to their sheared counterparts in order

to determine possible sources of the hydrating fluids.

Oxygen and carbon isotope analyses were also carried out on nine carbonate-bearing sheared samples, including six whole rock powders and three carbonate mineral separates. It was hoped that the results of the latter analyses would yield information on the source of the carbon in the shear zones bearing carbonate veins.

Sample Selection

Samples selected for oxygen isotope thermometry were those which showed textural equilibrium between the chlorite and the quartz. The quartz occurs in thin (0.5 to 2 cm) veins which are subparallel to the schistosity defined by the chlorite, and which anastomose along their length. In a few shear zones, carbonate (ankerite and/or Fe-dolomite) veinlets transect the quartz veins at low to moderate angles (10 to 50°), and are interpreted to post-date the equilibration of the quartz-chlorite pairs. The oxygen isotope compositions of the carbonate from three such veins were analyzed in order to see whether ^{18}O re-equilibrated during the emplacement of these later veins.

Analytical Techniques

Thirteen quartz-chlorite pairs - 11 from the Mirage Islands and 2 from the Octopus Islands - as well as 28 whole rock powders were analyzed. The mineral separates were crushed and hand-picked, then tested for purity by X-ray diffraction. Minor carbonate was optically identified in some of the whole rock samples. These samples were treated with HCl to remove the carbonate. Isotope analyses were carried out by Dr. Fred Longstaffe at the University of Alberta. The data are presented in Appendix B. Oxygen results are reported as $\delta^{18}O$ relative to standard mean ocean water (SMOW), and are expressed in ‰ (per mil) of total oxygen (Hoefs, 1973). The standard used for carbon isotopes was *bellefleuritella americana* from the Cretaceous Peedee Formation in South Carolina, (PDB), and is also reported in ‰ (ibid.). The results are precise to about 0.2‰.

Thermometry

Results and Calculations from Quartz-Chlorite Pairs

The relationship between the fractionation factor of an isotope between two minerals and temperature is given as:

$$(3.1) \quad 1000 \ln \alpha = \frac{A}{T^2} + B$$

(Taylor and Epstein, 1962; and Epstein and Taylor, 1967)

where α - fractionation factor

T - temperature

A, B - constants, dependent on the minerals being considered.

Faure (1977) has shown that for most values of α , $1000 \ln \alpha$ is approximately equal to $\delta^{18}O_1 - \delta^{18}O_2$, where 1 and 2 represent two minerals between which ^{18}O has equilibrated.

Thus the following relationship between $\Delta \delta^{18}O_{q-ch}$ and temperature was used:

$$(3.2) \quad \Delta \delta^{18}O_{q-ch} = 2.01 (10^6/T^2) + 1.99$$

(Wenner and Taylor, 1971)

where T - equilibrium temperature ($^{\circ}K$),

$\Delta \delta^{18}O_{q-ch}$ - difference in ^{18}O between quartz and chlorite (‰).

Equation 3.2 was calibrated for the Al-absent end member of chlorite (serpentine) (Weaner and Taylor, 1971). It has been shown by Mathews et al. (1983), and Aggarwal and Longstaffe (1987), however, that the chemistry of a mineral can affect the extent to which it fractionates oxygen. Therefore the mineral composition must be considered in determining its equilibration temperature. For example, at 550°C, the substitution of one Al into the tetrahedral site of a silicate mineral could decrease its equilibrium $\delta^{18}\text{O}$ content by 1.6‰ (Mathews et al., 1983). The same substitution into the octahedral site could increase the $\delta^{18}\text{O}$ content by 1.5‰ (ibid.).

Microprobe analyses of chlorites (Appendix A) from shear zones in the Mirage Islands reveal that Al comprises about 2.56 tetrahedral sites, and 2.65 octahedral sites. Calculating the net effect of these substitutions, it is likely that Al-absent chlorite would contain approximately 0.3‰ less ^{18}O than the Al-bearing chlorites in this study.

Microprobe analyses of chlorites (Appendix A) typically yielded weight % totals between 84 and 88%. Those with totals near 88% seem to be reasonable chlorite analyses, while those with lower totals (84-85%) appear to

have low SiO₂ contents. If the main source of error in these analyses results from poor silica determinations, and the SiO₂ contents of the chlorites is increased so that the weight % of all oxides is 88%, then the extra silica would displace some of the Al from the tetrahedral site. Therefore the magnitude of the decrease in $\delta^{18}\text{O}$ content due to tetrahedral Al would be smaller, and the magnitude of the increase in $\delta^{18}\text{O}$ content due to octahedral Al would be greater.

The net effect of an increased silica content was calculated for one chlorite analysis. Previously the silica occupied 5.5 tetrahedral sites, but upon normalizing the total oxides to 88% anhydrous, silica occupied 5.6 tetrahedral sites, leaving 2.4 sites for Al in tetrahedral coordination, and requiring that the octahedral site accommodate 2.8 Al atoms per unit cell. Using this distribution of Al to calculate the effect on the $\delta^{18}\text{O}$ content of the chlorite, it was estimated that Al-absent chlorite would contain about 0.4% more ^{18}O than the measured $\delta^{18}\text{O}$ value. Before normalization, the Al distribution for the same chlorite analysis predicted that Al-absent chlorite would contain about 0.3% less ^{18}O .

It is uncertain how reliable the measurement of silica in chlorite is (see discussion in Appendix A), therefore

calculating the magnitude of Al substitution into the silica site, and hence the net effect of Al distribution on the equilibrium $\delta^{18}\text{O}$ composition of the chlorite, is not meaningful.

In Table 3.1 the equilibrium temperatures calculated for quartz-chlorite pairs (data in Appendix B; sample calculation in Appendix C) in the shear zones are presented. The chlorite composition used was that of the Al-absent Fe/Mg chlorite. For the first shear zone presented (GWM-41C), two additional temperatures were calculated; those of the chlorite with its $\delta^{18}\text{O}$ content reduced by 0.3%, and increased by 0.4% (accounting for the possible effects of different proportions of Al in the tetrahedral and octahedral sites) The error range defined for these three temperatures overlap. Sample calculations are presented in Appendix C.

The equilibrium temperature of ^{18}O in the quartz-chlorite pairs was found to vary between 350°C and 620°C (Table 3.1 and Figure 3.1). Figure 3.1 shows that the temperatures are distributed into two distinct populations. This distinction is made only on the basis of ^{18}O fractionation, since petrographically the chlorite and quartz appear indistinguishable between the two sample sets. The temperature ranges of the M1 and M2 metamorphic

Figure 3.1 Histogram of temperature determinations from oxygen isotope fractionation between quartz and chlorite from shear zones on the Mirage and Octopus Islands. The temperatures have a bimodal distribution, with means of 590°C and 420°C.

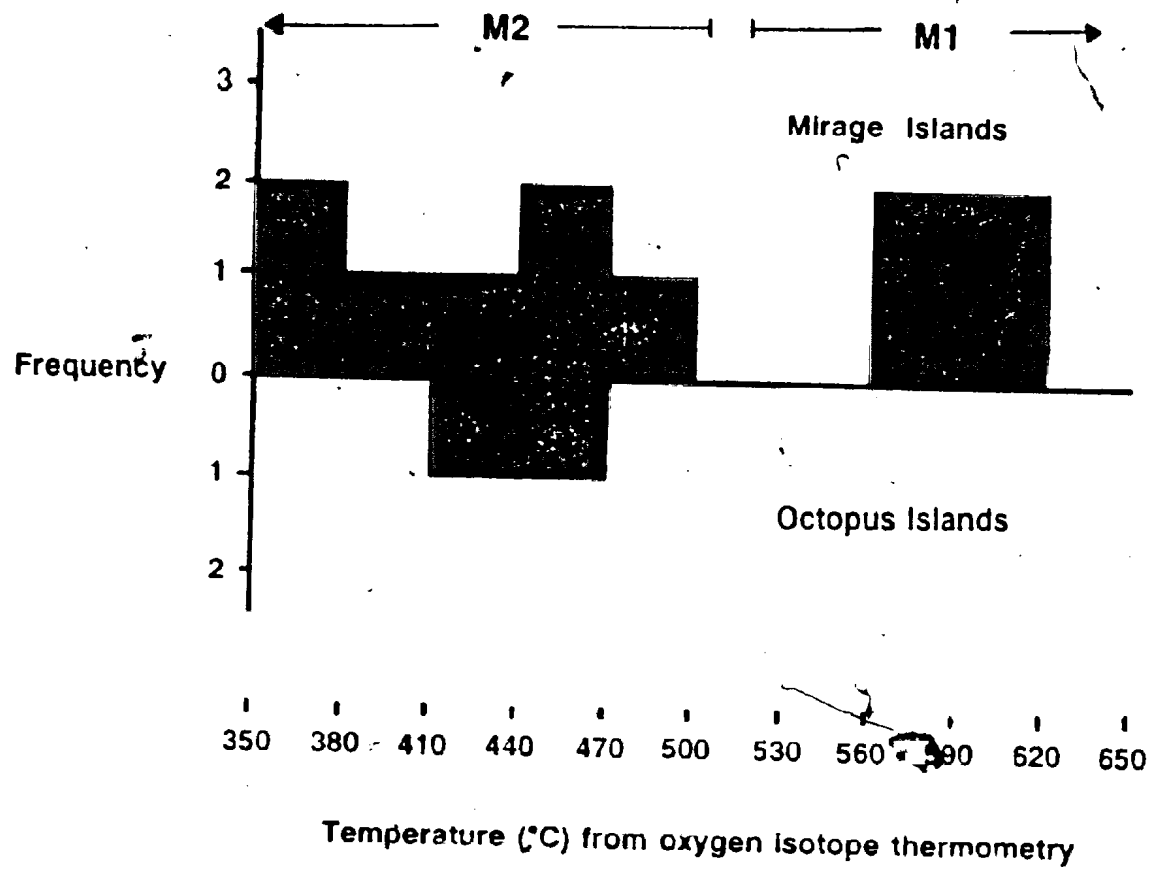


Table 3.1 Temperatures calculated from oxygen isotope fractionation between quartz and chlorite in shear zones from the Mirage Islands and Octopus Islands.

Results of Oxygen Isotope Thermometry

Sample Temperature (°C)

Mirage Island Samples:

CWM-41C	476 +/- 45
CWM-41C*	444 +/- 45
CWM-41C**	517 +/- 45
CWM-138 ¹	405 +/- 55
CWM-142E	574 +/- 50
CWM-143B	620 +/- 55
CWM-145B	366 +/- 25
CWM-146B	574 +/- 50
CWM-147B	442 +/- 40
CWM-154C	454 +/- 40
CWM-160C	433 +/- 35
CWM-163	596 +/- 60
CWM-164C	352 +/- 30

Octopus Island Samples:

CO-22C	430 +/- 30
CO-23C	441 +/- 30

* $\delta^{18}\text{O}$ content of chlorite reduced by 0.3‰ to approximate pure Al-absent chlorite (see discussion in text).

** $\delta^{18}\text{O}$ content of chlorite increased by 0.4‰ to approximate pure Al-absent chlorite with an increased silica content (see discussion in text).

events (as determined by geothermobarometry) are also included in Figure 3.1, and it can be seen that while a few of the shear zones have isotope fractions corresponding to M1 temperatures, most shear zones equilibrated at temperatures corresponding to M2.

The four shear zones which equilibrated at temperatures corresponding to M1 have a mean of $590^{\circ} \pm 55^{\circ}\text{C}$. Although this temperature lies above that normally considered stable for chlorite, Fleming and Fawcett (1976) have shown experimentally that quartz can coexist stably with 50% Fe/Fe+Mg chlorite at temperatures up to 590°C and 2 kbar $\text{P}_{\text{H}_2\text{O}}$, above which they break down to cordierite + talc + vapor. Furthermore, Aggarwal and Longstaffe (1987) report equilibrium temperatures as high as 588°C from oxygen isotope fractionation between quartz and "relatively iron rich" chlorite (ibid.). Outside the shear zones, M1 assemblages are characterized by amphibole and a lack of chlorite. However, inside the shear zones, the presence of abundant hydrothermal fluids (see Chapter 5 for fluid:rock ratios) appears to have stabilized the more hydrous assemblage.

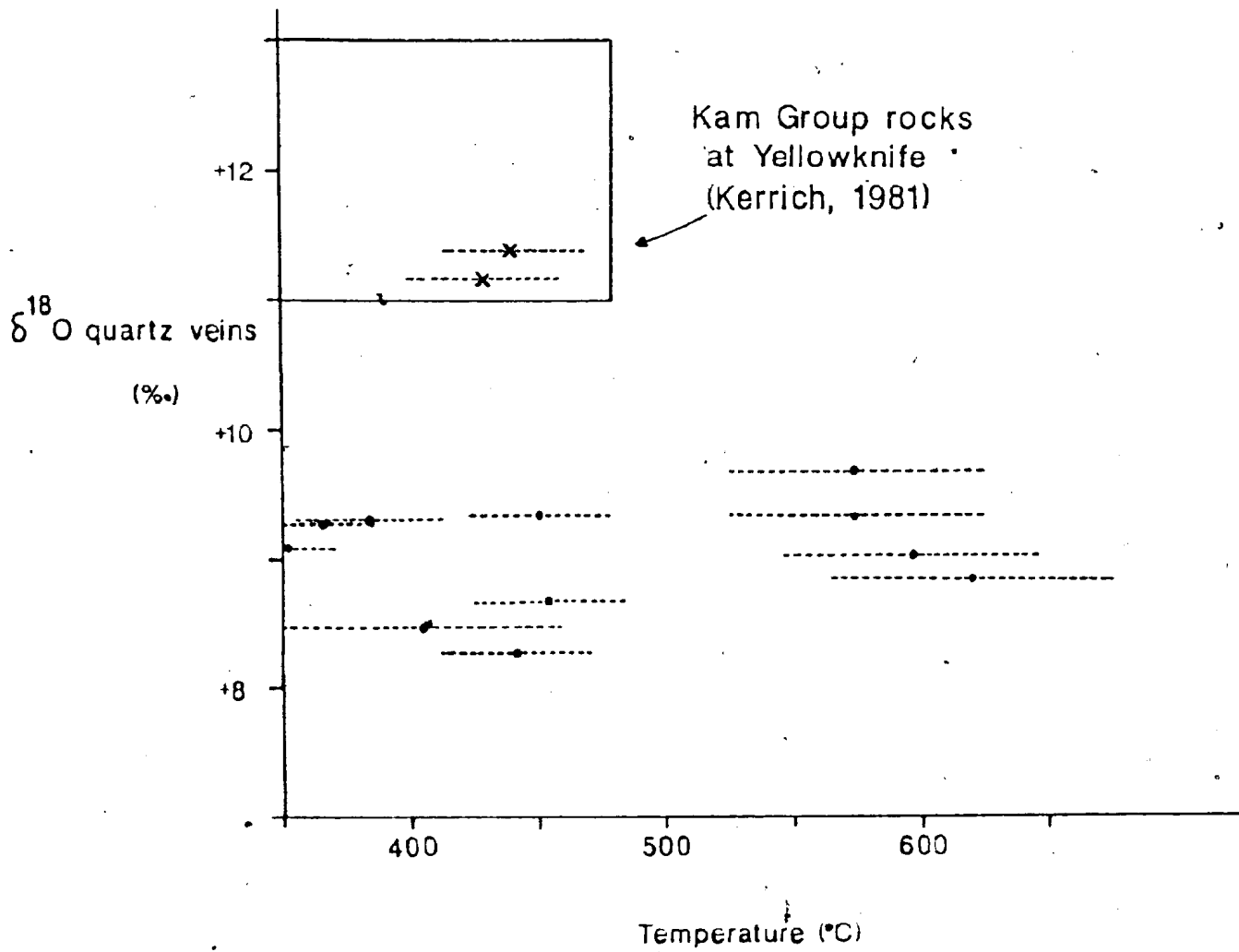
There does not appear to be a systematic variation in iron:magnesium ratios between the two populations of chlorites. Stoichiometric Fe:Mg ratios are between 1.13

and 1.34 in high temperature chlorites, and range from 0.60 to 1.30, with most near 1.0, in the low temperature chlorites (see Appendix A). SiO_2 occupancies are between 5.3 and 5.6 tetrahedral sites in the high temperature chlorites, and from 5.4 to 5.9 sites in the low temperature chlorites, but given the potential errors in the silica determinations in these analyses, the apparently greater silica contents of the low temperature chlorites may not be "real".

Since the bimodal temperature distribution of the shear zones calculated by ^{18}O partitioning between quartz and chlorite matches the temperature ranges for M1 and M2 from geothermometry, it is proposed that the high temperature shear zones equilibrated during M1, and the low temperature shear zones during M2.

Figure 3.2 depicts the relationship between temperature and ^{18}O of quartz veins from within the shear zones from the Mirage Islands and Octopus Islands, and compares them to the range of data from the gold-bearing shear zones at Yellowknife (after Kerrich, 1981). The two samples from the Octopus Islands have ^{18}O compositions between +11.2 and +11.3‰, which coincides with the range of quartz vein ^{18}O values found at Yellowknife (ibid.).

Figure 3.2 Graph of isotopic composition of quartz veins vs. shear zone temperature (from oxygen isotope thermometry) for shear zones on the Mirage Islands, Octopus Islands, and near Yellowknife. Yellowknife data from Kerrich (1981).



Mirage Island quartz veins have $\delta^{18}\text{O}$ contents between +8.6 and +9.6‰, which lie outside of this range.

The M2-equilibrated shear zones on the Mirage Islands have estimated temperatures which are coincident with those estimated for the shear zones on the Octopus Islands and at Yellowknife, implying that on a regional scale, the shear zones in the greenstone belt equilibrated during greenschist facies metamorphism. However, the isotopic compositions of the quartz veins from the Mirage Islands are distinctly different from those on the Octopus Islands and at Yellowknife.

The rocks which host the shear zones on the Octopus Islands and near Yellowknife are dominantly basalts and gabbros (Henderson and Brown, 1966; Helmstaedt *et al.*, 1981; Helmstaedt and Padgham, 1986), whereas the predominant lithology on the Mirage Islands is more felsic in composition, and felsic rocks have a greater capacity to concentrate ^{18}O than mafic rocks (Taylor and Epstein, 1962). If it is assumed that the shear zones equilibrated during regional greenschist facies metamorphism (with the exception of the four high temperature Mirage Island shear zones), then it is likely that the fluids present in the shear zones during their alteration were derived from

dehydration reactions accompanying metamorphism. Metamorphic fluids generated in and interacting with mafic rocks (such as at Yellowknife) would tend to have a higher ^{18}O content than fluids derived from a more felsic source, where ^{18}O would fractionate from the fluid into the siliceous host rock. Quartz veins precipitated from a relatively ^{18}O -depleted fluid would have lower ^{18}O contents than veins precipitated from an ^{18}O -rich fluid. Thus the differences in the oxygen isotopic compositions of quartz veins hosted in shear zones on the Mirage Islands, the Octopus Islands, and near Yellowknife do not necessarily imply a different fluid source, but may be a function of the chemistry of the host rocks.

It is possible to calculate the oxygen isotopic composition of the hydrothermal fluid which deposited the quartz veins, given an independent geothermometer. In Chapter 2, the equilibrium temperatures in two shear zones were calculated based on the plagioclase - hornblende thermometers of Spear (1980, 1981). However, the shear zones in which assemblages with plagioclase and amphibole are preserved are those which have not undergone extensive hydration, whereas the shear zones for which oxygen isotope fractionation has been measured have been exposed to high fluid:rock ratios, as evidenced by the presence of quartz veins and the absence of amphibole. Therefore the

temperature determined for plagioclase plus amphibole-bearing shear zones cannot be expected to yield reasonable fluid compositions for quartz plus chlorite - bearing shear zones.

Although it would be circular reasoning to use the temperatures determined from isotope thermometry to calculate the isotopic composition of the hydrothermal fluids, it is possible to estimate the range of fluid compositions that might be expected over the temperature limits calculated.

The isotopic composition of a fluid in equilibrium with quartz at a given temperature T (°K) can be estimated as:

$$(3.3) \quad \Delta\delta^{18}O_{q-w} = 3.38(10^6 * T^{-2}) - 2.90$$

(Friedman and O'Neil, 1977 after Clayton et al., 1972)

where $\Delta\delta^{18}O_{q-w}$ = the difference in $\delta^{18}O$ between quartz and water.

From Figure 3.2 it is clear that the quartz veins in the Mirage Island shear zones have a fairly uniform isotopic composition, with $\delta^{18}O$ ranging from +8.6 to +9.6‰. The M1-equilibrated shear zones have equilibrium

temperatures ranging from 574 to 620°C, and M2 shear zone temperatures vary between 352 and 476°C. From equation 3.3, the expected range of $\delta^{18}\text{O}$ for a fluid in equilibrium with quartz over the range of M1 temperatures is between +6.7 and +8.3%. That of a fluid at M2 temperatures is between +2.8 and +6.5%. Given the accumulated errors inherent in this calculation, it is possible that the range of fluid compositions for M1 and M2 shear zones actually overlap; however, the predicted $\delta^{18}\text{O}$ contents of the high temperature shear zones are consistently greater than those of the low temperature shear zones.

In Chapter 2 it was suggested that the thermal source for the amphibolite facies (M1) metamorphism was a pluton inferred to lie south of the West Mirage Islands, and/or the Western Plutonic Complex. If the estimated range of the fluid composition in the M1 shear zones (+6.7 to +8.3%) is correct, then these fluids overlap with the $\delta^{18}\text{O}$ content of igneous fluids (+6 to +10%, Taylor, 1967). Therefore fluids in the high temperature shear zones appear to be compatible with a magmatic source. However, a metamorphic source for M1 fluids cannot be ruled out, as the $\delta^{18}\text{O}$ range for metamorphic fluids (+5 to +25%, Taylor, 1967) also coincides with the fluid composition estimated for M1 shear zones.

Fluids in the M2-equilibrated shear zones have $\delta^{18}\text{O}$ contents estimated to lie between +2.8 and +6.5%. This is slightly below the range of $\delta^{18}\text{O}$ generally expected for metamorphic fluids (+5 to +25%, Taylor, 1967), but as described above, interaction of the fluid and wallrock as the fluids ascend and cool in the shear zone could have resulted in ^{18}O -depleted fluids.

Alternatively, the $\delta^{18}\text{O}$ range of meteoric fluids varies from 0 to $< -50\%$. (Taylor, 1967). If descending meteoric waters were to have come into contact with an isotopically heavier metamorphic (or igneous) fluid in the shear zones, the resultant mixture would have an intermediate isotopic composition, perhaps in the range of that found for the M2 shear zones.

The results of mapping in the West Mirage Islands (discussed in Chapter 1) were interpreted to indicate that all of the shear zones formed more or less synchronously. Since some shear zones have equilibrium temperatures corresponding to M1, it follows that the initial shearing event must have accompanied plutonism. It is suggested here that the shear zones were produced during M1 in the presence of fluids which accompanied plutonism and/or amphibolite facies metamorphism. Regional greenschist facies metamorphism followed - or accompanied and

outlasted - M1, during which the shear zones acted as conduits for M2-derived metamorphic fluids, and possibly for meteoric fluids as well. Most of the shear zones re-equilibrated during M2, and early (syn-M1) isotopic signatures have been overprinted, but a few shear zones have retained isotope fractions indicative of M1 temperatures.

Results from Carbonate-bearing Shear Zones

The results of analyses for $^{18}\text{O}_{\text{SMOW}}$ and $^{13}\text{C}_{\text{PDB}}$ in carbonate-bearing samples are presented in Appendix C. In two samples (CWM-151C and GWM-166C), ^{18}O values of +23.6‰ and +27.6‰ resemble those of marine carbonate (Longstaffe, personal communication, 1987). Oxygen in the remaining samples analyzed ranges in ^{18}O from +7.8 to +9.7‰. As noted earlier in this chapter, carbonate veinlets crosscut and post-date quartz veins, and ^{18}O values of carbonates indicate that ^{18}O in the carbonate minerals did not equilibrate with that in the quartz or chlorite. Furthermore, temperature calculations using a quartz-calcite pair and a chlorite-calcite pair yielded negative values of T^2 (see Appendix C), confirming that the carbonate veinlets are in disequilibrium with the quartz and chlorite.

Since the precipitation of the carbonate veinlets postdated that of the quartz veins, it is reasonable to assume that the temperature at which they formed was less than 350°C, which is the lowest temperature calculated for quartz-chlorite equilibration. If the carbonate is assumed to have precipitated at a temperature between 250 and 350°C, the $\delta^{18}\text{O}$ of the hydrothermal fluid from which it was deposited may be estimated using the following relationship:

$$(3.4) \quad \Delta\delta^{18}\text{O}_{\text{cc-w}} = \frac{2.78 * 10^6}{T^2} - 2.89$$

(Friedman and O'Neil, 1977)

where $\Delta\delta^{18}\text{O}_{\text{cc-w}}$ - the difference in $\delta^{18}\text{O}$ between calcite and water (‰)
 T - temperature (°K)

For carbonate with $\delta^{18}\text{O} = +8\%$, the isotopic composition of the equilibrium fluid would lie between 0 and +4‰ for this temperature range. This fluid composition is intermediate between that of meteoric water ($-50 < \delta^{18}\text{O} < 0\%$; Taylor, 1967) and one from a metamorphic ($+5 < \delta^{18}\text{O} < +25\%$; *ibid.*) or igneous ($+6 < \delta^{18}\text{O} < +10\%$; *ibid.*) source, and suggests that the fluids present in the shear zones in the late stages of shear zone alteration may have consisted of meteoric fluids

mixed with metamorphic and/or magmatic fluids.

Carbon isotope values from hydrothermal carbonate minerals found in the shear zones range from $^{13}\text{C} = -5.0$ to $+9.0\%$, with most values lying between -4 and -3% . In comparison, Fyon et al. (1983) found carbon isotope compositions of hydrothermal carbonates in 14 deposits near Timmins, Ontario to range from -5.9 to 0% , with a mean $^{13}\text{C}_{\text{PDB}}$ near -3.4% . The hydrothermal fluids which deposited the carbonates had an estimated fluid composition of $^{13}\text{C} = -4$ to -2% (Colvine et al., 1984). Hoefs (1980) showed that ^{13}C of magmatic CO_2 lies between about -7 and -3% , and thus Colvine et al. (1984) argue for a magmatic fluid source for these carbonates.

Because the carbon isotope composition of hydrothermal minerals is dependent not only on the ^{13}C content of the fluid, but also on the fluid's temperature, pH and oxygen fugacity, it is not possible to determine the carbon isotope composition of the fluids from the Mirage Island shear zones. It should be noted however, that the ^{13}C contents of vein carbonates in this study most closely resemble those typically associated with magmatic fluids.

Whole Rock Oxygen Isotopes

The whole rock oxygen isotope values of 10 sheared and 10 unsheared samples are given in Table 3.2. Unsheared mafic rocks (gabbros and basalts) from the Mirage Islands have $\delta^{18}\text{O}$ contents between +5.2 and +5.8‰, and record an increase in $\delta^{18}\text{O}$ into the shear zones by as much as 2.8‰. Sheared metabasites range in $\delta^{18}\text{O}$ from +5.4 to +8.4‰. Unsheared felsic to intermediate samples analyzed range from +7.9 to +8.6‰ in $\delta^{18}\text{O}$. Their sheared counterparts are slightly depleted in ^{18}O , ranging from +5.7 to +7.8‰.

The whole rock $\delta^{18}\text{O}$ values of the unsheared Mirage Island samples were found to lie near the ^{18}O -poor end of the usual range for their unaltered igneous protoliths (Figure 3.3) as defined by Faure, 1977.

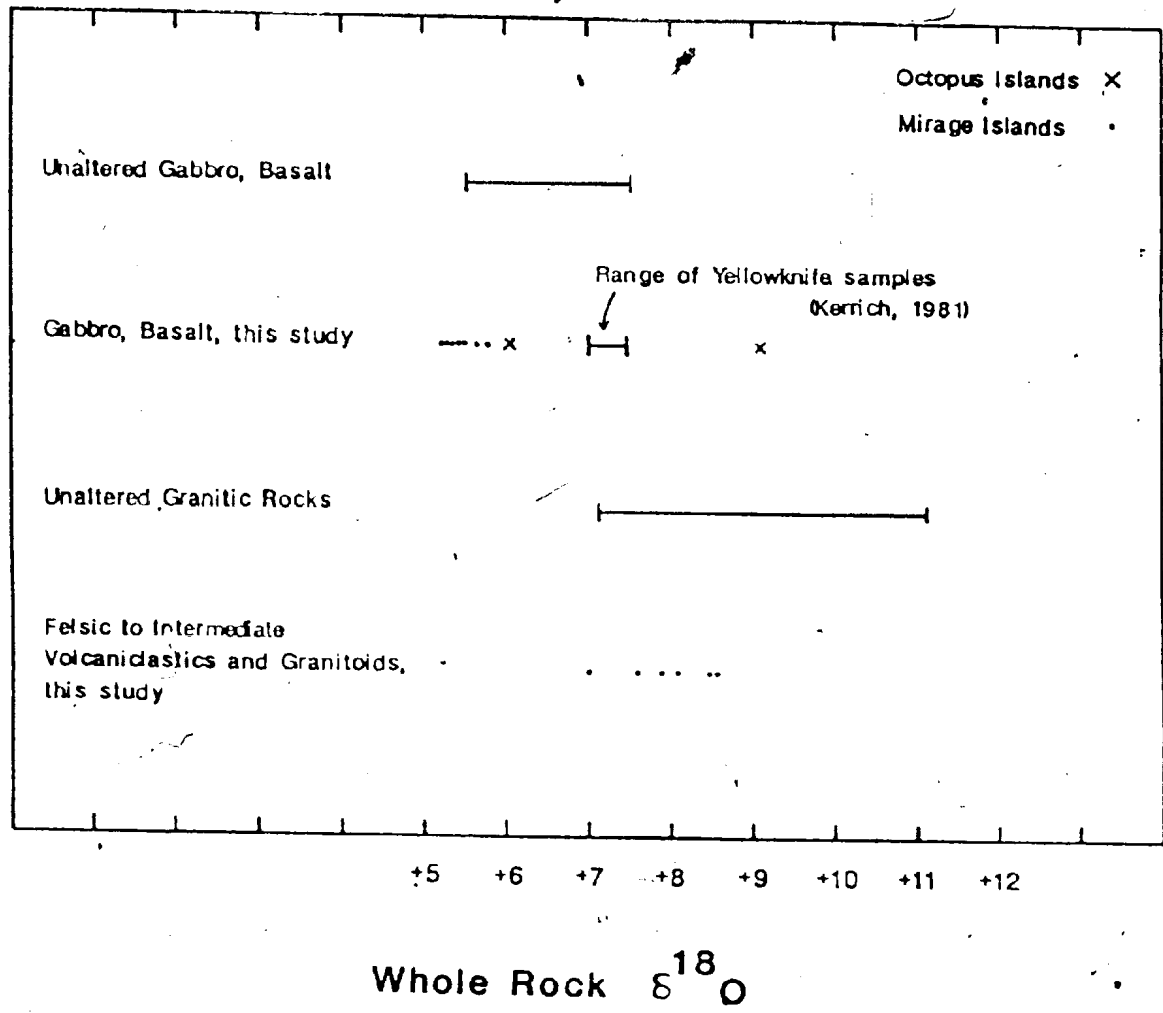
Four metabasite samples were analyzed from the Octopus Islands. The two unsheared samples contain more ^{18}O than the unsheared Mirage Island samples. One of them (CO-22A) is anomalously enriched in ^{18}O (9.1‰). Such high values are usually associated with oxygen exchange between basalt and seawater following deposition at active submarine volcanic centres (Muehlenbachs and Clayton, 1976). The

sheared equivalent of this rock has $\delta^{18}\text{O}$ of 8.8‰, and thus records a small depletion in ^{18}O . The second unsheared Octopus Island sample (CO-23A) lies within the igneous $\delta^{18}\text{O}$ range reported by Faure (1977) for fresh gabbro, and shows an increase in $\delta^{18}\text{O}$ from 6.1 to 6.7‰ into the shear zone.

With the exception of shear zone CO-22 whose protolith is anomalously rich in ^{18}O , all of the shear zones hosted in mafic rocks record an enrichment in ^{18}O compared to their unsheared protoliths. This trend is interpreted to indicate that isotopic exchange took place between the sheared rock and the hydrating fluids, which cooled with time and became progressively depleted in ^{18}O as the hydration reactions progressed. Hydrothermal fluids in the shear zones are estimated to have had $\delta^{18}\text{O}$ contents of +2.8 to +8.3‰. The variable extent of ^{18}O enrichment in the individual shear zones is believed to reflect the different degrees of hydration within them (see Chapter 6, Reaction Progress), and the different temperatures of equilibration.

Kerrick (1981) found that undeformed basalts of the Kam Group near Yellowknife have $\delta^{18}\text{O}$ values of +7 to 7.5‰. He attributed these high values to interaction.

Figure 3.3 Whole rock oxygen isotope compositions of typical unaltered mafic and felsic igneous rocks (after Faure, 1977). The ^{18}O compositions of unshered samples from the Mirage islands (dots) and Octopus Islands (X's) are superposed on the diagram, and they generally plot within the range of their unmetamorphosed equivalents. The range of ^{18}O compositions of unshered basalts from the Yellowknife area (after Kerrich, 1981) are also plotted.



with seawater following extrusion. Sheared mafic schists of the Kam Group show even greater enrichment in ^{18}O , with values near +12%, and the hydrous fluids in these shear zones were estimated to have had $\delta^{18}\text{O}$ values between +7 and +9%. (Kerrick, *ibid.*).

The mean increase of ^{18}O in Yellowknife shear zones is near 5%, while the increase in the Mirage Island shear zones has a mean of about 1%. (Table 3.2). Only two shear zones were analyzed from the Octopus Islands, and one unsheared sample^A was anomalously rich in ^{18}O , thus no meaningful estimate of the mean change in $\delta^{18}\text{O}$ content for these islands was possible. The greater ^{18}O enrichment in shear zones near Yellowknife is likely a result of larger fluid:rock ratios there, which are estimated to be an order of magnitude greater than those for the Mirage Islands (see Chapter 5 for fluid:rock ratios for the Mirage Islands).

The two shear zones cutting tuffaceous sediments (Unit 2) record unexpected results (Table 3.2). The unsheared samples have $\delta^{18}\text{O}$ compositions corresponding to unaltered felsic to intermediate igneous rocks (Figure 4.3), but there is a small decrease in $\delta^{18}\text{O}$ into the shear zones. Assuming that the conditions in these two shear zones were similar to those elsewhere, a greater enrichment of ^{18}O in

Table 3.2 Comparison of the whole rock oxygen isotope compositions of unsheared and sheared samples (with respect to SMOW) for eight shear zones from the Mirage Islands.

$^{18}\text{O} - ^{18}\text{O}_{\text{sheared}} - ^{18}\text{O}_{\text{unsheared}}$.

Wholerock Isotope Values

Sample	Rock type	$\delta^{18}O$ (unsheared)	$\delta^{18}O$ (sheared)	$\Delta\delta^{18}O$ (for shear zone)
--------	-----------	-------------------------------	-----------------------------	--

Mirage Island Samples:

CWM-34A,B	gabbro	+5.5	+6.5	+1.0
CWM-35A,B	gabbro	+5.4	+5.7	+0.3
CWM-145A,B	gabbro	+5.6	+8.4	+2.8
CWM-149A,B	gabbro	+5.4	+6.2	+0.8
CWM-154A,B	mafic flow	+5.3	+5.4	+0.1
CWM-160A,B	gabbro	+5.2	+6.5	+1.2
CWM-155A,B	felsic volcaniclastic	+8.6	+5.7	-2.9
CWM-162A,B	intermediate volcaniclastic	+7.9	+7.8	-0.1

the felsic shear zones than the mafic shear zones would intuitively have been expected, as felsic minerals have a greater tendency to concentrate heavy oxygen (Taylor and Epstein, 1962). Two possible explanations for this anomaly are suggested here: 1) if these two shear zones equilibrated at very high temperatures, (temperature data are not available), then ^{18}O could have fractionated into the fluid phase, thus accounting for the ^{18}O depletion in the sheared rock; or 2) if fluids in these two shear zones were descending and heating (such as would occur if meteoric water contributed to shear zone alteration) then the fluid could have become enriched in ^{18}O at the expense of the altered rock.

Conclusions

Hydrating fluids in the shear zones were at least in part basic, and appear to lie in two distinct populations:

1. high-temperature fluids estimated to have $\delta^{18}\text{O}$ contents between +6.7 and +8.3‰, which are interpreted to have been introduced into the shear zones during M1 metamorphism, and which were derived from either igneous fluids circulating about a crystallizing intrusive body, or from M1 metamorphic reactions likely resulting from heat imposed by the batholith, or both;

2. lower temperature, isotopically lighter (in the range of +2.8 to +6.5‰ ^{18}O) fluids believed to have been produced during M2 metamorphism from dehydration reactions, which subsequently reacted extensively with the wallrock, and became depleted in ^{18}O , or were mixed with meteoric fluids, or both.

With the exception of sample CO-22A, the ^{18}O content of the unshered rocks does not appear to have been affected by sea water alteration or metamorphism. Most of the shear zones show an enrichment in ^{18}O relative to their unshered protoliths, with the extent of enrichment being inversely proportional to the temperature of the fluid.

The variable extent of hydration between different shear zones, the possibility of isotopic exchange after peak metamorphism, and the likelihood of both the temperature and the ^{18}O content of the fluids varying with time all probably contributed to the range of temperature, ^{18}O fluid, and whole rock ^{18}O values within and outside of the shear zones.

Hydrothermal fluids in equilibrium with late cross-

cutting carbonate veinlets were estimated to have $\delta^{18}O$ contents between about 0 and +4‰, based on formation temperatures between 250 and 350°C. From this it is inferred that during the late stages of shear zone alteration, meteoric waters were mixed with either magmatic or metamorphic fluids (or possibly both). Carbon isotope data favour an interpretation involving a magmatic fluid source.

CHAPTER 4: FLUID INCLUSION ANALYSES

Introduction

Fluids trapped during the precipitation of vein minerals are relics of the hydrothermal fluid present during vein formation. An examination of fluid inclusions can therefore yield information about the composition of the hydrothermal fluid and the physical conditions under which the inclusion-bearing mineral was deposited.

Most fluid inclusions are made up of a liquid and a vapour phase at room temperature. Since the presence of different species in solution depresses the freezing point of a fluid by different amounts, a measure of the eutectic point of the fluid will allow qualitative identification of the species dissolved in the fluid. The salinity of the fluid may be estimated as "an equivalent weight percent NaCl, based on the melting temperature of ice in a liquid + vapour inclusion. Some inclusions contain one or more crystal phases[?] as well as liquid and vapour at 25°C. Usually the crystals are a chloride species (halite or sylvite), and can be distinguished optically. Salinity estimates of these inclusions can be made from their solution temperatures.

Fluid inclusions can be heated to determine the temperature at which the liquid and vapour (and solid) phases homogenize. Since it is assumed that the fluid was trapped as a supercritical (one phase) fluid, (Burrus, 1981), the homogenization temperature represents the minimum trapping temperature. If an independent estimate of pressure can be made, the trapping temperature may be calculated (Roedder, 1984). Conversely, given an independent estimate of temperature, the pressure of entrapment can be calculated.

Homogenization temperatures can be determined for all generations of inclusions in a given vein, although generally pressure-temperature work is restricted to primary inclusions, which are those inclusions trapped at the time of vein formation.

Selected samples of quartz veins from within shear zones from the Mirage Islands and Octopus Islands were examined for the presence of fluid inclusions. Analyses of inclusions were carried out to compare the minimum fluid trapping temperatures in the inclusions with the equilibrium temperatures determined by oxygen isotope thermometry and plagioclase-hornblende thermometry.

Analytical Techniques

Fluid inclusions were analyzed using a petrographic microscope equipped with a Fluid Inc. heating/freezing stage. The minimum size of inclusion analyzed was about 10 μm , although freezing and melting phenomena are more easily observed in larger inclusions. Condensation on the objective lens during heating from low temperatures (less than -60°C) occasionally prevented observation of melting temperatures.

Inclusions chosen for analysis were those which texturally appeared to be of possible primary origin. Some of the criteria which are used to identify primary inclusions are the presence of isolated, single inclusions with equant shapes and diameters greater than adjacent (secondary) inclusions, which are randomly distributed in all three dimensions (Roedder, 1984). Because of the planar nature of the samples, determination of the inclusions' distribution in the third dimension was limited by the sample thickness. Low homogenization temperatures of many of the inclusions suggest that they are in fact secondary in origin.

The vein quartz is coarse-grained (3-4mm), with

slightly undulose extinction. Subgrains and finely recrystallized grains are uncommon. Inclusions from strained or recrystallized areas were not examined, since leakage may occur from inclusions in strained grains (Roedder, 1984).

Temperatures measured were found to be reproducible to within about 3 - 4°C. Errors in temperature readings have been calibrated for true values between 60 and 260°C, and extrapolated above 260°C; and from 0 to -80°C (C. Saunders, oral communication, 1987). Between 0 and 60°C errors are less than about 1°C, and so have been ignored. The following linear regression equation was used for temperatures greater than 60°C:

$$T = 3.279 + 0.947 * T_{\text{meas}}, \quad \text{for } T > 60^{\circ}\text{C}. \quad (4.1)$$

(C. Saunders, oral communication, 1987)

Measurement errors on the thermometer have been estimated to be between +/- 1 and +/- 10°C, depending on the rate at which the temperature was increasing or decreasing.

Results

Data on freezing, melting and homogenization temperatures of 118 fluid inclusions are presented in Table 4.1. Homogenization temperatures of the inclusions range from near 12 to 415°C (see Figure 4.1), with a mean in most shear zones between 100 and 200°C. This temperature range suggests that most of the inclusions examined were not primary, but were trapped during cooling of the quartz veins. Of the thirteen quartz veins examined from different shear zones, eight have at least some inclusions with homogenization temperatures of 300°C or more (Figure 4.1). Assuming that the compositions of these high temperature inclusions have not changed since they were initially trapped (e.g. by leaking during subsequent straining of the quartz), the homogenization temperatures represent the minimum trapping temperatures. Based on this assumption, the eight samples bearing inclusions with high homogenization temperatures (>300°C), are interpreted to have been trapped at temperatures approaching the equilibrium temperatures in the shear zones. Although these inclusions may not be primary in origin, they are the oldest inclusions present, and thus they can be used to estimate the minimum pressure conditions in the shear zones following shear zone

Table 4.1 Comparison of the homogenization temperatures, eutectic temperatures and melting temperatures measured on fluid inclusions in quartz veins from shear zones on the Mirage Islands (CWM- samples) and Octopus Islands (CO- samples). The salinity (expressed as an equivalent wt % NaCl) may be estimated from the melting temperature of ice in liquid + vapour inclusions, and from the solution temperature of liquid + vapour + solid inclusions, and the species present in the fluid along with H₂O may be identified using the eutectic temperature of the fluid. Abbreviations used: T_h - homogenization temperature, T_{eu} - eutectic temperature, T_m - melting temperature.

Sample No.	T _h (°C)	T _{eu} (°C)	T _m (°C)	salinity (wt % NaCl)	composition* (+H ₂ O)
CWM-41C	87	-52.8	-22	24	NaCl+CaCl ₂
"	34.8	-52	-22	24	"
"	111	-52.8	-23	24.5	"
"	120	-53	-22.3	24	"
"	35.6		-22.7		CO ₂ +/-H ₂ S +/-SO ₂
"	200	-57.4	-30.1	27	NaCl+CaCl ₂ +MgCl ₂
"	240	-58.7	212	28	halite
"	204				
"	207				
"	183	-46.8	-21.5	23.8	NaCl+KCl +MgCl ₂
CWM-138		-42.1	-23.9	25	NaCl+KCl +MgCl ₂
"	174	-59.4	-17	20.4	NaCl+CaCl ₂ +MgCl ₂
"	189	-59.8	-16.4	20	"
"	200	-59.3	-14.3	17	"
"	204	-59.6	-13.4	16.5	"
"	131	-63.4	-31.2	27.5	
"	229	-42.8	-22	24	NaCl+KCl +MgCl ₂
"	170	-65.7	170	25	halite
"	26	-54.1	-20	22.7	NaCl+CaCl ₂
CWM-143B	189	-48	128	24	halite
"	156	-58.9	-20.4	23	NaCl+CaCl ₂ +MgCl ₂
"	173	-54.6	-18.8	22	NaCl+CaCl ₂
"	78		-47.8		
"	256.3	-58	256.3	29	halite
"	300	-62	195	27	halite
"	178	-68	-16.8	20.4	
"	154	-57	-20.1	22.6	NaCl+CaCl ₂ +MgCl ₂
CWM-145B	222	-26.1	150+/- 214	28	halite
"	229	-24			halite
"	232	-29.5			halite
"	120.5				halite
"	147				
"	129	-52.3			NaCl ₂ +CaCl ₂
"	271	-44.1	271	30.5	halite
"	331	-37.7	170	25	sylvite, halite
"			230		

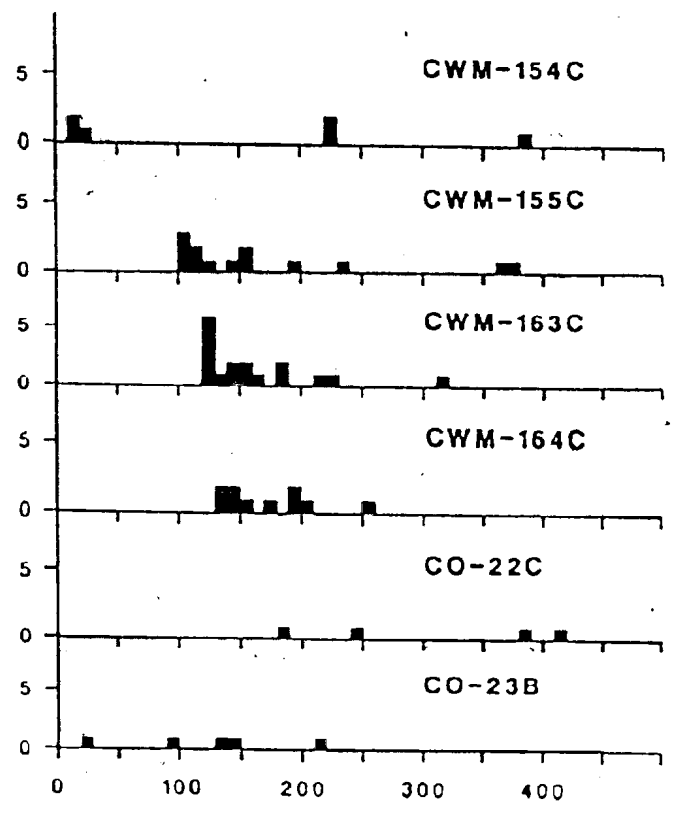
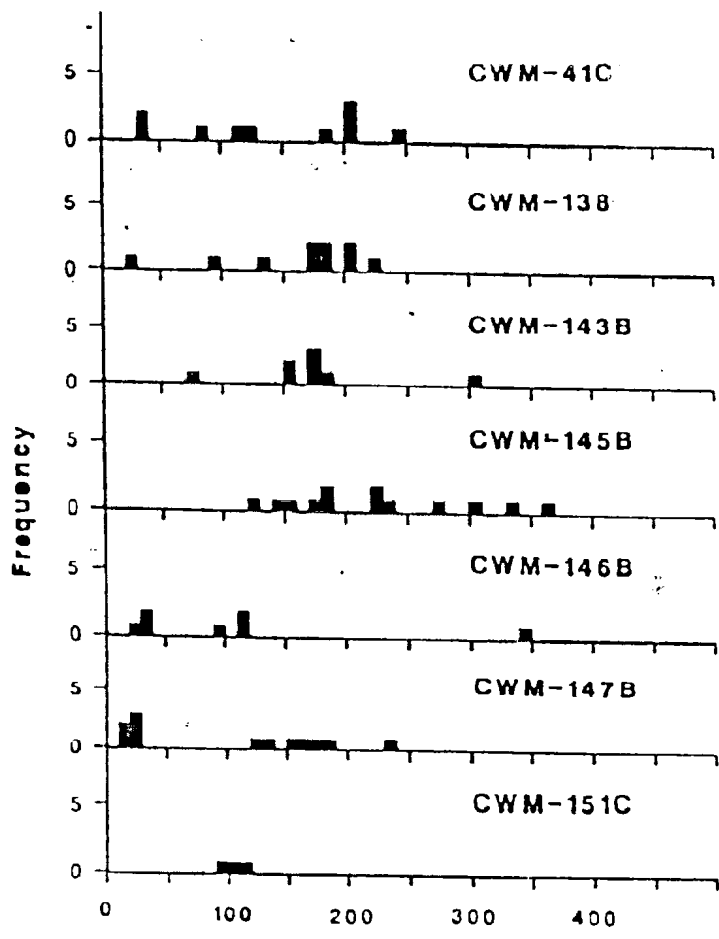
Sample No.	T _h	T _{eu}	T _m	salinity	composition
CWM-145B	364	-34.6	274	30	halite
"	308				
CWM-146B	95	-61.2	-3.2	5.1	NaCl+CaCl ₂ +MgCl ₂
"	117	-50.8	-10		NaCl+CaCl ₂
"	29.5				CO ₂ +?
"	120	-54	-20		NaCl+CaCl ₂
"	30.1	-58.8	-37.1		CO ₂
"	32	-72	-40		CO ₂ (+CH ₄ ?)
"	348		-18	18	
CWM-147B	124.5	-56.8	-24.1	25	NaCl+CaCl ₂ +MgCl ₂
"	154.5	-74.5	71.3	23	halite
"	168.4	-68.2	148	24	"
"	172	-64	130.5	24	"
"	189	-73.6	165	25	"
"	19.2	-48	-20.2		CO ₂ +CH ₄ +H ₂ S
"	20.1	-56	-30		"
"	19.8		-30		CO ₂ +?
"	26.3		-24.9		"
"	21.2	-40.1	30		CO ₂ +CH ₄ +H ₂ S
"	135				
"	232				
CWM-151C	99	-44.7	-14.7	18	NaCl+KCl +MgCl ₂
"	101	-40.1	-14.4	17.5	"
CWM-154C	382	-64.4	360	37	sylvite, halite
"	225	-38	382		NaCl+MgCl ₂
"	225	-46.6	-19.3	22.3	NaCl+KCl +MgCl ₂
"	14	-84	-55.7		CO ₂ +CH ₄
"	28.3	-80.2	-52.8		CO ₂ +CH ₄
"	11.6	-60	-5.7		CO ₂ +CH ₄

Sample No.	T _h	T _{eu}	T _m	salinity	composition*
CWM-155C	238				
"	107				
"	103				
"	128				
"	104				
"	151				
"	194				
"	154	-32.3	154	24	halite
"	140	-50.2	100+/- 140	23.5	sylvite, halite
"	376	-29.3	251	29	halite
"	110	-28.3			halite
"	314	-20.7			NaCl
"	189	-58.2			NaCl+CaCl ₂ +MgCl ₂
"	147	-62.6			
"	152	-60.1			NaCl+CaCl ₂ +MgCl ₂
"	187	-64.5			
"	360	-27.6	209	27.4	halite
CWM-163C	158	-57.8	-33.9	28	NaCl+CaCl ₂ +MgCl ₂
"	163	-55.2	-35.4	29	"
"	129.5	-64.4	-28.2	26.3	"
"	128	-65.5	-29.4	28	
"	220	-66.5			
"	213	-64.3			
"	148.5	-60	-5.7	7.6	NaCl+CaCl ₂ +MgCl ₂
"	131	-45.2	-27.7	27.5	NaCl+KCl +MgCl ₂
"	128	-44	-29.3	28	"
"	126	-52.2	-35.7	29	NaCl+CaCl ₂
"	129	-49.1	-30.1	28	"
"	123	-32			NaCl+MgCl ₂
"	314	-20.7			NaCl
"	189	-58.2			NaCl+CaCl ₂ +MgCl ₂
"	147	-62.6			
"	152	-60.1			NaCl+CaCl ₂ +MgCl ₂
"	187	-64.5			

Sample No.	T _h	T _{eu}	T _m	salinity	composition*
CWM-164B	164	-49.3	164	25	halite
"	305	-55.2	305	31	halite
"	193	-46.2	23	20	halite?
"	306	-46.8	306	31	halite
"	250	-48.6	-26	25.7	NaCl+CaCl ₂
"	150	-77.9	147	24	halite
"	176	-73.5	-35	28.5	
"	152	-78	152	24	halite
"	150	-79.2	100+/- 150	24	sylvite halite
CO22C	244	-65.3	-15.3	19	
"	186	-58.2	-10.6	14.5	NaCl+CaCl ₂ +MgCl ₂
"	415	-38.4	330.4	33	halite
"	386	-44.2	386	33.5	halite
CO23B	219	-54.6	-16.1	19.5	NaCl+CaCl ₂
"	149		-28	26.2	
"	133	-62.7	-26.5	26	
"	93	-46	-20	22.6	
"	29.6	-43	-15		CO ₂ +CH ₄ +H ₂ S

* "Composition" is a qualitative estimate of which phases are present (as chloride complexes) in solution; phases presented as minerals are daughter minerals, identified optically. Inclusions bearing MgCl₂ may also contain FeCl₂; these two species cannot be distinguished by temperature data alone (Crawford, 1981).

Figure 4.1 Histograms of homogenization temperatures of fluid inclusions in quartz veins from selected shear zones on the Mirage Islands (CWM- samples) and Octopus Islands (CO- samples).



Temperature (°C)

equilibration.

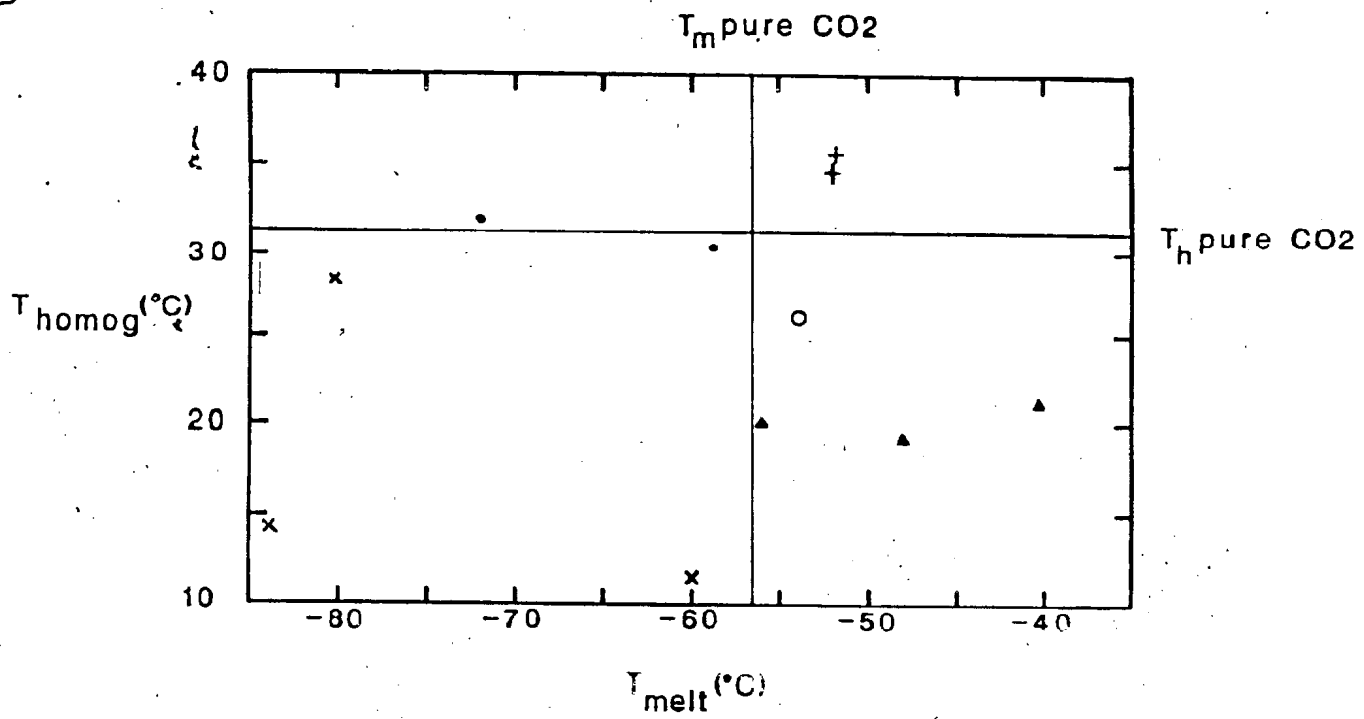
Compositions of Inclusions

It is difficult to determine the composition of inclusions quantitatively with non-destructive techniques. However, using data on freezing and melting temperatures of fluids, it is possible to infer which species, along with H₂O, are most likely to be present in the inclusion.

In Table 4.2, the critical point and triple point temperatures of various pure species are compared (after Burrus, 1981). For example, for a one-component fluid composed of CO₂, the homogenization temperature is 31.1°C, and melting occurs at -56.6°C (Burrus, 1981).

Inclusions which homogenized at temperatures between 11.6 and 32°C are present in a number of samples. Upon further heating they decrepitated. These characteristics suggest that the inclusions contain CO₂ (Burrus, 1981). In Figure 4.2, the homogenization temperature is plotted against the melting temperature of these inclusions. Of the eleven inclusions plotted in Figure 4.2, only one inclusion (in sample CWM-146B) appears to be almost pure CO₂.

Figure 4.2 Homogenization temperature versus melting temperature for CO₂-bearing inclusions. Homogenization temperature and melting temperature of pure CO₂ is indicated on the diagram.



- + CWM-41C
- o CWM-138
- CWM-146B
- ▲ CWM-147B
- x CWM-154C

Table 4.2 Critical point and triple point temperature of various species which are known to occur in fluid inclusions (after Burrus, 1981).

Component	Temperature* (critical point)	Temperature* (triple point)
H ₂ O	374	0.015
CO ₂	31.1	-56.6
SO ₂	157.8	-72.7
H ₂ S	100.4	-85.5
CH ₄	-82.1	-182.5

* temperature in °C

Three CO₂-bearing inclusions present in sample CWM-154C have homogenization and melting temperatures depressed below those of pure CO₂ (Figure 4.2). These fluids probably also contain CH₄, as the melting and homogenization temperatures lie between those of pure CO₂ and pure CH₄ (Table 4.2).

Sample CWM-41C contains two CO₂ inclusions with values of T_h and T_m slightly above those of pure CO₂ (Figure 4.2). The presence of a sulfur-bearing component in the fluid likely caused this increase in temperature (Burrus, 1981), although it is not possible to say whether H₂S or SO₂, or both, is present in the fluid.

The three inclusions studied in sample CWM-147B have homogenization temperatures less than that of CO₂, and melting temperatures greater than that of CO₂. Fluids in these inclusions may contain both CH₄ and a sulfur species - most likely H₂S.

Thus although CO₂ inclusions within any given quartz vein appear to contain the same species, the relative concentrations of the species appear to vary, as indicated by the range in melting and homogenization temperatures. However, this does not necessarily mean that more than one

trapping event of CO₂-rich fluid occurred in each quartz vein. Sterner and Bodnar (1984) and Roedder (1984) have pointed out that inclusions containing variable ratios of two or more end member components can be the result of trapping of a heterogeneous fluid. This may be the case with Mirage Island quartz veins.

Most fluid inclusions examined homogenized at temperatures between 100 and 200°C, and are interpreted to contain saline brines made up of H₂O + NaCl +/- other chlorides. The salinity of the trapped fluids in liquid plus vapor inclusions was calculated from the melting temperature using the following relationship:

$$(4.2) W_s = 1.76958 * \theta - (4.2884 * 10^{-2} * \theta^2) + (5.2778 * 10^{-4} * \theta^3)$$

(Potter et al., 1978),

where W_s = wt % NaCl

θ = melting point depression (°C)

The salinity is expressed as an equivalent weight % NaCl since volumetric data for NaCl-H₂O solutions are well studied, and approximate the behavior of brines bearing CaCl₂, MgCl₂, FeCl₂ and KCl to within about 0.1% (Roedder and Bodnar, 1980). Brines with more than 23.3 wt % sodium chloride are saturated with respect to NaCl (Potter et al., 1978), and yet several of the salinities reported in

Table 4.1 are greater than 24%, and have no daughter crystals present. Thus the main source of error must lie in the measurement of the melting temperature of the fluid inclusions, and the salinities reported therefore are only estimates. Nonetheless, it can be said that many of the liquid + vapor fluid inclusions have high salinities, commonly approaching saturation.

The eutectic temperatures of the fluids were used to identify which species are likely present in the fluids along with H₂O. The eutectic temperatures of saline fluids examined in this study are plotted in Figure 4.3. Crawford (1981) stated that saline inclusions in nature always contain NaCl, and may also contain other chloride species. The known eutectic temperatures of brines containing various chloride species are also plotted in Figure 4.3 (after Crawford, 1981).

Depression of the eutectic temperatures observed in fluid inclusions in this study indicates that few inclusions are simple NaCl brines, but that most contain more than one salt (Figure 4.3). MgCl₂ and FeCl₂ cannot be distinguished by temperature data alone (Crawford, 1981), thus inclusions interpreted to contain MgCl₂ may contain in part (or entirely) FeCl₂.

Figure 4.3 Histogram showing the range of eutectic temperatures found in inclusions in this study. The eutectic temperatures for brines containing various chloride species (after Crawford, 1981) are marked above the graph.



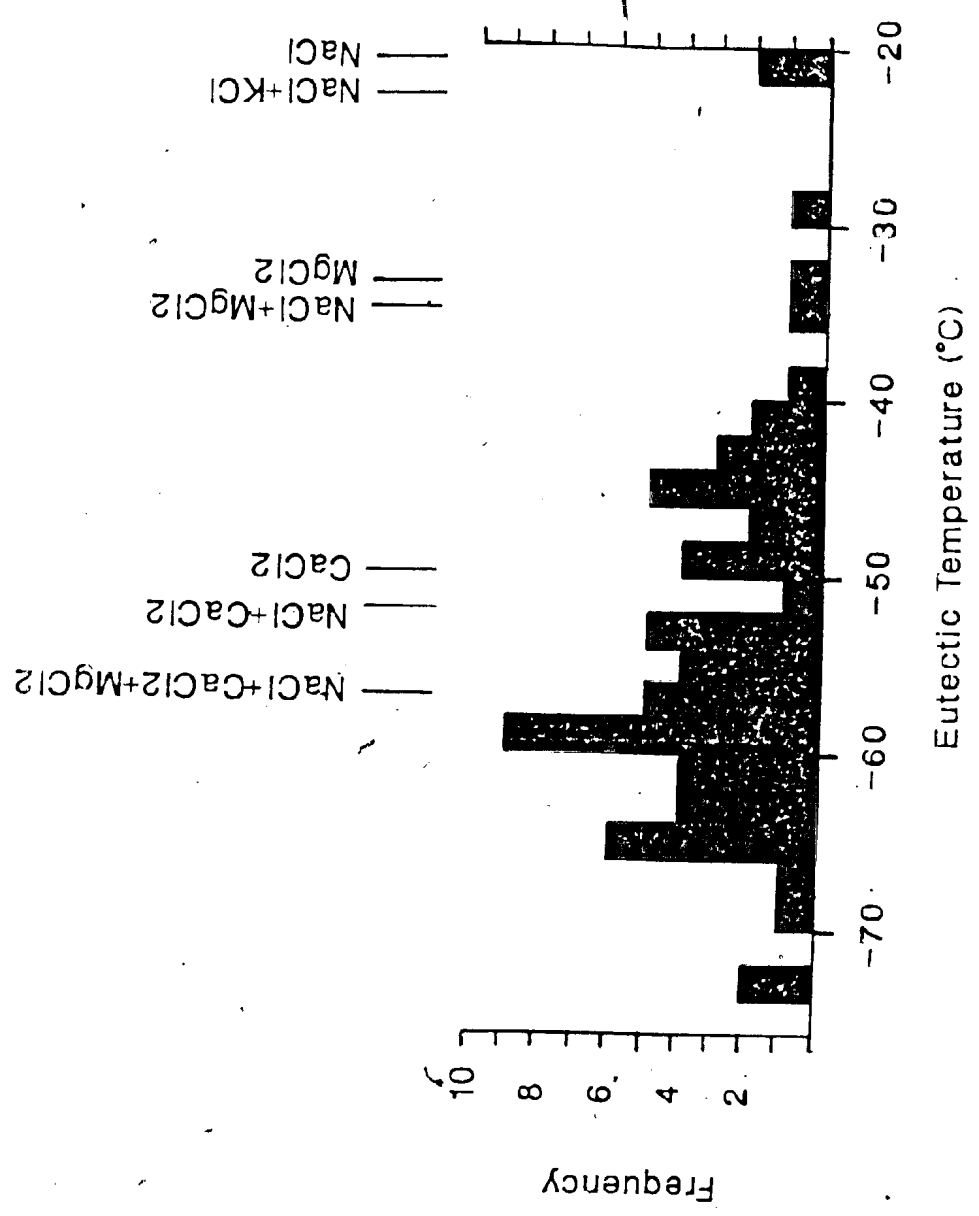


Table 4.1 lists the chloride species present in the fluids, and their salinities (expressed as equivalent wt % NaCl). The presence of iron and magnesium chloride in many of the fluid inclusions is compatible with the basic composition of the sheared rocks, and supports the hypothesis that the hydrothermal fluids were derived - at least in part - from a metamorphic source.

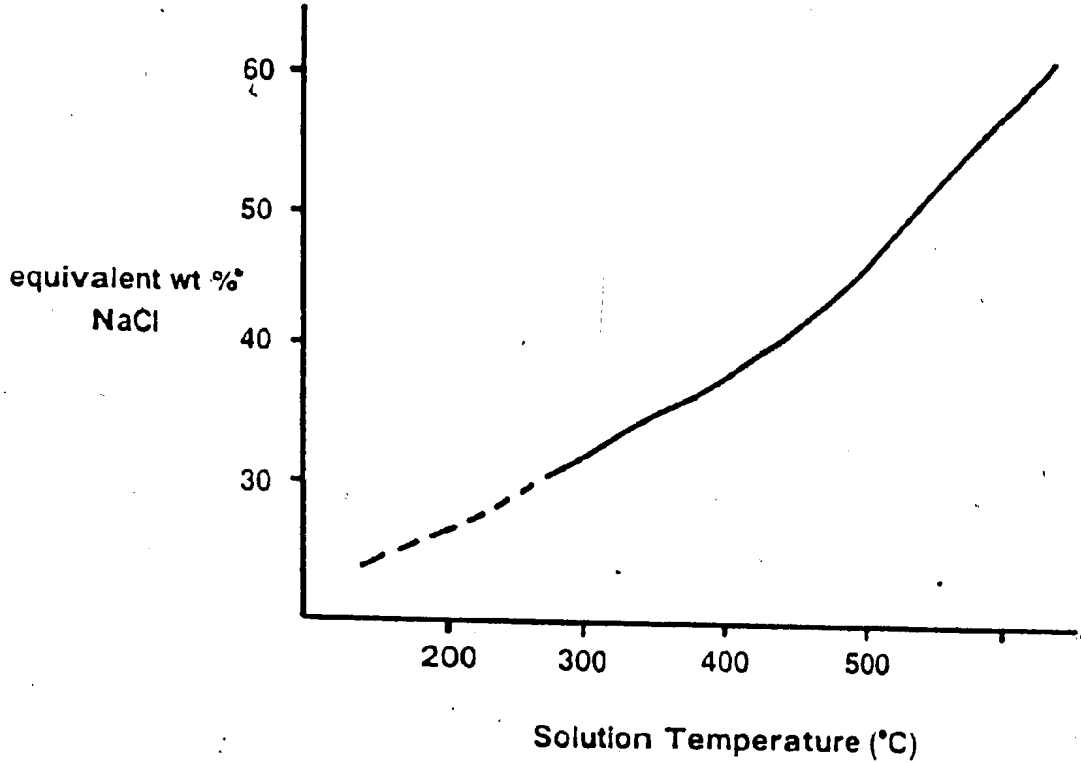
A large number of inclusions was observed which contained one or more cubic crystals, identified as halite, along with a liquid and a gas phase at room temperature. In some quartz veins, the ratio of liquid:gas:solid between inclusions was approximately equal, and it has been assumed that the crystals in them are daughter minerals. The fact that the solid phases within any one quartz vein dissolved at about the same temperature is interpreted to bear out this assumption.

In other quartz veins, the solution temperatures of the crystals are variable between inclusions. This may be interpreted in a number of ways. First of all, these inclusions may represent more than one trapping event, with the solid phases being daughter minerals which have crystallized from different fluids. Secondly, they may have been trapped at the same time from a heterogeneous

fluid, in which case the salinities of the resultant inclusions would be variable, and daughter minerals would precipitate out at more than one temperature. Finally, an original fluid containing a solid phase at the time of entrapment would produce inclusions with a range of salinities. If this is the case, then the NaCl crystals observed at room temperature are not daughter minerals, although some crystalline material present may have precipitated in the inclusions since trapping (Roedder, 1984).

Salinities of inclusions containing solid phases were determined from the homogenization temperatures of the fluids, using Figure 4.4 (Keevil, 1942). Values listed are the salinities of the fluids which, if the crystals are truly daughter minerals and were not trapped as solids, reflect the salinity of the fluid from which the inclusion was derived. Salinities range from 14 to 37 wt % NaCl equivalent. Fluids are composed of $H_2O + NaCl +/- CaCl_2 +/- KCl +/- MgCl_2 (+/- FeCl_2 +/- FeCl_3)$ (see Table 4.1).

Figure 4.4. Salinity (expressed as equivalent wt % NaCl) vs. solution temperature for fluid inclusions bearing daughter minerals (Keevil, 1942).



Thermobarometry

Unless a fluid inclusion can be shown to have been boiling at the time of entrapment, the homogenization temperature will be less than the trapping temperature (Roedder, 1984). Since no evidence was found in this study to suggest that the fluid was boiling (such as variable liquid:gas ratios of several inclusions which homogenize at the same temperature), it is believed that the homogenization temperatures presented in Figure 4.1 are less than the trapping temperatures. With an independent measure of pressure at the time of formation, the actual trapping temperature can be determined. Similarly, an independent estimate of temperature can allow an estimate of the pressure of entrapment.

The assemblage amphibole + plagioclase + epidote + calcite + quartz is preserved in two shear zones, and yields equilibrium pressures of between 2 and 4 kbars using the thermobarometer of Plyusnina (1982) (see Chapter 2). This is the only semiquantitative estimate of pressure obtained in this study, and is not sufficiently accurate to be applied to fluid inclusion data to determine the difference between homogenization and trapping temperatures. However it does give an indication

of the upper limit of trapping pressure of the fluids.

Oxygen isotope thermometry (Chapter 3) has yielded independent estimates of the temperature of formation for the quartz veins in which the fluid inclusions were examined. As these temperatures are not dependent on pressure, uncertainty associated with them is due solely to analytical, experimental and calculation errors. Furthermore, in Chapter 2, Spear's (1980, 1981) geothermometers were applied to sheared samples containing plagioclase and amphibole; these thermometers have only a very small dependence on pressure, and have yielded temperatures which are estimated to be near the maximum temperature occurring in the shear zones.

As noted in Chapter 4, temperatures determined from isotope thermometry cluster in two groups which are interpreted to reflect two thermal events - an amphibolite grade (M1) event with an average temperature near 590°C, and a greenschist grade (M2) event near 420°C. In Table 4.3 homogenization temperatures of the oldest (that is, the highest temperature) inclusions are compared to temperature estimates derived from oxygen isotopes and from plagioclase-hornblende equilibria.

The data have been divided into two groups: those

Table 4.3 Comparison of the homogenization temperature of fluid inclusions to the formation temperature, determined from oxygen isotope thermometry or plagioclase-hornblende thermometry. Given the salinity of the inclusions (from Table 4.1), the maximum formation pressure can be estimated from the difference between the formation temperature and the homogenization temperature. Abbreviations used: T_{hom} - homogenization temperature, T_{fm} - formation temperature, P_{fm} - formation pressure.

Thermal event	Sample no.	max T_{hom} (°C)	T_{fm} (°C)	$T_{\text{fm}} - T_{\text{hom}}$ (°C)	Salinity (wt % NaCl)	P_{fm} (kb)
M1	CWM-143B	300	620*	320	27	>3
	CWM-146B	348	574*	226	21	2.1
	CWM-155C	376	485**	109	29	1.1
	CWM-163C	314	596*	282	>25	3
M2	CWM-145B	364	366*	2	30	0
	CWM-154B	382	454*	72	37	0.75
	CWM-164B	306	352*	47	31	0.6
	CO-22C	415	430*	15	33	0.25

* T_{fm} determined from oxygen isotope thermometry

** T_{fm} determined from plagioclase-hornblende thermometry.

which equilibrated at amphibolite facies (M1) temperatures, and those that equilibrated at greenschist facies (M2) temperature, based on independent thermometers. Homogenization temperatures of inclusions from M2-equilibrated samples are slightly less than the equilibrium temperatures of their host shear zones, with a range in $T_{eqm} - T_{hom}$ from 2 to 72°C (Table 4.3). One of the inclusions in CWM-145B has a homogenization temperature almost identical to the equilibrium temperature of the shear zone from which it was sampled, suggesting that this inclusion was trapped during or immediately following equilibrium in that shear zone. Thus it is possible that this inclusion is primary.

The difference between equilibrium and homogenization temperatures ($T_{eqm} - T_{hom}$) can be used, together with compositional data, to estimate the maximum pressure of entrapment, using Figures 1 to 6 of Potter (1977), which give temperature corrections for different values of T_{hom} at various salinities (see Appendix D). If the inclusions are assumed to be primary, then the pressures represent the trapping pressures of the inclusions formed during vein precipitation. However, if the inclusions are secondary, then the trapping temperature of a given inclusion will be intermediate between the homogenization temperature and the equilibrium temperature of the shear

zone, and thus the trapping pressure estimated from $T_{\text{trap}} - T_{\text{hom}}$ will be lower. Maximum trapping pressures for quartz veins in M2-equilibrated shear zones range from 0 to 0.75 kbar (Table 4.3).

It seems likely that inclusions from the amphibolite facies (M1) shear zones are not primary, since the differences between T_{eqm} and T_{hom} are greater than 100°C. Oxygen isotopes from quartz-chlorite pairs in these veins and the plagioclase-hornblende thermometers of Spear (1980, 1981) yield temperatures indicative of the amphibolite facies (Chapter 3), implying that the veins were deposited during M1. However, the highest homogenization temperatures of the fluid inclusions correspond to greenschist facies temperatures, suggesting that these inclusions were trapped later, possibly during M2.

If an assumption is made that the fluid inclusions from the amphibolite facies shear zones are primary (that is, syn-M1), then the trapping pressures ranged from 1.1 to >3 kbars (Appendix E). If, on the other hand, they were trapped during M2, formation pressures would have been considerably lower. For the latter case, an approximation of maximum trapping pressure can be made using the average M2 temperature of 420°C from isotope

thermometry. $T_{\text{trap-Thom}}$ would then range from 44 to 120°C, and the corresponding pressures would range from 0.5 to 1.25 kbars. Clearly these pressures are approximate, and are only as reliable as the assumption that $T_{\text{trap}} = 420^\circ\text{C}$.

Another method commonly used to determine the temperature and pressure at which an inclusion was trapped is with intersecting isochores (lines of constant density) on a plot of pressure vs. temperature. If two inclusions with different compositions (such as CO_2 and H_2O) are trapped during the same event, then the point of intersection of their isochores will represent the pressure and temperature at the time of their entrapment (Roedder and Bodnar, 1980). This method can only be used if the two inclusions are pure components (ibid.).

Unfortunately this technique cannot be applied to the data from this study because the inclusions are not pure: the lowest salinity reported for an H_2O -rich inclusion is 5.1% NaCl, and only one sample (CWM-147B) appears to contain near-pure CO_2 . Furthermore, there is no evidence that the CO_2 -rich and H_2O -rich inclusions formed simultaneously; in fact, given the range of homogenization temperatures and fluid compositions, there appear to have been several trapping events. Finally, most low-salinity

inclusions have low homogenization temperatures (near 100°C), and since H₂O isochores are close to isothermal (low T/ P) for low values of T_{hom} , the trapping temperatures they would yield must also be fairly low. Therefore these inclusions would not provide information on the pressure and temperature conditions during shearing, but they would estimate the pressure and temperature at the time of their entrapment, following peak thermal conditions.

Discussion

Of the thirteen samples analyzed, eight quartz veins contain inclusions with homogenization temperatures sufficiently high to estimate the maximum pressure conditions in the shear zones during equilibration. Temperature estimates independent of fluid inclusion thermometry are available from oxygen isotope data and plagioclase-hornblende thermometry, and show that the shear zones, like the surrounding unsheared rocks, record two thermal events, M1 and M2.

M2-equilibrated shear zones have inclusions which yield maximum trapping pressures of 0 to 0.75 kbar for trapping temperatures between 350 and 450°C. These pressures would be lower for inclusions trapped after

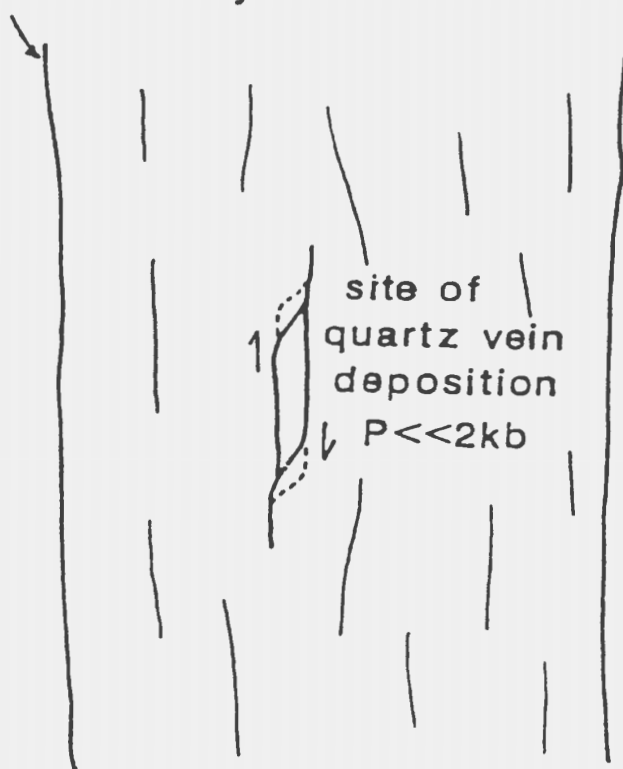
shear zone equilibration. Homogenization temperatures in M1 shear zones suggest that the inclusions are secondary. Assuming trapping temperatures corresponding to M2 conditions, maximum trapping pressures range to about 1.25 kbar.

This range of pressures is considerably lower than the 2 to 4 kbar indicated by Plyusnina's (1982) thermobarometer. However, 2 to 4 kbar is the upper limit of trapping pressures for primary inclusions, and all or most of the high temperature inclusions in this study are secondary inclusions.

Roedder (1984, Figure 9.5) proposed a model in which boiling can occur in a closed fluid-filled vein as a result of faulting. In this model, movement on a fault causes an increase in volume of the contained fluid, thus reducing pressure, and if the critical curve is reached, boiling will occur. Figure 4.5 demonstrates this thesis, for a shear zone in which the "regional" lithostatic pressure is 2 to 4 kbar. Following a component of movement in the shear zone, effective fluid pressure is reduced, resulting in a lowering of the solubility of SiO_2 in the fluid and precipitation of quartz in the shear zone. Primary fluid inclusions trapped during the formation of these quartz veins would have formation

Figure 4.5 Schematic diagram of a shear zone in which localized movement produces a dilatant zone, causing a drop in fluid pressure and the concomitant precipitation of silica. The trapping pressure of primary fluid inclusions in the quartz will thus be lower than the regional pressure of 2 to 4 kbar in the shear zone.

Shear Zone Boundary



pressures considerably lower than the lithostatic pressure in the shear zones. Secondary inclusions could also be trapped in this way, in low pressure zones produced during the straining of the vein resulting from incremental movement along the shear zone.

Shear zones on the Mirage Islands are characterized by strongly schistose zones, locally intruded by anastomosing quartz veins that are subparallel to the shear zone fabric. A process such as that illustrated in Figure 4.5 was probably operative during shear zone formation, with several episodes of movement along the shear zones resulting in a series - through time - of localized low pressure (dilatant) zones into which hydrothermal fluids flowed. Fluids trapped in quartz veins during these events record a range of pressures which are less than the regional greenschist (M2) pressure of approximately 2 to 4 kbar.

A large number of secondary inclusions was examined which have homogenization temperatures between 100 and 200°C. These inclusions contain fluids which were present in the shear zones during their cooling. No systematic relationship between salinity or fluid composition and homogenization temperature of the secondary inclusions was

found. If incremental movements along the shear zones continued during cooling (post-peak-M2), then these secondary inclusions would represent fluid pulses which moved through the shear zones, and were trapped in low pressure zones caused by the movement. The strained state of the quartz attests to movement in some shear zones subsequent to vein deposition.

The composition of the fluids which moved through the shear zones was variable. Most were saline fluids containing $H_2O + NaCl +/- CaCl_2, KCl, MgCl_2$ and/or $FeCl_2$, with salinities ranging from 4.8 to 37 wt % NaCl. Some fluids contained $CO_2 +/- CH_4, SO_2$ and/or H_2S and NaCl.

The compositions of the fluid inclusions suggests that the fluids present in the shear zones following their equilibration were derived - at least in part - from meteoric waters, since ground water typically has a high salinity (Fyfe et al., 1978).

In the previous chapter it was suggested from isotopic evidence that the late hydrothermal fluids may have been the product of a mixed source, composed of meteoric and either metamorphic or magmatic fluids. The composition of a low grade metamorphic brine from a well in the Salton Sea was found to contain significant CO_2 and CH_4 , as well

as H₂S in the gas phase, and >3000 ppm Na, Ca, K, Fe and Cl in the fluid phase (Fyfe et al., 1978). However, CO₂ is also known to be present (in lesser amounts) in fluids derived from a magmatic source (ibid.), and so it is not clear from this line of evidence whether the trapped fluids are a mixture of ground water and metamorphic or magmatic fluids (or both?).

The cations carried in solution were likely derived from the sheared rocks which host the quartz veins. Chemical changes in the shear zones which resulted from reaction with these fluids are discussed in the following chapter.

In general, given the large variation in fluid composition and homogenization temperatures, it appears that there were either several generations of fluid trapped over time, or a number of trapping events occurred (corresponding to incremental movements?) in the presence of an evolving brine following shear zone formation.

CHAPTER 5: SHEAR ZONE GEOCHEMISTRY AND REACTIONS

Introduction

Significant chemical changes commonly accompany hydrothermal alteration and metamorphism in shear zones, resulting in new mineral assemblages, different bulk chemistries, and changes in the oxidation state in the altered rocks (e.g. Kerrich, 1983). In this study, whole rock geochemical analyses were carried out on sheared/unsheared rock pairs, in order to document changes in bulk chemistry across the shear zones. Mineralogical changes in sheared rocks are characterized by balanced reactions.

It was found that, in general, the observed changes in major element abundances may be predicted from mineralogical changes in the shear zones.

Analytical Techniques

Analyses of major elements were done by atomic absorption spectrophotometry on solutions (by G. Andrews), and trace elements were analyzed by X-ray fluorescence on pressed powder pellets (by G. Viennott). Errors on major element analyses are estimated to be +/- 2% of the

reported values, and for trace elements errors are about +/- 5%. The data are presented in Appendix E.

In the following sections, the "protolith" of a sheared rock refers to a metamorphosed, lithologically equivalent rock outside of the shear zone.

Calculations and Results

Bulk Chemistry

Gresens (1967) has shown that in order to quantify the net chemical changes between any two rocks, one variable has to be assumed to be constant. This can be any element, or a parameter such as mass, volume or density. Considering the extent of hydration in the Mirage Island shear zones, it is unlikely that volume or mass remained unchanged during alteration. However, an assumption of constant Al has been made, which is qualitatively supported by the fact that the magnitude of the change in Al concentration between sheared and unsheared pairs is generally smaller than that of other elements. Most sheared samples show a change of 10% or less (1.5 wt % or less) in Al_2O_3 relative to their protoliths. In a few cases, the change in concentration of Al is significant (near 30%, or 5 wt %), but Al_2O_3 was still used as the

invariable parameter, in order to compare results between shear zones. Thus even if the assumption that Al_2O_3 was immobile during alteration is incorrect in some cases, it is still valid since it allows a comparison between shear zones of the changes in abundances of other elements relative to Al.

Grant (1986) devised a graphical means of determining relative gains and losses of material in an altered rock, which is simpler and more convenient to use than the equations of Gresens (1967). To use Grant's (1986) technique, the concentration of a given element in the unaltered rock is plotted on the horizontal axis, and its concentration in the altered rock is plotted on the vertical axis. All elements are plotted this way, then an isocon is drawn from the origin through the element whose concentration is assumed to have been unchanged during alteration. These diagrams can also be used for constant volume or constant mass alteration.

In interpreting the diagrams, all elements which lie on the isocon have maintained a constant concentration during alteration; those lying below the isocon were depleted during alteration, whereas those above the isocon were enriched. The amount by which an element is enriched or depleted is determined as the percent (positive or

negative) with respect to its concentration in the protolith by projection onto a vertical line that intersects the isocon at zero (see Figure 5.1).

Isocon diagrams were made for every sheared/unsheared pair analyzed from the Mirage Islands. An example is given in Figure 5.1 and the rest are presented in Appendix F.

The results determined using the isocon technique are assembled by element for shear zones in metabasic rocks (mainly sheared gabbros, Figure 5.2), and in felsic to intermediate volcanoclastic rocks (Figure 5.3). A number of patterns emerge.

In the metabasic rocks, all of the shear zones are predictably enriched in volatiles, most by more than 100%. Potassium and rubidium share similar trends: shear zones enriched in K are generally also enriched in Rb, and vice versa. Overall these two elements show the greatest amount of change, with a net increase within the sheared mafic rocks locally as high as 500%, and commonly greater than 50%. Calcium and strontium show a similar interdependence and are depleted in most shear zones, in places by more than 90%. The net depletion of calcium in

Figure 5.1 Isocon diagram for shear zone CWM-34. The concentrations of every element (multiplied by a factor to produce a value between 0 and 30, where necessary) in the unsheared sample (horizontal axis) and the sheared sample (vertical axis) are plotted on the graph. The isocon is a line from the origin through some element whose concentration is assumed to have remained constant during alteration, in this case Al. All other elements, when projected on to the vertical construction line on the right hand side of the figure, lie above the isocon (indicating that they were enriched during alteration); or below the isocon (indicating that they were depleted during alteration).

The vertical construction line may be scaled below the isocon from 0% to -100% at the point where it intersects the horizontal axis (where the concentration of an element in the altered sample = 0), and from 0% to infinity above the isocon, and then the magnitude of enrichment or depletion of the mobile elements can be read directly off the diagram.

LOI (loss on ignition) indicates the volatile content of the rock.

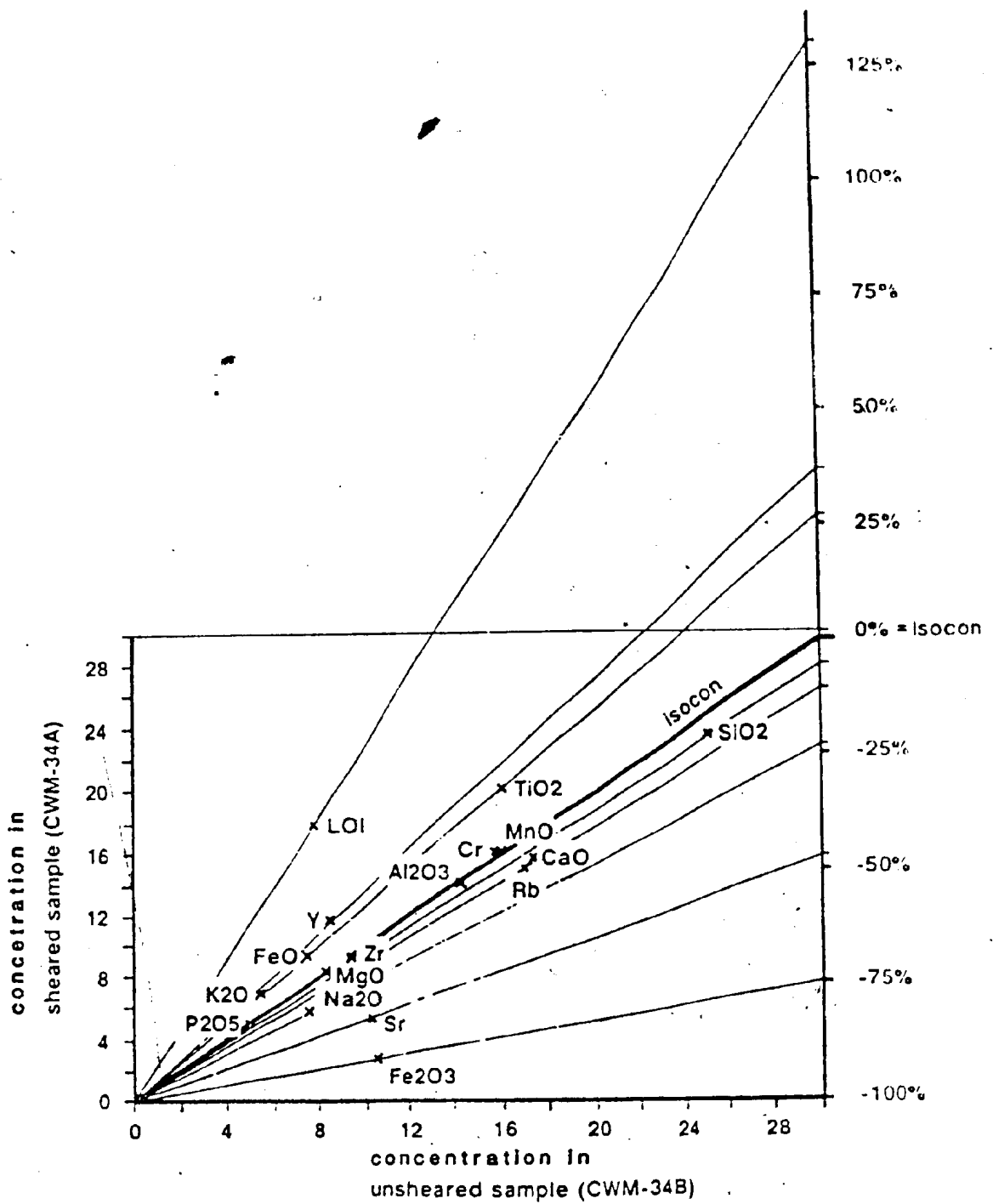
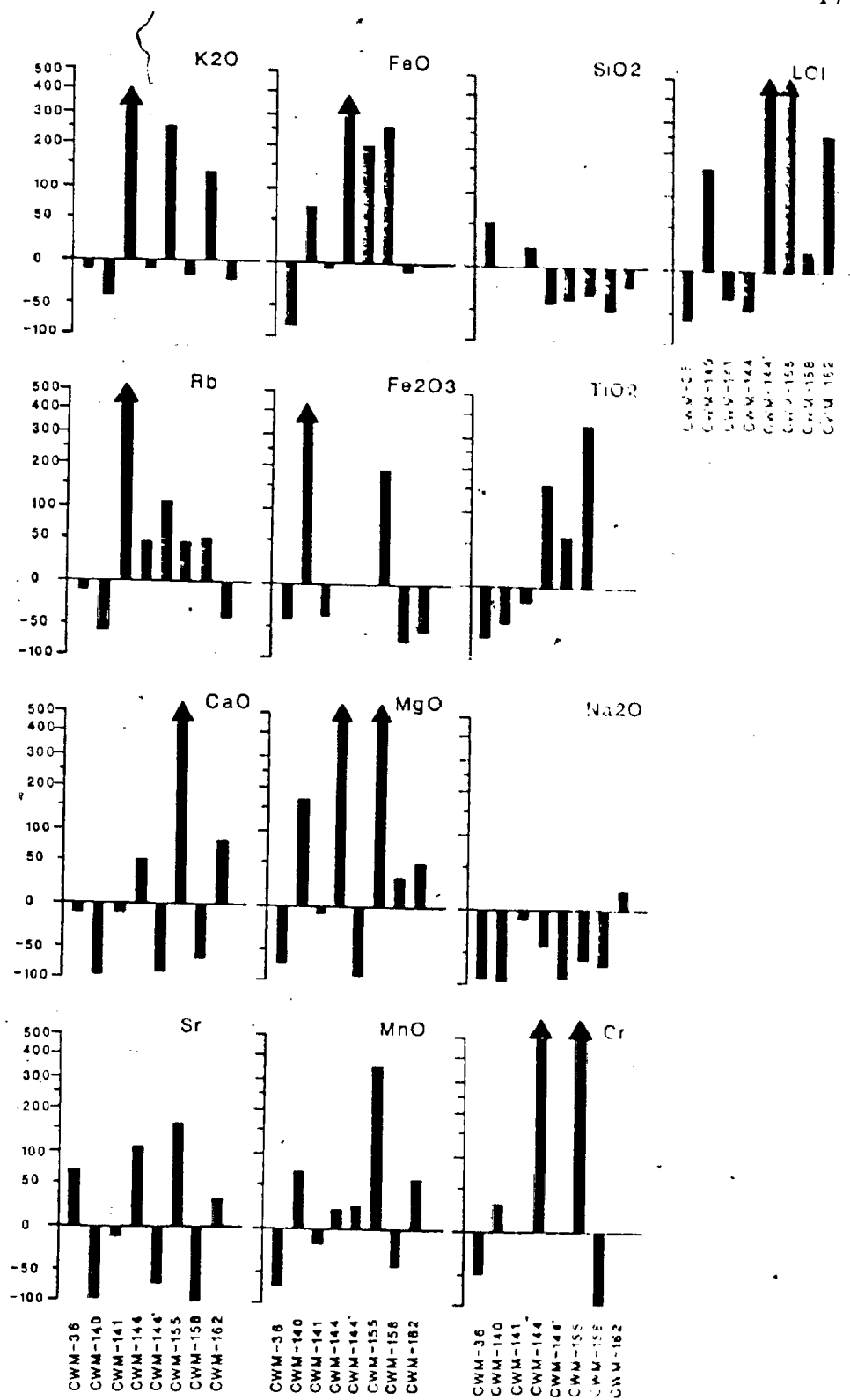


Figure 5.2 Graphs showing the gains (positive) or losses (negative) of various elements in each shear zone hosted in metabasic rocks, measured as a percent relative to the equivalent rock outside of the shear zone.

Figure 5.3 Graphs showing the gains (positive) or losses (negative) of various elements in each shear zone hosted in felsic to intermediate volcanoclastic rocks, measured as a percent relative to the equivalent rock outside of the shear zone.

Percent enrichment/depletion in shear zones



Sample Number

the sheared rocks is in accord with the change in plagioclase composition noted in Chapter 2 in which labradorite is replaced by albite in the shear zones. The calcium, liberated by the reaction must have been flushed from the system.

In the sheared rocks, total iron content generally shows a slight increase over the unsheared protolith (Figure 5.2), with a net increase in the amount of ferrous iron, and a net decrease in ferric iron. Thus most sheared rocks record a reduction of iron with respect to their protoliths. However, there are a few exceptions, and some shear zones were oxidized during alteration.

Magnesium and manganese display variable trends in the shear zones. Of the 21 shear zones analyzed, MgO is depleted in 7; enriched in 10; and remains approximately constant in 4. MnO is depleted in 11; enriched in 7; and is unchanged in 3. This is interpreted to indicate that MgO and MnO were mobile during shearing, although on a "regional" scale (encompassing all of the shear zones), the chemical system was approximately closed with respect to both elements.

Most sheared samples show little change in the silica


content. Ten shear zones are depleted in SiO_2 , 8 are enriched, and 3 remained constant. One shear zone (CWM-145) records a large increase in SiO_2 content; more than 500%. Although care was taken to select sheared samples which did not contain quartz veins, this significant enrichment in silica suggests that there was a quartz vein present in this sample.

Titanium and chromium each have apparently random chemical trends, with no consistent sense of enrichment or depletion. The magnitude of the change in concentration of these elements can be quite large. Locally TiO_2 is enriched by more than 100%; elsewhere it is depleted by more than 70%, while Cr enrichment can exceed 200% and depletion approaches 100% in places. However, the net change in concentration may only be on the order of a few parts per million, since these elements are present in trace amounts.

Sodium concentration shows an overall decrease in the shear zones. Although it is consumed by the formation of albite, more sodium is released during shear zone alteration than is used up, resulting in a net depletion in sodium. Mineral reactions are presented in the following section.

Kerrick (1983) also compiled chemical data for sheared metabasites from the Campbell and Con shear zones at Yellowknife. The Yellowknife shear zones, like those on the Mirage Islands, record a consistent enrichment in K and Rb, and a depletion in Na. Generally, more silica was deposited in the Yellowknife shear zones, probably because of lower equilibrium temperatures in the Yellowknife area (320 - 480°C; Kerrich, 1983) than in the Mirage Islands (360 to 600°C, this study), and thus silica solubility was lower near Yellowknife. Mg, Ca, Sr and Cr display similar chemical trends in the Yellowknife shear zones: with increasing intensity of alteration, these elements were initially depleted then subsequently enriched in the shear zones (Kerrick, 1983). In contrast, in the Mirage Island shear zones, Ca and Sr are consistently depleted and Mg and Cr behave variably. Ferric iron in the Campbell and Con shear zones is slightly enriched, whereas it is depleted in the Mirage Islands. Trends of ferrous iron were not presented by Kerrich (1983).

Changes in the concentrations of elements in sheared felsic to intermediate volcanogenic clastic rocks from the Mirage Islands are presented in Figure 5.3. Although volatiles show an overall enrichment in the shear zones, three samples (CWM-36, CWM-141, and CWM-144) record a net depletion. In Chapter 2 it was shown that the common



mineral assemblage of the fine-grained volcanoclastic rocks is quartz, feldspar, muscovite, biotite and chlorite; indicative of greenschist facies metamorphism. It appears likely that the anisotropy (bedding) of these rocks aided in hydration during M2, and so M1 (amphibolite facies) assemblages were only rarely preserved. The amphibolite facies assemblage of these rocks would have been quartz + feldspar + muscovite + biotite +/- an amphibole; the lack of chlorite being the distinguishing feature from the greenschist facies assemblage. Therefore, even if this assemblage was flushed through with large volumes of fluid, only a small amount of H₂O and CO₂ could be accommodated in the new mineral assemblage.

In shear zones in felsic rocks which record significant increases in volatile content, either biotite and/or amphibole were replaced by chlorite and/or biotite, or the modal abundance of micas increased significantly in the shear zone. However, where unsheared assemblages did not have the appropriate bulk composition to produce chlorite, very little change in volatile content occurred. If the protolith was a greenschist facies assemblage, a significant enrichment in water content would be unlikely. Perhaps the apparent dehydration of three of the sheared rocks is a function of sampling. As

these rocks are compositionally layered, if the sheared sample contained less mica and chlorite than the unsheared sample, an apparent reduction in H₂O content would be observed. Figure 5.3 indicates that volatiles were mobile during shearing, and regionally they are clearly enriched in the shear zones.

As in the sheared mafic rocks, K and Rb share similar trends and are, overall, enriched in the shear zones. Ca and Sr are also interdependent and show no apparent regional change, although their concentrations are quite variable between shear zones.

The patterns for iron are similar to those in the sheared metabasites - a net increase in total iron occurs, with ferrous iron enriched more than ferric iron, except in two shear zones (CWM-36 and CWM-140). Mg and Mn are enriched regionally, although of the 8 shear zones examined, 3 are depleted in MgO and 3 in MnO.

Silica is depleted in 5 of the 8 shear zones, and enriched in 2. Of the 3 shear zones depleted in volatiles, 2 are enriched in silica. This may indicate an increase in modal quartz and a concomitant decrease in mica content in these 2 shear zones, explaining the decrease in H₂O content, as described above.

Ti and Cr show no significant regional changes in concentration. Titanium content is increased in 3 shear zones, decreased in 3, and remained constant in 2. Chromium is increased in 3, decreased in 2, and is unchanged in 3.

Finally, Na in sheared felsic to intermediate volcanics is depleted in every shear zone but one, indicating a net regional depletion in sodium.

Generalizing on a regional scale, the shear zones have acted as approximately closed chemical systems with respect to magnesium, manganese, silica, titanium and chromium; and as open systems with respect to potassium, rubidium, calcium, strontium, iron, sodium and volatiles. The shear zones are enriched in potassium, rubidium, ferrous iron, and volatiles, and depleted in calcium, strontium, ferric iron and sodium.

Mineral Reactions

In this section, balanced reactions are presented in order to characterize the mineralogical changes that are observed in the shear zones. For a given reaction the modes of mineral phases in 100 cm³ of rock were determined

by point counting (1000 points), and the modes were converted to molar quantities (see Appendix G).

The reactants in a given equation are the minerals in the unsheared protolith; the products are the minerals in the sheared sample. Where a given phase occurs on both sides of a reaction and its composition is nearly the same, the difference between its abundance in the reactants and products is presented on one side of the equation, for simplicity. The compositions of amphiboles, chlorites and plagioclases were determined by microprobe analysis (see Appendix A), whereas those of sericite and epidote have been taken as the ideal end member compositions (sericite = $K_2Al_4Si_6Al_2O_{20}(OH)_4$, and epidote = $Ca_2Fe^{3+}Al_2OSi_3O_{11}(OH)$). Since biotite grains were too small to analyze with the microprobe, their formula was approximated as $K_2(Fe,Mg)_6Si_6Al_2O_{20}(OH)_4$. Fe:Mg ratios in biotites were assumed to be the same as Fe:Mg ratios in coexisting chlorite and/or amphibole. As in the previous section, Al is assumed to have remained constant during alteration, and thus the net chemical changes predicted by these reactions are relative to Al.

When the reactions were balanced for alumina, it was found that they did not balance for other elements. Cations were added (as oxides) on either side of the

equation as needed to balance the reactions, thereby providing a semi-quantitative estimate of the bulk chemical changes in a given shear zone. The cations are assumed to have been carried by the hydrothermal fluids which moved through the shear zones.

A sample reaction for a sheared gabbro is presented below. With the exception of a few elements, this balanced reaction predicts the behavior of the major elements successfully. Although the mobile elements are presented as oxides, they may in fact have been transported as complexes with other anions besides oxygen. This is discussed further in the following section.

(R5.1) CWM-142A to CWM-142B

.251(Ca_{.53}Na_{.45}Al_{1.53}Si_{2.46}O₈) + .052(Ca₂Fe⁺³Al₂OSi₃O₁₁OH)
(plagioclase) (epidote)

+ .171(K_{.03}(Ca_{1.80}Na_{.17})Fe_{1.68}Mg_{2.54}Mn_{.03}Fe_{.54}Al_{.14})
(actinolitic hornblende) (Si_{7.40}Al_{.60})O₂₂(OH)₂

+ (.017K₂O + .304FeO + .003MgO + .641H₂O + .056CO₂ +
.010SO₂)

(FLUID)

.100(Fe_{5.09}Mg_{3.99}Mn_{.03}Fe_{.08}Al_{2.62}(Si_{5.60}Al_{2.40})O₂₀(OH)₁₆)
(chlorite)

+ .074(Ca_{.06}Na_{.96}Al_{.99}Si_{2.99}O₈) + .328(SiO₂) +
(plagioclase) (quartz)

+ .005(FeS₂) + .056(CaCO₃) + .020(K₂Fe₄Mg₂Al₂Si₆O₂₀(OH)₄)
(pyrite) (calcite) (biotite)

+ (.036Na₂O + .485CaO + .068Fe₂O₃ + .002 MnO + .813SiO₂)

(FLUID)

In order to balance this reaction, K₂O, FeO, H₂O, CO₂, SO₂ and trace amounts of MgO are required as reactants, and Na₂O, CaO, Fe₂O₃, SiO₂ and minor MnO are required as products. Comparing these results with those of Figure 5.2, it can be seen that this reaction predicts the sense of movement (into or out of the shear zone) of most elements correctly, although the magnitudes of the

enrichments and depletions do not correlate well.

It is interesting to note that although the sodium content of plagioclase is increased in the shear zone (from labradorite to albite), the net sodium content of the sheared rock is less than its protolith. This is because more sodium was incorporated in the amphibole in the protolith than was required in albite in the sheared rock. Furthermore, there is a decrease in abundance of feldspar from 25% (modal) in the protolith to 19% in the altered rock from the shear zone.

From reaction R5.1 it can be seen that .641 moles of H₂O and .056 moles of CO₂ are consumed in producing the sheared mineral assemblage. Given a molar mass of water of 18.015 g/mol, and a specific volume near 1.3 cm³/g at the temperature and pressure of shearing (Fyfe, et al., 1978); and a mass of CO₂ of 12.011 g/mol and specific volume of 1250cm³/g (CRC Manual, 1983), this corresponds to 15 cm³ of H₂O and 840 cm³ of CO₂; or a minimum fluid:rock volume ratio of about 10:1. Note that this ratio is only an approximation, since it was calculated from volumetric data on pure H₂O and CO₂. Reaction R5.1 indicates that the fluid was not a pure H₂O-CO₂ mixture, but that several cations were dissolved in it. Given an average salinity of H₂O between 20 and 25 wt % NaCl

(indicated from fluid inclusion data), the specific volume of the fluid would be lower than pure H₂O for the same pressure and temperature conditions. Furthermore, it was concluded in the previous chapter that CO₂-bearing fluid inclusions were not pure CO₂, but contained CH₄ and locally H₂S, in unspecified quantities. The specific volume of an impure CO₂-rich fluid is different than that of pure CO₂.

It is not possible to calculate the exact fluid:rock ratio predicted by R5.1, since the true composition - and hence the physical properties - of the fluid is not known. However, the effect that impurities in H₂O and CO₂ would have on the final fluid:rock ratio, is negligible relative to the errors inherent in the assumption that a calculation of the volume of fluid which has reacted with 100 cm³ of rock, is representative of the fluid:rock volume ratio over the entire shear zone. Thus these values are only valid as indicators of the order of magnitude of fluid:rock ratios. It is interesting to note that the fluid:rock ratio calculated for R5.1 is an order of magnitude less than that calculated for shear zones at Yellowknife by Kerrich *et al.* (1977).

Fyfe, *et al.* (1978) reported concentrations of 54,000 ppm Na, 23,800 ppm K, 40,000 ppm Ca, and Si and Fe

concentrations on the order of .5 wt % in metamorphic waters. If the hydrothermal fluids in the Mirage Islands were of metamorphic origin and had compositions comparable to those reported by Fyfe et al. (1978), then a fluid:rock ratio on the order of 10:1 would be sufficient to produce the changes in element concentrations predicted by R5.1, assuming saturation of the elements and an efficient chemical system. The concentrations of species present in groundwater are of the same order of magnitude as metamorphic fluids (*ibid.*), and so similar fluid:rock ratios could be expected to produce the same chemical changes. On the other hand, the concentrations of these elements in igneous fluids are, on average, an order of magnitude or more lower (*ibid.*), and therefore the chemical changes would require a fluid:rock ratio on the order of 100:1 if the fluids in the shear zones were "typical" igneous fluids.

A total of eight balanced reactions were calculated for shear zones hosted in metabasic rocks. They are presented below, and the mineral compositions are presented in Appendix A. Table 5.1 and Figure 5.4 show the amounts of each major element predicted to be consumed or released by each reaction.

(R5.2) CWM-34A to CWM-34B

.312 (An₁₇) + .300 cpx + .060 hble + .114 ep + .021 py +
 (.018K₂O + .203FeO + .001MgO + .003MnO + .640H₂O +
 .186CO₂) - .402 qtz + .186 cc + .102 (An₀₄) + .089 chlor
 + .010 bio + .010 ser + (.091Na₂O + .355CaO + .077Fe₂O₃ +
 .944SiO₂ + .042SO₂)

(R5.3) CWM-35A to CWM-35B

.081 actin + .289 (An₅₆) + .277 cpx + .14 ep + .008 bio +
 .071 py + (.005Na₂O + .008K₂O + .162FeO + .119MgO +
 .003MnO + .823H₂O + .135CO₂) - .124 chlor + .154 (An₀₄)
 + .135 cc + .078 qtz + .001 ser + (.593GaO + .073Fe₂O₃ +
 .130SiO₂ + .142SO₂)

(R5.4) CWM-41A to CWM-41B

.159 actin + .240 (An₁₂) + .123 qtz + .006 ep + .011 cc +
 .009 bio + (.103FeO + .419H₂O + .148SO₂) - .073 chlor +
 .056 (An₀₀) + .007 ser + .074 py + (.085Na₂O + .004K₂O +
 .360CaO + .142MgO + .001MnO + .051Fe₂O₃ + 1.389SiO₂ +
 .011CO₂)

(R5.5) CWM-141A to CWM-141B

.284 (An₆₁) + .081 act-hble + .058 ep + .008 ser +
 (.042Na₂O + .640FeO + .135MgO + .001MnO + .385SiO₂ +
 .053TiO₂ + .589H₂O + .268CO₂ + .586SO₂) - .088 chlor +
 .780 qtz + .187 (An₀₃) + .003 bio + .268 cc + .296 py +
 .059 sph + (.006K₂O + .111CaO + .047Fe₂O₃)

(R5.6) CWM-142A to CWM-142B

.251 (An₅₄) + .171 act-hble + .052 ep + (.017K₂O + .304FeO
 + .003MgO + .641H₂O + .056CO₂ + .010SO₂) - .100 chlor +
 .074 (An₀₆) + .328 qtz + .056 cc + .020 bio + .005 py +
 (.036Na₂O + .485CaO + .068Fe₂O₃ + .002MnO + .813SiO₂)

(R5.7) CWM-149A to CWM-149B

.227 (An₁₁) + .204 hble + .032 ep + (.274FeO + .193MgO +
 .821H₂O + .177CO₂ + .044SO₂) - .130 chlor + .392 qtz +
 .177 cc + .002 (An₀₂) + .022 py + .0004 bio + (.129Na₂O +
 .006K₂O + .271CaO + .077Fe₂O₃ + .001MnO + 1.030SiO₂)

(R5.8) CWM-160A to CWM-160B

.149 hble + .125 (An₆₀) + .026 ep + .014 ser + .054 py +
 (.348FeO + .214MgO + .003MnO + .098H₂O + .871CO₂) - .131
 chlor + .125 (An₀₅) + .323 qtz + .006 bio + .098 cc +
 (.017Na₂O + .009K₂O + .435CaO + .047Fe₂O₃ + .567SiO₂ +
 .108SO₂)

RS.9) CWM-163A to CWM-163B

.265 (An₀₄) + .082 act-hble + .045 ep + (.042K₂O + .171FeO
 + .006Fe₂O₃ + .239H₂O + .029CO₂ + .034SO₂) - .033 chlor
 + .081 (An₀₀) + .290 qtz + .029 cc + .041 bio + .017 py +
 (.092Na₂O + .224CaO + .084MgO + .002MnO + .009TiO₂ +
 .649SiO₂)

where An = anorthite content of plagioclase, hble = hornblende, actin = actinolite, act-hble = actinolitic hornblende, cpx = clinopyroxene, ep = epidote, chlor = chlorite, qtz = quartz, bio = biotite, cc = calcite, py = pyrite, sph = sphene

The chemical changes predicted by these reactions (listed in Table 5.1 and shown in Figure 5.4), agree quite well with the measured whole rock chemical changes (Figure 5.2). Overall, ferrous iron, volatiles, potassium, magnesium and manganese are consumed in the shear zones, and sodium, calcium, ferric iron and silica are released. Calculations of minimum fluid:rock volume ratios for these reactions have been made based on the volume of volatiles consumed in the reactions, and are included in Table 5.1. The calculated ratios range from 4:1 to 130:1 in the metabasic rocks.

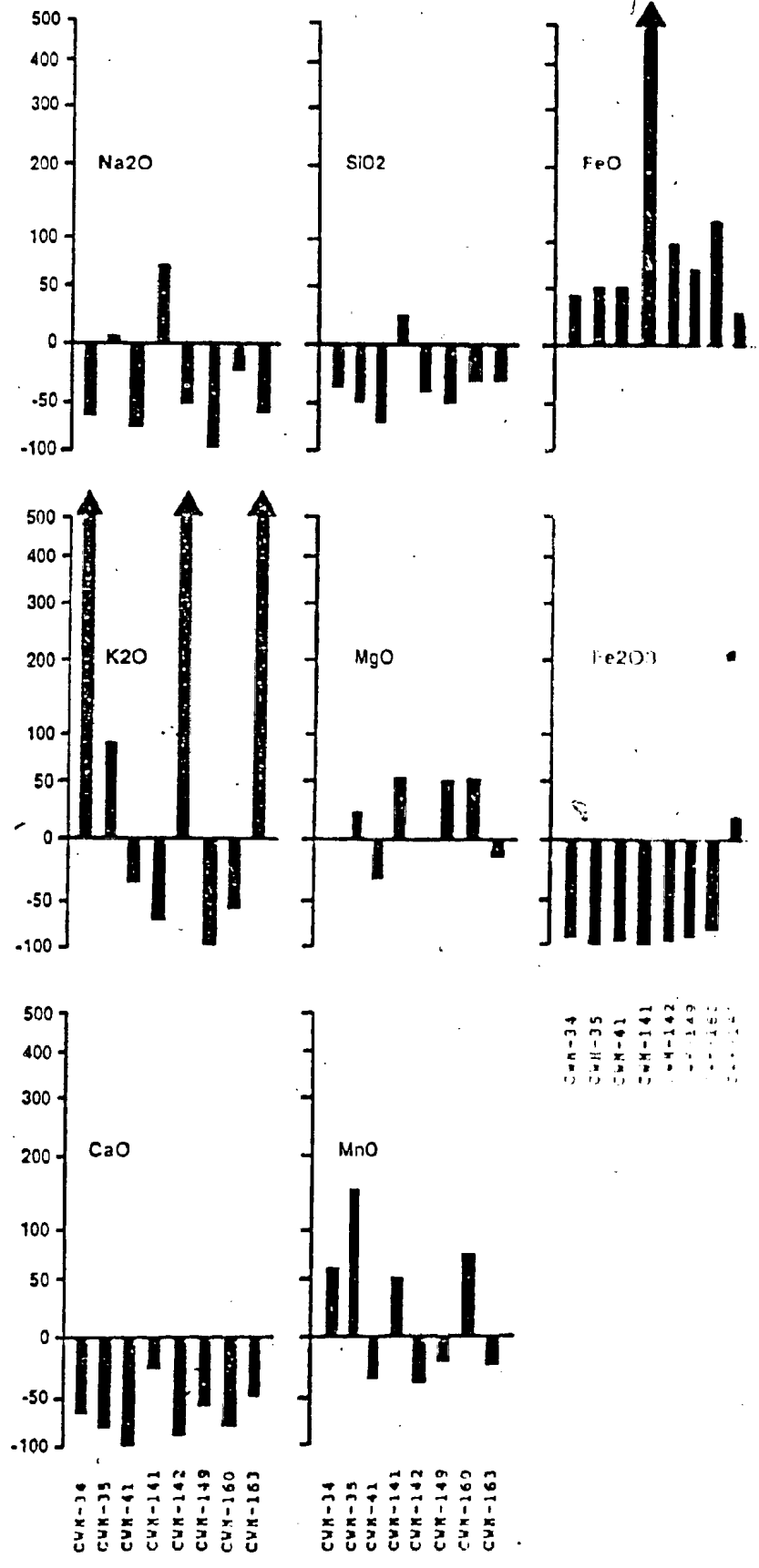
Two balanced reactions were calculated for shear zones

Table 5.1 Changes in concentrations of elements predicted by alteration reactions 5.2 to 5.11. Negative values represent a depletion in the sheared rock, and positive values indicate an enrichment. Minimum fluid:rock volume ratios are calculated from the volume of volatiles involved in the reactions, based on a reaction temperature of approximately 500°C, and a pressure of approximately 2 kbar.

	Na2O	K2O	CaO	FeO	MgO	MnO	Fe2O3	SiO2	TiO2	H2O	CO2	fl:rk
Mafic rocks:												
CWM 34	-.091	+.018	-.355	+.203	+.001	+.003	-.077	-.944		+.640	+.186	28:1
CWM 35	+.005	+.008	-.593	+.162	+.119	+.003	-.073	+.130		+.823	+.135	20:1
CWM 41	-.085	-.004	-.360	+.103	-.142	-.001	-.051	-1.39		+.419	-.011	54:1
CWM 141	+.042	-.006	-.111	+.640	+.135	+.001	-.047	+.385	+.053	+.589	+.268	40:1
CWM 142	-.036	+.017	-.485	+.304	+.003	-.002	-.068	-.813		+.641	+.056	10:1
CWM 149	-.129	-.006	-.271	+.274	+.193	-.001	-.077	-1.30		+.821	-.177	27:1
CWM 160	-.017	-.009	-.435	+.348	+.214	+.003	-.047	-.567		+.098	+.871	130:1
CWM 163	-.091	+.042	-.224	+.171	-.084	-.002	+.006	-.649	-.009	+.239	+.029	4:41
Felsic to intermediate volcaniclastic rocks:												
CWM 141	-.090	+.510	-.098	+.544	+.479			+2.62		-.582	-.027	4:1
CWM	-.014	+.143		+.675	+.575			+.272		+.317	-.016	2:1

Figure 5.4 Graphs showing the gains (positive) or losses (negative) of various elements in shear zones hosted in metabasic rocks, as predicted by balanced chemical equations between unsheared and sheared rock pairs.

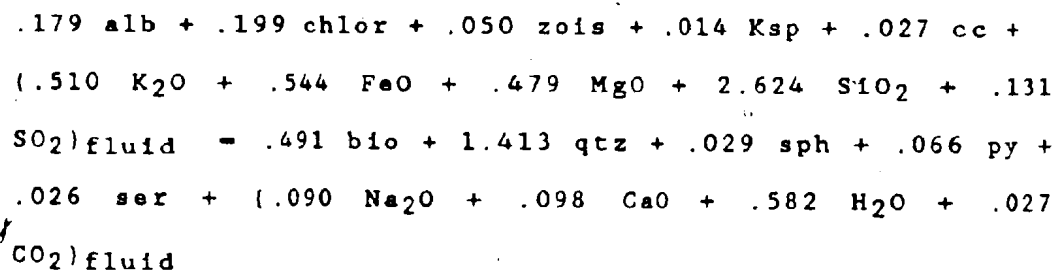
percent gains/losses of elements predicted by alteration reactions



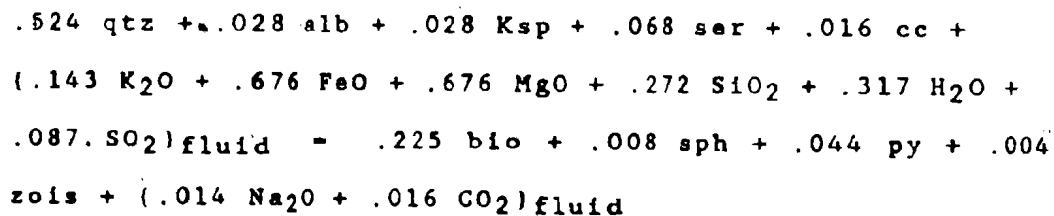
in the felsic to intermediate volcanogenic rocks. The compositions of mineral phases were taken as end-member compositions, since the rocks are too fine-grained for conventional microprobe analysis. These reactions therefore represent only a qualitative estimate of the chemical changes in these shear zones.

The two reactions are presented below, and the mineral formulas used are presented in Appendix I.

(R5.10) CWM-141C to CWM-141D



(R5.11) CWM-144A to CWM-144B



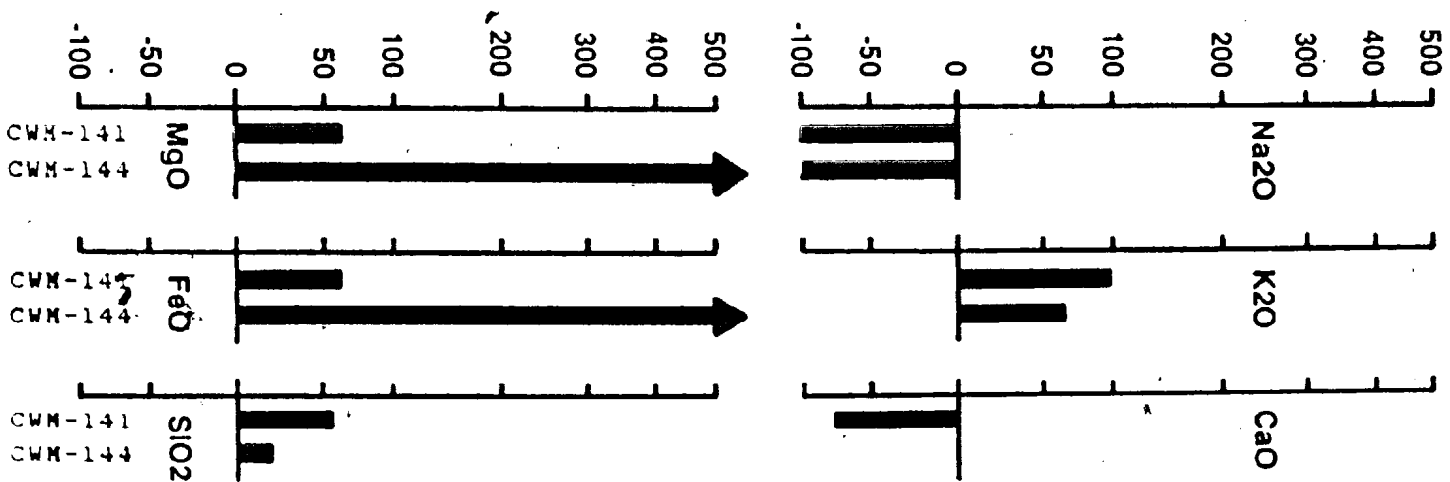
where alb = albite (identified optically in sample CWM-141C), Ksp = K-feldspar, zois = zoisite, ser = sericite, remaining mineral abbreviations are the same as those used in reactions 5.2 to 5.9

The results of these reactions are summarized in Table 5.1 and Figure 5.5. A comparison of Figures 5.3 and 5.5 shows that these reactions predict chemical trends fairly well, despite their qualitative nature. Sodium is released from both the mineral assemblages and from the shear zones, and potassium, iron and manganese are consumed, although the magnitude of the changes is not predicted very accurately. Ca seems to behave variably and unpredictably, in both diagrams. The reactions predict a silica increase in the shear zones which is not found in the whole rock data. Minimum fluid:rock volume ratios were calculated, based on the amount of H₂O and CO₂ consumed by the reactions, and they are presented in Table 5.1. The ratios are smaller than those determined for sheared metabasic rocks, varying from 2:1 to 4:1.

In summary, nearly every major element has been mobilized in the shear zones by the hydrothermal fluids. During alteration, fluids bearing K, Fe²⁺, Mg, Mn, +/- Si were flushed through the shear zones depositing these elements, and removing Fe³⁺, Na, Ca, +/- Si, and locally

Figure 5.5 Graphs showing the gains (positive) or losses (negative) of various elements in shear zones hosted in felsic to intermediate volcanoclastic rocks, as predicted by balanced chemical equations between unsheared and sheared rock pairs.

percent gains/losses of elements predicted by alteration reactions



Mg and Mn.) This changed the bulk compositions of the sheared rocks which, together with the changes in pressure and temperature conditions, resulted in the development of new mineral assemblages.

Composition of Hydrothermal Fluids

The cations present in the hydrous fluids were inferred in the previous section by balancing reactions between the mineral assemblages of the rocks inside and outside of the shear zones. In general, fluids which moved through the shear zones contained variable abundances of most major elements, as well as Sr, Rb, Ti, Cr and S.

Examination of fluid inclusions (Chapter 6) has shown that hydrothermal fluids trapped in quartz veins contain variable amounts of CO₂, CH₄, SO₂, H₂S, NaCl, CaCl₂, KCl, MgCl₂ and FeCl₂. With the exception of silica, these major elements are the same as those predicted from the bulk chemical and mineral assemblage data described above.

Microprobe analyses of chlorites (Appendix A) from a number of shear zones show that chlorine is not present in detectable quantities (i.e. <0.02 wt. %). This, together

with the presence of several chloride species in fluid inclusions, suggests that chlorine complexed with ions in solution in fluids in the shear zones, but did not itself react with the sheared rock. Thus chlorine does not need to be considered as a participant in the reactions, and can be considered a catalyst.

Oxidation State

The oxidation state is calculated as ferrous iron divided by the sum of $\text{FeO} + \text{Fe}_2\text{O}_3$. The oxidation state of iron in sheared and unsheared samples is summarized in Table 5.2. Abundances of ferrous and ferric iron from major element analyses are presented in Appendix E.

Most sheared samples are reduced with respect to their protoliths, with a mean $\text{FeO}/(\text{FeO} + \text{Fe}_2\text{O}_3)$ of 0.80 outside of the shear zones, and 0.89 inside the shear zones. Of 36 shear zones analyzed, there is a reduction of Fe in 32. In three shear zones, iron is oxidized relative to unsheared samples, with means of 0.89 and 0.78 outside and inside the shear zones, respectively. One shear zone has preserved the same oxidation state (0.84) as its protolith (see Table 5.2).

Table 5.2 Comparison of oxidation state of iron (FeO/FeO+Fe₂O₃) in unsheared and sheared samples from the Mirage Islands. Most shear zones (32 out of 36) are reduced relative to their protoliths, three are oxidized and one has remained unchanged. Data on the oxidation state of shear zones at Yellowknife are from Kerrich et al., 1977.

Mirage Islands metabasites

	Unsheared	Sheared	Total number of samples
$\frac{\text{FeO}}{\text{FeO}+\text{Fe}_2\text{O}_3}$	range - 0.70 to 0.92	range - 0.74 to 0.97	32 - reduced
	mean - 0.80	mean - 0.89	
	range - 0.85 to 0.97	range - 0.70 to 0.94	3 - oxidized
	mean - 0.89	mean - 0.78	
	0.84	0.84	1 - unchanged

Yellowknife basalts: mean unsheared - 0.76
 mean sheared - 0.78
 mean ore-bearing - 0.95

(Kerrick et al., 1977)

At Yellowknife, Kerrich et al. (1977b) found that unsheared basalts have an average ferrous iron to total iron ratio of 0.76. Sheared basalts are slightly more reduced (0.78), and ore-bearing parts of the shear zones (that is, those parts which have undergone extensive sericitization and chloritization) contain 95% Fe²⁺. Although the trend between sheared and unsheared rocks at Yellowknife is similar to that found in the Mirage Islands, unsheared samples in this study are, on average, more reduced than unsheared Yellowknife basalts. The oxidation state in the shear zones lies between those of the incipiently sheared rocks and the ore-bearing rocks near Yellowknife.

Fyfe et al. (1978) and Fyfe and Kerrich (1976) noted that, in general, regional metamorphism does not notably change the oxidation state of a rock, but where large volumes of fluid have interacted with a rock, significant changes in the Fe²⁺/Fe³⁺ ratio may occur. Ascending, cooling fluids are usually accompanied by reduction, whereas descending, heating fluids oxidize a rock (Fyfe et al., 1978).

Consider a model in which fluids ascending from 3-4 kbars pressure (10-12 km) to about 2 kbars pressure (about

7 km) in the shear zones cool with time from $>500^{\circ}\text{C}$ to about 350°C (as estimated in Chapters 2, 3 and 4). The solubility of quartz would then drop from about 0.7 wt % to 0.2 wt % (see Fyfe *et al.*, 1978, Figure 4.15A), resulting in the deposition of 0.5 g of silica per 100 g of fluid.

In shear zone CWM-145, almost 37 g of quartz have been deposited in a 100 g sample of sheared rock by a fluid with a temperature estimated to be 366°C (determined from oxygen isotope fractionation). The deposition of 37 g of silica would require 7400 g of solution according to the above model, which corresponds to a fluid:rock volume ratio of about 280:1, based on 100 g of rock with a density of 3 g/cm^3 , and a fluid density near 0.8 g/cm^3 (determined from a specific volume of pure H_2O of $1.3 \text{ cm}^3/\text{g}$). For a saline fluid, the density would be slightly higher, and would result in a slightly lower fluid:rock ratio.

In a similar way, fluid:rock ratios can be approximated for all shear zones, based on the amount of silica which has been added to or removed from the system. Whole rock data show the change in silica content in 100 g of a sheared rock relative to its protolith. In a few shear zones, fluid temperature has been determined

from oxygen isotopes, and has a bimodal distribution with means of 420 and 590°C (see Chapter 4); in the remaining shear zones it is estimated to be 500°C. The solubilities of silica in fluids at these three temperatures and about 3 kbars pressure are 0.30, 0.50 and 0.75 wt % in order of increasing temperature (Fyfe *et al.*, 1978). The density of the fluid is approximated as 0.8 g/cm³, and that of the rock is taken as 3 g/cm³ and 2.6 g/cm³ for mafic and felsic to intermediate volcanogenic rocks, respectively.

Although the temperature estimate of 500°C may be in error in some cases, it is likely to be correct to within about 100°C. Changing the estimated temperature in any shear zone by 100°C affects the silica solubility by approximately 0.3 wt % SiO₂, but does not change the order of magnitude of the fluid:rock ratio. Similarly, increasing or decreasing the fluid density by up to 0.2 g/cm³ (which would account for the range of salinities estimated in the previous chapter), does not affect the fluid:rock ratio by a significant amount.

Table 5.3 shows the fluid:rock ratios required to produce the observed changes in silica content at a given temperature. These ratios range from 10:1 up to 350:1, but all are only minimum ratios, since they assume that: 1) the fluid was saturated with respect to silica;

Table 5.3 Table showing the net increase (positive) or decrease (negative) of silica in sheared rocks from the Mirage Islands, and the minimum fluid:rock volume ratios required to produce these changes. The solubility of quartz is estimated to be 0.3, 0.5 and 0.75 wt % at 420, 500 and 590°C and 3 kbar pressure (see text), and the rock volume is based on densities of 3 g/cm³ for basic rocks and 2.6 g/cm³ for felsic to intermediate rocks. Fluid density is estimated to be 0.8 g/cm³.

206

Shear Zone	SiO2	Solubility of qtz (wt %)	H2O required (g)	rock vol (cm ³)	fluid:roc (vol)
<u>metabasic rocks</u>					
CWM-34	-3.3	.5	660	33.3	20:1
CWM-35	-7.2	.5	1440	33.3	40:1
CWM-41	-14.2	.3	4730	33.3	140:1
CWM-137	-2.2	.5	440	33.3	15:1
CWM-139	-1.5	.5	300	33.3	10:1
CWM-141	+2.9	.5	580	33.3	20:1
CWM-142	-2.1	.75	280	33.3	10:1
CWM-145	+36.7	.3	12230	33.3	350:1
CWM-149	-3.9	.5	780	33.3	20:1
CWM-151	+1.3	.5	260	33.3	10:1
CWM-154	-5.7	.3	1900	33.3	60:1
CWM-159	-5.3	.5	960	33.3	30:1
CWM-160	-3.3	.3	1100	33.3	30:1
CWM-161	-3.8	.5	760	33.3	25:1
CWM-163	-1.5	.75	200	33.3	10:1
CO-13	-5.3	.5	1060	33.3	30:1
CO-14	-1.3	.5	260	33.3	10:1
CO-20	-4.7	.5	940	33.3	30:1
CO-22	+9.0	.3	3000	33.3	90:1
CO-23	-5.4	.3	1800	33.3	50:1

felsic to intermediate volcaniclastic rocks

CWM-36	+19.4	.5	3880	38.5	100:1
CWM-140	-4.8	.5	960	38.5	25:1
CWM-141	+1.3	.5	260	38.5	10:1
CWM-144	-12.9	.5	2580	38.5	70:1
CWM-149	+1.8	.5	360	38.5	10:1
CWM-155	-20.0	.5	4000	38.5	100:1
CWM-158	-18.7	.5	3400	38.5	100:1
CWM-162	-8.7	.5	1740	38.5	50:1

and 2) the chemical system was 100% efficient at adding or removing SiO_2 from the mineral assemblage.

Large fluid:rock ratios are cited by Fyfe et al., 1978 and Fyfe and Kerrich (1976) as a means by which the oxidation state of an altered rock may be changed.

From the above calculations, and from chemical reactions presented earlier in this chapter, it is clear that large volumes of fluid have penetrated the Mirage Island shear zones. The oxidation state of the sheared rocks is interpreted to indicate that the majority of these fluids were ascending and cooling - derived, presumably, from a metamorphic or possibly an igneous source at depth.

The local presence of oxidized iron in the shear zones implies that in places fluids were descending in the shear zones. Further evidence of descending hydrothermal fluids comes from the presence of carbonate veins locally. While the solubility of silica decreases with decreasing temperature, that of calcite increases under the same conditions, thus carbonate veins would be expected to precipitate out where hydrothermal fluids are descending, and temperature is increasing.

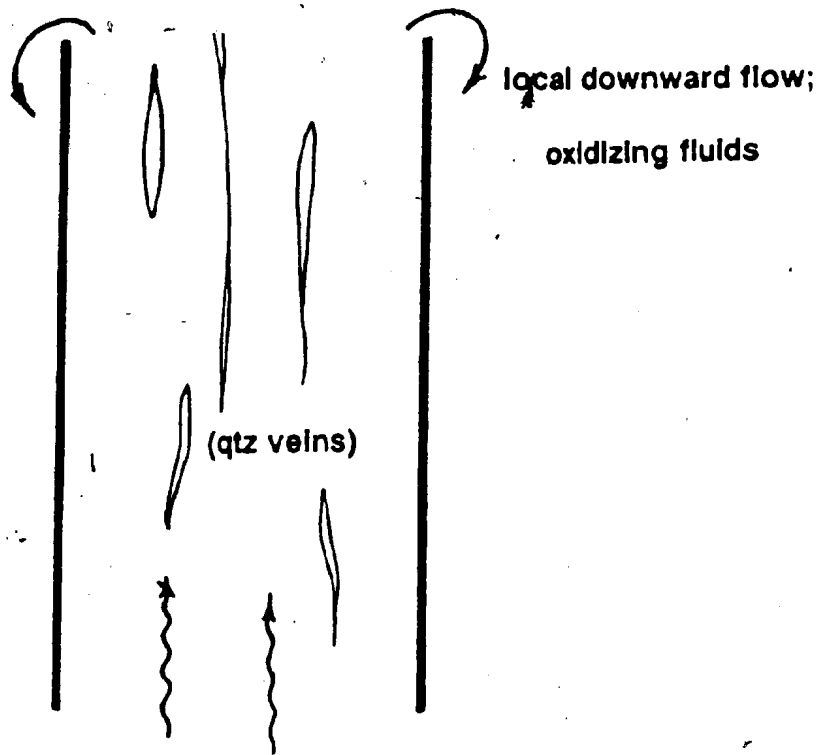
One possible origin for descending fluids is from a meteoric source. Isotope studies (Chapter 3) have revealed that some of the hydrothermal fluids have oxygen isotopic compositions compatible with a fluid composed of a mixture of metamorphic (or igneous) and meteoric waters. However the shear zones in which these fluids occur do not correspond to those which have been oxidized. Unfortunately, the oxidized shear zones have not been analyzed for stable isotopes, and so no estimate of the isotopic composition of their fluids exists. Therefore, it is difficult to evaluate whether meteoric water contributed to the alteration.

Alternatively, it is possible that hydrothermal fluids underwent convection in the shear zones, circulating downwards locally, with a net upward flow direction (see Figure 5.6). In this model, local oxidation in the shear zones indicates the sites where downward flow has occurred. It is possible that meteoric fluids comprised part of the circulating hydrothermal fluid.

Summary

In this chapter, it was shown that the shear zones acted as open chemical systems during alteration, being enriched in some elements, and depleted in others with

Figure 5.6 Schematic diagram showing the local downward convection of hydrothermal fluids in a shear zone system with a net upward flow direction. Overall, fluids in this model would be rising and cooling with time, but locally downward-directed fluids would be increasing in temperature.



net upward flow; reducing fluids

respect to their protoliths outside the shear zones. By balancing reactions between the sheared and unsheared mineral assemblages,³ it is possible to predict fairly successfully which elements have increased in concentration, and which have decreased.

Estimates of fluid compositions based on these reactions, coupled with results from fluid inclusion analyses, indicate that most elements were transported in the shear zones as chloride complexes, and that chlorine has not reacted with the sheared rocks.

In most shear zones (about 90%), iron is in a more reduced state than in unsheared samples. This is evidence that: 1) large volumes of fluid have moved through the shear zones, and 2) these fluids were ascending and cooling with time. Minimum fluid:rock volume ratios estimated from silica enrichment/depletion are in the order of 10:1, and locally are as high as 350:1, supporting the former conclusion.

A few shear zones are oxidized relative to their protoliths, from which the presence locally of descending, heating fluids can be inferred. These fluids may have been derived from meteoric waters which mixed with isotopically heavier metamorphic and/or magmatic fluids.

Alternatively, the oxidized shear zones may be evidence for convective circulation in the shear zone system, with net upward-directed flow, but locally downward-flowing cells.

CHAPTER 6: REACTION PROGRESS

Introduction

Based on the results presented in previous chapters, it can be seen that the rocks in the shear zones on the Mirage Islands have undergone alteration to variable extents, with some elements being consistently enriched or depleted, whereas others behave unpredictably. In this chapter, the extent to which a reaction has proceeded in a given shear zone is quantified, using the techniques of Ferry (1980, 1983, 1985) and Thompson (1982).

Ferry (1980, 1983, 1985) has defined two parameters which can be used to track the degree to which a rock is altered. The first method is a measure of the alteration index, which is defined simply as the modal quantity of secondary (or alteration) minerals in a sample, divided by the sum of the primary (unaltered) and secondary minerals (Ferry, 1985). A completely unaltered rock will contain no secondary minerals, and so will have an alteration index of zero, whereas a completely altered rock with no primary minerals preserved will have an alteration index of one. This parameter may be applied to any sample for which modal quantities of minerals are known, and does not

require that chemical analyses of individual minerals be carried out.

The second measure of alteration progress is given by ξ , the reaction progress variable, which may be defined as the number of moles of a specified mineral produced by a given reaction (Ferry, 1983). In order to calculate the reaction progress for a given rock, its initial, unaltered state must be defined, and the reaction(s) which produced the mineral assemblage in the final, altered state must be identifiable. A reaction progress variable equal to zero indicates that no reaction has occurred, and a value of one implies that the reaction has gone to completion.

Methodology

For several shear zones in metabasic rocks from the Mirage Islands, modal proportions and mineral compositions have been determined for unsheared and sheared rock pairs. Therefore the reaction progress variables and alteration indices may be calculated for the shear zones, using the unsheared samples as the initial and the sheared samples as the final alteration states. This provides a measure of the extent of alteration specific to each shear zone, but does not provide a means of comparing the reaction progress between the shear zones.

In the following sections, Ferry's (1985) alteration index has been modified slightly to accommodate the fact that the initial "unaltered" states in fact display variable degrees of alteration in the different protoliths. Thus, instead of presenting the absolute values of the alteration indices for each unsheared and sheared rock, the differences between the final and initial states are determined. The values calculated represent the amount of alteration each shear zone has undergone, with no reference to a given starting point. Thus a sheared rock whose change in alteration index (ΔAI) is 0.8 is not necessarily more altered than one whose ΔAI is 0.7; it has merely undergone more alteration from its initial (unsheared) state.

The reaction progress variables for the net transfer reactions which characterize the alteration in the shear zones are useful in demonstrating that the shear zones acted as open chemical systems, and that the fluid composition played an important role during alteration.

Alteration Index

The alteration index of a rock was defined by Ferry (1985) as:

$$(6.1) \quad AI = \frac{\text{mode of secondary minerals}}{\text{mode of primary + secondary minerals}}$$

In this study, the change in alteration index between a sheared rock and its protolith is defined as:

$$(6.2) \quad \Delta AI = AI_{\text{sheared}} - AI_{\text{unsheared}}$$

In samples from the Mirage Islands, the mafic minerals are used to track the alteration state. Since most of the shear zone alteration occurred under M2 (greenschist facies) conditions, the mafic alteration minerals are those which equilibrated during M2 - namely chlorite and biotite. Primary mafic minerals are therefore defined as those minerals which were present before M2 metamorphism - that is, amphibole and clinopyroxene (The latter is preserved in only two samples). The alteration indices (AI) of 8 unsheared and 8 sheared gabbros and the changes in alteration indices

(ΔAI) between the sheared and unsheared pairs are presented in Table 6.1. A sample calculation is presented

Table 6.1 Alteration index (AI) for unsheared and sheared rock samples, and the change in alteration index (AI) calculated for unsheared/sheared pairs across each shear zone. See text for definitions of AI and AI.

Unsheared Sample	AI	Sheared Sample	AI	Δ AI
CWM-34A	.21	CWM-34B	1.00	.79
CWM-35A	.14	CWM-35B	1.00	.86
CWM-41A	.35	CWM-41B	1.00	.65
CWM-141A	.59	CWM-141B	1.00	.41
CWM-142A	.17	CWM-142B	1.00	.83
CWM-149A	.01	CWM-149B	1.00	.99
CWM-160A	.26	CWM-160B	1.00	.74
CWM-163A	.12	CWM-163B	.40	.28

in Appendix C.

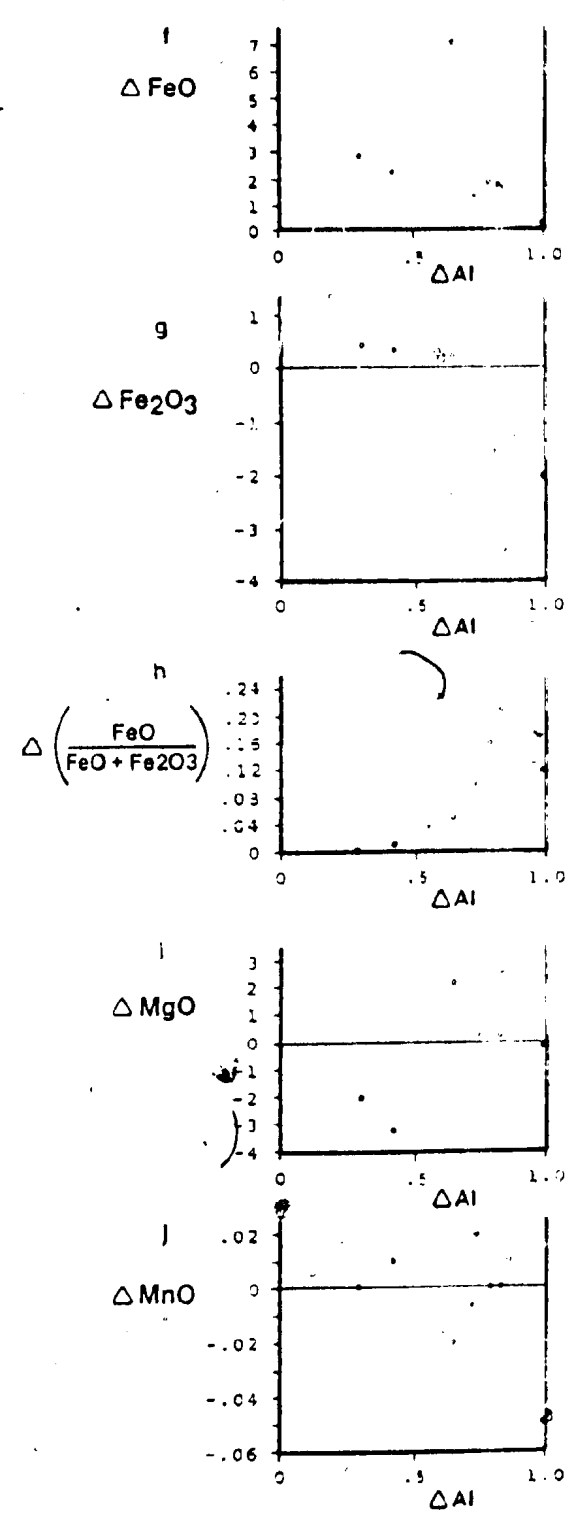
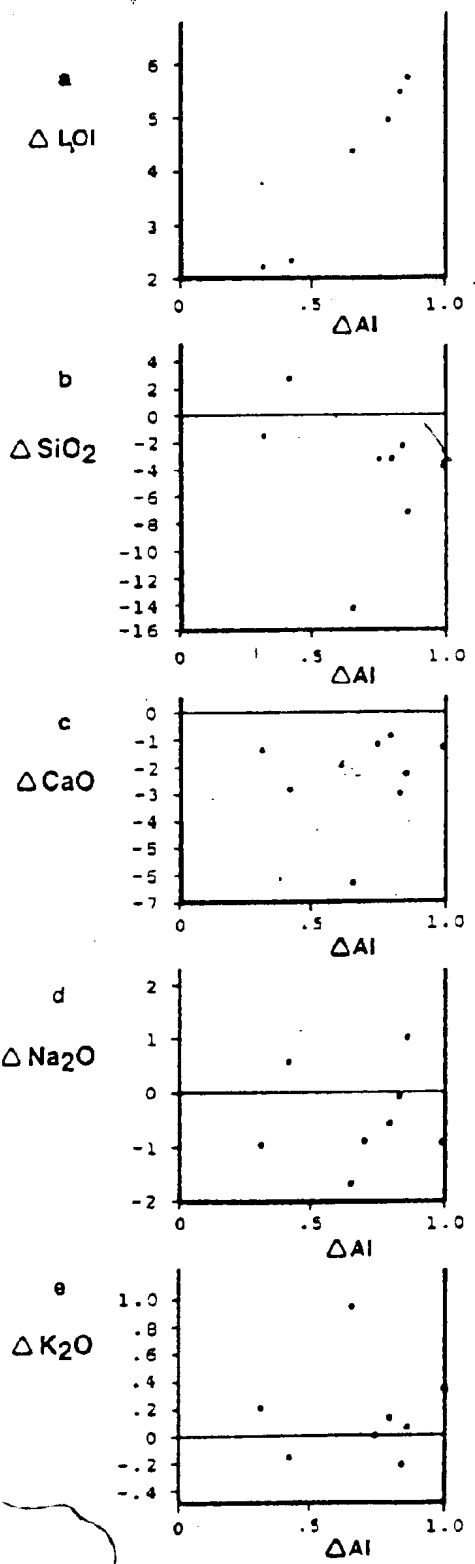
With the exception of sample CWM-163B, all of the sheared rocks have alteration indices of 1.00, indicating that primary minerals have been entirely replaced in most shear zones. The alteration state of the unsheared rocks ranges from .01 (99% primary minerals) to .59 (more than half the primary minerals replaced by secondary minerals). The degree of alteration in the shear zones can be compared by reference to the calculated values of ΔAI . From Table 6.1 it can be seen that shear zone CWM-149 has undergone the most alteration from its initial state ($\Delta AI = .99$), and CWM-163 the least ($\Delta AI = .28$).

In the previous chapter, it was found that some major elements behave predictably in the sheared gabbros. Volatiles, Fe^{2+} , and K generally were concentrated in the shear zones, and Fe^{3+} , Na and Ca were removed. Other elements, in particular Si, Mg and Mn, have no apparent pattern in their distribution. In Table 6.2 and Figures 6.1 a - j, the changes in alteration state are compared to the changes in concentration of these elements, to determine whether the extent to which they are enriched or depleted varies systematically with the amount of alteration the sheared rocks have undergone.

Table 6.2 Comparison of AI (arranged in order of increasing magnitude) with the change in concentration of various elements (positive values have increased in concentration; negative values have decreased) across shear zones on the Mirage Islands. The change in concentration of elements was calculated by subtracting the concentration of a given element in the 'unsheared' state from that in the sheared state; thus a positive value indicates an enrichment, and a negative value indicates a depletion of the element.

Shear Zone	CWM 162	CWM 141	CWM 41	CWM 160	CWM 34	CWM 142	CWM 35	CWM 149
Δ Al	.28	.41	.65	-.74	.79	.83	.86	.99
Δ LOI	2.27	2.31	4.39	7.82	4.97	5.48	5.74	7.67
Δ SiO ₂	-1.5	-2.9	-14.2	-3.3	-3.3	-2.1	-7.2	-3.9
Δ CaO	-1.40	-2.90	-6.44	-1.12	-.88	-3.04	-2.34	-1.28
Δ Na ₂ O	-.95	.52	-1.71	-.89	-.60	-.07	1.01	-.91
Δ K ₂ O	.21	-.17	.95	0.0	.14	-.20	.07	.34
Δ FeO	2.70	2.09	7.01	1.34	1.87	1.77	1.58	.31
Δ Fe ₂ O ₃	.40	.30	.24	-1.21	-1.55	-3.45	-1.23	-2.07
Δ MgO	-2.08	3.14	2.16	.13	-.09	.15	.22	-.20
Δ MnO	0.0	.01	-.02	.02	0.0	0.0	.01	-.05
$\Delta \frac{\text{FeO}}{\text{Fe}_{\text{tot}}}$	0.0	.01	.05	.10	.16	.21	.11	.12

Figure 6.1 Graphs of AI vs. the change in concentration of various major elements across shear zones on the Mirage Islands. Results are discussed in text.



As expected, the increase in volatile content of the sheared rocks corresponds to an increase in the alteration index (Fig. 6.1a). Since a major difference between the primary and secondary minerals used to define the alteration index is the abundance of water in the secondary minerals, it is to be expected that the data would roughly define a straight line with an intercept close to the origin.

Figures 6.1c, d and e are plots of ΔCaO , $\Delta\text{Na}_2\text{O}$ and $\Delta\text{K}_2\text{O}$ respectively, against ΔAI . The changes in concentration of these alkaline elements do not appear to be functions of the extent of alteration, even though each of these elements was found to be consistently enriched or depleted in the shear zones.

Figure 6.1b is a plot of ΔSiO_2 vs ΔAI . The behaviour of silica between shear zones is apparently unrelated to the difference in alteration index.

In Figure 6.1f, the change in Fe^{2+} content is plotted against ΔAI . The data are somewhat scattered, but most appear to define a line with a negative slope, implying that the more alteration a sheared rock has undergone with respect to its protolith, the smaller the magnitude of the

Fe^{2+} enrichment in that shear zone. Since the alteration indices of most sheared rocks were found to be unity, then unsheared rocks for which alteration indices are low (and therefore have high values of ΔAI) must have Fe^{2+} contents near those of their sheared counterparts, while those with high alteration indexes (and therefore low values of ΔAI) must be depleted in Fe^{2+} relative to their sheared equivalents.

This suggests that at least some of the Fe^{2+} which has been enriched in the shear zones was derived from the adjacent unsheared rock. Low values of AI in unsheared rocks most likely resulted from hydrothermal fluids in the shear zones penetrating into the surrounding wallrocks. Interaction between these fluids and the wallrocks caused Fe^{2+} to be removed from the protolith and concentrated in the shear zones, resulting in the coincidence of low ΔAI and high ΔFe^{2+} .

The difference in Fe^{3+} content is plotted against ΔAI in Figure 6.1g. The two shear zones with the lowest values of ΔAI are slightly enriched in Fe^{3+} , and the rest are depleted. Overall, the magnitude of the Fe^{3+} depletion increases with the amount of alteration experienced by the shear zone.

It was noted in Chapter 5 that the oxidation state of iron is more reduced within the shear zones than outside of them. Figure 6.1h is a plot of the change in oxidation state against ΔAI . It shows that the shear zones in which the most alteration occurred are also the most reduced. Combining the results of Figure 6.1h with 6.1a, it can be concluded that the shear zones which are the most enriched in volatiles have undergone the most reduction, and that the fluids therefore must have been reducing fluids, as suggested in the previous chapter.

In Figures 6.1i and j, ΔMgO and ΔMnO are plotted against ΔAI . Like SiO_2 , these elements were found to behave unpredictably between the shear zones, and Figure 6.1 reveals that there is no systematic variation between their enrichment or depletion and the change in alteration index.

Reaction Progress

In order to monitor the reaction progress in each shear zone, the reactant and product minerals must be identified, and the reaction(s) which produced the final assemblage must be known. Although modal quantities and mineral compositions vary between the shear zones, the unaltered basic assemblages are composed of various

proportions of amphibole +/- clinopyroxene + plagioclase + epidote +/- chlorite +/- calcite +/- quartz +/- sericite +/- pyrite +/- sphene, and the altered assemblages contain chlorite + albite + quartz + calcite +/- biotite +/- epidote +/- sericite +/- amphibole +/- sphene +/- pyrite. A simplified net reaction between these two assemblages would involve the hydration and carbonation of amphibole, plagioclase, epidote and locally clinopyroxene to produce chlorite, albite, calcite, quartz, and locally biotite (Chapter 5). All of the net shear zone reactions presented in Chapter 5 are modelled as open chemical systems.

In Table 6.3, the additive components for each mineral involved in the reactions are presented. To simplify calculations, pyrite and sphene have been left out, since they are accessory minerals, and do not play a significant role in the reactions. The additive components are idealized formulae as recommended by Thompson (1982), which lie near the average formula determined from all chemical analyses of each mineral. Mg in the formulae represent the sum of Mg + Fe + Mn.

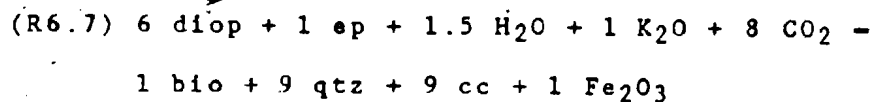
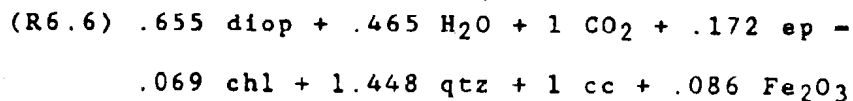
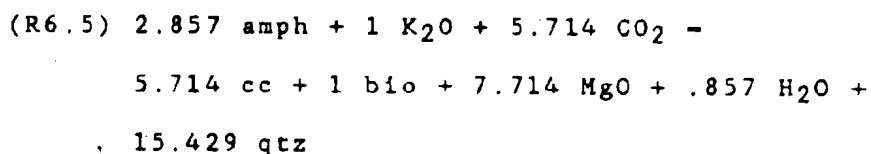
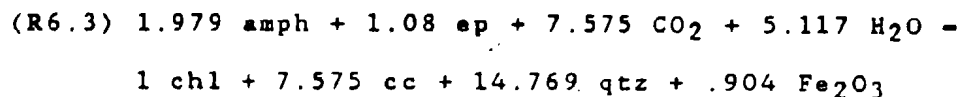
These additive components can be combined with the appropriate exchange components from Table 6.3 to produce the true compositions of the minerals in a given reaction.

Table 6.3 Additive and exchange components for the minerals involved in the net transfer reactions used to characterize alteration in shear zones on the Mirage Islands.

Phase	Additive Component	Exchange Components
albite	$\text{NaAlSi}_3\text{O}_8$	$\text{CaAlNa}_{.1}\text{Si}_{.1}$
andesine	$\text{Ca}_{.35}\text{Na}_{.65}\text{Al}_{1.35}\text{Si}_{1.65}\text{O}_8$	$\text{CaAlNa}_{.1}\text{Si}_{.1}$
Quartz	SiO_2	
Calcite	CaCO_3	
Epidote	$\text{Ca}_2\text{Fe}^3\text{Al}_2\text{OSi}_3\text{O}_{11}(\text{OH})$	
Diopside	$\text{CaMgSi}_2\text{O}_6$	$\text{FeMg}_{.1}, \text{MnMg}_{.1}$
		$\text{CaMg}_{.1}$
Amphibole	$\text{Ca}_2\text{Mg}_{4.8}\text{Al}_{.2}\text{Si}_{7.5}\text{Al}_{.5}\text{O}_{22}(\text{OH})_2$	$\text{FeMg}_{.1}, \text{MnMg}_{.1}$
		$\text{CaMg}_{.1}, \text{FeAl}_{.1}$
Chlorite	$\text{Mg}_{9.5}\text{Al}_{2.5}\text{Si}_{5.5}\text{Al}_{2.5}\text{O}_{20}(\text{OH})_{16}$	$\text{FeMg}_{.1}, \text{MnMg}_{.1}$
		$\text{FeAl}_{.1}$
Biotite	$\text{K}_2\text{Mg}_6\text{Si}_6\text{Al}_2\text{O}_{20}(\text{OH})_4$	$\text{FeMg}_{.1}$

As in Chapter 5, epidote is taken as ideal epidote ($\text{Ca}_2\text{Fe}^{3+}\text{Al}_2\text{OSi}_3\text{O}_{11}(\text{OH})$), and the only exchange component considered for biotite is $\text{FeMg}_{.1}$, for simplicity.

Five independent net transfer reactions have been identified which characterize the reactions that have occurred within the shear zones. They are:



Abbreviations: amph - amphibole, ep - epidote, chl - chlorite, qtz - quartz, and - andesine, alb - albite, bio - biotite, diop - diopside

Two of these reactions produce chlorite, two produce

biotite, one produces albite and four produce calcite. R6.6 and R6.7 are only applicable to two shear zones (CWM-34 and CWM-35), since pyroxene is only preserved in two unsheared samples. Reactions in the remaining six shear zones can be characterized by R6.3 to R6.5. From these reactions five different reaction progress variables (ϵ) may be defined as follows:

(R6.8) ϵ_1 - no. moles chl produced by R7.3

(R6.9) ϵ_2 - no. moles alb produced by R7.4

(R6.10) ϵ_3 - no. moles bio produced by R7.5

(R6.11) ϵ_4 - no. moles cc produced by R7.6

(R6.12) ϵ_5 - (no. moles ep produced by R7.7)

Combining equations R6.3 to R6.12, the following five equations can be written for the two shear zones with pyroxene preserved in the protoliths:

(R6.13) no. moles chl in sheared sample - $\epsilon_1 + .069\epsilon_4$

(R6.14) no. moles alb in sheared sample - ϵ_2

(R6.15) no. moles bio in sheared sample - $\epsilon_3 + \epsilon_5$

(R6.16) no. moles cc in sheared sample - $7.575\epsilon_1 + 5.714\epsilon_3 + \epsilon_4 + 9\epsilon_5$

(R6.17) no. moles ep in sheared sample - $-1.08\epsilon_1 - .172\epsilon_4 - \epsilon_5$

For the remaining shear zones, no pyroxene is preserved in the unsheared rocks, and the following equations have been determined from R6.3 to R6.5 and R6.8 to R6.10:

$$(R6.18) \text{ no. moles chl in sheared sample} = \epsilon_1$$

$$(R6.19) \text{ no. moles alb in sheared sample} = \epsilon_2$$

$$(R6.20) \text{ no. moles bio in sheared sample} = \epsilon_3$$

The two shear zones with pyroxene involved in the alteration reaction are considered first. In R6.13 to R6.17, the number of moles of each mineral produced by the alteration can be taken from R5.2 and R5.3 (in Chapter 5), which give the net alteration reactions for each of these shear zones. For shear zone CWM-34 (reaction R5.2), the following substitutions have been made:

$$(R6.13) \text{ moles chl} = .089 - \epsilon_1 + .069\epsilon_4$$

$$(R6.14) \text{ moles alb} = .102 - \epsilon_2$$

$$(R6.15) \text{ moles bio} = .010 - \epsilon_3 + \epsilon_5$$

$$(R6.16) \text{ moles cc} = .186 - 7.575\epsilon_1 + 5.714\epsilon_3 + \epsilon_4 + 9\epsilon_5$$

$$(R6.17) \text{ moles ep} = -.114 - 1.08\epsilon_1 - .172\epsilon_4 - \epsilon_5$$

Solving these five equations algebraically yields the following values for : $\epsilon_1 = .25$, $\epsilon_2 = .10$, $\epsilon_3 = -.23$,

$\xi_4 = -2.3$, $\xi_5 = .24$. Only values of ξ between 0 and 1 are meaningful; the negative values result from the fact that the chemical system was open, and several elements were introduced to or removed from the system which were not a part of the initial or final mineral assemblages. Thus, calculations of the reaction progress variables using a model for a closed chemical system yield meaningless results.

It is therefore necessary to try a slightly different approach. The reaction progress variables may be approximated using the molar proportions of the reactant minerals in the unshered rock, together with modal ratios of minerals in R6.3 to R6.7.

If the only reaction to produce albite in shear zone CWM-34 was R6.4, then $\xi_2 = .102$. If some albite was produced from elements introduced by the fluid (for instance, in Chapter 5 it was found that some Na was introduced into the fluid by the breakdown of amphibole), then ξ_2 would be less than .102, and if some of the albite produced by R6.4 was subsequently removed by the fluid, then ξ_2 would be greater than .102. Since the chemical system was open, it is difficult to determine how much albite was produced or consumed by the fluid phase, and so ξ_2 is approximated as .102, based on the assumption that

the majority of albite in the sheared sample was produced by R6.4.

Chlorite was produced in R6.3 from amphibole, and in R6.6 from diopside. The molar ratio of amphibole:chlorite in R6.3 is approximately 2:1, and that of diopside:chlorite in R6.6 is about 10:1; therefore, given that the other reactants are present in excess quantities, 1 mole of chlorite can be produced from 2 moles of amphibole or 10 moles of cpx.

The net alteration reaction in shear zone CWM-34 (R5.2) has .300 moles of cpx and .060 moles of amphibole among the reactants. These molar quantities imply that .03 moles of chlorite may be produced from cpx by R6.6, and .03 moles chlorite may be produced from amphibole by R6.3, assuming that both reactions go to completion (that is, $\epsilon_1 - \epsilon_4 = 1$). The total number of moles of chlorite from R6.3 and R6.6 would therefore be about .06. This is slightly less than the total amount of chlorite actually produced in the shear zone (.089 moles); however elements introduced into the shear zone by the hydrothermal fluids have not been considered here, and they could account for the remainder of the chlorite. The total number of moles of FeO + MgO + MnO estimated to have been put into the system by the fluid is .207 (R5.2). Generally, Fe, Mg and

Mn were found to occupy about 9.35 octahedral sites per mole of chlorite in sheared samples (Appendix A, Chapter 3), therefore the number of moles of chlorite that .207 moles of FeO, MgO and MnO could produce (when combined with enough Al, Si and H₂O) is $.207/9.35 = .022$ moles. Thus the total amount of chlorite expected in the sheared rock, given $\xi_1 - \xi_4 = 1$, and considering the input of elements by the hydrothermal fluid would be approximately $.06 + .022 = .082$, which corresponds more closely to the actual molar quantity of chlorite found in the shear zone (.089 moles).

Biotite is produced by R6.5 from amphibole, and by R6.7 from diopside. The ratio amphib:bio is about 3:1 in R6.5, and diop:bio is 6:1 in R6.7. The molar quantities of amphibole and cpx in the reactants in shear zone CWM-34 (R5.2) suggest that the amphibole could produce up to .02 moles of biotite by R6.5 and the cpx could produce up to .05 moles of biotite by R6.7, for a total biotite content of .07 moles.

Since the total amount of biotite present in the sheared sample is .010 moles, then ξ_3 and ξ_5 must be less than 1. If ξ_3 and ξ_5 are each .14, then the total number of moles of biotite produced would be approximately .01. ξ_3 and ξ_5 will have slightly lower values if some biotite

is considered to have been produced from elements introduced from an external source.

Thus the reaction progress variables for shear zone CWM-34 may be approximated as $\epsilon_1 \approx 1.0$, $\epsilon_2 \approx .10$, $\epsilon_3 \approx .14$, $\epsilon_4 \approx 1.0$ and $\epsilon_5 \approx .14$. The number of moles of epidote produced by R6.3, R6.6 and R6.7, given by R6.17 should be:

$$\begin{aligned} \epsilon_p &= -1.08\epsilon_1 - .172\epsilon_4 - \epsilon_5 \\ &= -1.392 \text{ moles; or } +1.392 \text{ moles consumed.} \end{aligned}$$

In fact only .114 moles are consumed, implying that the remaining 1.278 moles of epidote were released into the fluid. This is compatible with the losses of Ca and Fe^{3+} recorded in the shear zone (Chapter 5), and suggests that some of the epidote was consumed by reactions other than R6.3, R6.6 and R6.7.

Similarly, less calcite is actually present in the sheared rock than would be predicted from R6.16:

$$\begin{aligned} \epsilon_{\text{Ca}} &= 7.575\epsilon_1 + 5.714\epsilon_3 + \epsilon_4 + 9\epsilon_5 \\ &= 10.63 \text{ moles.} \end{aligned}$$

If the approximations of reaction progress variables

are correct, then a large amount of calcite was removed from the system by the hydrothermal fluids.

For shear zone CWM-35, similar estimates of reaction progress variables can be made. Once again, solving R6.12 to R6.17 for the molar quantities of minerals in R5.3 (below) yields meaningless values of ϵ . From R5.3 the following substitutions have been made:

$$\text{chlor} = .124 - \epsilon_1 + .069\epsilon_4$$

$$\text{alb} = .154 - \epsilon_2$$

$$\text{bio} = 0 - \epsilon_3 + \epsilon_5$$

$$\text{cc} = .135 - 7.575\epsilon_1 + 5.714\epsilon_3 + \epsilon_4 + 9\epsilon_5$$

$$\text{ep} = -.140 - 1.08\epsilon_1 - .172\epsilon_4 - \epsilon_5$$

If the only source of albite in the sheared rock is from reaction R6.4, then ϵ_2 is approximately .15. The maximum number of moles of chlorite produced from amphibole by R6.3 would be about .03, and from cpx by R6.6 would be about .03 (assuming $\epsilon_1 = \epsilon_4 = 1$, and the other reactants in R6.3 and R6.6 are present in excess amounts), which accounts for .06 moles, or approximately half of the chlorite.

The reactants in R5.3 include .008 moles of biotite, which is assumed here to have been present in the

protolith. No biotite is present in the products, inferring that none was produced by R6.5 or R6.7, so that $\epsilon_3 = \epsilon_5 = 0$. (Alternatively, the biotite produced by these reactions was removed by the fluids, in which case estimates of ϵ_3 and ϵ_5 are not possible.) The biotite on the reactant side of the alteration reaction was probably hydrated to produce chlorite plus K_2O , accounting for some of the excess chlorite on the reactants side. The remainder of the chlorite must have come from elements introduced into the shear zone by the fluids.

For shear zone CWM-35: $\epsilon_1 \approx 1$, $\epsilon_2 \approx .15$, $\epsilon_3 \approx 0$, $\epsilon_4 \approx 1$ and $\epsilon_5 \approx 0$. Therefore the maximum amount of epidote produced from R6.3, R6.6 and R6.7 would be:

$$\begin{aligned} ep &= -1.08\epsilon_1 - .172\epsilon_4 - \epsilon_5 \\ &= -1.25 \text{ moles, or } +1.25 \text{ moles consumed.} \end{aligned}$$

The maximum amount of calcite that could be produced from R6.3, R6.5, R6.6 and R6.7 would be:

$$\begin{aligned} cc &= 7.575\epsilon_1 + 5.714\epsilon_3 + \epsilon_4 + 9\epsilon_5 \\ &= 8.57 \text{ moles.} \end{aligned}$$

Clearly, significant amounts of these two minerals have been mobilized by the hydrothermal fluids.

The remaining six shear zones have no cpx preserved in their protoliths, and so the calculation of reaction progress variables is simplified. R6.18 to R6.20 define ξ_1 , ξ_2 and ξ_3 as the number of moles of chlorite produced by R6.3, the number of moles of albite from R6.4 and the number of moles of biotite from R6.5, respectively. As demonstrated for shear zones CWM-34 and CWM-35, the fact that the chemical systems are open to elements from external sources complicates the calculation of the reaction progress variables.

In shear zone CWM-41, no biotite is produced by the alteration, although a small amount of biotite is present among the reactants (R5.4). Thus ξ_3 is approximately 0.

In the same shear zone, .073 moles of chlorite were produced from .159 moles of actinolite. From the molar proportions of amphibole and chlorite in R6.3, the maximum amount of chlorite that could be produced from .159 moles of actinolite by R6.3 is about .079, which suggests that ξ_1 is roughly $.073/.079 = .92$, and that some amphibole is left over which has not been altered. In fact the sheared rock contains no amphibole (see Appendix G), which means that: 1) R6.3 went to completion and used up all of the amphibole (and therefore $\xi_1 = 1$), but some of the chlorite was removed by the fluids; or 2) ξ_1 is less than one, and

the remaining amphibole that was not consumed by the formation of chlorite was removed by the fluids. Since the major compositional difference between amphibole and chlorite is the higher calcium and silica contents in the amphibole (as well as a greater volatile content in chlorite), the net depletion of Ca and Si measured for this shear zone (Figure 5.2) would suggest that the latter was the case, and that excess amphibole went into solution. Based on this assumption, ϵ_1 is probably closer to .92 than to 1.0.

If R6.4 was the exclusive source of albite in the sheared assemblage of this shear zone, then $\epsilon_2 = .06$. If some of the albite produced by R6.4 has subsequently been removed by fluids, then ϵ_2 will be greater than .06, and conversely if some of the albite was produced from elements put into the shear zone by fluids, then ϵ_2 will be less than .06.

From ϵ_1 , ϵ_2 and ϵ_3 , the number of moles of calcite can be estimated as:

$$\begin{aligned} \text{mol cc} &= 7.575\epsilon_1 + 5.714\epsilon_3 \\ &= 6.8 \end{aligned}$$

In fact no calcite was found in the sheared sample, and

.011 moles of calcite were consumed by the net alteration, (see R5.4) suggesting that calcite was mobilized in the shear zone by the fluid.

Estimates of the reaction progress variables for the remaining five shear zones are presented in Table 6.4. The values of ξ_1 are generally high ($>.8$), while those of ξ_2 and ξ_3 are low ($<.25$). The high values of ξ_1 are in accord with the observation that in every shear zone, all or nearly all of the amphibole has been replaced by chlorite.

The amount of calcite produced from R6.3 and R6.5, given the values of ξ_1 and ξ_3 from Table 6.4 exceeds the amount of calcite found among the products in every sheared rock. However, in an open chemical system with ascending cooling fluids, the solubility of calcite would be increasing, thus the removal of calcite from the sheared assemblage would be expected.

Conclusions

It can be seen that the reaction progress variable can be used to track the extent of mineralogical changes. However, its application to open chemical systems is limited by the uncertainties involved in estimating the

Table 6.4 Estimates of reaction progress variables for
the net transfer reactions which characterize alteration
in the Mirage Island shear zones. 1.5 defined in text.

Shear Zone	E1	E2	E3	E4	E5
CWM-34	1.0	.10	.14	1.0	.14
CWM-35	1.0	.15	0	1.0	0
CWM-41	.9 to 1.0	.06	0	---	---
CWM-141	1.0	.19	.11	---	---
CWM-142	.8 to 1.0	.07	.24	---	---
CWM-149	1.0	.01	.06	---	---
CWM-160	1.0	.12	.12	---	---
CWM-163	.8 to .9	.08	1.0	---	---

effect the fluid has had on a given reaction.

In open chemical systems such as the shear zones on the Mirage Islands, alteration index is a simple and effective means of monitoring the reaction progress and of comparing the alteration states of different altered rocks. The change in alteration index (ΔAI) between unsheared-sheared pairs seems to vary systematically with the changes in concentration of volatiles, Fe^{2+} and Fe^{3+} , but does not appear to be a function of the changes in concentration of alkaline elements, Si, Mg or Mn.

Alteration in the shear zones entailed the hydration of amphibole and clinopyroxene to produce chlorite and biotite, and albitization of plagioclase. These mineralogical changes can be represented by a few independent net transfer reactions which, when added together, produce the net alteration reaction which has occurred in each shear zone (presented in Chapter 5). A reaction progress variable can be defined for each net transfer reaction; however solving for these variables is complicated by the fact that the chemical system was not closed. In every shear zone it is likely that reactions involving elements carried in solution by the hydrothermal fluids have contributed to the mineralogical changes

observed. Unfortunately, since the fluid compositions can only be estimated from fluid inclusion data and from changes in mineral chemistry, the effects of these open reactions cannot be quantified. Overall it was found that reactions involving the formation of chlorite at the expense of amphibole (+/- cpx) have values near 1, and albite-forming reactions and reactions involving biotite formation have low reaction progress variables (<.25).

CHAPTER 7: DISCUSSION AND CONCLUSIONS

Summary

The volcanic rocks of the Mirage Islands comprise a felsic to intermediate volcaniclastic suite with intercalated basaltic flows, intruded by gabbro dykes and sills. Primary textures preserved in the supracrustal rocks imply a subaqueous origin at a depth near that of a continental margin. The suite is interpreted to be correlative to the Banting Group of the Yellowknife Supergroup. The Mirage Island rocks were intruded to the west by a composite batholith known as the Western Plutonic Complex, and possibly in the south by another inferred plutonic body.

Rocks on the Mirage Islands have undergone two phases of metamorphism: a mid-amphibolite facies event (M1), during which temperatures reached 600°C and pressure is estimated to have been between 2 and 5 kbars; and a retrograde greenschist facies event (M2) with temperatures of 400 to 500°C, and pressures near 2 to 4 kbars.

Temperatures during M1 are compatible with conditions adjacent to a granitic pluton, in this case the Western

Plutonic Complex and/or the pluton inferred to be present south of the West Mirage Islands, and so the heat source for the amphibolite facies metamorphism is interpreted to be plutonic.

It is believed that shearing was initiated during M1 since temperatures from oxygen isotopes show that a few shear zones have preserved isotope fractions which equilibrated near 600°C.

Following peak M1 metamorphism and shear zone initiation, regional greenschist metamorphism (M2) prevailed on the Mirage Islands. Low pressure greenschist facies metamorphism has occurred throughout the Yellowknife Supergroup, and it is believed that this low grade metamorphism accompanied and outlasted M1, the latter being spatially controlled by plutonism. Retrogression in the permeable volcanoclastic rocks is extensive, whereas the less permeable gabbros have locally preserved amphibolite facies mineral assemblages.

The shear zones developed during M1 acted as conduits for the flow of hydrothermal fluids during M2. Extensive hydration, chemical alteration, and isotope exchange ensued as large volumes of fluid ascended through the shear zones, cooling with time. The presence of several

generations of secondary fluid inclusions attests to continued fluid flow during cooling.

The extent of hydration is variable between the shear zones, and as a result the re-equilibration of oxygen isotopes varied, thereby yielding a range of formation temperatures for the shear zones. Equilibrium temperatures in shear zones which re-equilibrated during M2 range from 470 to 350°C. Formation pressures, estimated from primary fluid inclusions in quartz veins, are low - from 0 to 0.75 kbar - and from this it is inferred that movement and deposition of quartz in the shear zones continued during M2. Displacement produced local dilatant zones in the shears, in which pressures may have been reduced sufficiently to cause boiling of the fluid.

The fluid which moved through the shear zones was not in equilibrium with the rock, since fluid-rock interaction produced not only changes in the mineral assemblages, but also in the bulk chemical compositions (including the oxygen isotopic compositions) of the sheared rocks. In general, sheared metabasites were enriched in volatiles, K, Rb, Fe^{2+} , and ^{18}O , and were depleted in Na, Ca, Sr, Fe^{3+} , and Si as a result of hydrothermal alteration. Mg and Mn do not show a consistent pattern. Sheared felsic

to intermediate volcanoclastic rocks were enriched in volatiles, K, Fe^{2+} , Mg, Mn; and were depleted in Fe^{3+} , Si, and Na.

Oxygen isotopic compositions calculated for the hydrothermal fluids lie in the ranges defined for metamorphic and igneous fluids. The source of the hydrothermal fluids is therefore not known for certain. However, during shear zone initiation it is likely that the magmatic fluids circulating about the Western Plutonic Complex or the inferred pluton (or both) were present in the shear zones, since the shear zones were formed during M1, which accompanied plutonism. As shear zone alteration continued into M2, it is probable that metamorphic fluids contributed to shear zone alteration, although the possible role of igneous fluids cannot be disproven. The oxygen isotopic compositions calculated for the fluids in the M2-equilibrated shear zones imply either that:

- 1) there was local input by circulating meteoric water; or
- that 2) the fluids reacted extensively in the shear zones, thus becoming depleted in ^{18}O .

Iron in the shear zones is generally in a more reduced state than in the adjacent unsheared rocks, implying that large volumes of hydrothermal fluids were ascending and cooling with time. The presence of a few oxidized shear

zones implies the existence of descending fluids, either due to convection of the metamorphic (+/- igneous) fluids, or the presence locally of meteoric water.

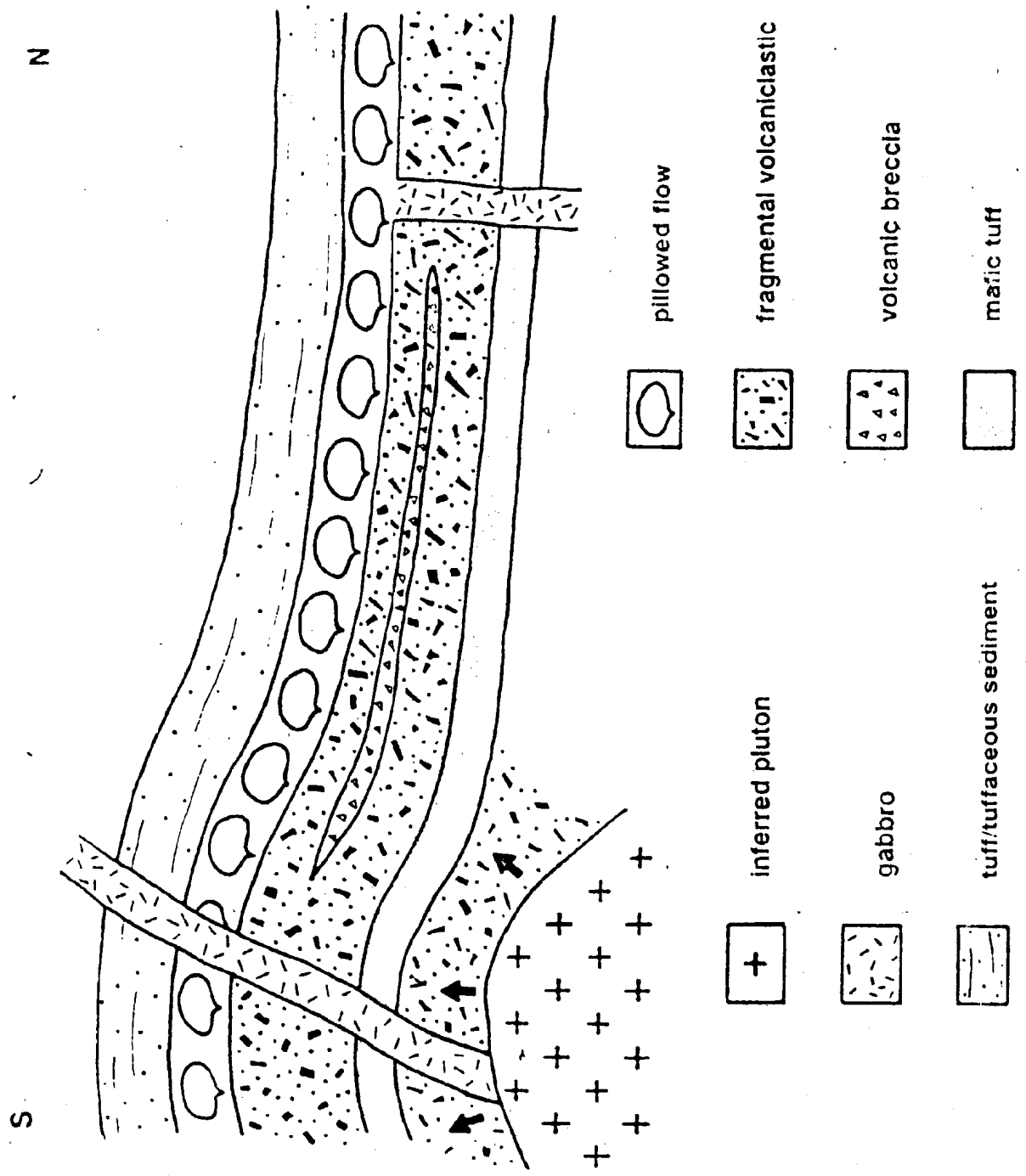
Fluid:rock ratios have been estimated from the amount of volatiles incorporated into the sheared mineral assemblages, and from the amount of silica consumed or released during alteration. Generally the minimum ratios are on the order of 10:1.

Shear Zone Model

In this section, a model is proposed for the formation and alteration history of the Mirage Island shear zones, in light of the metamorphic history and interpreted geology. It is subdivided into three stages, involving the intrusion of the plutonic bodies into the volcanic pile; the formation of the shear zones during M1 as a result of plutonism; and the subsequent flushing of large volumes of fluid through the shear zones during M2.

The first stage is illustrated schematically in Figure 7.1. The intrusion of a plutonic body into the supracrustal sequence produced a thermal aureole and

Figure 7.1 Deposition of the Mirage Island supracrustal sequence was followed by the intrusion of one or more plutonic bodies. Their intrusion produced amphibolite facies contact metamorphic aureoles on the surrounding rocks. Arrows indicate the direction of movement of the pluton.



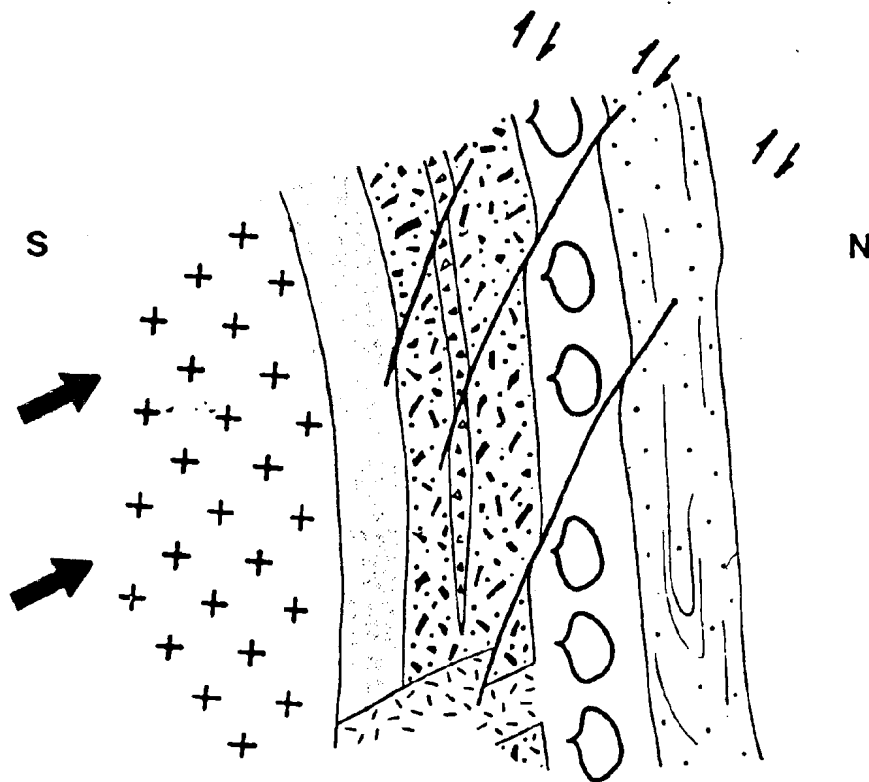
initiated M1 amphibolite facies metamorphism. It is uncertain whether the supracrustal rocks were undergoing regional greenschist facies metamorphism at the time, as contact metamorphism and subsequent retrogression have overprinted any possible evidence of it.

In the second stage (Figure 7.2), the volcanic package was deformed and tilted into its present, near vertical orientation as the pluton continued to intrude. In this model, the principle compressive stresses imposed on the country rocks by the intruding body would have been approximately horizontal and oriented north-south in the area of the West Mirage Islands, resulting in faults that were steeply-dipping east-west structures with south side up displacement. Limited kinematic data from the West Mirage Islands indicate that displacement was actually oblique slip locally.

Following plutonism and shear zone initiation during M1, regional greenschist facies metamorphism (M2) ensued. The final stage of the shear zone history entails the focussing of large volumes of metamorphic fluids in the shear zones. Ascending hydrothermal fluids derived from dehydration reactions at depth (plus possibly some relict igneous fluids associated with the adjacent cooling pluton) moved through the shear zones, changing both the

Figure 7.2 During the intrusion of the inferred pluton the volcanic units were tilted into a subvertical orientation. Subhorizontal north-south stresses around the pluton produced a series of steeply-dipping, east-west striking, south side up shear zones in the overlying rocks. Arrows indicate the direction of movement of the pluton.

Shear Zone Formation
south side up displacement



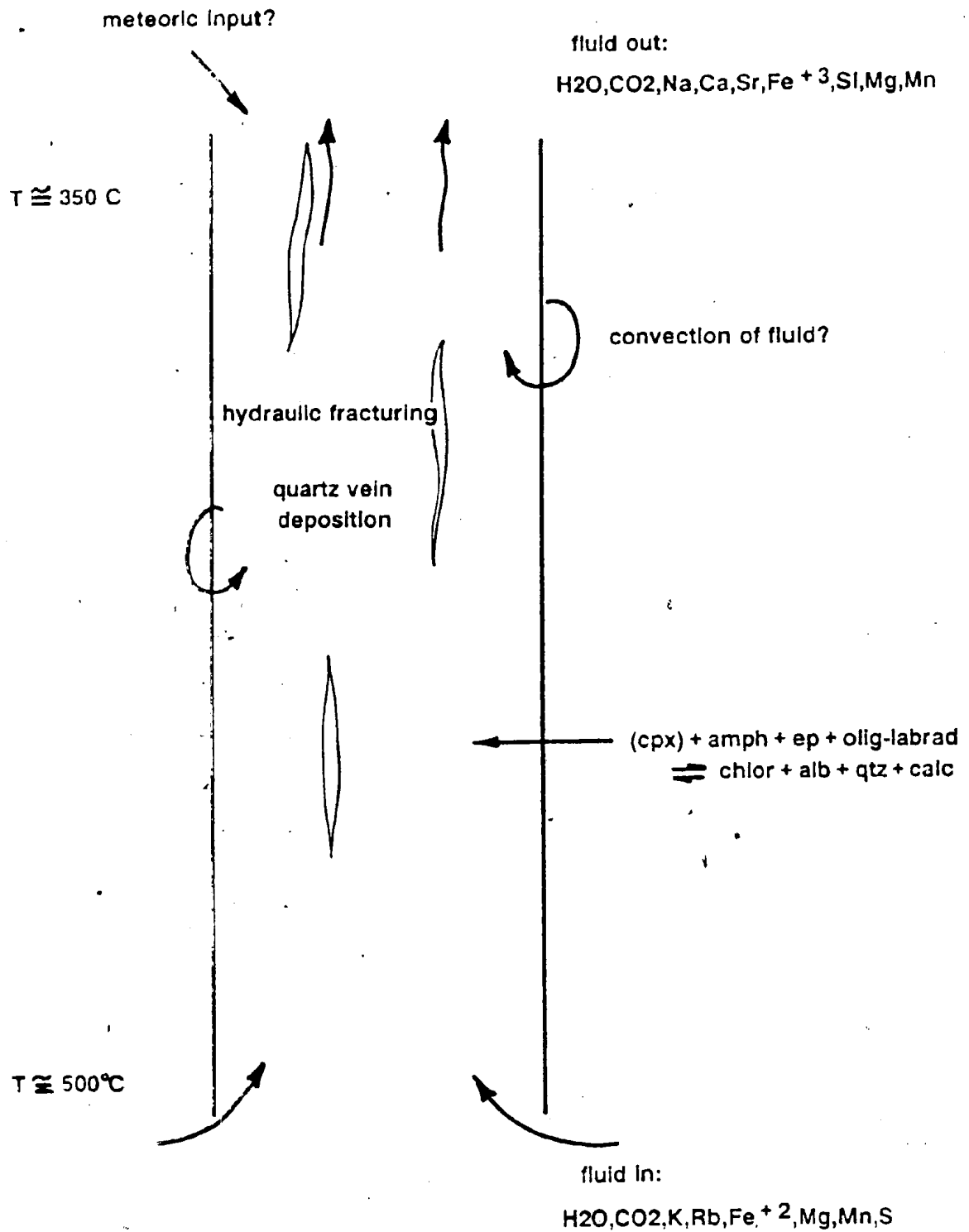
mineral assemblage and the bulk chemistry of the sheared rock (Figure 7.3).

As the fluids ascended and the temperature dropped, anastomosing, schistosity-parallel quartz veins were deposited. Locally, hydrothermal fluids descended in the shear zones, and caused the precipitation of carbonate veins. The behavior of the fluid caused an overall reduction of iron in the shear zones, but local zones of oxidation occurred. The descending fluid may have been derived from meteoric water near the surface, or it may represent localized convection of the fluid, which has a net upward flow direction (Figure 7.3).

Incremental movements along the shear zones continued during (M2), producing localized offsets inside the shear zones, and resulting in several generations of secondary fluid inclusions.

In the Mirage Islands, the amount of alteration and the equilibrium temperature is variable between the shear zones. This is not interpreted to imply that the formation of individual shear zones occurred at different times, but rather that the final "closing" of the shear zones varied with time. In Figure 7.4, this is

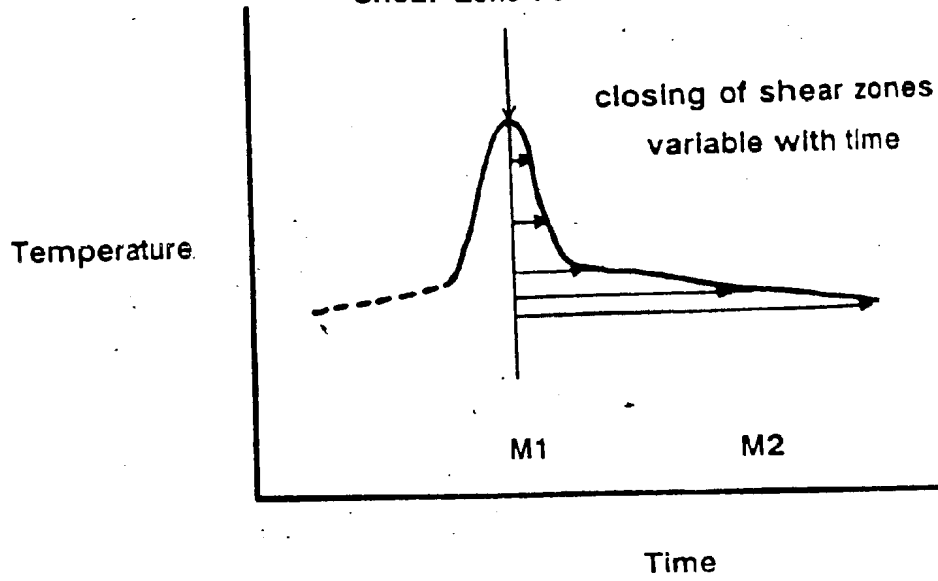
Figure 7.3 Following the formation of the shear zones, hydrothermal fluids derived from regional greenschist facies metamorphic reactions (perhaps accompanied by magmatic fluids associated with cooling of the inferred pluton) were focussed in the shear zones. Amphibolite facies (M1) assemblages were re-equilibrated to greenschist facies (M2) assemblages in the presence of these fluids, which also produced changes in the bulk chemical compositions of the rocks in the shear zones. The net flow-direction of hydrothermal fluids in the shear zones was upward, but locally downward-directed flow of fluids (either from a meteoric source or as a result of convection) occurred.



illustrated schematically on a temperature-time plot. The shear zones were formed during M1, which accompanied plutonism, and were initially altered by fluids derived from a magmatic source. Hydrothermal alteration continued after the cooling of the pluton, with metamorphic fluids derived from M2. Alteration in some shear zones ended following M1, while in others it lasted well into M2, resulting in a range of final alteration stages and measured equilibrium temperatures.

Figure 7.4 Schematic temperature - time plot showing the interpreted timing of shear zone formation (syn-M1), and the variable timing of shear zone closure (during M2). Because the closure of the shear zones varied with time, a wide range of equilibrium temperatures and alteration states is observed.

Shear Zone Formation



REFERENCES

- Aggarwal, P.K. and Longstaffe, F.J., 1987. Oxygen-isotope geochemistry of metamorphosed, massive sulfide deposits of the Flin Flon - Snow Lake Belt, Manitoba. Contributions to Mineralogy and Petrology, 96, pp. 314-325.
- Allison, I. and Kerrich, R., 1981. Deformation and fluid transport in shear zones at Yellowknife: structural controls, hydrostatic regime, and chemical mass balance, in Gold Workshop Volume, ed. by R.D. Morton, Yellowknife Geo-Workshop Committee, Yellowknife, pp. 202-222.
- Baragar, W.R., 1975. Miscellaneous data from volcanic belts at Yellowknife, Wolverine Lake, and James River, in Report of Activities, Part A. Geological Survey of Canada Paper 75-1A, pp. 281-286.
- Bostock, H.H., 1980. Geology of the Itchen Lake area, District of Mackenzie. Geological Survey of Canada Memoir 391, 101 p.

Boyle, R.W., 1961. The geology, geochemistry and origin of the gold deposits of the Yellowknife District. Geological Survey of Canada Memoir 310, 193 p.

Boyle, R.W., 1979. The geochemistry of gold and its deposits, Geological Survey of Canada Bulletin 280, 584 p.

Burrus, R. C., 1981. Analysis of phase equilibria in C-O-H-S fluid inclusions, in M.A.C. Short Course in Fluid Inclusions: Applications to Petrology, ed. by L.S. Hollister and M.L. Crawford. 304 p.

Clayton, R.N., O'Neil, J.R. and Mayeda, T.K., 1972. Oxygen isotope exchange between quartz and water. Journal of Geophysical Research, vol.77, pp. 3057-3067.

Colvine, A.C., Andrews, A.J., Cherry, M.E., Durocher, M.E., Fyon, A.J., Lavigne, M.J. Jr., MacDonald, A.J., Marmont, S., Poulsen, K. H., Springer, J.S. and Troop, D. C., 1984. An integrated model for the origin of Archean lode gold deposits. Ontario Geological Survey Open File Report 5524, 98 p.

Crawford, M.L., 1981. Phase equilibria in aqueous fluid inclusions. in M.A.C. Short Course in Fluid Inclusions: Applications to Petrology, ed. by L.S. Hollister and M.L. Crawford, 304 p.

CRC Handbook of Chemistry and Physics, 1983, 63rd edition. Copyright 1983 by CRC Press, Inc.

Drury, S.A., 1977. Structures induced by granite diapirs in the Archean greenstone belt of Yellowknife, N.W.T.: implications for Archean geotectonics. *Journal of Geology*, 85, pp. 345-358.

Easton, R.M., 1984. Compilation of geochronologic data for the Yellowknife greenstone belt (85J/8, 85J/9) and vicinity, District of Mackenzie, N.W.T. in Contributions to the Geology of the N.W.T., ed. by J.A. Brophy, Vol. 1, Northern Affairs Program, pp.1-20.

Epstein, S. and Taylor, H.P. Jr., 1967. Variation of $^{18}O/^{16}O$ in minerals and rocks. in Researches in Geochemistry vol. 2, ed. by P.H. Abelson. J. Wiley and Sons, New York, Copyright, pp. 29-62.

Faure, G., 1977. Principles of Isotope Geology. John Wiley and Sons, New York, Copyright, 464p.

Ferry, J.M., 1980. A case study of the amount and distribution of heat and fluid during metamorphism. Contributions to Mineralogy and Petrology, 71, pp. 373-385.

Ferry, J.M., 1983. Applications of the reaction progress variable in metamorphic petrology. Journal of Petrology, 24, pp. 343-376.

Ferry, J.M., 1984. Phase composition as a measure of reaction progress and an experimental model for the high-temperature metamorphism of mafic igneous rocks. American Mineralogist, 69, pp. 677-691.

Ferry, J.M., 1985. Hydrothermal alteration of Tertiary igneous rocks from the Isle of Sky, NW Scotland, parts I and II. Contributions to Mineralogy and Petrology, 91, pp. 264-304.

Fleming, P.D. and Fawcett, J.J., 1976. Upper stability of chlorite and quartz in the system MgO-FeO-Al₂O₃-SiO₂-H₂O at 2 kbar water pressure. American Mineralogist, 61, pp. 1175-1193.

Friedman I. and O'Neil J.R., 1977. Compilation of stable isotope fractionation factors of geochemical interest. 6th edition. United States Geological Survey Professional Paper 440-KK, 12 p.

Fyfe, W.S., Price, N.J. and Thompson, A.B., 1978. Fluids in the Earth's Crust. Elsevier Scientific Publishing Company, Amsterdam, Copyright 1978, 303 p.

Fyfe, W.S., and Kerrich, R., 1976. Geochemical prospecting: extensive versus intensive factors. Journal of Geochemical Exploration, 6, pp. 117-192.

Fyon, J.A., Crocket, J.H. and Schwarz, H.P., 1983. Application of stable isotope studies to gold metallogeny in the Timmins-Porcupine camp. Ontario Geological Survey Open File 5464, 182 p.

Goldak, G.R., 1987. Marine Seismic Survey, Marlin Claim Group, Yellowknife Bay, N.W.T. Confidential Assessment Report filed by Golden Marlin Mines Limited.

Gresens, R.L., 1967. Composition-volume relationships of metasomatism, Chemical Geology 2, pp. 47-55.

Grant, J.A., 1986. The isocon diagram - a simple solution to Gresen's equation for metasomatic alteration. *Economic Geology*, 81, pp. 1976-1982.

Harte, B. and Graham, C.M., 1975. The graphical analysis of greenschist to amphibolite facies mineral assemblages in metabasites. *Journal of Petrology*, 16, pp. 347-370.

Helmstaedt, H. and Padgham, W.A., 1986. A new look at the stratigraphy of the Yellowknife Supergroup at Yellowknife, N.W.T. - Implications for the age of gold-bearing shear zones and Archean basin evolution. *Canadian Journal of Earth Sciences*, 23, pp. 454-475.

Helmstaedt, H., Padgham, W.A. and Brophy, J.A., 1986. Multiple dikes in Lower Kam Group, Yellowknife greenstone belt: Evidence for Archean sea-floor spreading? *Geology*, 14, pp.562-566.

Helmstaedt, H., King, J.E., Goodwin, J.A. and Patterson, J.G., 1981. Geology of the southwest end of the Yellowknife greenstone belt. in *Proceedings of the Gold Workshop, Yellowknife*, ed. by R.D. Morton. Geoworkshop Committee, Yellowknife, N.W.T., pp. 232-249.

Henderson, J.B., 1981. Archean basin evolution in the Slave Province, Canada. in Plate Tectonics in the Precambrian, ed. by A.E. Kroner, Elsevier Scientific Publishing Company, Amsterdam. pp. 213-235.

Henderson, J.B., 1978. Age and origin of the gold-bearing shear zones at Yellowknife, N.W.T. Geological Survey of Canada Paper 78-1A, pp. 259-262.

Henderson, J.B., 1970. Stratigraphy of the Yellowknife Supergroup, Yellowknife Bay - Prosperous Lake area, District of Mackenzie, Geological Survey of Canada Paper 70-26.

Henderson, J.F. and Brown, I.C., 1966. Geology and structure of the Yellowknife greenstone belt, District of MacKenzie. Geological Survey of Canada Bulletin 141.

Hoefs, J., 1973. Stable Isotope Geochemistry. Copyright 1973, Springer-Verlag, New York, 140 p.

Hoefs, J., 1980. Stable Isotope Geochemistry. Copyright 1980, Springer-Verlag, New York, 208 p.

Hoffman, P.F., 1986. Crustal accretion in a 2.7-2.5 Ga "Granite-Greenstone" terrane, Slave Province, N.W.T.: a prograding trench-arc system?. GAC/MAC Abstracts, 11, p. 82.

Jolliffe, A.W., 1938. Yellowknife Bay-Prosperous Lake Area, N.W.T. Geological Survey of Canada Paper 38-21.

Jolliffe, A.W. 1946. Yellowknife Bay, District of MacKenzie, N.W.T. Geological Survey of Canada Map 709A.

Keevil, 1942. Vapor pressures of aqueous solutions at high temperatures. Journal of the American Chemistry Society, 64, pp. 841-850.

Kerrich, R., Fyfe, W.S. and Allison, I., 1977a. Iron reduction around gold-quartz veins, Yellowknife District, N.W.T., Canada. Economic Geology, 72, pp.657-663.

Kerrich, R., Fyfe, W.S., Gorman, B.E. and Allison, I., 1977b. Local modification of rock chemistry by deformation. Contributions to Mineralogy and Petrology, 65, pp. 183-190.

Kerrich, R. and Allison, I., 1978. Vein geometry and hydrostatics during Yellowknife mineralization. Canadian Journal of Earth Sciences, 15, pp. 1653-1660.

Kerrich, R. and Fryer, B.J., 1979. Archaean precious-metal hydrothermal systems, Dome Mine, Abitibi Greenstone Belt. II. REE and oxygen isotope relations, Canadian Journal of Earth Sciences, 16, pp. 440-458.

Kerrich, R., 1981. Archean lode gold deposits: a synthesis of data on metal distribution, fluid inclusions and stable isotopes, with special reference to Yellowknife. in Gold Workshop Volume, ed. by R.D. Morton, Yellowknife Geo-Workshop Committee, Yellowknife, pp. 95-171.

Kerrich, R. and Fyfe, W.S., 1981. The gold-carbonate association: source of CO₂, and CO₂ fixation reactions in Archean lode deposits. Chemical Geology, 33, pp. 265-294.

Kerrich, R., 1983. Geochemistry of gold deposits in the Abitibi Greenstone Belt. Canadian Institute of Mining and Metallurgy, Special Volume 27, Perry Printing, Lachine, Quebec, 71 p.

King, J.E., Davis, W.J., Relf, C. and Avery, R.W., in press. Deformation and plutonism in the western Contwoyto Lake map area (86E), central Slave Province, District of Mackenzie, N.W.T. in Current Research, Part A, G.S.C. Paper 88-1A.

Laird, J. and Albee, A.L., 1981. Pressure, temperature, and time indicators in mafic schist: Their application to reconstructing the polymetamorphic history of Vermont. *American Journal of Science*, 281, pp. 127-175.

Leake, B.E., 1978. Nomenclature of Amphiboles. *American Mineralogist*, 16, pp. 501-520.

Mathews A., Goldsmith, J.R. and Clayton, R.N., 1983. Oxygen isotope fractionations involving pyroxenes: the calibration of mineral-pair geothermometers. *Geochimica et Cosmochimica Acta*, 47, pp. 631-644.

Matsuhisa, Y., Goldsmith, J.R., and Clayton, R.N., 1979. Oxygen isotope fractionation in the system quartz-albite-anorthite-water. *Geochimica et Cosmochimica Acta*, 43, pp. 1131-1140.

McGlynn, J. and Henderson, J.F., 1972. The Slave Province. in Variations in Tectonic Styles in Canada. ed. by R.A. Price and R.G.W. Douglas. Geological Association of Canada Special Paper 11, pp. 506-526.

Meuhlenbachs, K. and Clayton, R.N., 1976. Oxygen isotope composition of the oceanic crust and its bearing on seawater. Journal of Geophysical Research, 81, pp. 4365-4369.

Padgham, W.A., 1981. Archean crustal evolution - a glimpse from the Slave Province. Special Publication of the Geological Society of Australia, 7, pp. 99-110.

Padgham, W.A., 1983. Gold deposits of the N.W.T.: Classes, styles, genesis, exploration methods and success probabilities. 11th annual Geoscience Forum, December 1983, Yellowknife, N.W.T.

Padgham, W.A., 1985. Observations and speculations on supracrustal successions in the Slave Structural Province. Geological Association of Canada, Special Paper 28, pp. 133-151.

Plyusnina, L.P., 1982. Geothermometry and geobarometry of plagioclase-hornblende-bearing assemblages. Contributions to Mineralogy and Petrology, 80, pp. 140-146.

Potter, R.W., 1977. Pressure corrections for fluid-inclusion homogenization temperatures based on the volumetric properties of the system NaCl-H₂O. United States Geological Survey Journal of Research, 5, pp. 603-607.

Potter, R.W. and Brown, D.L., 1975. The volumetric properties of aqueous chloride solutions from 0 to 500°C at pressures up to 2000 bars based on a regression of the available literature data. United States Geological Survey Open File Report. 31 p.

Potter, R.W., Clynne, M.A. and Brown, D.C., 1978. Freezing point depression of aqueous sodium chloride solutions. Economic Geology 73, pp. 284-285.

Powell, R. and Evans, J., 1983. A new geobarometer for the assemblage biotite-muscovite-chlorite-quartz. Journal of Metamorphic Geology, 1, pp. 331-336.

Relf, C., 1986a. The Geology of the West Mirage Islands. 13th annual Geoscience Forum, December, 1983, Yellowknife, N.W.T.

Relf, C., 1986b. Geology of the West and East Mirage Islands. Department of Indian and Northern Affairs Canada, Open File map.

Rice, J.M. and Ferry, J.M., 1982. Buffering, infiltration and the control of intensive variables during metamorphism, in Characterization of Metamorphism through Mineral Equilibria, ed. by J.M. Ferry, Mineralogical Society of America, volume 10.

Robinson, P., Spear, F.S., Schumacher, J.C., Laird, J., Klein, C., Evans, B.W. and Doolan, B.L., 1983. Phase relations of metamorphic amphiboles: natural occurrence and theory. in Reviews in Mineralogy vol 9b, Amphiboles: Petrology and Experimental Phase Relations. ed. by D.R. Veblen and P.H. Robins, pp. 1-227.

Roedder, E., 1984. Fluid Inclusions, Mineralogical Society of America volume 12, pp. 221-250.

Roedder, E. and Bodnar, E.J., 1980. Geologic pressure determinations from fluid inclusion studies. Annual Review of Earth and Planetary Science, 8, pp. 1-41.

Roedder, E., 1979. Fluid Inclusions as samples of ore fluids, in Geochemistry of Hydrothermal Ore Deposits, second edition, ed. by H.L. Barnes, pp. 684-737.

Spear, F.S., 1980. NaSi - CaAl exchange equilibria between plagioclase and amphibole: an empirical model. Contributions to Mineralogy and Petrology, 72, pp. 33-41.

Spear, F.S., 1981. Amphibole + plagioclase equilibria: An empirical model for the relation albite + tremolite = edenite + 4 quartz. Contributions to Mineralogy and Petrology, 77, pp. 355-364.

Sterner, S.M. and Bodnar, R.J., 1984. Synthetic fluid inclusions in natural quartz I. Compositional types synthesized and applications to experimental geochemistry. Geochimica et Cosmochimica Acta., 48, pp. 2659-2668.

- Taylor, H.P. Jr. and Epstein, S., 1962. Relationships between $^{18}\text{O}/^{16}\text{O}$ ratios in coexisting minerals of igneous and metamorphic rocks. Bulletin of the Geological Society of America 73, pp. 461-480.
- Taylor, H.P. Jr., 1967. Oxygen isotope studies of hydrothermal mineral deposits. in Geochemistry of Hydrothermal Ore Deposits, ed. by H.L. Barnes, Holt, Rinehart and Winston, Inc., New York, pp. 109-142.
- Thompson, J.B. Jr., 1982. Composition space: an algebraic and geometric approach. in Characterization of Metamorphism through Mineral Equilibria, ed. by J.M. Ferry, Mineralogical Society of America, 10, 397 p.
- Wenner, D.B. and Taylor, H.P. Jr., 1971. Temperatures of serpentinization of ultramafic rocks based on $^{18}\text{O}/^{16}\text{O}$ fractionation between coexisting serpentine and magnetite. Contributions to Mineralogy and Petrology, 32, pp. 165-185.

APPENDIX AMicroprobe Analyses

Minerals were analyzed on a Jeol JXA50A electron probe X-ray microanalyzer. The standard used was a clinopyroxene (ACPX) with the following composition (expressed as wt % of oxides): Na₂O - 1.27, MgO - 16.65, Al₂O₃ - 7.86, SiO₂ - 50.73, K₂O - 0, CaO - 15.82, TiO₂ - 0.74, MnO - 0.13, FeO - 6.76.

The results were found to be reproducible to within about +/- 0.05 wt %, and most elements, with the exception of Si and Na, have an estimated accuracy of +/- 5 % of the reported values (H. Longrich, personal communication, 1986). The lower limit of detection of an element is approximately 0.02 wt %.

Results of mineral analyses used in this study are presented on the following pages. "Wt %" refers to the weight percent oxide in a mineral, and "form" refers to the stoichiometric number of each cation in one formula unit of a mineral. Calcic amphiboles were normalized to 13 cations excluding Ca, Na, and K, after Robinson et al. (1982). Plagioclase formulae were calculated to 8 oxygen, and chlorite to 28 oxygen.

The quality of analyses is variable. In particular, plagioclase wt % totals were found to have a wide range. Because the standard used to calibrate the probe has a low Na content, Na is likely a major source of error in albite analyses.

In the section on plagioclase chemistry (Chapter 2), analyses with wt % totals outside of the range 98 - 102 %, but which yielded constant Ca:Na ratios were taken as acceptable, since they were only used to compare anorthite contents of plagioclases. In the section on thermometry (also in Chapter 2), calculations were restricted to those plagioclases with totals between 98 and 102 wt %. Those with totals outside of 99 - 101%, but between 98 and 102% are indicated in the text with an asterisk (*). Errors inherent in the temperature calculations using Spear's (1980, 1981) thermometers are estimated to be +/- 70°C for plagioclases with totals between 98 - 99% and 101 - 102%, versus +/- 50 C for plagioclases with totals between 99 - 101%.

Chlorite analyses were found to have wt % totals between about 85 and 88%. Analyses near the lower end of this range have silica contents lower than expected for chlorite, and therefore the main source of error in these analyses is believed to be a result of poor silica totals.

Unsheared gabbro sample: CWM-15 (plagioclase)

	wt %	form
Na2O	1.18	1.02
Al2O3	18.93	1.00
SiO2	67.08	2.99
K2O	0.03	.00
CaO	0.15	.01
FeO	0.01	.00
Total:	98.80	5.02

Unsheared gabbro sample: CWM-34A (plagioclase)

	wt %	form	wt %	form	wt %	form	wt %	form
Na2O	10.11	.86	10.92	.92	10.51	.89	10.41	.9
Al2O3	21.01	1.08	20.46	1.05	20.73	1.07	20.06	1.06
SiO2	66.39	2.90	66.87	2.91	66.63	2.91	65.16	2.91
K2O	0.10	.00	0.04	.00	0.70	.00	0.20	.01
CaO	2.98	.14	2.78	.13	2.88	.13	2.60	.13
FeO	0.10	.00	0.06	.00	0.07	.00	0.06	.00
Total:	99.69	4.98	101.13	5.01	100.89	5.00	98.50	5.01

Na2O	10.20	.87
Al2O3	21.59	1.12
SiO2	65.02	2.85
K2O	0.05	.00
CaO	3.83	.18
FeO	0.10	.00
Total:	100.79	5.02

Unsheared gabbro sample: CWM-34A (amphibole)

	wt %	form	wt %	form	wt %	form	wt %	form
Na2O	.83	.24	.94	.27	.75	.21	.86	.25
MgO	12.15	2.73	13.06	2.88	12.64	2.72	12.15	2.74
Al2O3	5.31	.95	6.44	1.12	5.43	.92	5.31	.95
SiO2	47.26	6.99	47.04	6.96	50.42	7.28	47.26	7.00
K2O	0.27	.05	0.34	.06	0.29	.05	0.27	.05
CaO	10.25	1.66	11.57	1.84	11.20	1.73	10.25	1.66
TiO2	1.09	.12	.58	.06	.63	.05	1.09	.11
MnO	.39	.05	.34	.04	.31	.04	.39	.05
Fe _{tot}	16.95	2.08	15.55	1.93	16.32	1.97	16.97	2.09
Total:	94.62	14.82	95.86	15.16	97.96	14.97	94.55	14.90

Sheared gabbro sample: CWM-34B (plagioclase)

	wt %	form	wt %	form
Na2O	11.91	1.02	11.81	1.04
Al2O3	20.23	1.05	19.88	1.07
SiO2	65.99	2.92	62.94	2.84
K2O	0.05	.00	0.25	.00
CaO	1.21	.03	0.93	.04
FeO	0.17	.00	1.61	.06
Total:	99.46	5.04	97.42	5.06

Sheared gabbro sample: CWM-34B (chlorite)

	wt %	form	wt %	form
Na2O	.00	.000	.04	.012
MgO	16.50	5.209	16.68	5.337
Al2O3	20.57	5.135	20.41	5.161
SiO2	25.77	5.458	24.72	5.306
K2O	.02	.000	.02	.000
CaO	.02	.000	.03	.006
TiO2	.06	.006	.05	.004
MnO	.28	.049	.25	.044
FeO	22.95	4.065	23.07	4.140
Cl	.01	.000	.03	.000
Total:	86.29	19.941	85.48	20.037

Unsheared gabbro sample: CWM-35A (plagioclase)

	wt %	form	wt %	form	wt %	form	wt %	form
Na2O	4.00	.35	6.14	.54	5.55	.49	4.97	.44
Al2O3	29.14	1.57	27.00	1.41	27.12	1.46	27.96	1.51
SiO2	52.19	2.40	55.88	1.41	54.58	2.49	53.02	2.44
K2O	0.15	.01	0.08	.00	0.10	.01	0.54	.03
CaO	12.91	.63	10.15	.49	11.21	.54	11.60	.57
FeO	0.60	.02	0.57	.02	0.70	.20	0.91	.03
Total:	99.00	4.98	99.82	5.01	99.26	5.01	99.00	5.02
Na2O	3.87	.34	5.42	.48				
Al2O3	28.82	1.55	27.46	1.47				
SiO2	52.49	2.40	54.36	2.47				
K2O	0.05	.00	0.13	.01				
CaO	13.42	.66	11.38	.55				
FeO	0.81	.03	0.80	.02				
Total:	99.46	4.98	99.55	5.00				

Unsheared gabbro sample: CWM-35A (clinopyroxene)

	wt %	form	wt %	form
Na ₂ O	.22	.015	.57	.042
MgO	17.10	.927	12.88	.735
Al ₂ O ₃	2.04	.086	4.05	.182
SiO ₂	55.70	2.027	50.49	1.935
K ₂ O	.04	.001	.20	.009
CaO	12.64	.492	9.16	.375
TiO ₂	.06	.001	.18	.004
MnO	.22	.006	.41	.012
FeO	12.18	.370	19.70	.631
Total:	100.31	3.927	98.71	3.957

Unsheared gabbro sample: CWM-35A (amphibole)

	wt %	form	wt %	form	wt %	form	wt %	form
Na ₂ O	.51	.14	.12	.03	.30	.11	.51	.15
MgO	12.15	2.65	14.17	3.26	14.58	3.10	12.15	2.64
Al ₂ O ₃	4.93	.85	1.14	.19	3.25	.55	4.93	.85
SiO ₂	50.21	7.35	52.14	7.73	53.16	7.66	50.12	7.35
K ₂ O	.24	.05	.04	.01	.11	.02	.24	.04
TiO ₂	.50	.05	.09	.01	.10	.01	.50	.05
MnO	.43	.05	.25	.03	.23	.03	.43	.05
Fe _{tot}	16.61	2.03	14.20	1.80	13.76	1.64	16.61	2.04
Total:	97.06	14.97	94.50	14.86	98.00	15.02	96.97	14.97

Sheared gabbro sample: CWM-35B (plagioclase)

	wt %	form	wt %	form
Na ₂ O	11.73	1.01	11.23	.96
Al ₂ O ₃	19.21	1.00	19.92	1.04
SiO ₂	66.99	2.97	67.22	2.96
K ₂ O	0.03	.00	0.10	.00
CaO	0.96	.04	0.79	.04
FeO	0.09	.00	0.14	.00
Total:	99.01	5.02	99.40	4.97

Sheared gabbro sample: CWM-35B (chlorite)

	wt %	form	wt %	form
Na ₂ O	.00	.000	.01	.000
MgO	16.36	6.635	16.32	6.741
Al ₂ O ₃	20.18	6.476	20.46	6.684
SiO ₂	26.25	7.147	24.74	6.863
K ₂ O	.00	.000	.01	.000
CaO	.04	.008	.04	.004
TiO ₂	.07	.008	.06	.008
MnO	.28	.063	.29	.065
FeO	22.76	5.180	22.92	5.316
Cl	.00	.000	.01	.000
Total:	86.19	25.564	85.03	25.716

Unsheared gabbro sample: CWM-41A (plagioclase)

	wt %	form
Na ₂ O	10.29	.87
Al ₂ O ₃	21.67	1.11
SiO ₂	66.01	2.88
K ₂ O	0.18	.01
CaO	1.74	.12
FeO	0.08	.00
Total:	99.91	4.99

Unsheared gabbro sample: CWM-41A (amphibole)

	wt %	form	wt %	form	wt %	form	wt %	form
Na ₂ O	.30	.08	.25	.07	.38	.11	.32	.09
MgO	15.24	3.21	15.61	3.25	13.66	2.98	15.61	3.27
Al ₂ O ₃	3.16	.52	3.44	.57	5.93	1.02	3.06	.51
SiO ₂	52.53	7.67	52.69	7.65	48.20	7.05	53.51	7.65
K ₂ O	.08	.01	.07	.01	.17	.03	.07	.01
CaO	11.52	1.74	12.54	1.89	12.40	1.94	12.78	1.92
TiO ₂	.19	.02	.05	.00	.86	.09	.07	.01
MnO	.19	.02	.24	.03	.18	.02	.25	.03
Fe _{tot}	13.09	1.54	12.59	1.48	14.77	1.81	13.07	1.26
Total:	96.30	14.81	97.48	14.95	94.70	15.05	96.74	14.75

	wt %	form	wt %	form
Na2O	.17	.05	.29	.08
MgO	16.57	3.51	15.05	3.18
Al2O3	1.17	.19	3.80	.63
SiO2	53.71	7.24	52.18	7.53
K2O	.02	.00	.09	.02
CaO	12.78	1.95	12.09	1.84
TiO2	.10	.01	.08	.01
MnO	.20	.02	.18	.02
Fe _{tot}	11.83	1.41	13.72	1.63
Total:	96.55	14.98	97.48	14.94

Sheared gabbro sample: CWM-41B (plagioclase)

	wt %	form	wt %	form
Na2O	11.16	.982	11.88	1.026
MgO	.00	.000	.00	.000
Al2O3	19.53	1.044	18.91	.993
SiO2	65.27	2.963	67.05	2.991
K2O	.04	.001	.03	.001
CaO	.26	.012	.15	.006
TiO2	.00	.000	.00	.000
MnO	.03	.000	.00	.000
FeO	.01	.000	.01	.000
Total:	96.30	5.002	98.05	5.018

Sheared gabbro sample: CWM-41B (chlorite)

	wt %	form	wt %	form	wt %	form	wt %	form
Na2O	.01	.000	.04	.012	.00	.000	.04	.012
MgO	16.51	5.019	16.66	5.153	16.37	5.109	16.14	5.025
Al2O3	20.82	5.007	21.30	5.208	21.34	5.269	21.08	5.184
SiO2	27.67	5.647	25.90	5.372	25.46	5.331	26.17	5.466
K2O	.03	.006	.00	.000	.00	.000	.01	.000
TiO2	.06	.005	.04	.004	.07	.006	.02	.001
MnO	.20	.030	.21	.036	.18	.030	.25	.042
FeO	23.96	4.090	24.25	4.208	24.08	4.218	23.85	4.161
Cl	.01	.000	.03	.000	.00	.000		
Total:	89.31	19.805	88.49	19.995	87.62	19.975	87.69	19.902

Unsheared gabbro sample: CWM-82 (plagioclase)

	wt %	form	wt %	form	wt %	form	wt %	form
Na ₂ O	6.34	.52	5.25	.46	5.77	.51	5.82	.51
Al ₂ O ₃	26.98	1.43	26.33	1.41	27.31	1.45	26.90	1.44
SiO ₂	56.44	2.54	56.70	2.57	55.46	2.50	55.66	2.52
K ₂ O	0.04	.00	0.79	.04	0.07	.00	0.04	.00
CaO	9.95	.48	10.02	.49	11.23	.54	10.66	.52
FeO	0.04	.00	0.21	.01	0.12	.00	0.21	.01
Total:	99.79	4.98	99.30	4.98	99.96	5.00	99.29	5.00
Na ₂ O	5.71	.50	6.00	.52	5.85	.51	5.64	.49
Al ₂ O ₃	26.91	1.44	26.93	1.43	26.81	1.43	27.50	1.46
SiO ₂	55.61	2.52	56.36	2.53	56.07	2.54	55.58	2.51
K ₂ O	0.07	.00	0.10	.00	0.06	.00	0.10	.01
CaO	11.04	.53	10.86	.52	10.26	.50	10.79	.52
FeO	0.21	.01	0.18	.00	0.15	.00	0.21	.01
Total:	99.55	5.00	100.43	5.00	99.20	4.98	99.82	5.00

Unsheared gabbro sample: CWM-82 (amphibole)

	wt %	form
Na ₂ O	.54	.15
MgO	15.07	3.20
Al ₂ O ₃	4.82	.81
SiO ₂	49.82	7.23
K ₂ O	.33	.06
CaO	11.34	1.73
TiO ₂	1.01	.10
MnO	.21	.03
Fe _{tot}	13.66	1.62
Total:	96.80	14.93

Unsheared gabbro sample: CWM-83 (plagioclase)

	wt %	form	wt %	form	wt %	form
Na2O	11.94	1.01	12.20	1.02	11.40	.95
Al2O3	18.94	.98	20.59	1.05	20.43	1.03
SiO2	68.00	2.98	66.70	2.90	69.30	2.96
K2O	0.13	.01	0.07	.00	0.04	.00
CaO	0.88	.04	1.72	.08	0.98	.05
FeO	0.08	.00	0.18	.01	0.03	.00
Total:	99.97	5.02	101.46	5.05	102.18	4.99

Unsheared gabbro sample: CWM-126 (plagioclase)

	wt %	form	wt %	form	wt %	form
Na2O	9.26	.79	11.41	.99	11.07	.95
Al2O3	22.03	1.14	20.27	1.07	19.65	1.02
SiO2	65.11	2.85	67.52	1.07	67.84	2.99
K2O	0.44	.02	0.03	.00	0.29	.01
CaO	2.83	.13	0.09	.00	0.04	.01
FeO	0.20	.00	0.02	.00	0.02	.00
Total:	99.87	4.97	99.34	5.02	98.91	4.98

Na2O	11.83	.97	11.19	.95
Al2O3	20.31	1.05	30.98	1.08
SiO2	66.49	2.93	66.16	2.90
K2O	0.03	.00	0.03	.00
CaO	1.51	.07	1.69	.08
FeO	0.03	.00	0.04	.00
Total:	99.76	5.02	100.09	5.01

Unsheared gabbro sample: CWM-126 (amphibole)

	wt %	form	wt %	form	wt %	form	wt %	form	wt %	form
Na2O	1.29	.37	1.42	.42	1.17	.35	1.42	.45	1.52	.46
MgO	5.23	1.17	5.35	1.22	4.90	1.11	4.34	.98	4.79	1.11
Al2O3	12.83	2.27	12.75	2.30	12.77	2.30	14.58	2.66	13.43	2.46
SiO2	43.26	6.48	43.84	6.41	42.43	6.48	39.28	6.13	41.39	6.43
K2O	.33	.06	.29	.06	.28	.05	.37	.07	.30	.06
CaO	10.87	1.75	11.46	1.88	11.47	1.88	11.48	1.86	10.78	1.79
TiO2	.24	.03	.21	.02	.26	.03	.27	.03	.25	.03
MnO	.34	.04	.27	.03	.34	.04	.33	.04	.28	.03
Fe _{tot}	23.98	3.01	23.39	3.00	23.77	3.03	24.32	3.16	22.64	2.94
Total:	98.30	15.18	96.98	15.32	97.39	15.27	96.39	15.38	95.38	15.31

Unsheared gabbro sample: CWM-127 (plagioclase)

	wt %	form	wt %	form
Na2O	7.82	.67	6.81	.58
Al2O3	24.09	1.26	26.36	1.36
SiO2	61.18	2.72	69.88	2.62
K2O	0.07	.00	0.04	.00
CaO	6.83	.32	7.78	.41
FeO	0.04	.00	0.10	.00
Total:	100.03	4.97	100.97	4.97

Unsheared gabbro sample: CWM-127 (amphibole)

	wt %	form	wt %	form	wt %	form
Na2O	.88	.25	1.03	.30	1.21	.34
MgO	10.54	2.28	9.78	2.17	7.05	1.54
Al2O3	8.91	1.52	8.68	1.52	13.68	2.70
SiO2	47.18	6.84	46.61	6.93	41.79	6.11
K2O	.07	.01	.21	.04	.54	.10
CaO	10.36	1.61	11.41	1.82	11.77	1.84
TiO2	.29	.03	.39	.04	.32	.02
MnO	.41	.05	.24	.03	.23	.03
Fe _{tot}	18.87	2.29	18.51	2.30	20.23	2.47
Total:	97.50	14.88	96.86	15.15	96.85	12.72

Unsheared gabbro sample: CWM-141A (plagioclase)

	wt %	form	wt %	form	wt %	form
Na2O	3.79	.35	3.80	.35	4.33	.39
Al2O3	29.39	1.63	28.18	1.57	28.68	1.60
SiO2	49.94	2.35	50.73	2.40	50.39	2.38
K2O	0.14	.01	0.04	.00	0.10	.00
CaO	12.45	.63	12.32	.63	12.00	.61
FeO	0.63	.02	0.60	.02	.063	.02
Total:	96.74	4.99	95.70	4.97	96.13	5.00

Unsheared gabbro sample: CWM-141A (amphibole)

	wt %	form	wt %	form	wt %	form
Na2O	.30	.09	.34	.10	.34	.10
MgO	14.08	3.09	14.09	3.12	13.20	2.95
Al2O3	4.61	.80	3.30	.58	3.64	.64
SiO2	49.41	7.28	50.07	7.44	51.30	7.55
K2O	.13	.02	.09	.02	.11	.02
CaO	10.74	1.70	11.96	1.90	11.38	1.83
TiO2	.06	.01	.71	.08	.09	.01
MnO	.21	.03	.28	.03	.26	.03
Fe _{tot}	14.14	1.78	13.90	1.73	14.13	1.77
Total:	94.09	14.80	94.96	15.00	94.61	14.90

Sheared gabbro sample: CWM-141B (plagioclase)

	wt %	form	wt %	form
Na2O	12.48	1.08	11.34	.98
Al2O3	19.25	1.02	18.09	.95
SiO2	65.75	2.94	67.98	3.02
K2O	0.04	.00	0.05	.00
CaO	0.62	.03	0.80	.04
FeO	0.10	.00	0.07	.00
Total:	98.24	5.07	98.33	4.99

Sheared gabbro sample: CWM-141B (chlorite)

	wt %	form	wt %	form	wt %	form
Na2O	.01	.000	.07	.022	.07	.022
MgO	12.73	3.615	12.93	3.647	12.66	3.592
Al2O3	20.05	4.504	20.25	4.520	19.96	4.487
SiO2	24.48	4.667	24.28	4.597	24.44	4.661
K2O	.00	.000	.02	.005	.00	.000
CaO	.04	.005	.02	.000	.02	.000
TiO2	.07	.005	.03	.002	.03	.000
MnO	.27	.039	.22	.033	.26	.039
FeO	26.41	4.208	26.98	4.270	26.89	4.286
Total:	84.10	17.043	84.93	17.110	84.35	17.088

Unsheared gabbro sample: CWM-142A (plagioclase)

	wt %	form	wt %	form
Na2O	5.89	.52	5.12	.44
Al2O3	26.36	1.41	28.82	1.53
SiO2	56.61	2.57	54.55	2.46
K2O	0.07	.00	0.04	.00
CaO	9.44	.46	10.89	.53
FeO	0.34	.01	0.37	.01
Total:	98.71	4.97	99.79	4.97

Unsheared gabbro sample: CWM-142A (amphibole)

	wt %	form	wt %	form
Na2O	.61	.17	.87	.24
MgO	11.45	2.54	9.82	2.19
Al2O3	4.35	.75	5.30	.89
SiO2	50.35	7.40	48.82	7.14
K2O	.15	.03	.09	.02
CaO	11.37	1.80	9.65	1.49
TiO2	.50	.05	.62	.06
MnO	.27	.03	.52	.05
Fe _{tot}	17.48	2.22	21.83	2.63
Total:	96.56	14.99	97.52	14.71

Sheared gabbro sample: CWM-142B (chlorite)

	wt %	form	wt %	form	wt %	form
Na2O	.01	.000	.03	.012	.02	.006
MgO	14.06	4.432	13.26	4.256	14.36	4.515
Al2O3	20.11	5.009	20.38	5.173	20.30	5.047
SiO2	26.26	5.555	25.38	5.471	25.97	5.481
K2O	.01	.000	.01	.000	.00	.000
CaO	.02	.000	.00	.000	.05	.006
TiO2	.04	.000	.04	.000	.07	.005
MnO	.31	.049	.29	.050	.24	.037
FeO	27.40	4.848	27.36	4.927	27.33	4.824
Total:	88.29	19.898	86.85	19.901	88.41	19.928

Sheared gabbro sample: CWM-142B (chlorite)

	wt %	form	wt %	form
Na ₂ O	.01	.000	.00	.000
MgO	12.68	4.088	12.10	3.941
Al ₂ O ₃	20.78	5.294	20.12	5.187
SiO ₂	24.72	5.345	24.98	5.462
K ₂ O	.02	.000	.01	.000
CaO	.02	.000	.04	.005
TiO ₂	.02	.000	.01	.000
MnO	.21	.032	.29	.051
FeO	28.91	5.230	28.84	5.276
Cl	.01	.001	.00	.000
Total:	87.55	20.084	86.50	19.988

Sheared gabbro sample: CWM-142B (plagioclase)

	wt %	form	wt %	form	wt %	form
Na ₂ O	11.35	.96	10.95	.95	11.74	1.04
Al ₂ O ₃	19.17	.99	19.28	1.02	19.89	1.07
SiO ₂	68.28	2.98	66.30	2.97	63.45	2.89
K ₂ O	0.03	.00	0.02	.00	0.03	.00
CaO	1.23	.06	1.21	.06	1.25	.05
FeO	0.12	.00	0.13	.00	0.18	.00
Total:	100.18	4.99	99.89	5.00	96.54	5.05

Sheared gabbro sample: CWM-142B (amphibole)

	wt %	form
Na ₂ O	1.36	.40
MgO	6.52	1.47
Al ₂ O ₃	12.27	2.19
SiO ₂	43.14	6.52
K ₂ O	.39	.07
CaO	11.42	1.85
TiO ₂	.04	.00
MnO	.20	.03
Fe _{tot}	22.07	2.79
Total:	97.41	15.32

Unsheared gabbro sample: CWM-143A (amphibole)

	wt %	form
Na ₂ O	.51	.15
MgO	10.45	2.36
Al ₂ O ₃	4.67	.83
SiO ₂	48.24	7.31
K ₂ O	.20	.04
CaO	10.59	1.72
TiO ₂	.12	.01
MnO	.23	.03
Fe _{tot}	19.31	2.45
Total:	94.41	14.90

Unsheared intermediate volcanoclastic sample:
CWM-144A (plagioclase)

	wt %	form	wt %	form
Na ₂ O	10.18	.86	11.61	.96
Al ₂ O ₃	19.40	.99	19.29	.96
SiO ₂	68.48	2.98	71.49	3.04
K ₂ O	0.63	.03	0.06	.00
CaO	0.43	.02	0.03	.00
FeO	0.04	.00	0.00	.00
Total:	99.16	4.88	102.48	4.96

Sheared intermediate volcanoclastic sample:
CWM-144B (plagioclase)

	wt %	form
Na ₂ O	11.81	.98
Al ₂ O ₃	19.80	1.00
SiO ₂	69.58	2.99
K ₂ O	0.09	.00
CaO	0.22	.01
FeO	0.02	.00
Total:	101.52	4.98

Sheared gabbro sample: CWM-146B (plagioclase)

	wt %	form
Na ₂ O	10.73	.92
Al ₂ O ₃	19.33	1.01
SiO ₂	67.76	3.00
K ₂ O	0.10	.01
CaO	0.54	.02
FeO	0.18	.01
Total:	98.64	4.97

Unsheared gabbro sample: CWM-149A (plagioclase)

	wt %	form	wt %	form	wt %	form	wt %	form
Na ₂ O	10.82	.92	10.74	.90	10.04	.84	10.35	.87
Al ₂ O ₃	21.10	1.09	20.60	1.06	22.34	1.13	22.26	1.14
SiO ₂	65.88	2.89	67.89	2.95	66.65	2.87	65.15	2.84
K ₂ O	0.04	.00	0.09	.01	0.03	.00	0.04	.00
CaO	2.52	.12	1.12	.05	2.71	.13	3.18	.15
FeO	0.18	.00	0.14	.00	0.10	.00	0.13	.00
Total:	100.54	5.02	100.58	4.97	101.87	4.97	101.11	5.01

Unsheared gabbro sample: CWM-149A (amphibole)

	wt %	form	wt %	form	wt %	form
Na ₂ O	1.21	.35	.91	.27	.43	.12
MgO	7.50	1.67	8.23	1.87	13.39	2.90
Al ₂ O ₃	12.47	2.20	9.35	1.68	4.49	.77
SiO ₂	42.96	6.44	44.74	6.84	49.85	7.25
K ₂ O	.44	.08	.31	.06	.14	.03
CaO	11.82	1.90	10.74	1.76	12.48	1.95
TiO ₂	.23	.03	.38	.04	.44	.05
MnO	.24	.03	.25	.03	.25	.03
Fe _{tot}	20.95	2.63	19.68	2.52	16.24	1.98
Total:	97.82	15.30	94.61	15.07	97.71	15.05

Sheared gabbro sample CWM-149B (plagioclase)

	wt %	form
Na2O	11.77	.98
Al2O3	20.47	1.04
SiO2	68.13	2.92
K2O	0.13	.01
CaO	0.56	.02
FeO	0.06	.00
Total:	101.12	4.97

Sheared gabbro sample: CWM-149B (chlorite)

	wt %	form	wt %	form	wt %	form
Na2O	.01	.000	.00	.000	.05	.019
MgO	13.64	4.410	13.94	4.428	14.29	4.535
Al2O3	20.75	5.301	19.98	5.016	20.72	5.205
SiO2	24.33	5.275	25.81	5.497	25.43	5.417
K2O	.00	.000	.05	.012	.00	.000
CaO	.01	.000	.02	.000	.02	.000
TiO2	.06	.006	.02	.000	.11	.012
MnO	.21	.032	.22	.037	.18	.031
FeO	27.33	4.957	27.67	4.928	26.55	4.729
Total:	86.47	20.000	87.90	19.949	87.45	19.960

Sheared gabbro sample: CWM-155B (plagioclase)

	wt %	form	wt %	form	wt %	form
Na2O	9.81	.86	10.65	.93	10.52	.92
Al2O3	21.84	1.16	20.13	1.08	20.86	1.11
SiO2	62.58	2.83	64.52	2.90	63.36	2.86
K2O	0.06	.00	0.52	.03	0.64	.04
CaO	3.34	.17	1.63	.08	1.65	.08
FeO	0.08	.00	0.13	.00	0.28	.01
Total:	97.81	5.02	97.76	5.02	97.31	5.02

Sheared gabbro sample: CWM-155B (amphibole)

	wt %	form
Na ₂ O	.74	.21
MgO	13.27	2.92
Al ₂ O ₃	7.23	1.26
SiO ₂	47.99	7.09
K ₂ O	.08	.01
CaO	11.15	1.77
TiO ₂	.20	.02
MnO	.25	.03
Fe _{tot}	13.50	1.67
Total:	94.41	14.98

Unsheared gabbro sample: CWM-156 (plagioclase)

	wt %	form
Na ₂ O	8.82	.77
Al ₂ O ₃	23.76	1.26
SiO ₂	60.17	2.72
K ₂ O	0.04	.00
CaO	5.76	.28
FeO	0.03	.00
Total:	98.57	5.03

Unsheared gabbro sample: CWM-156 (amphibole)

	wt %	form	wt %	form
Na ₂ O	.90	.26	.84	.25
MgO	10.95	2.48	9.14	2.08
Al ₂ O ₃	9.33	1.66	11.45	2.06
SiO ₂	46.20	6.83	44.16	6.58
K ₂ O	.16	.03	.14	.03
CaO	10.97	1.78	10.77	1.76
TiO ₂	.35	.04	.20	.02
MnO	.29	.04	.33	.04
Fe _{tot}	15.34	1.94	17.35	2.21
Total:	94.50	15.05	94.44	15.03

Unsheared gabbro sample: CWM-160A (plagioclase)

	wt %	form	wt %	form	wt %	form	wt %	form
Na ₂ O	4.90	.43	4.59	.40	6.02	.52	3.72	.33
Al ₂ O ₃	28.47	1.55	28.78	1.53	27.56	1.46	30.43	1.63
SiO ₂	51.98	2.41	53.61	2.42	56.15	2.52	51.55	2.35
K ₂ O	0.11	.00	0.09	.00	0.05	.00	0.03	.00
CaO	11.93	.59	12.61	.61	10.19	.49	13.79	.67
FeO	0.70	.02	0.70	.03	0.49	.01	0.58	.01
Total:	98.09	5.00	100.38	4.99	100.45	5.00	100.09	4.99
Na ₂ O	4.41	.38	3.97	.35				
Al ₂ O ₃	29.00	1.54	29.83	1.60				
SiO ₂	54.10	2.43	52.01	2.36				
K ₂ O	0.02	.00	0.11	.00				
CaO	12.54	.61	13.58	.66				
FeO	0.61	.01	0.53	.02				
Total:	100.68	4.97	100.03	4.99				

Unsheared gabbro sample: CWM-160A (amphibole)

	wt %	form	wt %	form	wt %	form
Na ₂ O	.56	.16	.86	.25	.46	.13
MgO	11.90	2.67	8.33	1.86	12.07	1.49
Al ₂ O ₃	5.42	.96	10.59	1.84	5.73	1.01
SiO ₂	47.11	7.09	43.71	6.56	48.07	7.18
K ₂ O	.15	.03	.27	.05	.10	.02
CaO	11.78	1.90	11.63	1.87	12.01	1.92
TiO ₂	.18	.02	.25	.03	.25	.03
MnO	.25	.03	.34	.04	.23	.03
Fe _{tot}	17.62	2.22	20.63	2.59	16.49	2.06
Total:	94.97	15.06	96.84	15.09	95.41	13.97

Sheared gabbro sample: CWM-160B (plagioclase)

	wt %	form
Na ₂ O	11.16	.94
Al ₂ O ₃	20.87	1.07
SiO ₂	66.62	2.91
K ₂ O	0.91	.05
CaO	1.67	.08
FeO	0.16	.01
Total:	101.39	5.02

Sheared gabbro sample: CWM-160B (chlorite)

	wt %	form	wt %	form	wt %	form
Na2O	.00	.000	.05	.019	.00	.000
MgO	14.23	4.516	14.97	4.778	14.45	4.554
Al2O3	20.02	5.029	19.58	4.942	20.23	5.038
SiO2	25.77	5.492	25.82	5.527	26.13	5.521
K2O	.25	.063	.13	.031	.14	.037
CaO	.05	.006	.03	.006	.02	.000
TiO2	.04	.006	.03	.000	.04	.000
MnO	.30	.050	.26	.044	.29	.049
FeO	26.98	4.810	25.78	4.615	26.83	4.740
Cl	.01	.000	.02	.000		
Total:	87.71	19.978	86.76	19.980	88.28	19.963

Unsheared gabbro sample: CWM-163A (plagioclase)

	wt %	form	wt %	form
Na2O	11.50	.97	11.55	.95
Al2O3	19.50	1.00	20.52	1.02
SiO2	68.23	2.98	66.70	2.82
K2O	0.11	.00	0.04	.00
CaO	0.82	.04	0.62	.03
FeO	0.11	.01	1.45	.08
Total:	100.27	4.99	100.88	4.90

Unsheared gabbro sample: CWM-163A (amphibole)

	wt %	form	wt %	form	wt %	form
Na2O	.26	.07	.66	.19	.79	.23
MgO	16.36	2.84	11.18	2.42	10.22	2.31
Al2O3	4.90	.83	5.59	.96	5.82	1.04
SiO2	51.29	7.33	49.77	7.24	48.75	7.28
K2O	.05	.01	.30	.06	.22	.04
CaO	11.74	1.80	11.07	1.73	11.33	1.84
TiO2	.39	.04	1.00	.10	.55	.06
MnO	.30	.04	.33	.04	.31	.04
Fe _{tot}	16.08	1.92	18.32	2.23	17.12	2.17
Total:	98.32	14.88	98.20	14.97	95.11	15.11

Unsheared gabbro sample: CWM-163A (chlorite)

	wt %	form	wt %	form
Na2O	.01	.000	.06	.018
MgO	15.01	4.633	15.55	4.892
Al2O3	21.17	5.168	19.83	4.892
SiO2	26.78	5.545	26.83	5.629
K2O	.00	.000	.02	.000
CaO	.03	.006	.02	.000
TiO2	.04	.000	.02	.003
MnO	.29	.048	.32	.055
FeO	25.57	4.426	25.14	4.400
Total:	89.08	19.850	88.07	19.879

Sheared gabbro sample: CWM-163B (plagioclase)

	wt %	form
Na2O	11.58	.99
Al2O3	20.13	1.04
SiO2	67.84	2.96
K2O	0.06	.00
CaO	0.20	.00
FeO	0.07	.00
Total:	99.88	4.99

Sheared gabbro sample: CWM-163B (amphibole)

	wt %	form	wt %	form	wt %	form
Na2O	.96	.28	1.17	.35	1.32	.39
MgO	9.37	2.14	6.02	1.38	5.64	1.27
Al2O3	8.60	1.55	13.39	2.44	14.14	2.52
SiO2	44.45	6.80	41.22	6.36	42.50	6.42
K2O	.16	.03	.46	.09	.48	.09
CaO	11.03	1.81	11.02	1.82	11.38	1.84
TiO2	.05	.01	.06	.00	.05	.01
MnO	.23	.03	.19	.03	.25	.03
Fe _{tot}	19.33	2.47	21.46	2.77	21.84	2.76
Total:	94.20	15.12	95.18	15.24	97.60	15.33

Sheared gabbro sample: CWM-163B (chlorite)

	wt %	form	wt %	form
Na ₂ O	.02	.006	.00	.000
MgO	12.91	4.059	13.36	4.243
Al ₂ O ₃	19.92	4.950	20.27	5.094
SiO ₂	26.99	5.687	26.33	5.613
K ₂ O	.04	.006	.05	.012
CaO	.06	.012	.05	.006
TiO ₂	.03	.005	.02	.000
MnO	.29	.049	.23	.037
FeO	28.04	4.944	27.00	4.813
Cl	.01	.000	.00	.000
Total:	88.36	19.750	87.46	19.887

Sheared gabbro sample: CWM-164B (plagioclase)

	wt %	form	wt %	form
Na ₂ O	8.61	.74	7.51	.68
Al ₂ O ₃	23.35	1.22	24.61	1.29
SiO ₂	65.54	2.79	60.71	2.69
K ₂ O	0.20	.00	0.04	.00
CaO	4.44	.21	6.99	.33
FeO	0.05	.00	0.10	.00
Total:	99.19	4.79	100.40	4.99

Sheared gabbro sample: CWM-164B (amphibole)

	wt %	form
Na ₂ O	.75	.22
MgO	10.86	2.48
Al ₂ O ₃	10.44	1.89
SiO ₂	44.54	6.52
K ₂ O	.13	.02
CaO	11.78	1.93
TiO ₂	.06	.01
MnO	.16	.02
Fe _{tot}	15.89	2.02
Total:	95.08	15.11

Unsheared gabbro sample: CO-22A (plagioclase)

	wt %	form	wt %	form
Na ₂ O	10.38	.88	10.49	.89
Al ₂ O ₃	21.53	1.11	21.51	1.11
SiO ₂	65.46	2.87	65.70	2.87
K ₂ O	0.49	.03	0.03	.00
CaO	2.46	.12	2.82	.13
FeO	0.25	.01	0.12	.00
Total:	100.57	5.02	100.67	5.00

Unsheared gabbro sample: CO-22A (amphibole)

	wt %	form	wt %	form	wt %	form	wt %	form
Na ₂ O	.48	.13	.77	.22	.48	.13	.74	.21
MgO	12.88	2.76	11.73	2.62	13.07	2.81	13.96	3.01
Al ₂ O ₃	4.30	.73	6.90	1.22	4.06	.69	3.62	.62
SiO ₂	51.34	7.52	47.16	7.07	50.36	7.31	51.77	7.48
K ₂ O	.07	.01	.09	.02	.09	.02	.11	.02
CaO	11.22	1.73	11.14	1.79	11.41	1.76	10.86	1.68
TiO ₂	.11	.01	.21	.02	.10	.01	.07	.01
MnO	.23	.03	.30	.04	.36	.04	.29	.04
Fe _{tot}	16.23	1.95	16.07	2.01	16.15	2.01	15.23	1.84
Total:	97.86	14.87	94.44	15.01	96.08	14.78	96.65	14.91

Unsheared gabbro sample: CO-23A (plagioclase)

	wt %	form	wt %	form
Na ₂ O	5.00	.43	5.85	.51
Al ₂ O ₃	28.64	1.51	26.82	1.43
SiO ₂	55.16	2.46	55.93	2.53
K ₂ O	0.08	.00	0.16	.01
CaO	11.57	.55	10.34	.50
FeO	0.78	.03	0.66	.02
Total:	101.23	4.98	99.76	5.00

Unsheared gabbro sample: CO-23A (amphibole)

	wt %	form	wt %	form
Na ₂ O	.75	.22	.14	.04
MgO	10.76	2.40	15.68	3.40
Al ₂ O ₃	7.15	1.26	1.98	.34
SiO ₂	46.79	7.01	52.26	7.61
K ₂ O	.12	.02	.05	.01
CaO	10.89	1.75	12.75	1.99
TiO ₂	.26	.03	.01	.00
MnO	.41	.05	.19	.02
Fe _{tot}	17.92	2.24	13.30	1.57
Total:	95.05	14.98	96.36	14.98

APPENDIX BOxygen and Carbon Isotope Data on Whole rock and Mineral Separates:

Whole rock samples were crushed and weighed. Approximately 5 to 10 milligrams were analyzed for ^{18}O (measured relative to standard mean ocean water - SMOW) and ^{13}C (measured relative to *bellemnitella americana* from the Cretaceous Peedee Formation in South Carolina - PDB). Oxygen isotope samples containing trace amounts of carbonate were treated with HCl to remove the carbonate.

Mineral separates were hand picked from crushed samples, and tested for purity (>95%) by X-ray diffraction before analysis for ^{18}O and ^{13}C . Isotope analyses were carried out in the laboratories of Dr. F. J. Longstaffe at the University of Alberta.

Oxygen Isotope Data on Mineral Separates

Sample	Quartz	Chlorite	Carbonate	
	$\delta^{18}\text{O}_{\text{SMOW}}$	$\delta^{18}\text{O}_{\text{SMOW}}$	$\delta^{18}\text{O}_{\text{SMOW}}$	$\delta^{13}\text{C}_{\text{PDB}}$
CWM-41C	+9.3	+3.7		
CWM-138	+8.7	+2.4		
CWM-142E	+9.3	+4.5		
CWM-143B	+8.8	+4.3		
CWM-145B	+9.3	+2.4		
CWM-146B	+9.6	+4.8		
CWM-147B	+9.3	+3.4	+7.8	-3.1 (calcite)
CWM-151C		+3.3	+23.6	-4.3 (Fe-dolomite)
CWM-154C	+8.7	+2.9		
CWM-160C	+9.3	+3.3		
CWM-163C	+9.0	+4.4		
CWM-164B	+9.1	+2.0		
CWM-166C	+9.6		+27.6	+0.9 (Fe-dolomite)
CO-22C	+11.2	+5.1		
CO-23C	+11.4	+5.5		

303

Whole Rock Oxygen Isotope Data

Sample	$\delta^{18}\text{O}_{\text{SMOW}}$	Calcite Results	
		$\delta^{18}\text{O}_{\text{SMOW}}$	$\delta^{13}\text{C}_{\text{PDB}}$
<u>Sheared Samples:</u>			
CWM-34B	+6.5	+7.8	-4.0
CWM-35B	+5.7	+8.1	-2.8
CWM-84	+9.9		
CWM-140B	+5.0		
CWM-145B	+8.4		
CWM-149B	+6.2		
CWM-154B	+5.4	+7.8	-5.0
CWM-155B	+5.7		
CWM-160B	+6.5	+8.1	-2.97
CWM-162B	+7.8		
CO-22B	+8.8	+9.7	-3.5
CO-23B	+6.7	+9.1	-3.5

Sample $\delta^{18}\text{O}_{\text{SMOW}}$

Unsheared Samples:

CWM-24	+7.6
CWM-34A	+5.5
CWM-35A	+5.4
CWM-57	+5.8
CWM-118	+8.5
CWM-145A	+5.6
CWM-149A	+5.4
CWM-154A	+5.3
CWM-155A	+8.6
CWM-156	+7.0
CWM-157	+8.1
CWM-160A	+5.2
CWM-162A	+7.9
CO-22A	+9.1
CO-23A	+6.1

APPENDIX GSELECTED SAMPLE CALCULATIONSSample Calculation of Temperature from ^{18}O Data

$$\Delta\delta^{18}\text{O}_{\text{q-ch}} = 2.01 (10^6 * T^{-2}) + 1.99$$

(from Wenner and Taylor, 1971)

For CWM-41C, $\delta^{18}\text{O}_{\text{q}} = +9.3\%$ and $\delta^{18}\text{O}_{\text{ch}} = +3.7$

$$9.31 - 3.74 = 2.01 (10^6 * T^{-2}) + 1.99$$

$$T^2 = 561452.51$$

$$T = 749.3^\circ\text{K} = 476^\circ\text{C}$$

Sample Calculation of Fluid Composition in equilibrium with Quartz

$$\Delta\delta^{18}\text{O}_{\text{q-w}} = 3.38 (10^6 * T^{-2}) - 2.90$$

(from Friedman and O'Neil, 1977 after Clayton et al., 1972)

For an estimated temperature of 723°K and $\delta^{18}\text{O}_{\text{q}} = +9.0\%$

$$9.0 - w = \frac{3.38 * 10^6}{(723)^2} - 2.90$$

$$w = 6.72 \%$$

Sample Calculation of Temperature from Quartz-Calcite

$$\Delta\delta^{18}\text{O}_{\text{q-c}} = .6 (10^6 * T^{-2}) - .01$$

(from Friedman and O'Neil, 1977)

for CWM-166C: $9.6 - 27.6 = -.6 (10^6 * T^{-2}) - .01$

$$T^2 = -33352$$

unsolvable equation

Sample Calculation of Alteration Index

$$\text{AI} = \frac{\text{mode of secondary mins}}{\text{mode of primary + secondary mins}}$$

For sample CWM-141A, primary minerals - 22.0 % actinolitic
hornblende

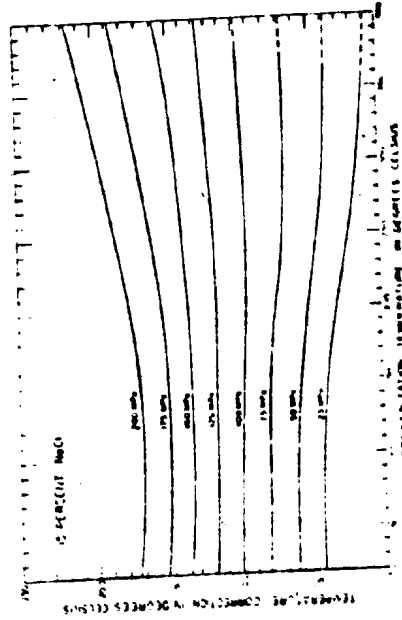
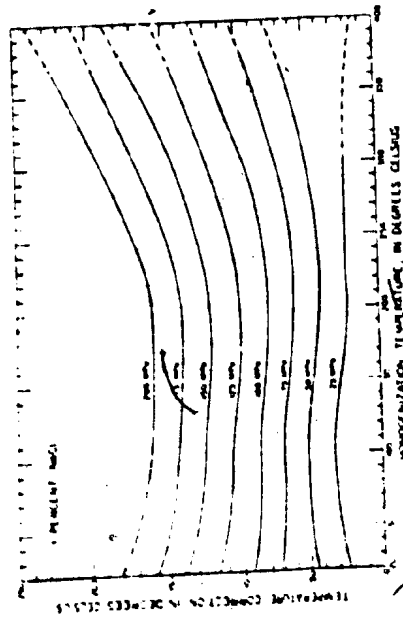
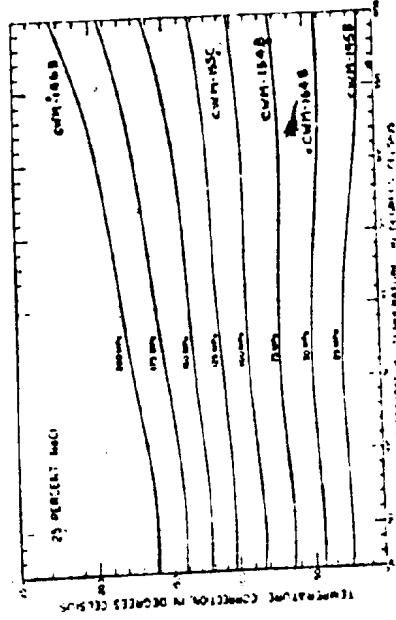
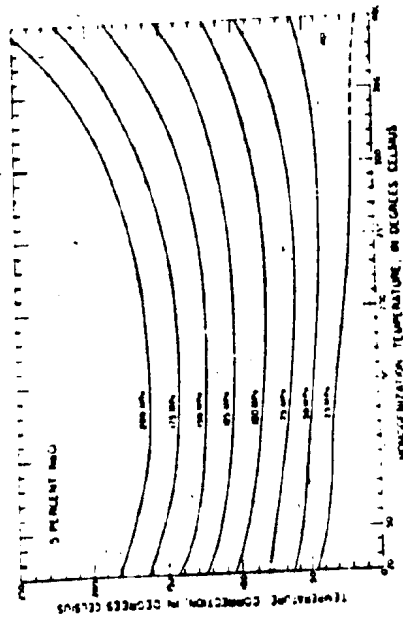
secondary minerals - 5.2 % biotite
26.5 chlorite

$$\text{So AI} = \frac{5.2 + 26.5}{5.2 + 26.5 + 22.0} = 0.59$$

APPENDIX D

Selected figures from Potter (1977) used to estimate trapping pressures of fluid inclusions from Mirage Island samples

The graphs plot formation pressure curves relative to temperature correction ($- T_{\text{formation}} - T_{\text{homogenization}}$) (vertical axis), and homogenization temperature (horizontal axis), for different salinities of fluid. In this study, homogenization temperature was measured, and temperature correction was calculated using the formation temperatures determined from oxygen isotope thermometry, and therefore the trapping pressures of the fluid inclusions can be estimated using these diagrams.



APPENDIX EGeochemical Analyses

Whole rock major element analyses were carried out on solutions by atomic absorption spectrophotometry at Memorial University by G. Andrews. The results are presented as a weight percent. Errors are estimated to be +/- 2% of the reported values. Ferrous and ferric iron were distinguished by titration.

Trace elements were analyzed by X-ray fluorescence on pressed powder pellets by G. Viennott at Memorial. The results are presented in parts per million (ppm). A standard was run a total of eight times with the unknowns, and its results were reproduceable to within about 5%.

RESULTS OF MAJOR ELEMENT ANALYSES OF METABASIC ROCKS

Oxide	CWM-34A	CWM-34B	CWM-35A	CWM-35B	CWM41A	CWM-41B
SiO ₂	50.0	46.7	48.4	41.2	49.2	35.3
TiO ₂	0.64	0.80	0.88	1.12	0.60	0.68
Al ₂ O ₃	14.5	13.6	14.1	15.7	12.8	17.6
FeO	7.42	9.29	9.00	10.58	10.28	17.29
Fe ₂ O ₃	2.10	0.55	2.49	1.26	1.90	2.14
MnO	0.16	0.16	0.18	0.19	0.17	0.15
MgO	8.38	8.29	9.12	9.34	11.0	13.2
CaO	8.66	7.78	9.48	7.14	6.98	0.54
Na ₂ O	2.51	1.91	1.83	2.84	2.43	0.72
K ₂ O	0.55	0.69	0.51	0.58	0.78	1.73
P ₂ O ₅	0.05	0.05	0.05	0.07	0.07	0.26
LOI	3.88	8.85	3.22	8.96	2.53	6.92
Total	99.66	99.69	100.25	100.14	100.23	98.44

Oxide	CWM-92	CWM-137A	CWM-137B	CWM-139A	CWM-139B
SiO ₂	59.0	47.8	45.6	46.0	44.2
TiO ₂	0.72	0.76	0.84	1.08	1.08
Al ₂ O ₃	14.7	14.4	14.4	15.3	14.1
FeO	7.26	8.89	9.57	10.54	12.05
Fe ₂ O ₃		2.48	1.12	1.94	1.06
MnO	0.11	0.18	0.16	0.18	0.19
MgO	5.81	8.84	8.93	7.79	8.21
CaO	6.36	10.6	7.68	8.88	7.42
Na ₂ O	3.74	1.60	2.02	2.80	1.70
K ₂ O	1.31	0.26	0.37	0.19	0.13
P ₂ O ₅	0.16	0.07	0.11	0.08	0.10
LOI	0.63	2.49	7.53	2.78	6.52
Total	99.80	99.31	99.38	98.52	98.52

Oxide	CWM141A	CWM141B	CWM142A	CWM142B	CWM145A	CWM145B
SiO ₂	44.7	47.6	49.6	47.5	42.8	86.5
TiO ₂	1.24	1.60	1.32	1.36	1.44	0.00
Al ₂ O ₃	14.8	11.8	12.9	12.3	12.9	3.33
FeO	10.62	12.71	11.70	13.47	11.46	3.73
Fe ₂ O ₃	2.34	2.64	4.51	1.06	3.76	0.64
MnO	0.18	0.19	0.20	0.20	0.20	0.04
MgO	9.37	5.96	6.16	6.31	5.69	2.05
CaO	8.54	5.64	8.92	5.88	7.74	0.50
Na ₂ O	1.14	1.66	1.93	1.86	1.79	0.20
K ₂ O	0.82	0.65	0.39	0.19	0.28	0.10
P ₂ O ₅	0.11	0.28	0.12	0.13	0.10	0.00
LOI	4.34	6.65	1.67	7.15	4.10	1.65
Total	99.37	98.78	98.62	98.89	100.53	99.15

Oxide	CWM149A	CWM149B	CWM149C	CWM149D	CWM151A	CWM151B
SiO2	49.1	45.2	53.0	54.8	47.0	48.3
TiO2	1.60	1.24	1.00	0.60	0.92	0.48
Al2O3	12.8	11.9	13.6	11.6	14.3	11.2
FeO	11.59	11.90	5.13	11.10	10.43	11.78
Fe2O3	3.47	1.40	1.10	2.12	1.90	4.93
MnO	0.21	0.16	0.10	0.15	0.17	0.17
MgO	6.84	6.64	3.78	6.96	9.47	9.42
CaO	8.86	7.58	8.94	4.72	7.78	1.98
Na2O	2.28	1.37	3.62	3.12	2.00	0.02
P2O5	0.15	0.14	0.27	0.16	0.09	0.06
LOI	1.14	8.81	6.45	8.29	3.33	7.88
Total	99.88	98.56	98.81	99.32	99.01	99.29

Oxide	CWM152A	CWM152B	CWM154A	CWM154B	CWM160A	CWM160B
SiO2	48.0	48.0	50.9	45.2	49.1	45.8
TiO2	1.04	0.68	0.88	0.96	1.20	0.88
Al2O3	14.3	14.7	13.8	14.4	13.9	11.7
FeO	11.51	11.99	7.47	8.44	10.67	12.01
Fe2O3	1.73	1.15	2.28	1.70	1.87	0.66
MnO	0.20	0.17	0.16	0.16	0.20	0.22
MgO	9.23	10.1	9.39	8.79	7.36	7.49
CaO	7.24	2.88	9.50	9.16	10.0	8.88
Na2O	2.58	0.81	2.01	2.40	1.81	0.92
K2O	1.01	1.09	1.34	1.15	0.49	0.49
P2O5	0.08	0.09	0.12	0.11	0.09	0.06
LOI	2.43	6.73	1.58	6.25	1.82	9.64
Total	100.62	99.67	100.25	99.65	99.68	100.07

Oxide	CWM161A	CWM161B	CWM163A	CWM163B	CO13A	CO13B
SiO2	49.1	45.3	48.5	47.0	49.1	43.8
TiO2	1.56	1.28	0.92	1.72	0.92	0.76
Al2O3	13.1	12.0	13.6	11.7	14.3	14.1
FeO	12.05	12.16	10.75	13.45	9.87	9.83
Fe2O3	3.05	1.35	2.12	2.52	2.13	0.75
MnO	0.22	0.20	0.22	0.22	0.22	0.14
MgO	5.36	4.90	8.18	6.10	7.36	6.49
CaO	8.10	8.56	10.2	8.80	10.1	8.18
Na2O	2.18	2.27	2.15	1.20	2.80	3.47
K2O	0.49	0.92	0.30	0.51	0.30	0.23
P2O5	0.12	0.20	0.06	0.16	0.08	0.08
LOI	1.92	8.03	2.12	4.39	0.77	9.66
Total	98.77	99.51	99.51	99.11	99.02	98.57

Oxide	CO14A	CO14B	CO22A	CO22B	CO23A	CO23B
SiO2	48.6	47.3	48.6	57.6	47.0	41.6
TiO2	1.00	0.96	0.84	0.68	0.80	0.60
Al2O3	14.4	14.1	13.4	14.1	14.9	14.6
FeO	10.05	9.45	11.29	4.74	10.19	11.09
Fe2O3	1.98	1.55	1.67	1.09	2.27	0.67
MnO	0.18	0.14	0.15	0.08	0.17	0.15
MgO	8.19	9.77	9.19	2.88	10.1	9.11
CaO	10.0	6.24	4.68	7.78	7.64	7.54
Na2O	2.04	1.90	1.74	1.97	1.80	2.37
K2O	0.23	1.29	1.36	1.95	0.60	0.40
P2O5	0.08	0.09	0.07	0.07	0.04	0.05
LOI	1.14	1.29	5.30	6.30	3.76	10.01
Total	100.14	98.90	99.53	99.76	99.77	99.41

RESULTS OF MAJOR ELEMENT ANALYSES FROM FELSIC TO INTERMEDIATE ROCKS

Oxide	CWM-36A	CWM-36B	CWM140A	CWM140B	CWM141D	CWM141D
SiO2	58.2	77.6	64.7	59.5	59.7	61.0
TiO2	0.88	0.40	0.60	0.36	0.64	0.56
Al2O3	14.7	10.7	13.2	12.5	15.7	16.2
FeO	6.72	1.35	4.49	7.23	5.23	5.11
Fe2O3	1.16	0.57	0.12	0.48	1.05	0.68
MnO	0.12	0.03	0.06	0.10	0.08	0.07
MgO	5.80	1.30	4.42	11.4	4.13	3.87
CaO	4.66	3.56	3.22	0.28	3.74	3.30
Na2O	4.92	3.05	3.34	0.12	4.45	4.38
K2O	0.97	0.07	2.07	1.19	0.34	1.63
P2O5	0.26	0.18	0.14	0.13	0.16	0.27
LOI	1.31	0.47	2.01	4.98	2.78	1.99
Total	100.44	99.46	98.86	99.45	98.57	99.62

Oxide	CWM144A	CWM144B	CWM155A	CWM155B	CWM158A	CWM158B
SiO2	76.9	38.7	74.8	54.8	61.2	42.5
TiO2	0.16	0.20	0.16	0.80	0.64	1.04
Al2O3	11.2	8.92	12.8	14.1	15.8	25.4
FeO	1.24	29.9	1.37	5.52	4.52	6.87
Fe2O3			0.59	1.90	1.40	0.76
MnO	0.03	0.03	0.03	0.14	0.08	0.08
MgO	0.26	1.36	0.62	8.00	3.83	7.84
CaO	1.72	0.12	0.96	7.14	5.36	2.88
Na2O	4.48	0.36	4.70	2.10	3.41	1.78
K2O	2.19	6.03	2.89	2.71	1.27	4.53
P2O5	0.04	0.08	0.01	0.14	0.13	0.23
LOI	1.24	13.26	0.39	2.29	2.49	4.83
Total	99.46	99.54	99.48	100.51	100.63	99.49

Oxide	CWM162A	CWM162B
SiO2	72.2	63.5
TiO2	0.72	0.76
Al2O3	13.1	14.5
FeO	3.48	3.58
Fe2O3	0.31	0.13
MnO	0.05	0.08
MgO	1.51	2.50
CaO	3.12	5.74
Na2O	2.49	1.78
K2O	1.98	1.70
P2O5	0.13	0.20
LOI	0.70	2.74
Total	99.51	99.11

TRACE ELEMENT ANALYSES OF METABASIC ROCKS

Sample	Rb	Sr	Y	Zr	Nb	Ti/100	Cr
CWM-34A	17	103	17	56	5	62	314
CWM-34B	15	53	23	55	6	59	320
CWM-35A	11	112	25	56	3	75	314
CWM-35B	14	52	27	73	5	119	435
CWM-41A	23	85	16	82	4	76	443
CWM-41B	11	13	22	141	7	267	296
CWM-92	34	252	20	100	7	77	148
CWM-137A	2	103	18	51	4	71	337
CWM-137B	4	72	15	45	4	59	495
CWM-139A	0	100	24	67	5	112	164
CWM-139B	0	52	21	59	4	91	229
CWM-141A	17	117	22	73	5	116	353
CWM-141B	14	39	42	162	9	208	56
CWM-142A	5	101	30	90	7	138	73
CWM-142B	1	41	29	89	5	136	86
CWM-145A	6	92	40	98	7	136	28
CWM-145B	4	14	6	6	3	2	21
CWM-149A	14	137	37	123	9	156	156
CWM-149B	23	59	37	110	9	153	151
CWM-151A	6	151	25	74	3	102	253
CWM-151B	14	12	19	61	4	106	267
CWM-152A	14	74	27	73	6	108	189
CWM-152B	6	57	24	76	4	140	575
CWM-154A	30	235	16	70	5	82	417
CWM-154B	26	95	17	75	7	74	409
CWM-160A	17	104	29	81	8	92	158
CWM-160B	17	54	29	57	7	77	229
CWM-161A	9	123	33	110	9	177	0
CWM-161B	28	75	36	100	5	151	2
CWM-163A	5	120	24	62	2	92	78
CWM-163B	11	70	36	125	9	145	94
CO-13A	4	110	21	65	2	91	227
CO-13B	1	42	16	66	5	106	245
CO-14A	2	108	24	69	4	94	258
CO-14B	27	91	18	61	5	93	235

TRACE ELEMENT ANALYSES OF FELSIC TO INTERMEDIATE ROCKS

Sample	Rb	Sr	Y	Zr	Nb	Ti/100	Cr
CWM-36A	24	130	17	147	7	89	91
CWM-36B	14	198	17	86	6	53	37
CWM-140A	54	125	21	155	10	62	138
CWM-140B	18	3	16	149	6	76	176
CWM-141C	2	178	17	157	7	72	0
CWM-141D	36	170	18	159	8	74	0
CWM-144A	39	72	23	133	12	20	0
CWM-144B	83	204	19	140	6	67	5
CWM-155A	70	69	30	255	13	21	0
CWM-155B	110	199	16	100	7	70	318
CWM-158A	33	209	18	151	7	65	4
CWM-158B	82	93	21	254	12	106	0
CWM-162A	61	163	28	225	14	65	0
CWM-162B	38	227	28	250	15	83	0

APPENDIX FIsocon Technique (Grant, 1986)

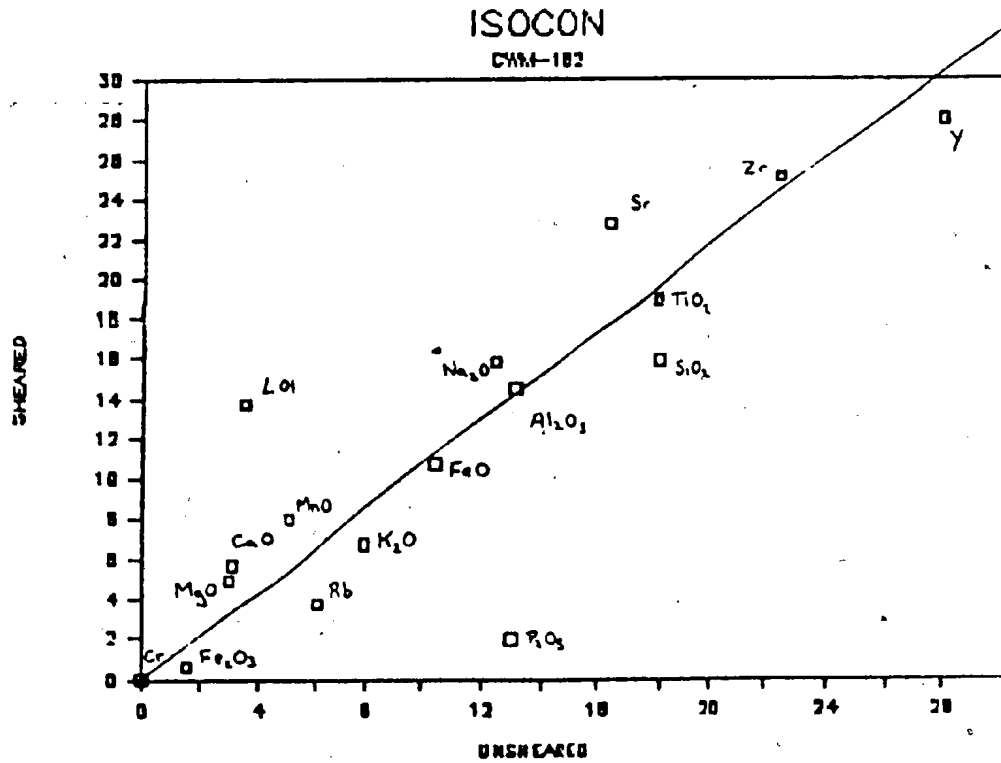
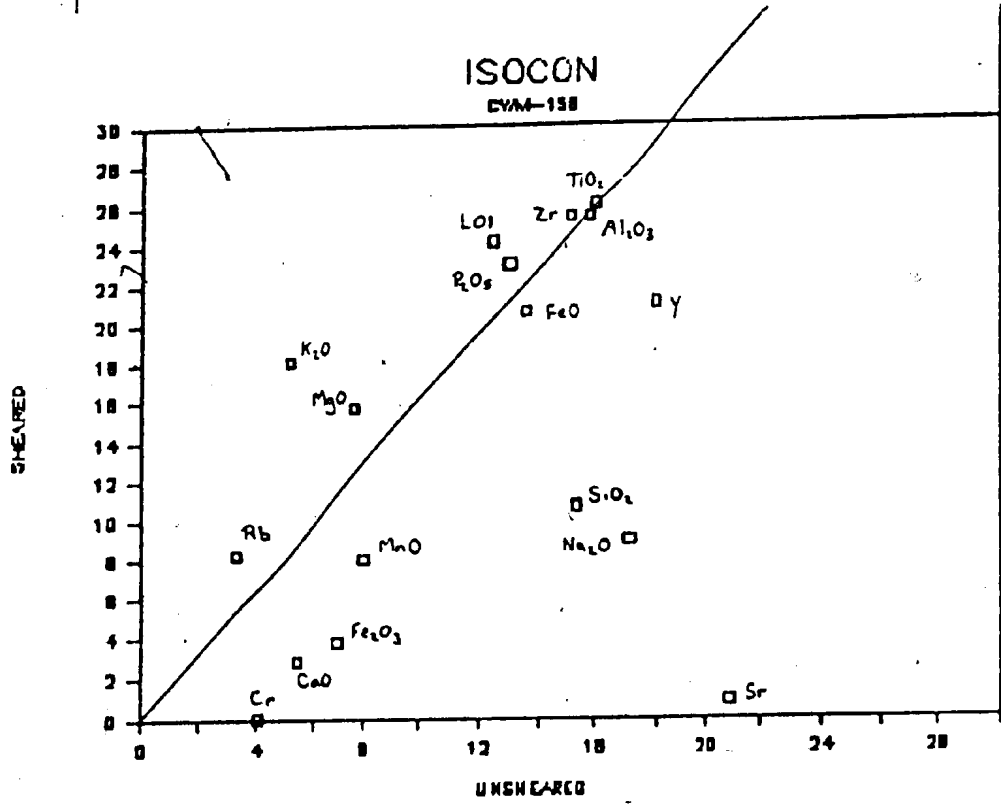
The isocon technique, devised by Grant (1986), is a method of determining the relative gains and losses of elements as a result of chemical alteration. In order to use this method, it must be assumed that one element, or a parameter such as mass or volume, has remained unchanged during alteration, and then the relative enrichment or depletion of other elements may be estimated. The horizontal axis represents the concentration of an element in the unaltered state, while the vertical axis represents the concentration of the same element in the altered state. The axes are scaled from 0 to 30, and values which lie outside of this range are multiplied by a factor such that the product lies between 0 and 30.

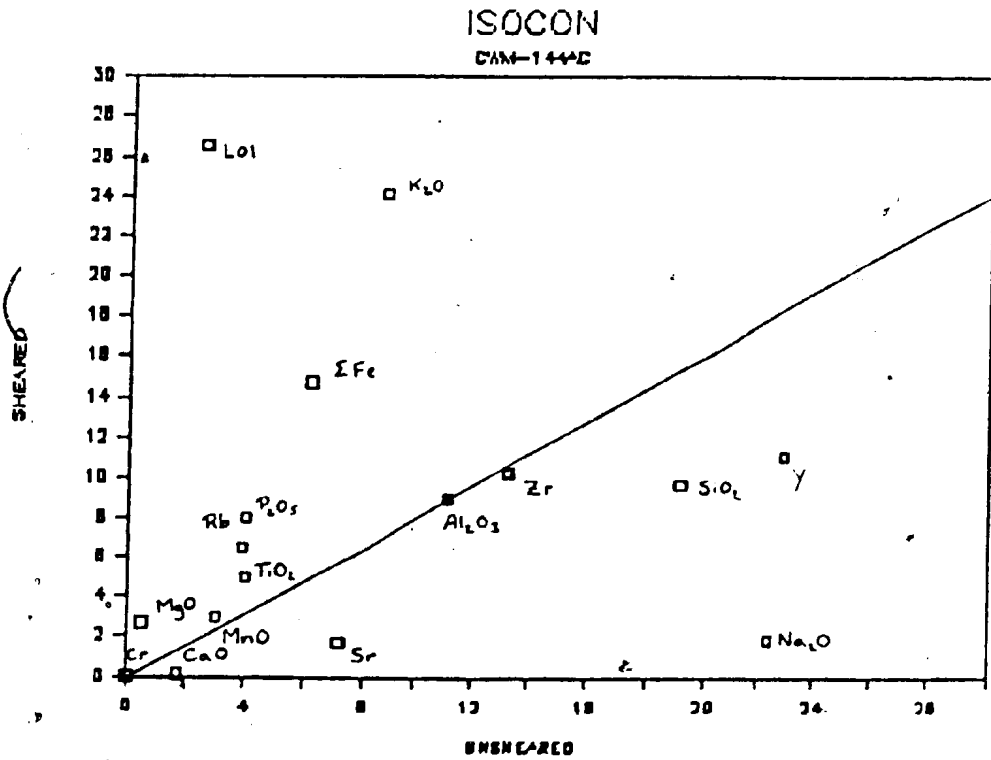
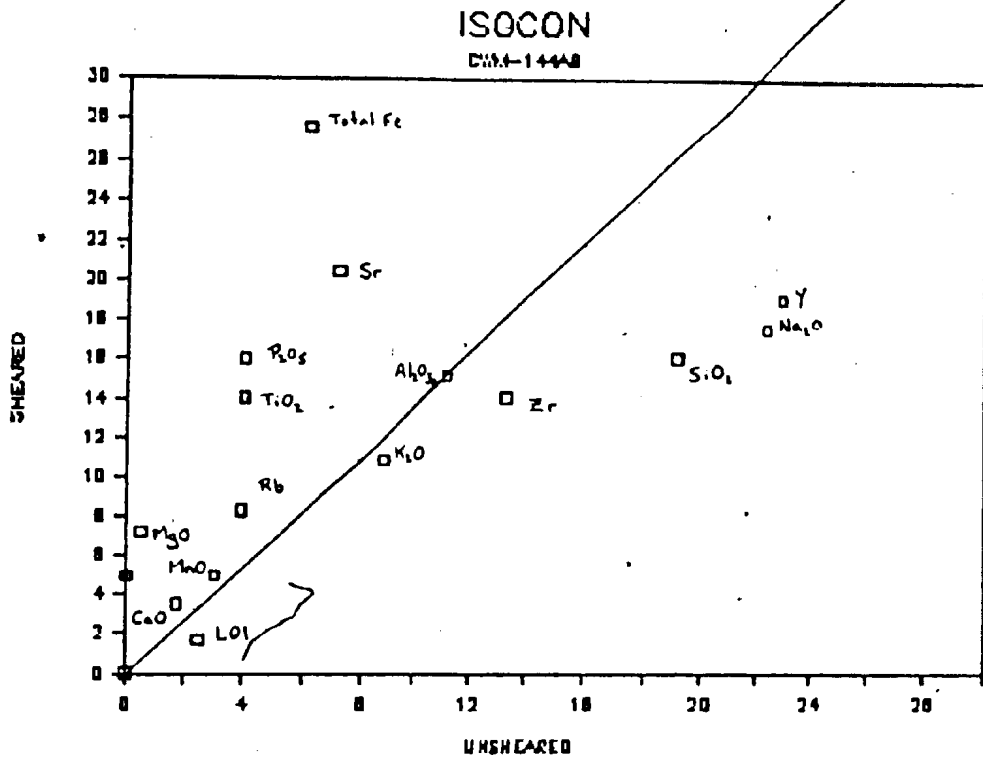
The constant parameter (in this study, Al_2O_3) is plotted on the diagram by plotting its unaltered concentration on the horizontal axis, and its altered concentration on the vertical axis. The isocon (which represents a line of constant concentration) is then drawn from the origin through this point, so that it intersects the vertical axis on the right hand side of the diagram. This point of intersection represents an enrichment/depletion of zero. Where the vertical line intersects the horizontal axis of the diagram, the

enrichment is equal to -100%, or 100% depletion. The space between these points can be scaled between 0 and 100.

The same scale can be used above the point 0, and represents positive values of enrichment. There is no upper limit to the extent of enrichment possible.

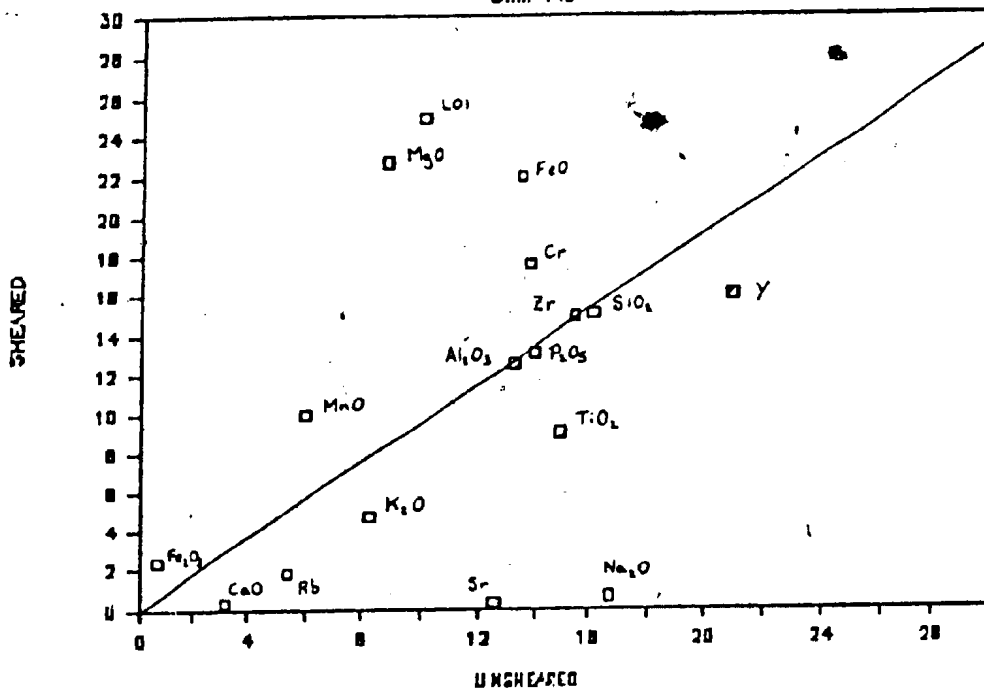
To determine the magnitude of enrichment or depletion of a given mobile element, it is plotted on the diagram and a line is drawn from the origin through that point to intersect the scaled vertical line on the right hand side of the diagram. The amount of depletion or enrichment is determined from the position of intersection on the vertical axis on the right hand side of the diagram.





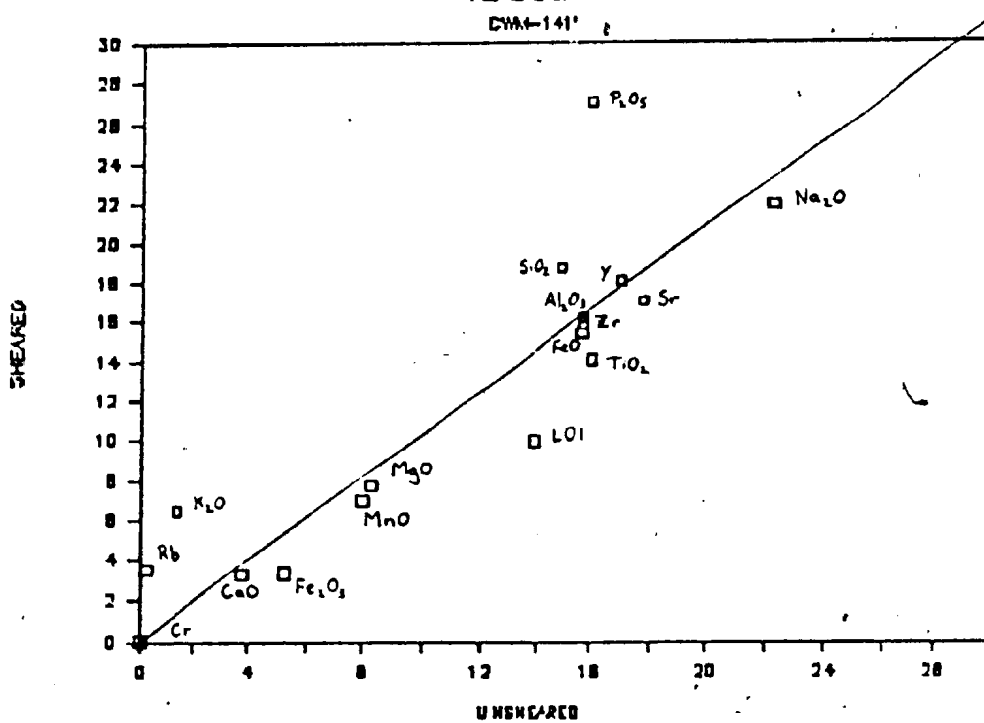
ISOCON

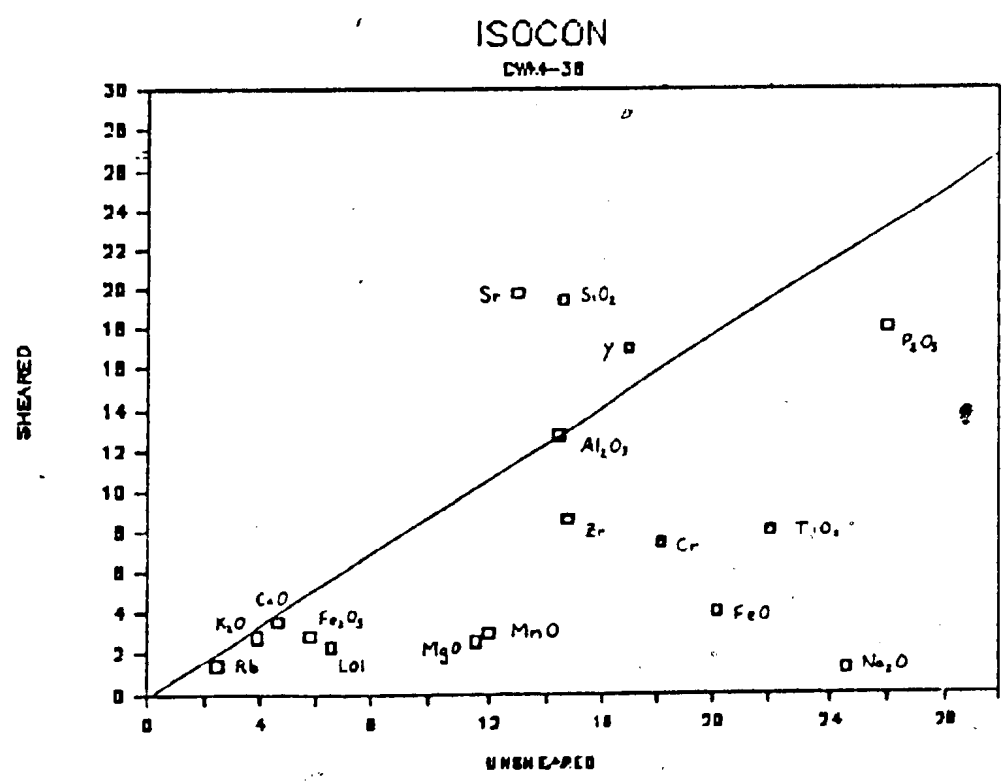
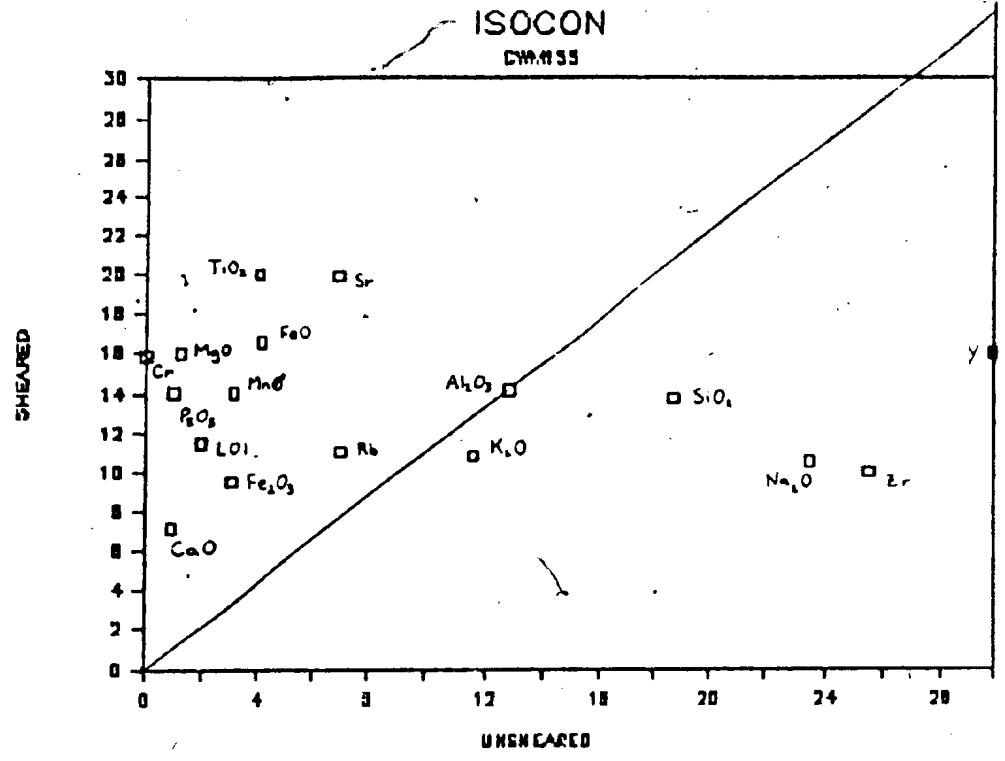
CWA-140

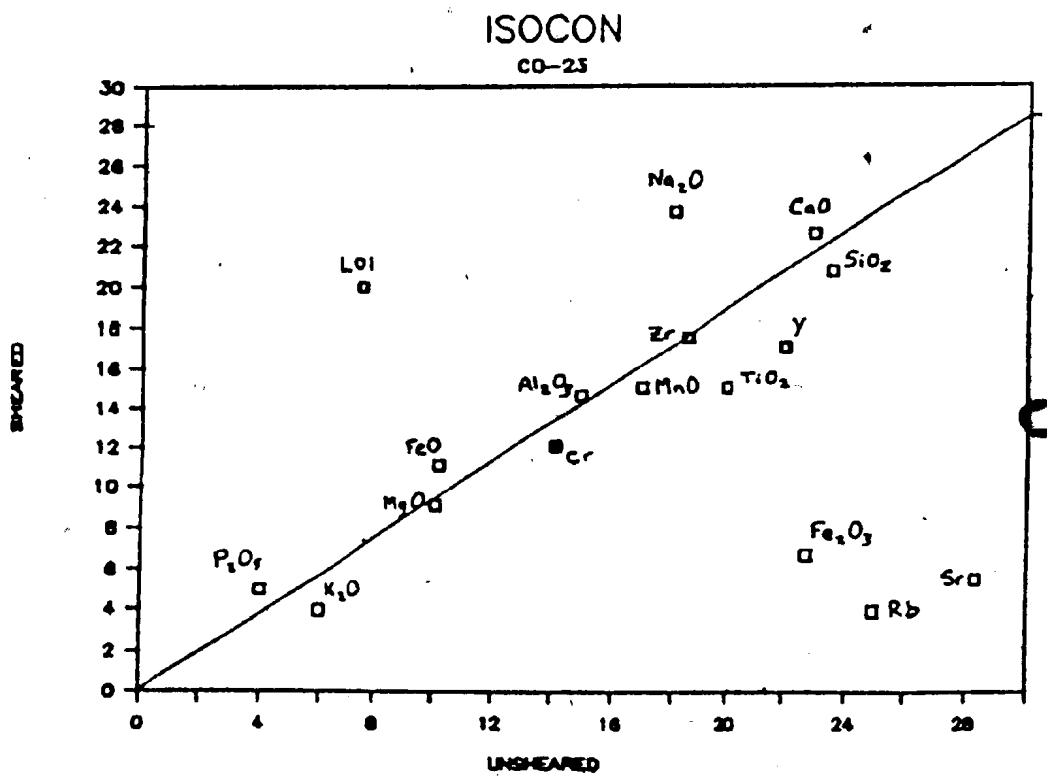
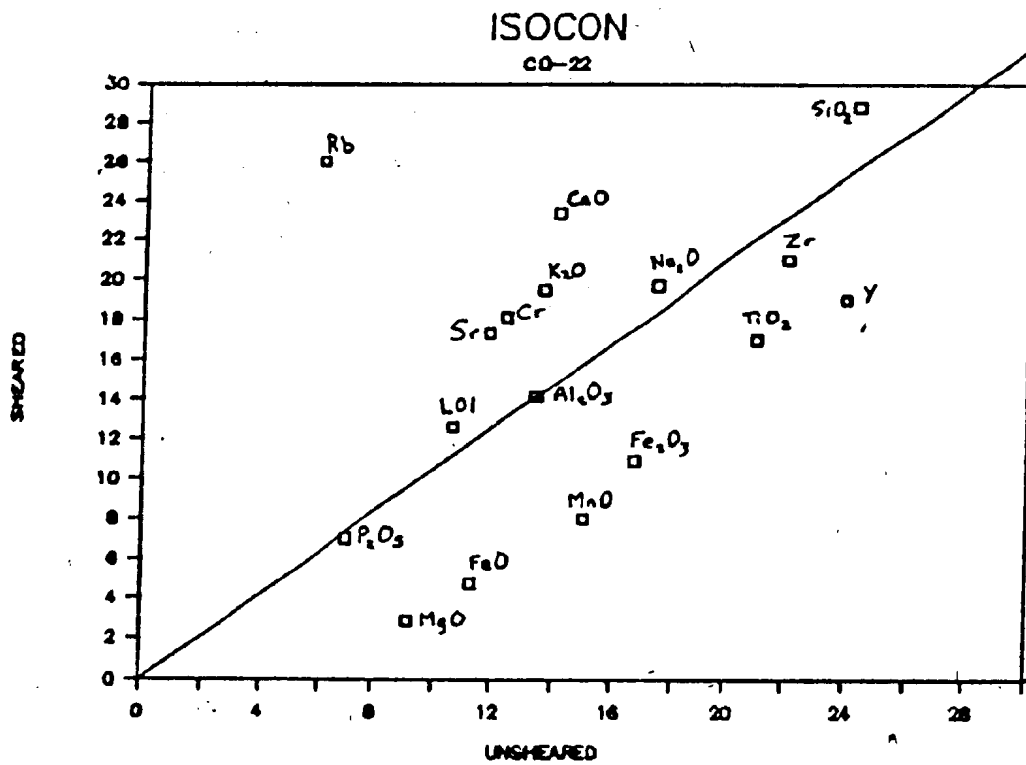


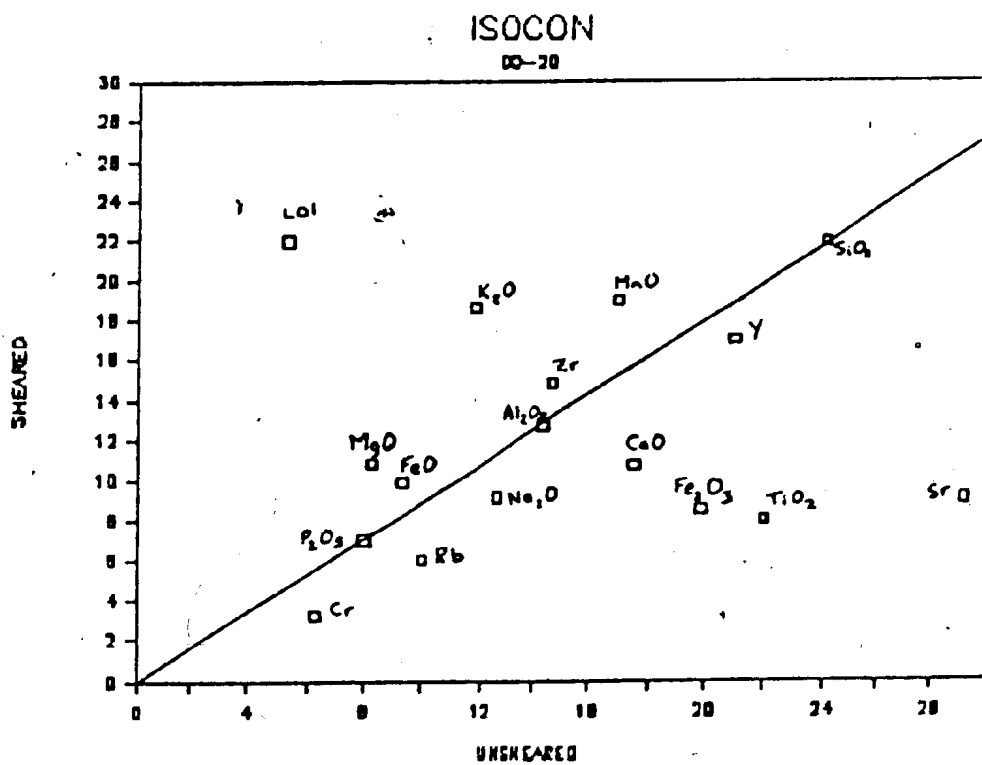
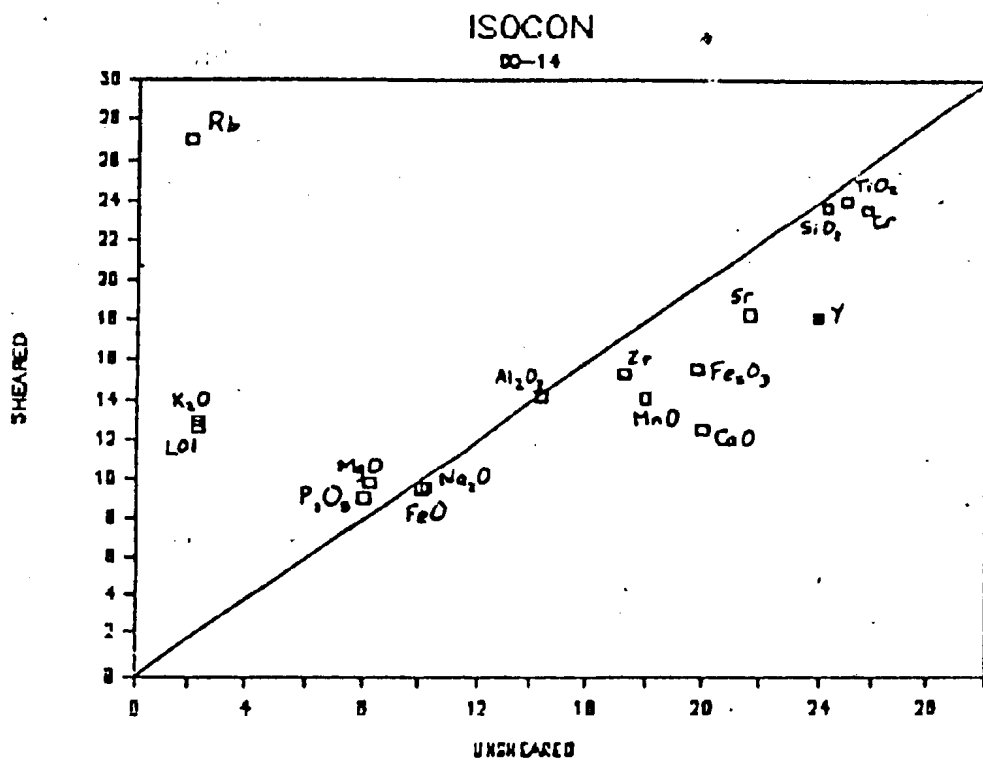
ISOCON

CWA-141

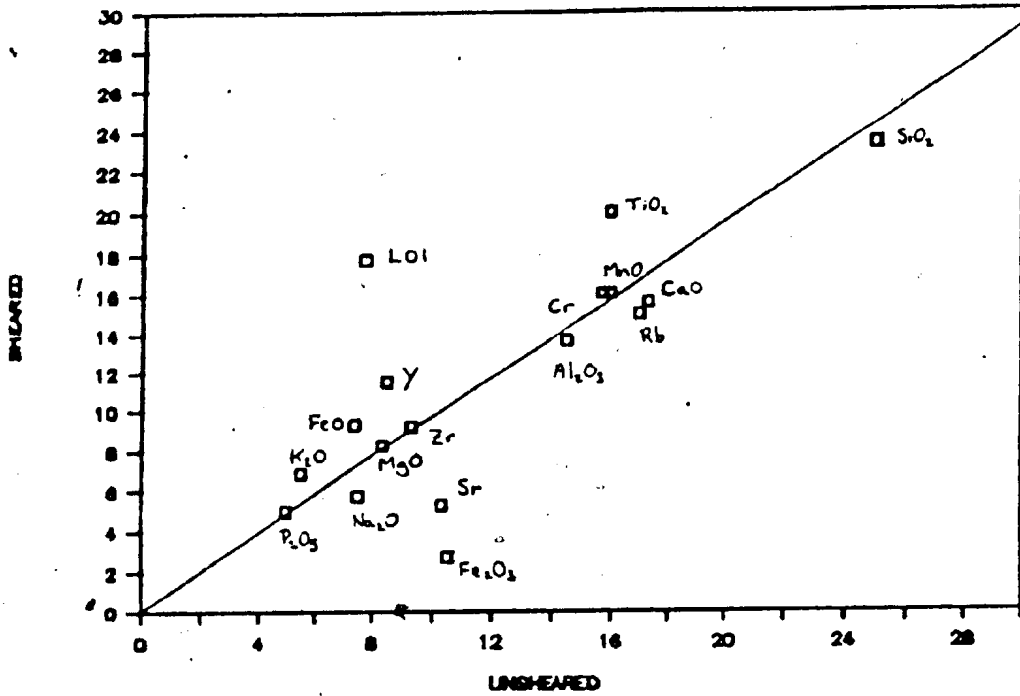




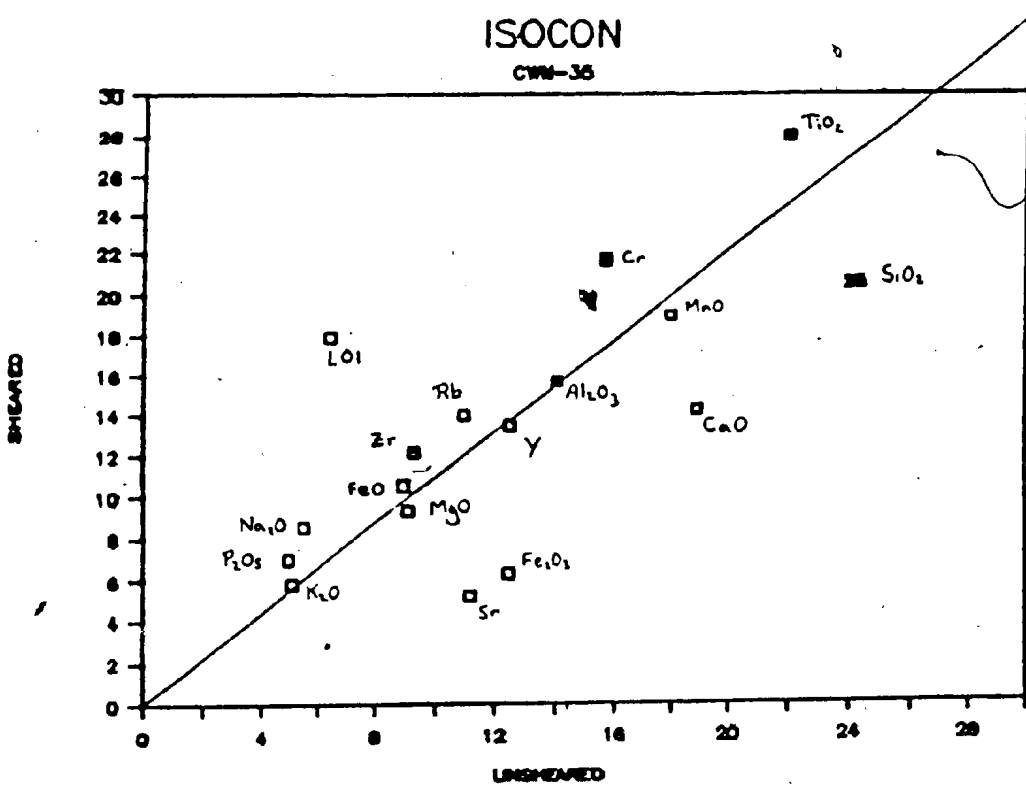


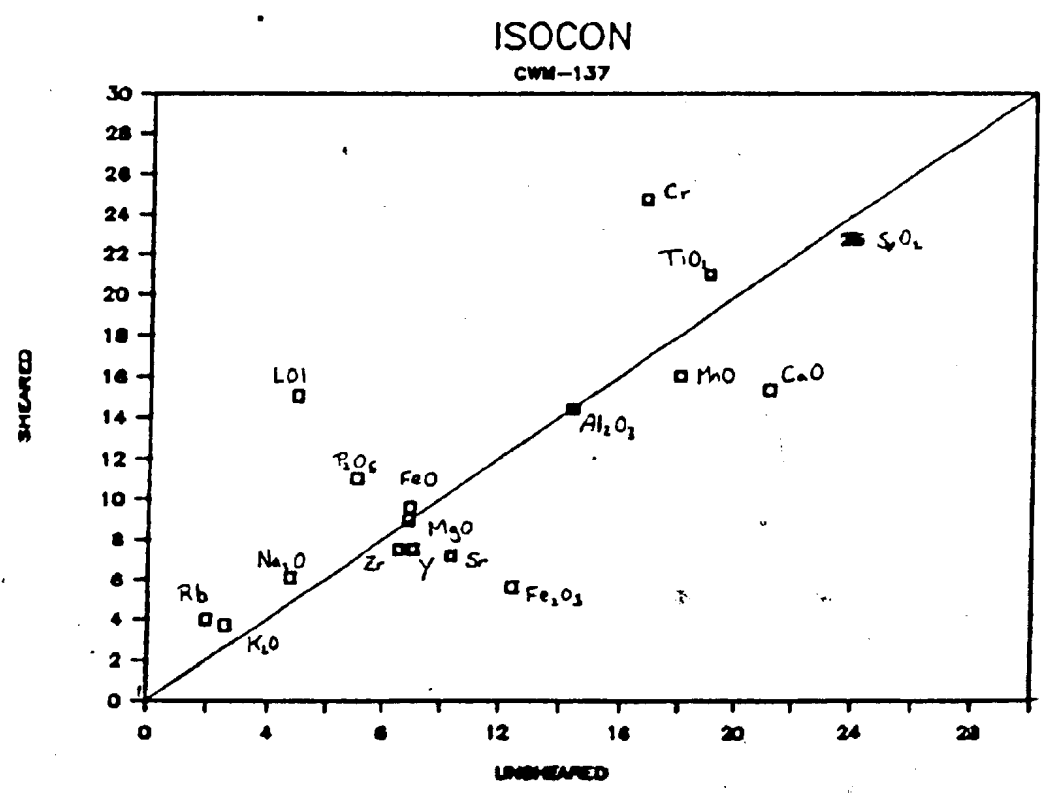
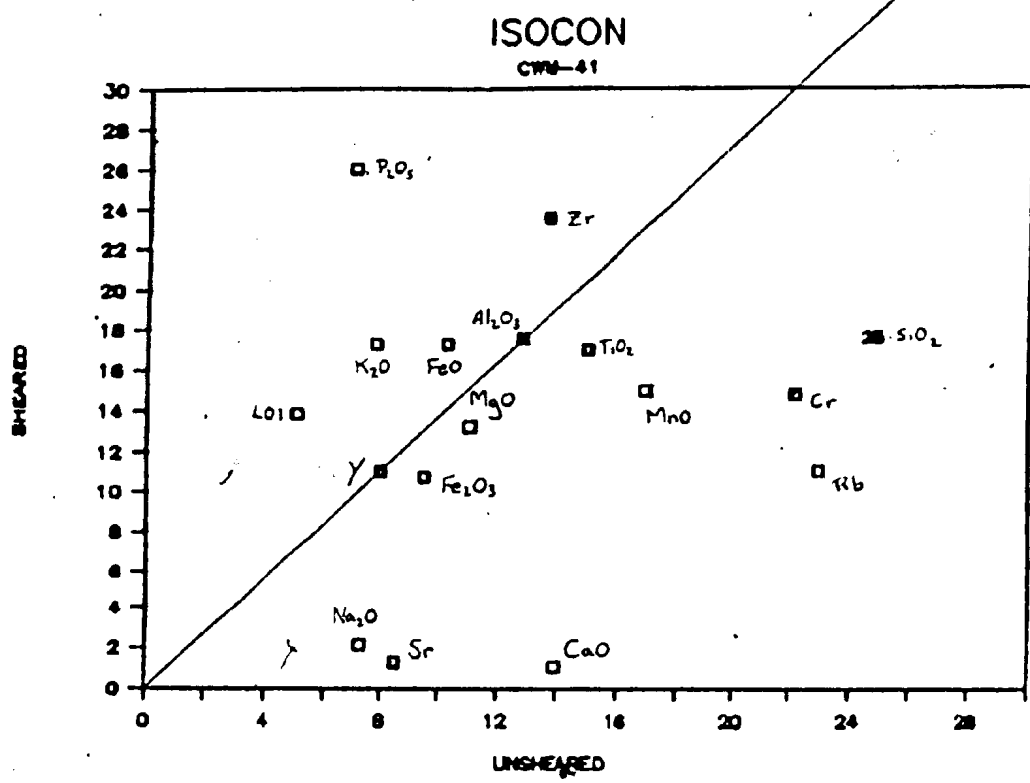


ISOCON
CVM-34

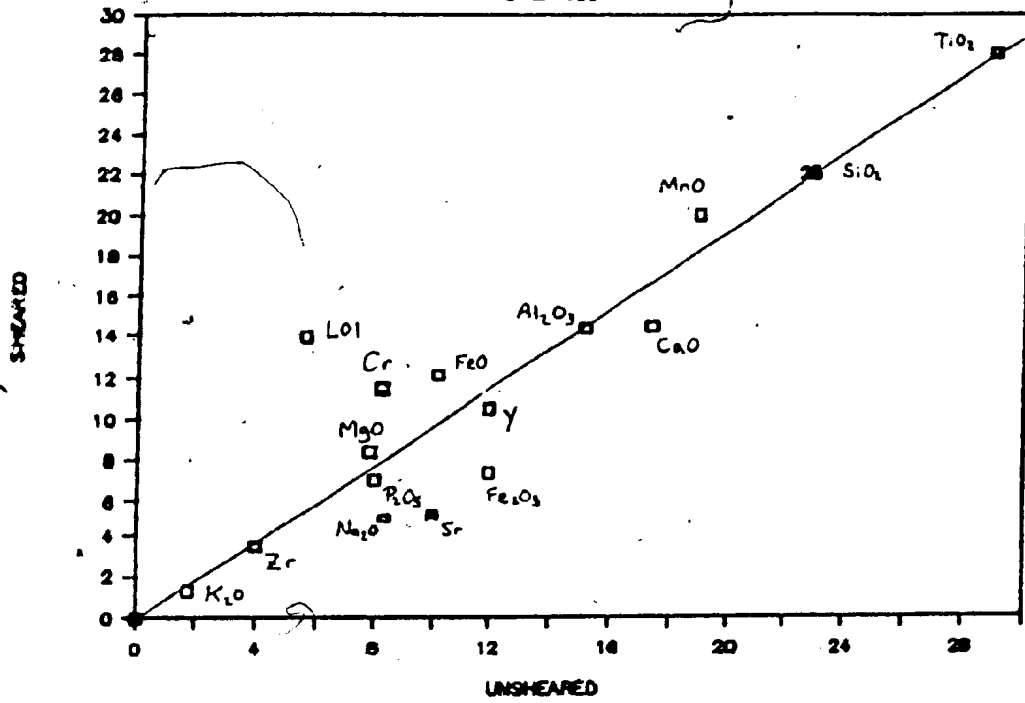


ISOCON
CVM-35

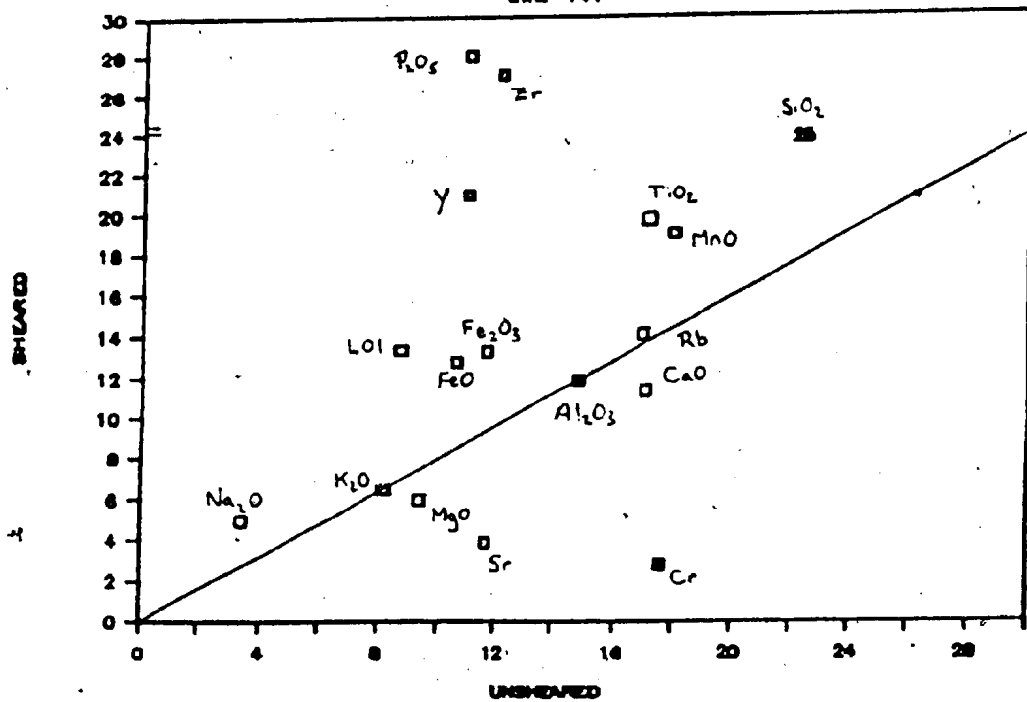




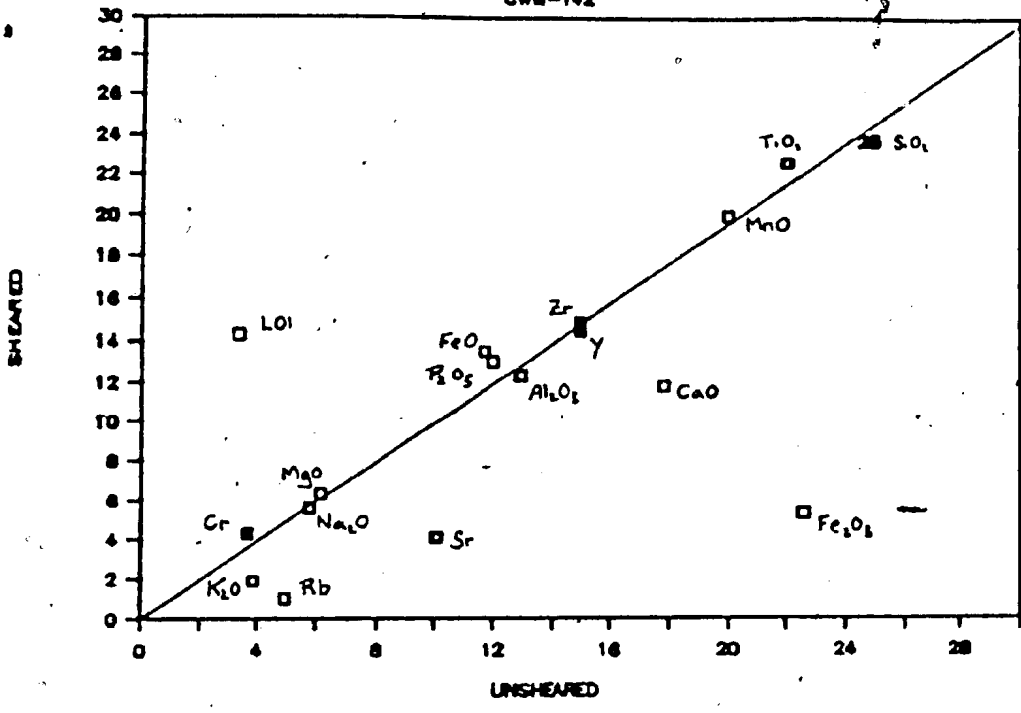
ISOCON
CWM-130



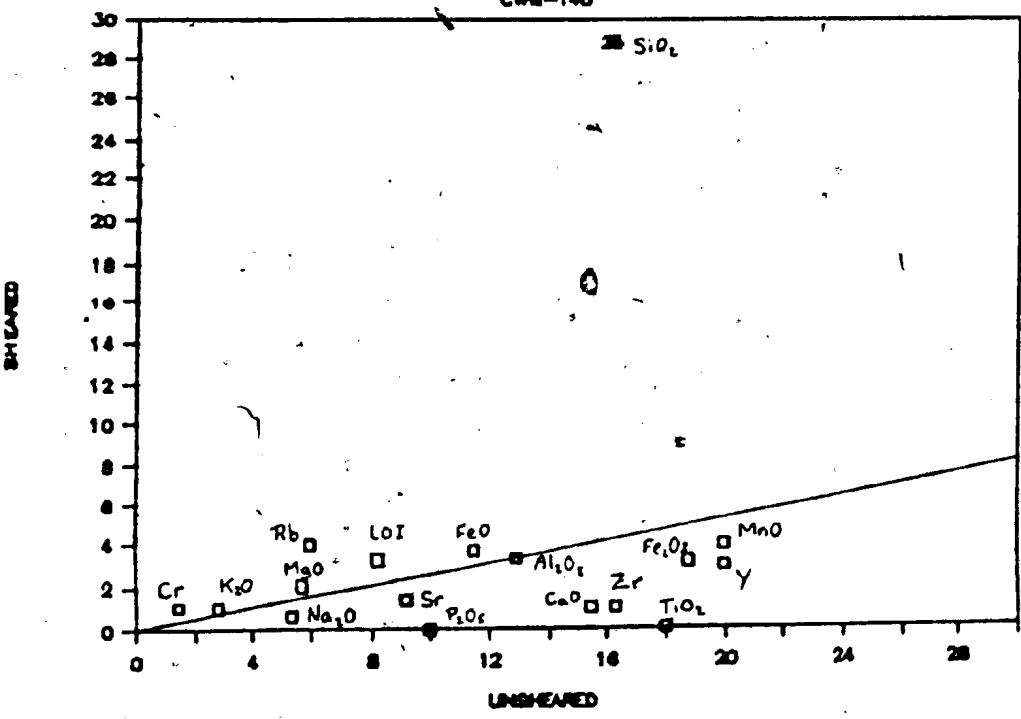
ISOCON
CWM-141



ISOCON CWI-142

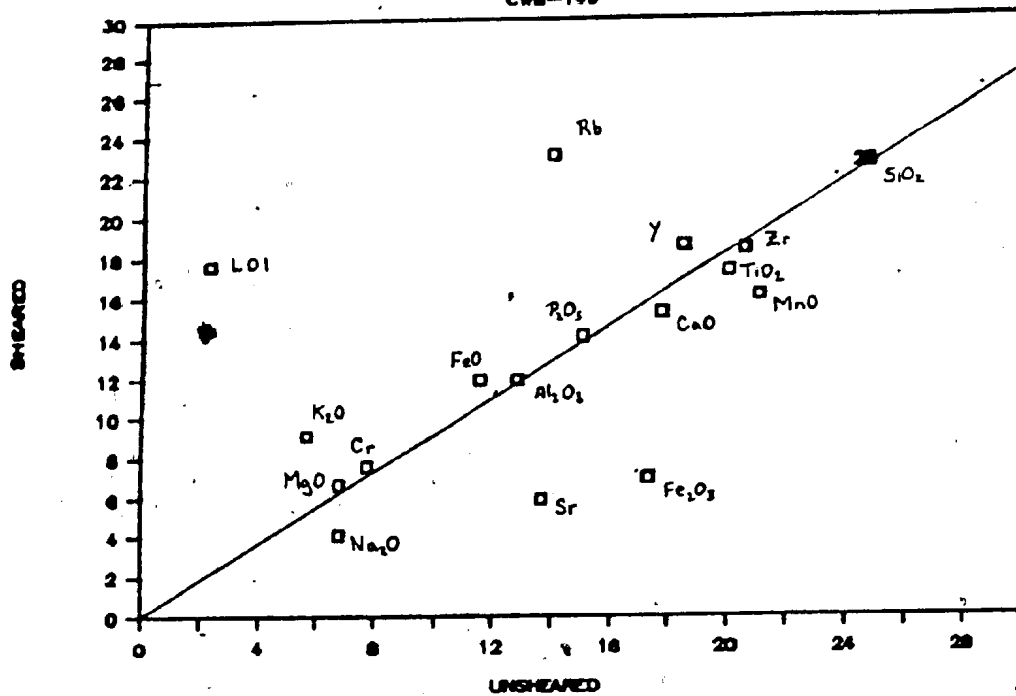


ISOCON | CWI-145



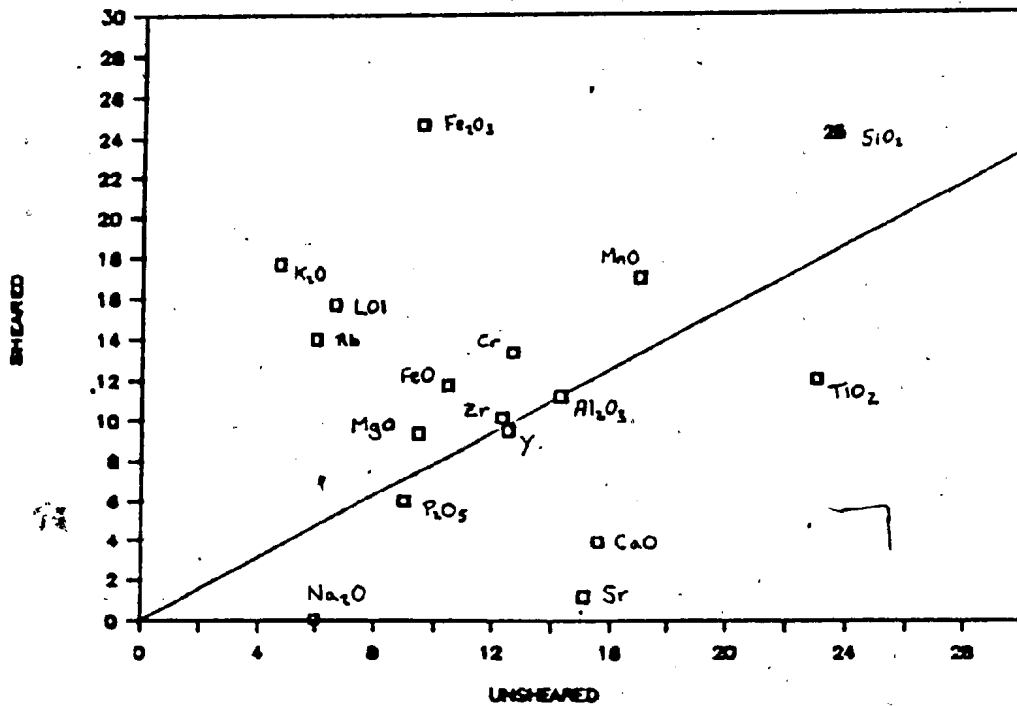
ISOCON

CWM-149

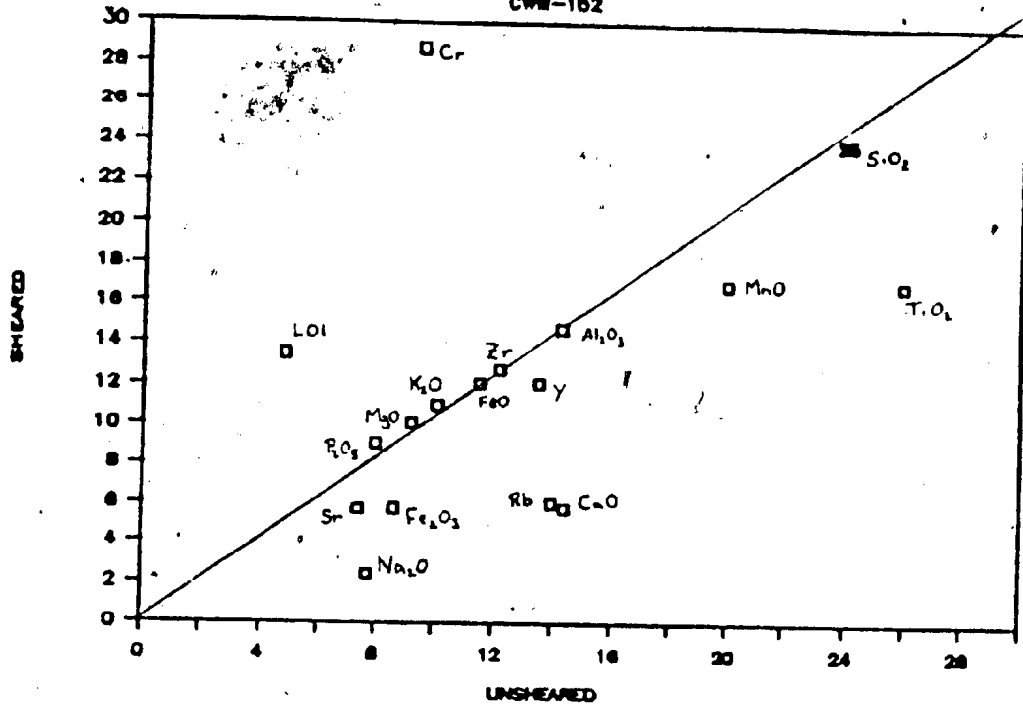


ISOCON

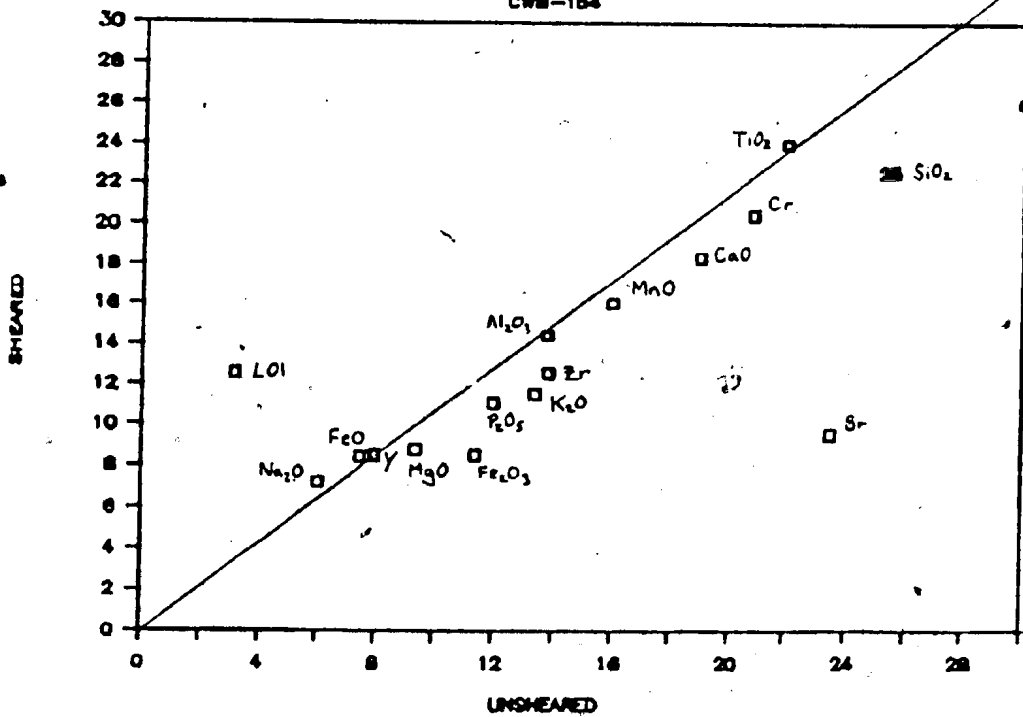
CWM-181



ISOCON CWM-162

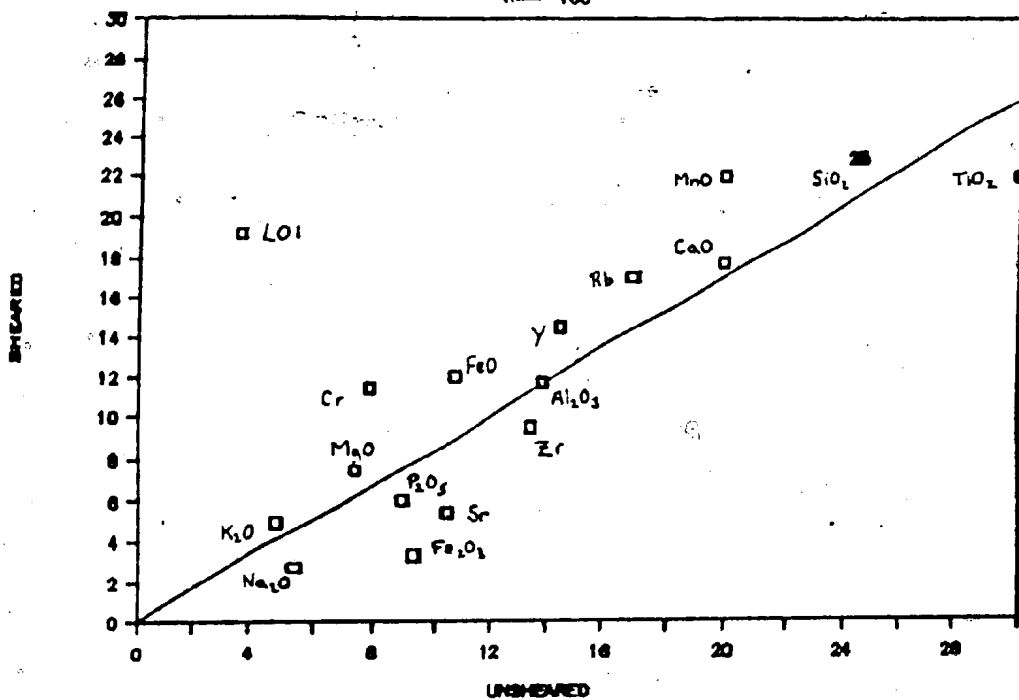


ISOCON CWM-154



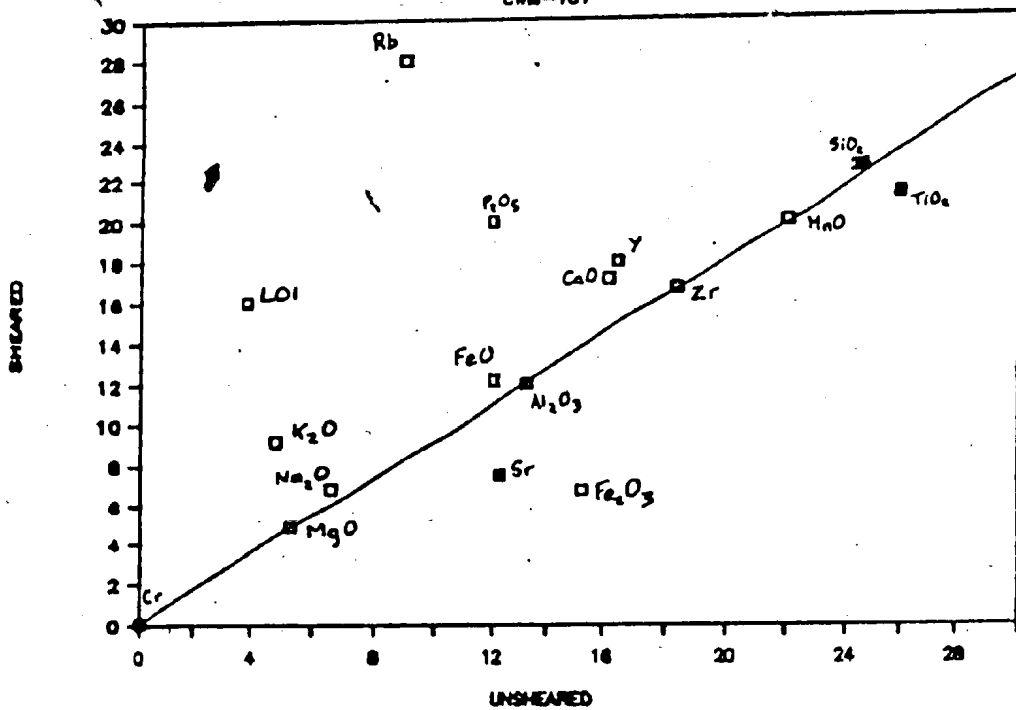
ISOCON

CWM-160



ISOCON

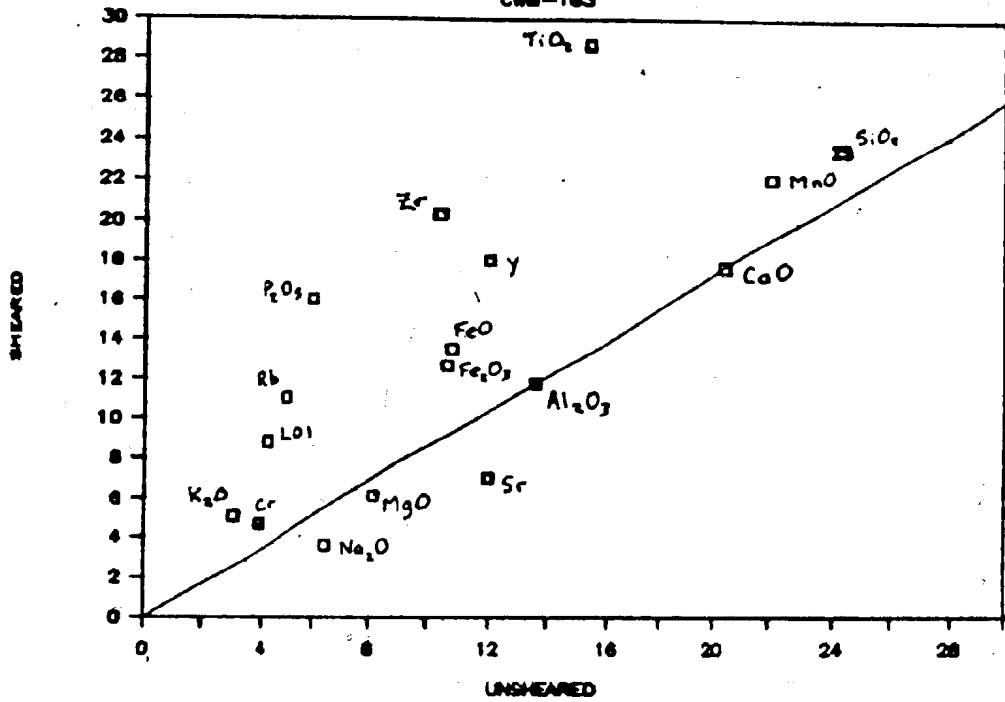
CWM-161



ISOCON

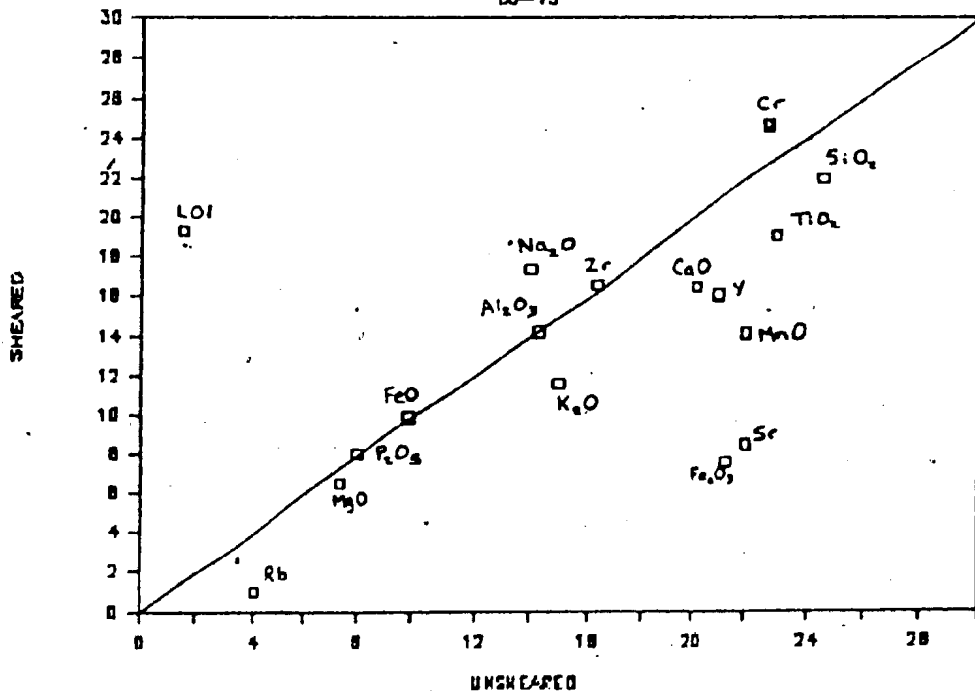
CW-163

33°



ISOCON

00-13



APPENDIX GModal and Molar Quantities of Samples

Modal abundances of minerals were determined from thin sections by point counting (1000 points). These values were converted to molar quantities using the following molar volumes (cm^3/mol): amphibole - 273, albite - 100.2, anorthite - 100.8, chlorite - 141, epidote - 139, carbonate - 37, biotite - 151, sericite/muscovite - 150, quartz - 22.7, pyrite - 24, K-feldspar - 108.

metabasite samples

Sample #	plag	amph	chl	epi	carb	bio	ser	qtz	py
CWM-34A	31.3	35.0	9.3	16.0	2.0			4.2	2.2
moles:	.312	.128	.068	.115	.054			.185	.09
CWM-34B	18.5		39.1	0.2	14.4	2.8	2.6	20.7	1.7
moles:	.184		.285	.001	.390	.018	.018	.912	.071
CWM-35A	29.0	39.2	4.7	21.2	0.8	1.5		1.8	1.8
moles:	.289	.144	.034	.152	.021	.010		.079	.071
CWM-35B	35.7		43.7	1.7	12.3	0.3	0.3	5.9	0.1
moles:	.356		.319	.012	.330	.002	.002	.260	.004
CWM-41A	24.2	43.4	21.7	2.7	0.4	1.3	1.1	4.0	1.2
moles:	.241	.159	.158	.019	.011	.009	.008	.176	.050
CWM-41B	22.2		61.6	1.9	0.2		4.7	1.2	8.2
moles:	.222		.450	.014	.005		.033	.053	.343
CWM-141A	22.2	23.2	25.8	13.1	4.3	6.2	1.6	1.8	1.8
moles:	.221	.085	.188	.094	.116	.041	.011	.079	.075
CWM-141B	17.5		34.8	4.1	10.9	5.0	1.5	19.6	6.
moles:	.175		.254	.029	.295	.033	.011	.864	.255
CWM-142A	25.6	46.7	9.4	11.7	0.4	0.4		2.6	3.2
moles:	.255	.171	.069	.084	.011	.003		.115	.134
CWM-142B	19.0		44.5	4.5	5.7	1.1		21.7	3.3
moles:	.190		.325	.032	.154	.007		.956	.146
CWM-149A	22.8	55.7	0.7	5.4	1.1	4.4		5.8	
moles:	.227	.204	.005	.039	.030	.029		.256	
CWM-149B	0.6		44.0	1.0	17.0	4.6		27.4	3.4
moles:	.006		.321	.007	.461	.030		1.208	.226
CWM-160A	33.1	40.8	14.2	5.4			3.1	0.6	2.8
moles:	.330	.149	.104	.039			.022	.026	.117
CWM-160B	23.8		48.4	1.8	6.9	1.8	1.2	14.6	1.5
moles:	.237		.353	.013	.187	.012	.008	.643	.063
CWM-163A	26.6	47.2	6.2	12.8	2.6			1.0	3.5
moles:	.265	.173	.045	.092	.070			.044	
CWM-163B	12.1	37.1	15.9	6.6	4.2	9.2		10.8	4.1
moles:	.120	.136	.116	.047	.114	.061		.476	.171

felsic to intermediate volcanoclastic samples

Sample #	plag	Ksp	chl	epi	carb	bio	ser	qtz	py	sph
CWM-141C	37.9	9.1	20.9	8.4	1.2	1.2	2.6	17.6		1.1
moles:	.378	.091	.152	.061	.032	.008	.018	.776		.023
CWM-141D	20.0	7.7	4.6	1.5	0.2	29.4	4.6	29.8	0.6	1.6
moles:	.200	.077	.036	.011	.005	.195	.033	1.313	.002	.034
CWM-144A	27.3				1.4	3.2	21.7	46.1		0.3
moles:	.272				.038	.021	.154	2.032		.006
CWM-144B	21.6			0.4	0.8	28.9	12.2	34.2	0.8	0.6
moles:	.216			.003	.022	.191	.087	1.507	.033	.013

Abbreviations used: plag - plagioclase, amph - amphibole, chl chlorite, epi - epidote, carb - carbonate, bio - biotite, ser sericite, qtz - quartz, py - pyrite, Ksp - K-feldspar, sph - sphene

APPENDIX H

Idealized formulae of mineral grains too small to obtain microprobe analyses for are as follows:

sericite: $K_2Al_4Si_6Al_2O_{20}(OH)_4$

epidote: $CaFe^3Al_2OSi_3O_{11}(OH)$

chlorite (intermediate volcanoclastic samples):
 $Mg_6Fe_6Si_6Al_2O_{20}(OH)_{16}$

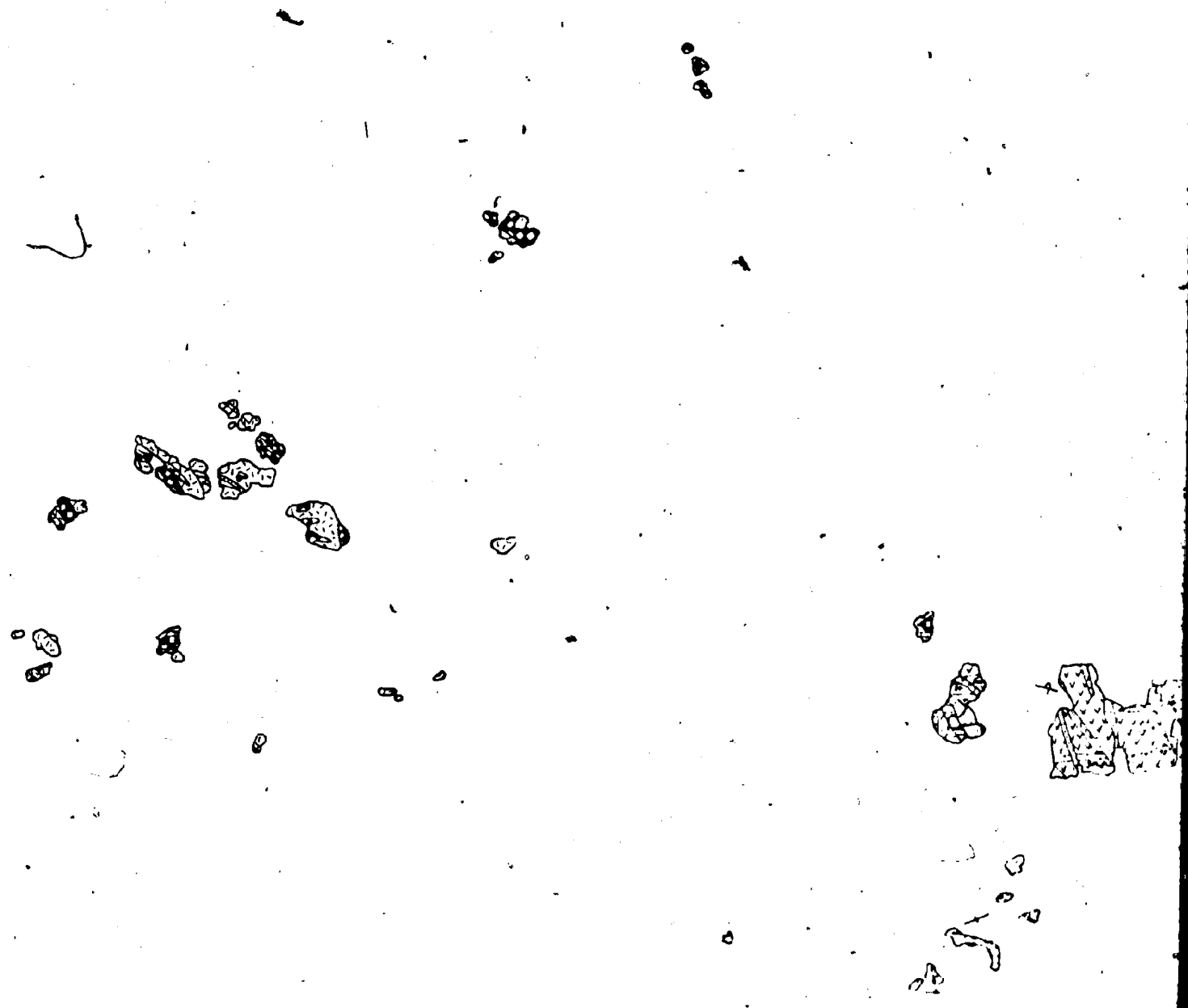
sphene: $CaTiSiO_4(OH)$

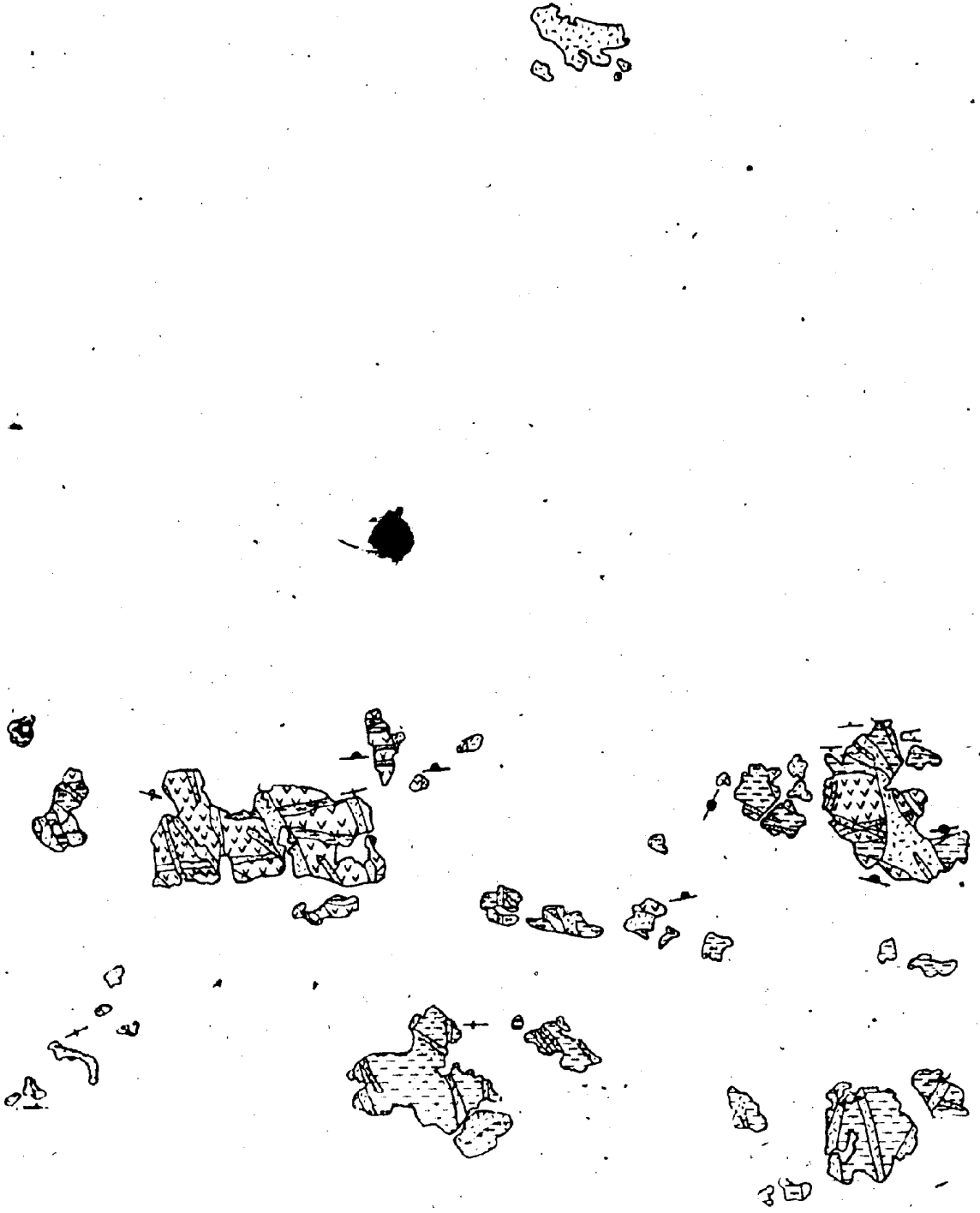
pyrite: FeS_2

clinozoisite: $Ca_2Al_3OSi_3O_{11}(OH)$

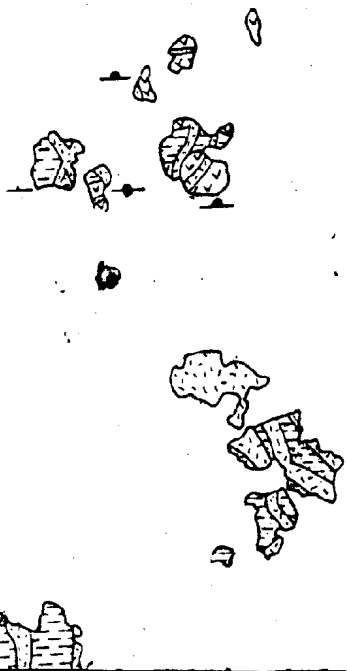
GEOLOGY OF THE WEST

EST MIRAGE ISLANDS





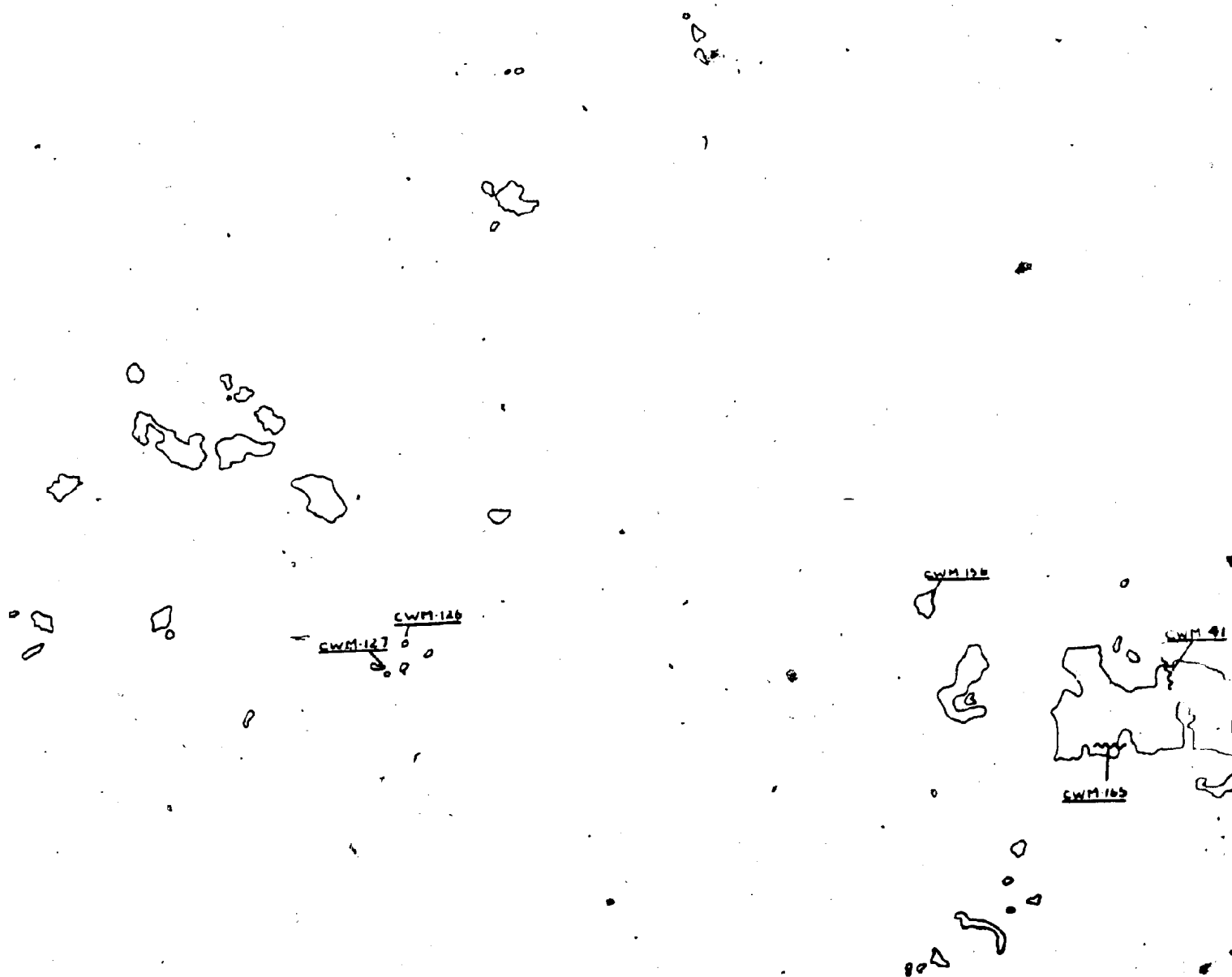
N



SAMPLE LOCATION MA

OCTOPUS ISLANDS

MAP: WEST MIRAGE ISLANDS



LANDS



CWM-126

CWM-41

CWM-165

CWM-26

CWM-22

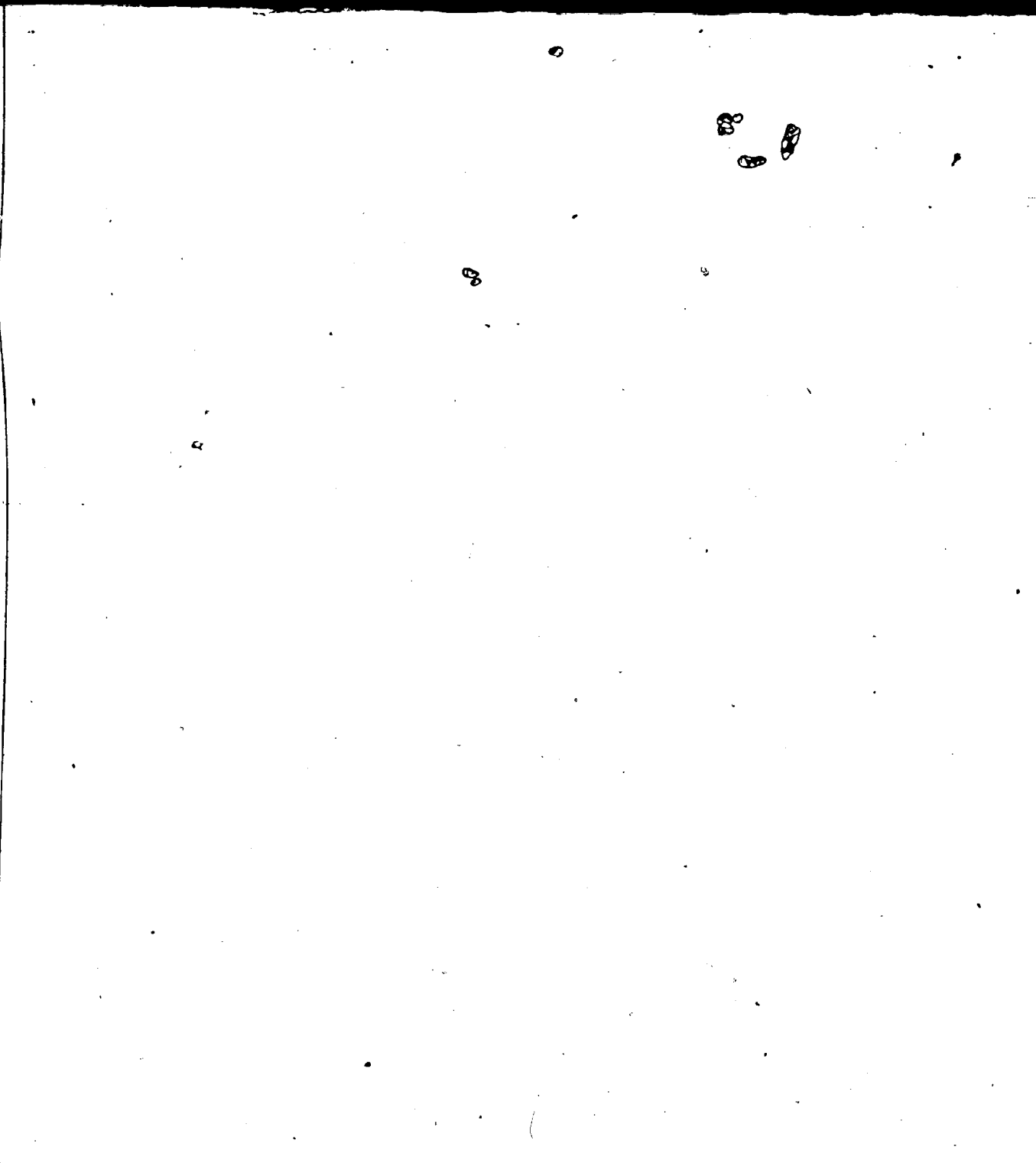
CWM-34

CWM-162

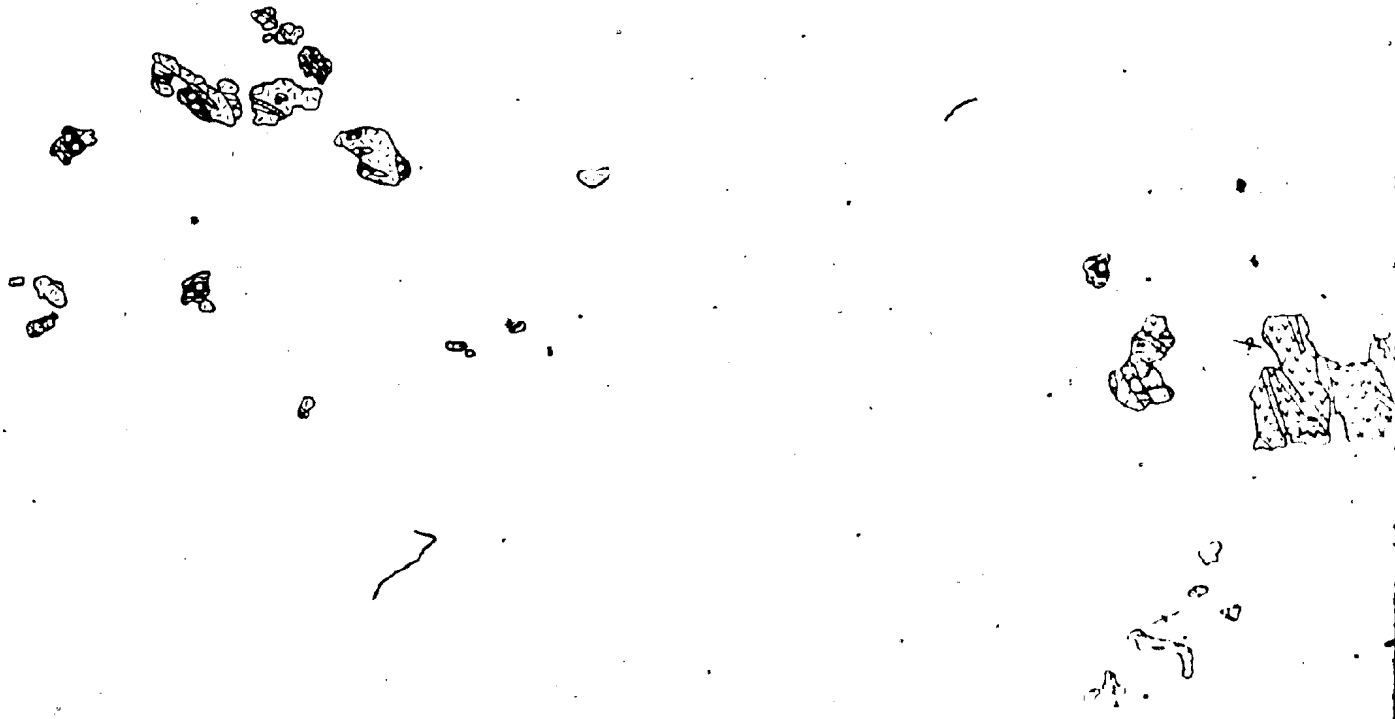
0 m 500

N





- | | | |
|--|------------------------------|--------------|
| | 8 Diabase Dykes | beddi |
| | 7 Granitoid | tops known |
| | 6 Tonalite | tops unknown |
| | 5 Metagabbro Dykes and Sills | overturned |
| | | (dips subv |
| | | pillov |

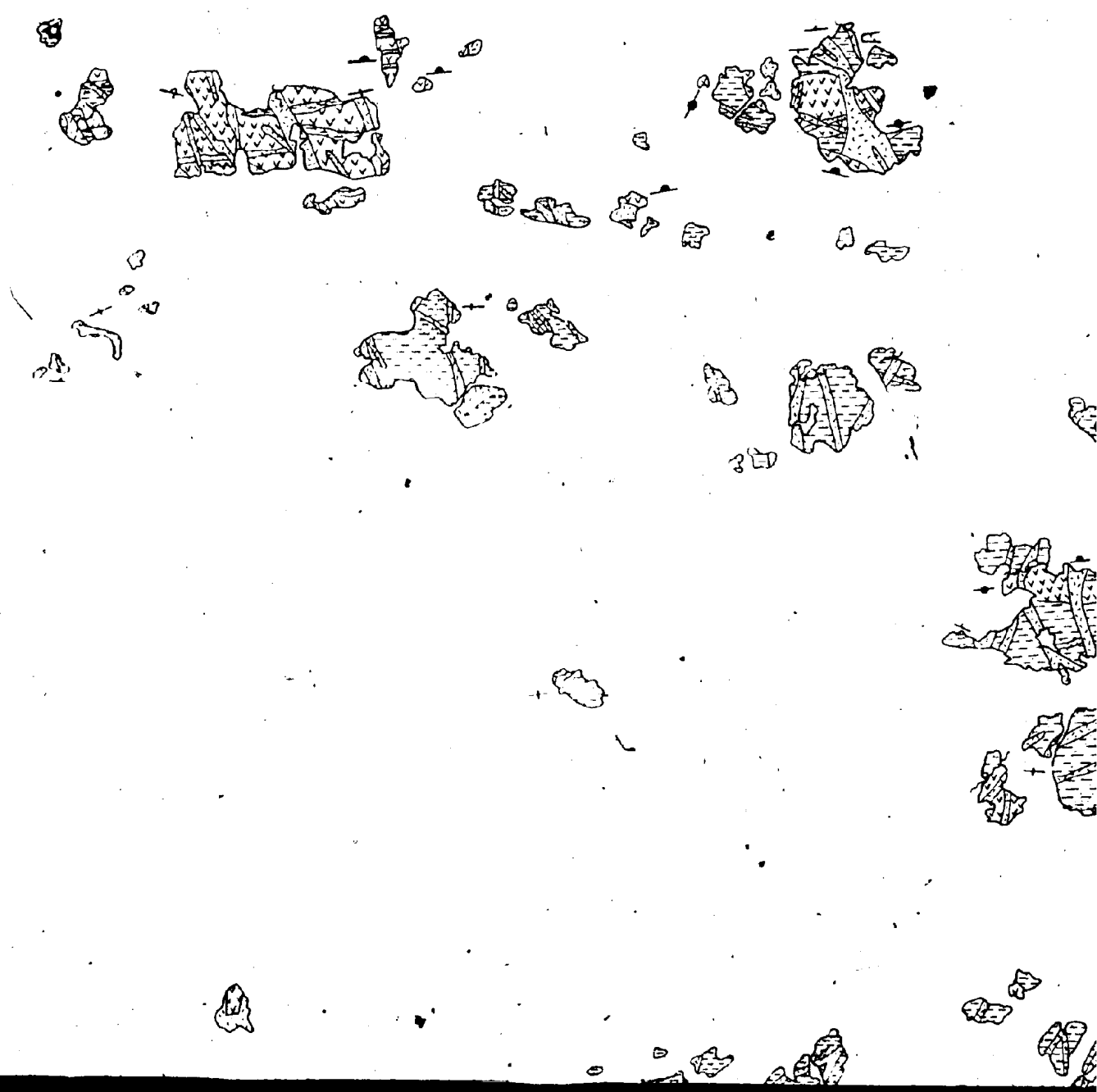


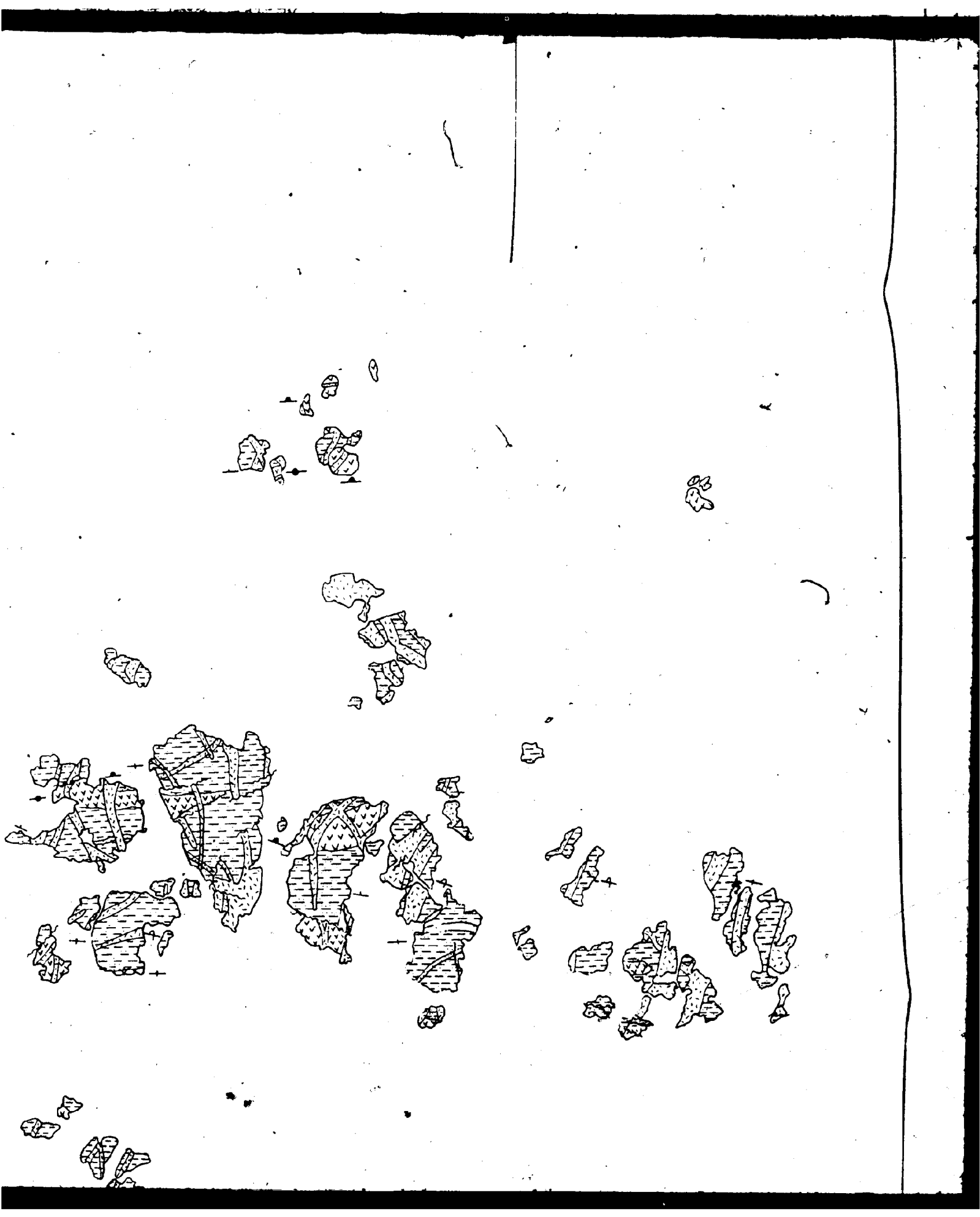
dding

n +

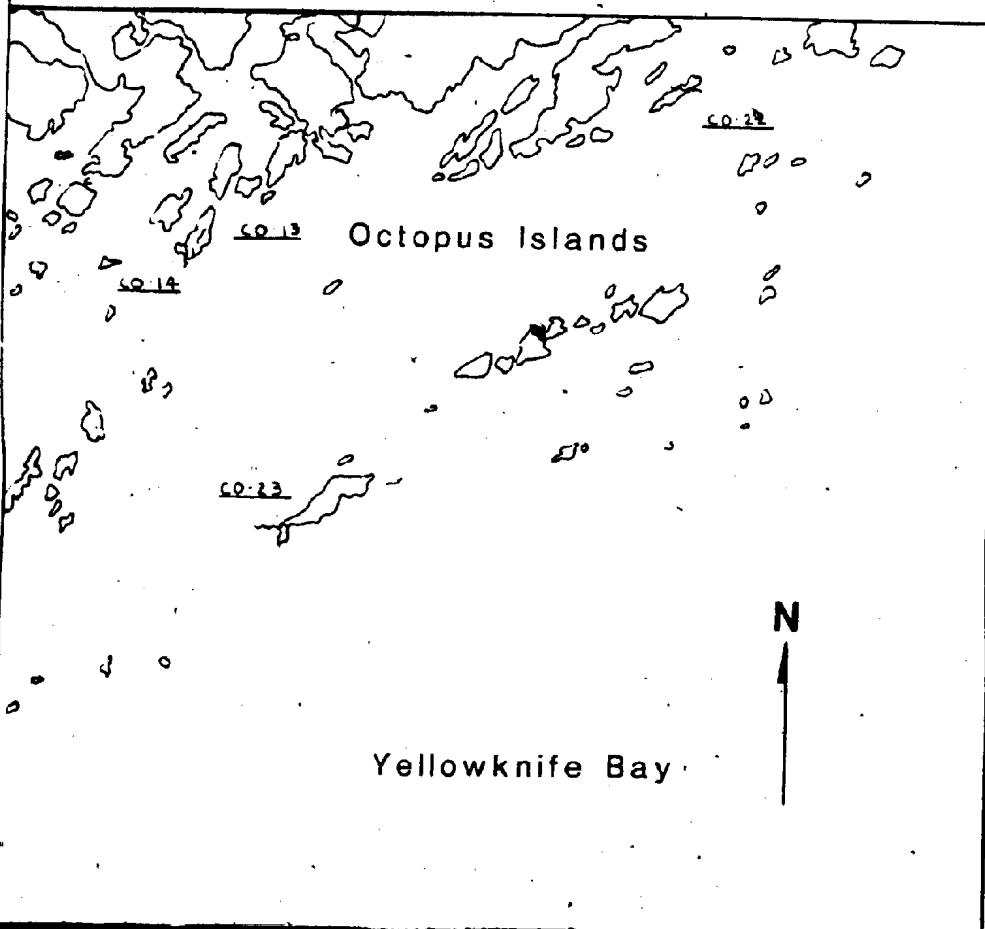
ubvertical)

illows





OCTOPUS ISLANDS



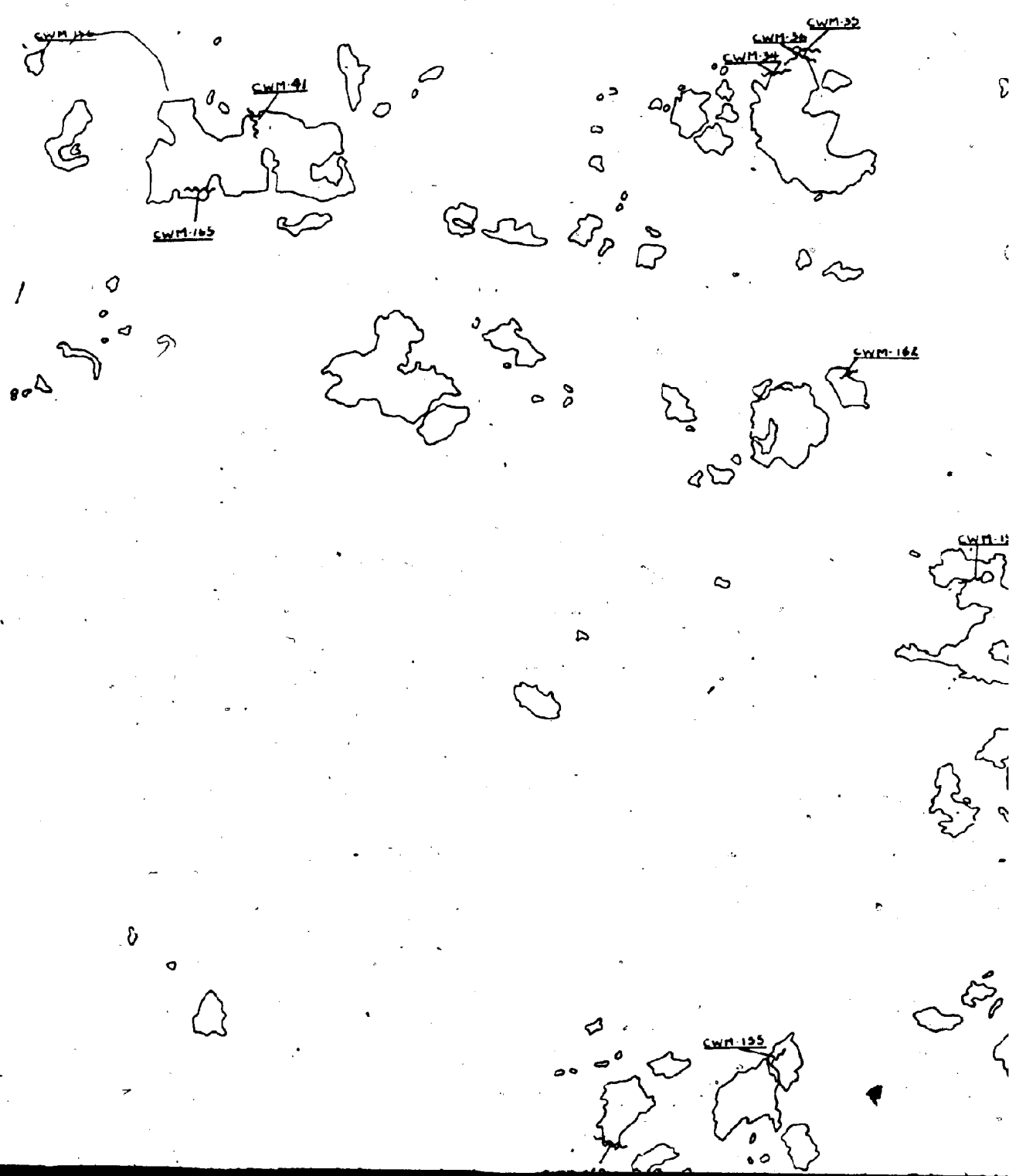


CWM 127
CWM 128

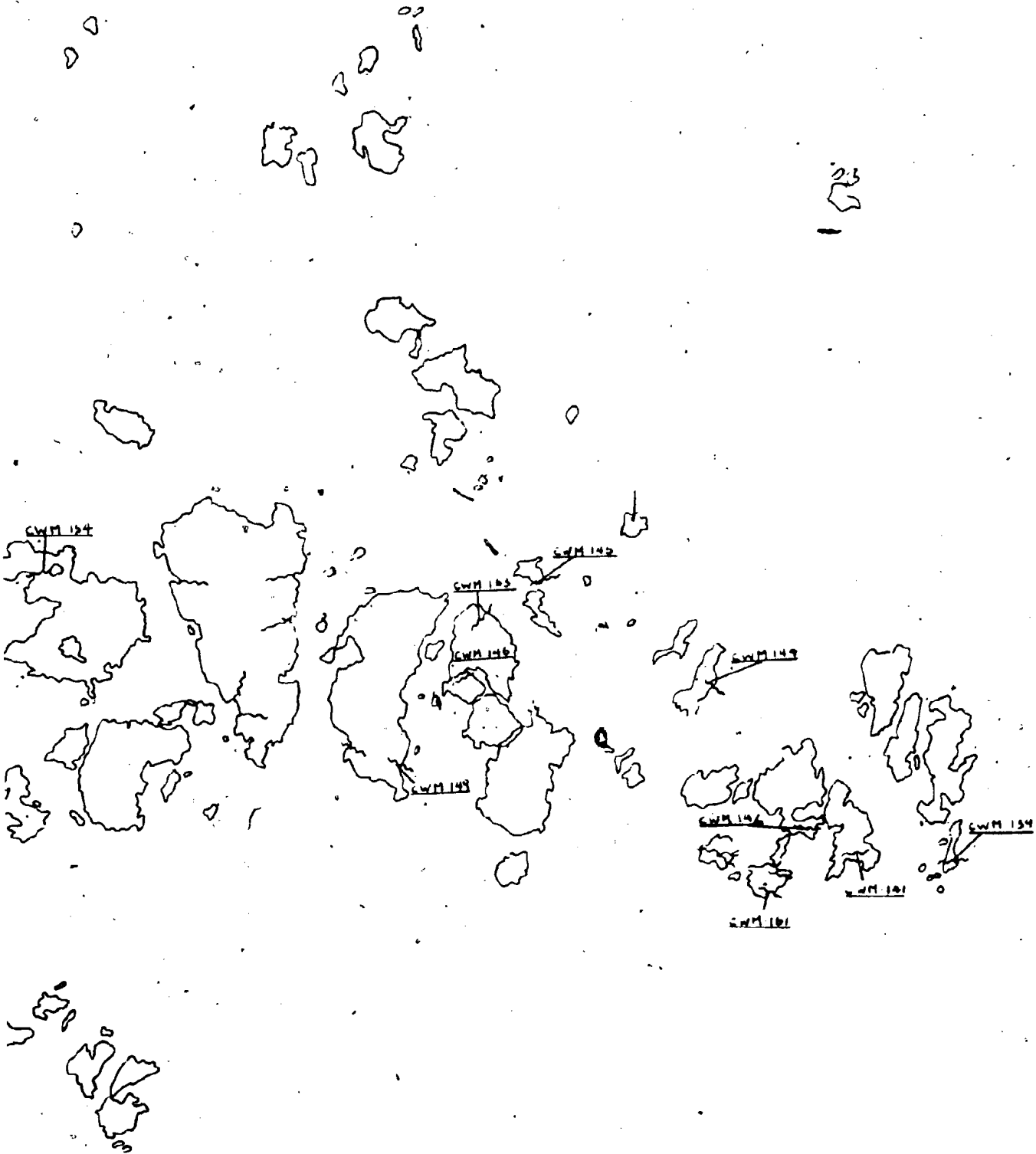
CWM 128

CWM 41
CWM 165





0 m 500



ARCHEAN



8 Diabase Dykes



7 Granitoid



6 Tonalite



5 Metagabbro Dykes and Sills



4 Felsic Dykes



3 Plagioclase Porphyry

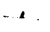

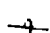


2 Felsic to Intermediate Metavolcaniclastics





1 Mafic Metavolcanics

bedding

tops known 
tops unknown 
overturned 

(dips subvertical)

pillows

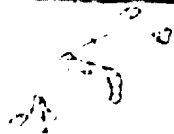
tops known 
tops unknown 

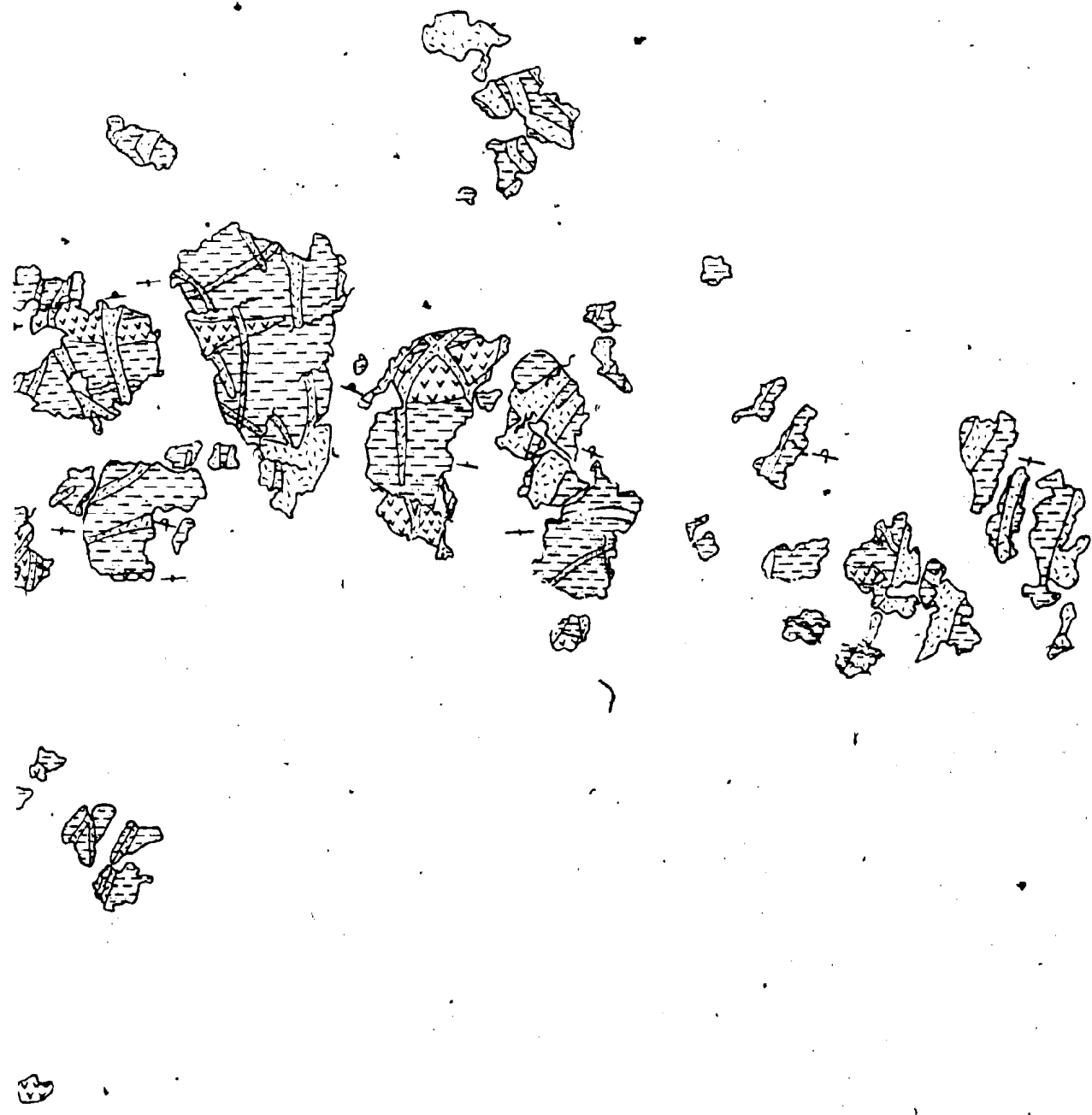
fault/shear zone



a)

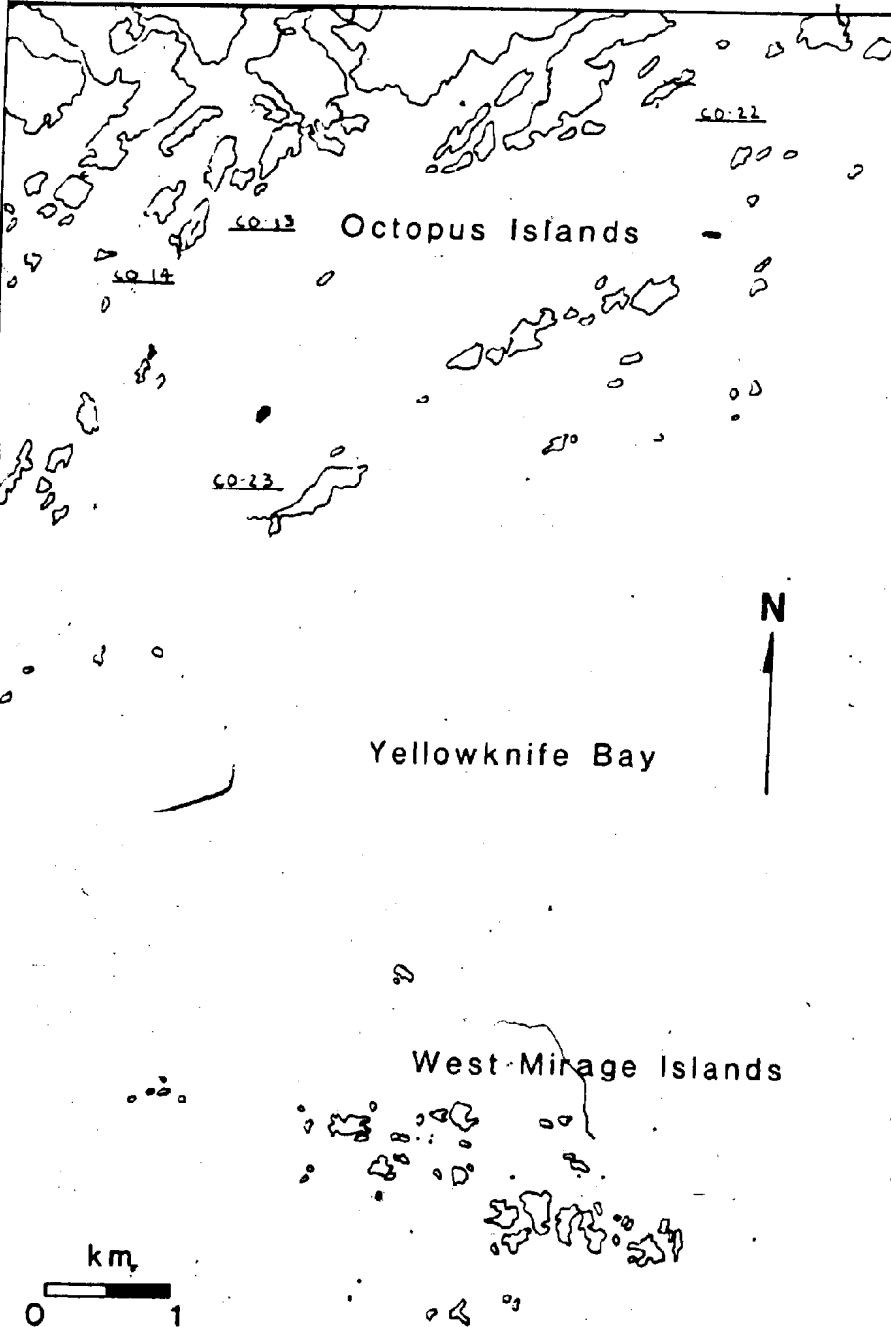
e



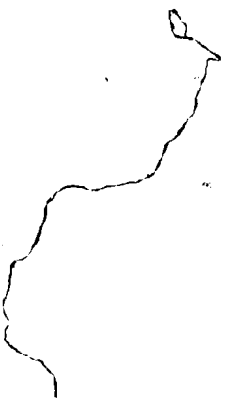


0 m 500

OCTOPUS ISLANDS



800



804

CWM-184

CWM-184

CWM-185

CWM-180

